

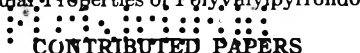
258 - v

THE JOURNAL OF PHYSICAL CHEMISTRY

(Registered in U. S. Patent Office)

Founded by Wilder D. Bancroft

TWENTY-SIXTH NATIONAL COLLOID SYMPOSIUM, LOS ANGELES, JUNE, 1952

Melvin A. Cook, Ivan B. Cutler, George Richard Hill, Milton E. Wadsworth and Alex G. Oblad: A Mechanism of Cation and Anion Exchange Capacity.....	1
F. J. Williams, M. Neznayko and D. J. Weintritt: The Effect of Exchangeable Bases on the Colloidal Properties of Bentonite.....	6
W. O. Milligan and B. G. Holmes: X-Ray Diffraction Studies in the System $Al_2O_3-SnO_2-TiO_2$	11
R. C. Wilhoit and Malcolm Dole: Specific Heat of Synthetic High Polymers. II. Polyhexamethylene Adipamide and Sebacamide.....	14
Samuel Krimm: X-Ray Studies on Crystalline and Amorphous Order in High Polymers.....	22
Marjorie J. Vold: Packing Orientation of Soap Crystallites.....	26
W. H. Peterson and A. Bondi: A Study of Soap Aerogels from Lubricating Greases.....	30
R. M. Barrer: A New Approach to Gas Flow in Capillary Systems.....	35
R. T. Johansen, P. B. Lorenz, C. G. Dodd, Frances D. Pidgeon and J. W. Davis: The Permeation of Water and Isooctane through Plugs of Microscopic Particles of Crushed Quartz.....	40
George John Bouyoucos: Capillary Rise of Water in Soils under Field Conditions.....	45
B. Roger Ray and F. E. Bartell: Wetting Characteristics of Cellulose Derivatives. II. Interrelations of Contact Angles.....	49
P. C. Carman: Properties of Capillary-Held Liquids.....	56
Conway Pierce and R. Nelson Smith: Adsorption in Capillaries.....	64
J. Kohl and R. D. Zentner: The Preparation and Utilization of Metallic Aerosols for Filter Paper Testing.....	68
A. Bondi and C. J. Penther: Some Electrical Properties of Colloidal Suspensions in Oils.....	72
Kenneth E. Hayes and Robert B. Dean: Adsorption on Monolayers. VI. Adsorption of the Isomeric Hexanes on Condensed Stearic Acid Monolayers and on Clean Water Surfaces.....	80
S. Chu Liang: A Study of Physical Adsorption at Low Coverages.....	84
G. D. Halsey, Jr.: On the Structure of Micelles.....	87
R. O. Gumprecht and C. M. Sliepcevich: Scattering of Light by Large Spherical Particles.....	90
R. O. Gumprecht and C. M. Sliepcevich: Measurement of Particle Sizes in Polydispersed Systems by Means of Light Transmission Measurements Combined with Differential Settling.....	95
Frederick M. Fowkes: Role of Surface Active Agents in Wetting.....	98
Karol J. Mysels and D. Stigter: A New Method of Measuring Diffusion Coefficients.....	104
F. D. Maslan, M. Altman and E. R. Aberth: Prediction of Gas-Adsorbent Equilibria.....	106
L. E. Miller and F. A. Hamm: Macromolecular Properties of Polyvinylpyrrolidone: Molecular Weight Distribution	110
 CONTRIBUTED PAPERS	
H. W. Foote and Michael Fleischer: The Addition of Iodine to Tetramethylammonium Iodide.....	122
P. A. Charlwood: Estimation of Heterogeneity from Diffusion Measurements.....	125



Founded by Wilder D. Bancroft

THE JOURNAL OF PHYSICAL CHEMISTRY

(Registered in U. S. Patent Office)

W. ALBERT NOYES, JR., EDITOR

ALLEN D. BLISS

ASSISTANT EDITORS

ARTHUR C. BOND

EDITORIAL BOARD

R. P. BELL

R. E. CONNICK

J. W. KENNEDY

E. J. BOWEN

E. A. HAUSER

S. C. LIND

G. E. BOYD

C. N. HINSHELWOOD

W. O. MILLIGAN

MILTON BURTON

E. A. MOELWYN-HUGHES

Published monthly (except July, August and September) by the American Chemical Society at 20th and Northampton Sts., Easton, Pa.

Entered as second-class matter at the Post Office at Easton, Pennsylvania.

The *Journal of Physical Chemistry* is devoted to the publication of selected symposia in the broad field of physical chemistry and to other contributed papers.

Manuscripts originating in the British Isles, Europe and Africa should be sent to F. C. Tompkins, The Faraday Society, 6 Gray's Inn Square, London W. C. 1, England.

Manuscripts originating elsewhere should be sent to W. Albert Noyes, Jr., Department of Chemistry, University of Rochester, Rochester 3, N. Y.

Correspondence regarding accepted copy, proofs and reprints should be directed to Assistant Editor, Allen D. Bliss, Department of Chemistry, Simmons College, 300 The Fenway, Boston 15, Mass.

Business Office: American Chemical Society, 1155 Sixteenth St., N. W., Washington 6, D. C.

Advertising Office: American Chemical Society, 332 West 42nd St., New York 18, N. Y.

Articles must be submitted in duplicate, typed and double spaced. They should have at the beginning a brief Abstract, in no case exceeding 300 words. Original drawings should accompany the manuscript. Lettering at the sides of graphs (black on white or blue) may be pencilled in, and will be typeset. Figures and tables should be held to a minimum consistent with adequate presentation of information. Photographs will not be printed on glossy paper except by special arrangement. All footnotes and references to the literature should be numbered consecutively and placed on the manuscript at the proper places. Initials of authors referred to in citations should be given. Nomenclature should conform to that used in *Chemical Abstracts*, mathematical characters marked for italic, Greek letters carefully made or annotated, and subscripts and superscripts clearly shown. Articles should be written as briefly as possible consistent with clarity and should avoid historical background unnecessary for specialists.

Symposium papers should be sent in all cases to Secretaries of Divisions sponsoring the symposium, who will be responsible for their transmittal to the Editor. The Secretary of the Division by agreement with the Editor will specify a time after which symposium papers cannot be accepted. The Editor reserves the right to refuse to publish symposium articles, for valid scientific reasons. Each symposium paper may not exceed four printed pages (about sixteen double spaced typewritten pages) in length except by prior arrangement with the Editor.

Remittances and orders for subscriptions and for single copies, notices of changes of address and new professional connections, and claims for missing numbers should be sent to the American Chemical Society, 1155 Sixteenth St., N. W., Washington 6, D. C. Changes of address for the *Journal of Physical Chemistry* must be received on or before the 30th of the preceding month.

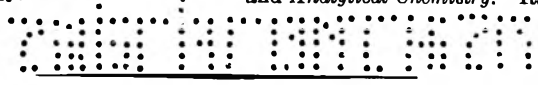
Claims for missing numbers will not be allowed (1) if received more than sixty days from date of issue (because of delivery hazards, no claims can be honored from subscribers in Central Europe, Asia, or Pacific Islands other than Hawaii), (2) if loss was due to failure of notice of change of address to be received before the date specified in the preceding paragraph, or (3) if the reason for the claim is "missing from files."

Subscription Rates: to members of the American Chemical Society, \$8.00 for 1 year, \$15.00 for 2 years, \$22.00 for 3 years; to nonmembers, \$10.00 for 1 year, \$18.00 for 2 years, \$26.00 for 3 years. Postage free to countries in the Pan American Union; Canada, \$0.40; all other countries, \$1.20. Single copies, \$1.25; foreign postage, \$0.15; Canadian postage \$0.05.

The American Chemical Society and the Editors of the *Journal of Physical Chemistry* assume no responsibility for the statements and opinions advanced by contributors to

THIS JOURNAL.

The American Chemical Society also publishes *Journal of the American Chemical Society*, *Chemical Abstracts*, *Industrial and Engineering Chemistry*, *Chemical and Engineering News* and *Analytical Chemistry*. Rates on request.



THE JOURNAL OF PHYSICAL CHEMISTRY

(Registered in U. S. Patent Office) (Copyright, 1953, by the American Chemical Society)

Founded by Wilder D. Bancroft

VOLUME 57

FEBRUARY 2, 1953

NUMBER 1

A MECHANISM OF CATION AND ANION EXCHANGE CAPACITY¹

BY MELVIN A. COOK, IVAN B. CUTLER, GEORGE RICHARD HILL AND MILTON E. WADSWORTH
College of Mines and Mineral Industries, University of Utah, Salt Lake City

AND ALEX G. OBLAD
Houdry Process Corporation, Linwood, Pennsylvania

Received July 22, 1952

Cation and anion exchange capacity in aluminous clay minerals and polyamine resins, respectively, are attributed to an (acid-base) "ion-pair" adsorption process in which one ion of the "ion-pair" is adsorbed on the solid or colloidal particle in the "compact double layer" while the other remains hydrated and occupies the "diffuse double layer." In cation exchange clays the "compact double layer" ion is the hydroxyl ion, in anion exchange resins it is the hydrogen ion. This mechanism for ion exchange is here developed thermodynamically and correlations with available experimental data are discussed. Equilibrium constants and adsorption potentials obtained in these analyses are shown to have the magnitudes required by the theory. Previously obscure effects of the ionic strength of the aqueous solution are derived quantitatively and the general feature of ion exchange explained.

Introduction

In this paper the mechanism of cation and anion exchange in (1) aluminous clay mineral and synthetic zeolites and (2) polyamine resins, respectively, is considered. The factors affecting exchange capacity are then presented. The phenomena of ion exchange and especially the mechanisms involved in the systems mentioned have been objects of great activity by workers in many fields. Recent published material which initially was concerned with the mechanism of heterogeneous catalysis has shed very considerable light on the subject of the mechanism of ion exchange.

In this article we shall employ the model proposed by Milliken, Mills and Oblad² to discuss the chemistry and thermodynamics of base adsorption and BEC (base exchange capacity) of clays and synthetic zeolites and anion exchange capacity (AEC) of resins. It will be seen that strong support for the mechanism proposed is obtained from (1) the equilibrium constants and adsorption potentials result-

ing from the theory proposed, (2) the general correlation of the data, and (3) the explanation of the effects of ionic strength which hitherto have remained obscure.

No attempt will be made here to discuss cation exchange by the sulfonated resin type of ion exchange medium. This type of cation exchange is well understood.

Discussion

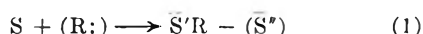
Milliken, Mills and Oblad (MMO)² associate catalytic activity of natural and synthetic alumina-silica and related acid catalysts with "promoted" structural changes on the surface of the catalyst. These changes are shown to correspond to a shift in coordination of the aluminum ions in alumina "micelles" from the 6-coordinated (octahedral) to the 4-coordinated (tetrahedral) forms. In the 6-coordinated state the calcined catalyst is a potential Lewis acid. The catalyst is prepared in such a way as to minimize the "activation energy" for the transformation. This is accomplished by forming the catalyst under conditions where the aluminum ions exist as extensively as possible in the 4-coordinated or acid state by means of promotional influences of (cristobalite) silica and NH_4^+ . In the calcining process NH_3 and water are removed and the alumina consequently goes over to the 6-coordinated state. Because of the influence of cristobalite at the linear interface between alumina and silica micelles and the fact that alumina in the original or precalcined hydroaluminum silicate is originally largely 4-coordinated, the system acquires appreciable strain or surface warp when the alumina contained therein goes over to the 6-coordinated structure on calcination. The influence of this strain is to lower the energy level of the

(1) Presented before the twenty-sixth National Colloid Symposium which was held under the auspices of the Division of Colloid Chemistry of the American Chemical Society in Los Angeles, California, June 16-18, 1952.

(2) T. H. Milliken, G. A. Mills, and A. G. Oblad, "Heterogeneous Catalysis," Faraday Society Discussion, 279, No. 8 (1950); Volume III, "Advances in Catalysis," Academic Press, Inc., New York, N. Y., in press.

transition state so that it becomes easier for the alumina to change over from the 6-coordinated to the 4-coordinated state under the influence of basic materials. Under the (promotec.) condition in which even a hydrocarbon may act as a free base toward the catalyst, however, stronger bases such as alkali, quinoline, etc., "poison" the catalyst by rendering the 4-coordinated state energetically more stable than the 6-coordinated one. In order that the catalyst remain spontaneously regenerative it is necessary for the 6-coordinated state to be the more stable one; for catalytic activity, it is necessary for the energy difference between the two states to be sufficiently small that the surface may oscillate rapidly back and forth between the two structures under the influence of temperature and the weak base adsorbate.

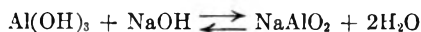
The warped or strained surface is one in which the surface unsaturation is satisfied under the restrictions of limited mobility of a solid by sharing of the unsaturation bonds, between, for example, two sites on the unstrained structure. An adsorption site, represented by S, is thus broken into two joined sites (kinetically still a single site) in the transition to the higher energy level by adsorption of the weak base. The adsorption reaction may, therefore, be represented by the equation



where R: is the (chemisorbed) radical or ion carrying the free electron pair. In the reaction of the alumina-silica catalyst with hydrocarbon, R: is the hydride ion (H:)⁻. The benefit of the catalyst then results from the rearrangements which take place in the carbonium ion under the highly polar environment of the catalyst surface. Here S represents the strained catalyst surface.

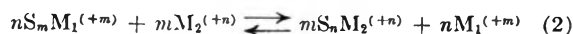
Milliken, Mills and Oblad² further showed that natural and synthetic hydroaluminum silicates contain "acid" sites and that the catalytic activity of the calcined form of these materials is a function of this "acidity," implying that the "acid" sites in the hydroaluminum silicates correspond to (but are not identical with) the seat of catalytic activity of the calcined catalyst. Greensfelder, *et al.*,³ have given a discussion of the reactions occurring on these "acid" catalysts.

Milliken, Mills and Oblad² also showed that base adsorption by clays and synthetic hydroaluminum silicates is related to the number of "acid" sites in a one to one correspondence with the active alumina content of the adsorptive material. They propose that base adsorption, like catalytic activity by aluminum silicates, involves a change of coordination of the aluminum from a 6-state to a 4-state. They point out that base adsorption by these materials is related not only to the cation involved but is also dependent on the OH⁻ concentration. For example, the amphoteric nature of aluminum hydroxide, Al(OH)₃, is related to the concentration of OH⁻



The amphoteric nature of aluminum is not lost when alumina is combined with silica. However, according to the MMO model, the pH level at which the amphoteric or coordination shift takes place is lowered from 10-12 to 3-4 or lower.

It is well known that BEC is related to pH. The conventional exchange equilibrium expressed by the equation



however, does not account for the BEC. Here M₁^(+m) and M₂⁽⁺ⁿ⁾ are two cationic species of charge +m and +n, respectively, and the site S corresponds to the S'' of equation (1) and carries a (-ε) charge, where ε is the electronic charge. It may be shown that the family of adsorption curves one obtains in the titration of a pure clay (usually referred to as H⁺ clay) represented at constant pH by the equation

$$\theta^* = f(A_M^{+n}) \quad (3)$$

(3) B. L. Greensfelder, H. H. Voge and G. M. Good, *Ind. Eng. Chem.*, 41, 2573 (1945).

may all be superimposed when plotted according to the equation

$$\theta = g(A_M^{+n} A_{OH^-}^n) \quad (4)$$

Here θ is the fraction of S sites occupied by base, f is a function of the activity of the M⁺ⁿ alone and g is a function of the product (M⁺ⁿ) (OH⁻)ⁿ (γM⁺ⁿγ_{OH⁻}ⁿ). Equation (3) at constant pH and equation (4) resemble the Langmuir isotherm except that they do not become constant at high base concentrations, instead experimentally θ continues to increase slowly as the base concentration increases.

Equation (4) implies that base adsorption by clays is an "ion-pair" process and that BEC, therefore, depends not only on the exchangeable ion concentrations, but also on the hydroxyl ion concentration. We recognize three possible types of adsorption conforming to this condition, namely: (a) hydrated ion-pair adsorption, (b) hydrated-dehydrated ion-pair adsorption, (c) dehydrated ion-pair (or free base-free acid) adsorption.

Type (a) involves only DDL ("diffuse-double layer") adsorption and is perhaps best exemplified by K⁺OH⁻ adsorption on mercury resulting in the "ideal" electrocapillarity curve. It is clear that this type is not involved in base adsorption by clays. Type (b) involves the adsorption of one ion in the CDL ("compact-double layer") in a dehydrated condition and the other in the DDL in a hydrated condition. The MMO model of clays indicates that this type of adsorption is involved in the extraction of bases from aqueous solutions by clays. Type (c) occurs prominently in cationic and anionic collectors and corresponding depressants in flotation,⁴⁻⁷ and in acid and base adsorption by wool.⁸ Cook and Wadsworth discussed these three types of acid and base adsorption and showed how free energy and selectivity considerations may be used to distinguish between them. The equivalent of model (b) was proposed for anion exchangers by Bishop⁹ and was implied by the equations for anion exchange capacity written by Kunin and Myers¹⁰ and by Jenny.¹¹

On the basis of the MMO model of clays one concludes that a pure (dialyzed) clay has no BEC; this property is acquired by the CDL adsorption (chemisorption) of OH⁻, according to the equation (1), specifically



where S represents an inactive site and $\bar{\text{SOH}}^-$ the active site. The symbol $\bar{\text{SOH}}^-$ is intended to imply no particular structure for the hydroxyl ion activated site. Reaction (5) allows the accumulation of charge on the surface which in turn causes adsorption of the counter-ions (M⁺ⁿ) in the DDL.

(4) M. A. Cook and J. C. Nixon, *THIS JOURNAL*, 54, 445 (1950).

(5) M. A. Cook and A. W. Last, *Utah Engineering Experiment Station Bulletin No. 47*, 40; No. 14 (May, 1950).

(6) G. A. Last and M. A. Cook, "Theory of Collector Depressant Equilibria," *THIS JOURNAL*, 56, 637, 643 (1952).

(7) M. E. Wadsworth, R. G. Conrady and M. A. Cook, *THIS JOURNAL*, 55, 1219 (1951).

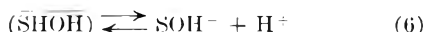
(8) M. A. Cook and M. E. Wadsworth *Utah Engineering Experiment Station Bulletin No. 51*, 41; No. 9 (May, 1951), part I.

(9) J. A. Bishop, *THIS JOURNAL*, 50, 6 (1945); 54, 697 (1950).

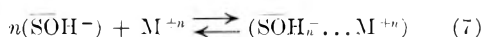
(10) R. K. Kunin and R. J. Myers, *ibid.*, 51, 1111 (1947)

(11) H. Jenny, *Colloid Sci.*, 1, 33 (1945)

MMO pointed out that the dialyzed clay is really not a H^+ clay. They show that H^+ must be adsorbed, because of ionic dimensions, as a hydronium ion H_3O^+ . The 4-coördinate structure of aluminum thus formed with H_3O^+ as the positive ion is not a stable structure and shifts over to the 6-coördinate hydragillite form of alumina, the molecular composition being unchanged in this shift. Anticipating the results of the present treatment one finds additional evidence for this shift from potential energy considerations. It will be shown that the OH^- adsorption potential on silica-alumina is in the range 12-14 kcal., or at least has this value as a minimum. The DDL adsorption of H^+ would amount to less than 3 kcal. Hence, the sum of the CDL adsorption of OH^- and DDL adsorption of H^+ probably is less than the potential for formation of water from OH^- and H^+ , unless the lower limit given above differs by more than 3-5 kcal. from the true value which seems unlikely. Hence, the H^+ clay should be unstable. Thus, if the counter-ion to the \overline{SOH}^- site were a H^+ , either water would form regenerating the S site, or the H^+ would chemisorb to eliminate the surface charge depending on whether the potential for the latter reaction were less or greater than that for free water formation. The work of MMO seems to establish the latter. The hydroaluminum silicate is acidic and one must, therefore, take into account the reaction



The BEC is related directly to the concentration of \overline{SOH}^- sites which by virtue of their $(-\epsilon)$ charge interact electrostatically with the hydrated counterion M^{+n} with a negative potential energy approximately $-n\epsilon^2/D\bar{r}$. (D is the dielectric constant and \bar{r} the average or effective distance between the CDL and DDL). The formation of this DDL structure is described by the equation



Equations (5), (6) and (7), together with the surface site balance equation

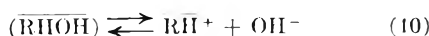


constitute the conditions determining the BEC. The actual exchange reaction (2) may be applied accurately only when all of these conditions are simultaneously determined.

Anion Exchange Capacity (AEC).—While detailed surface structure relations are unknown in this case the assumption is made that the same factors apply in determining AEC as in the BEC of zeolites. The equations in this case may be written as follows: For the CDL the important reaction in the polyamine resins is

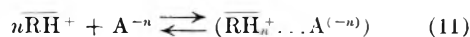


The surface charge may be removed by the reaction



implying the instability of the DDL when the counter-ion is the OH^- . This is the exact counterpart of the non-existence of the H^+ clay discussed by MMO. The third equation for AEC is the

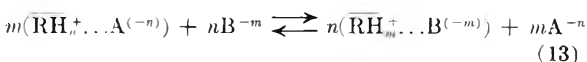
DDL formation with exchangeable anions, namely



The surface balance equation is, as before



Finally the anion exchange reaction is



The g Function.—By introducing the appropriate equilibrium constants and solving equations (5), (6), (7) and (8) simultaneously one obtains

$$\left[\frac{1-n\theta}{\theta^{1/n}} \right] A_M^{1/n} A_{OH^-} = K_3^{(1/n)} S_0^{(1/n-1)} \gamma_3^{(1/n)} \left[\frac{A_{OH^-}}{\gamma_1} + \frac{K_w}{\gamma_2 K_2} + \frac{1}{\gamma_3 K_1} \right] \quad (14)$$

where K_1 , K_2 and K_3 are the equilibrium constants of equations (5), (6) and (7), respectively. K_w is the dissociation constant of water, $\theta = (\overline{SOH}_n^- \dots M^{+n})/S_0$, and γ_1 , γ_2 , γ_3 and γ_4 are the activity coefficients of the sites \overline{SOH}^- and \overline{SHOH} , $(\overline{SOH}_n^- \dots M^{+n})$ and S, respectively. The equilibrium constants are here defined as

$$\begin{aligned} K_1 &= A_{\overline{SOH}^-} / A_S A_{OH^-} \\ K_2 &= A_H^+ S_{\overline{SOH}^-} / A_{\overline{SHOH}} \\ K_3 &= A_M^{+n} A_{\overline{SOH}^-}^n / A_{\overline{SOH}_n^- \dots M^{+n}} \end{aligned} \quad (15)$$

A plot of the left side of equation (14) (all quantities of which are measurable) against a_{OH^-} should give a straight line of intercept

$$I = \left(\frac{\gamma_1 K_w}{\gamma_2 K_2} + \frac{\gamma_1}{\gamma_3 K_1} \right) (K_3 \gamma_3)^{1/n} \frac{S_0^{(1-1/n)}}{\gamma_1} \quad (16)$$

and slope

$$S = \frac{(K_3 \gamma_3)^{(1/n)} S_0^{(1-1/n)}}{\gamma_1} \quad (17)$$

under conditions where the activity coefficients are constant. The condition under which I and S are constants is that the total ionic strength of the aqueous solution must remain constant. This is not *a priori* obvious but will be shown to be true later in this paper.

The equations of this section all have their counterpart in the corresponding anion exchange systems. These are

$$\left[\frac{1-n\theta}{\theta^{1/n}} \right] A_{H^+} A_{A^{-n}}^{1/n} = K_3^{1/n} R_0^{(1/n-1)} \gamma_3^{1/n} \left[\frac{A_{H^+}}{\gamma_1} + \frac{K_w}{\gamma_2 K_2} + \frac{1}{\gamma_3 K_1} \right] \quad (18)$$

where γ_1 , γ_2 , γ_3 and γ_4 are the activity coefficients of the sites \overline{RH}^+ , \overline{RHOH} , $(\overline{RH}_n^+ \dots A^{(-n)})$ and R, respectively, θ is $(\overline{RH}_n^+ \dots A^{(-n)})/R_0$ and the K 's are defined as

$$\begin{aligned} K_1 &= A_{\overline{RH}^+} / A_R A_{H^+} \\ K_2 &= A_{OH^-} A_{\overline{RH}^+} / A_{\overline{RHOH}} \\ K_3 &= A_{A^{-n}} A_{\overline{RH}^+}^n / A_{(\overline{RH}_n^+ \dots A^{-n})} \end{aligned} \quad (19)$$

Base Adsorption on Clays.—The data of Marshall, *et al.*,^{12,13} describing the titration of various dialyzed clay minerals by NaOH, KOH and NH_4OH

(12) C. E. Marshall and W. E. Bergman, *THIS JOURNAL*, **46**, 52, 327 (1942).

(13) C. E. Marshall and C. A. Krinbill, *ibid.*, **46**, 1072 (1942).

were studied in detail by Cutler and Cook.¹⁴ For these bases equation (14) becomes

$$\left[\frac{1-\theta}{\theta} \right] A_M^+ A_{OH^-} = K'_3 \left[A_{OH^-} + \frac{K_w}{K'_2} + \frac{1}{K'_1} \right] \quad (14a)$$

where $K'_3 = K_3\gamma_3/\gamma_1$, $K'_2 = K_2\gamma_2/\gamma_1$ and $K'_1 = K_1\gamma_3/\gamma_1$. Values of $(SOH^-\dots M^+)$ were obtained by means of membrane electrodes¹² and the original concentration of base before clay additions; values of S_0 were determined semiempirically by Cutler and Cook.¹⁴

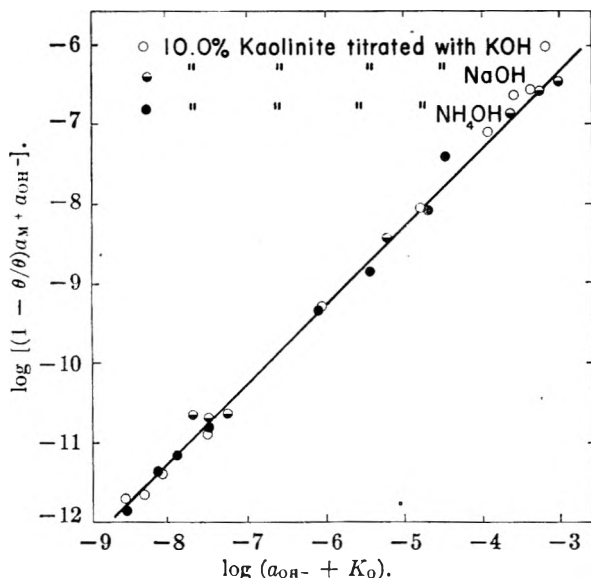


Fig. 1.—Titration data of dialyzed Kaolinite, plotted according to the logarithmic form of equation (14a).

Table I lists the value of S_0 , K'_3 and $(K_w/K'_2 + 1/K'_1)$ obtained from plots made according to equation 14a. In all cases the data were found to conform to this theory. A sample plot according to equation 14a is given in Fig. 1 for the titration of kaolinite by KOH, NaOH and NH_4OH .

The observed magnitude of K'_3 is essentially correct for the DDL formation potential, assuming that $\gamma_3/\gamma_1 \sim 1.0$. If it is assumed that $K_w/K'_2 \ll (K'_1)^{-1}$, and that $\gamma_3/\gamma_1 \sim 1.0$, the potential of OH^- adsorption would be 12 to 14 kcal. There is, of course, a possibility that the two constants are approximately equal. In any event it is clear from the data in the last column in Table I that 12 to 14 kcal. is a minimum for the CDL formation potential for OH^- on clay minerals. One thus obtains strong support for the type (b) adsorption mechanism from the adsorption potentials derived from the theory itself.

It is of interest also to note that the minimum potential for the chemisorption of H^+ to give $SHOH$ is 5–6 kcal. according to the data in Table I. The fact that this is greater than can be explained by the DDL potential adds further evidence in favor of the present theory. Unfortunately it is not pos-

(14) I. B. Cutler and M. A. Cook, "Theory of Ion Exchange Reactions with Clay Minerals" paper presented at April, 1952, Chicago Meeting of American Ceramic Soc.

TABLE I
CONSTANTS OF EQ. 14a FOR BASE ADSORPTION BY CLAYS

Mineral	Suspension concn., %	Base	S_0 (meq. per 100 g. clay)	$K'_3 \times 10^3$	$K_w/K'_2 + 1/K'_1$ ($\times 10^{10}$)
Kaolinite	10.0	NaOH	3.0	0.6	100
Kaolinite	10.0	KOH	3.0	0.6	8.3
Kaolinite	10.0	NH_4OH	3.0	0.45	4.5×10^4
Montmorillonite	2.8	NaOH	100	5.0	4.0
Montmorillonite	1.0	NaOH	100	0.6	5.0
Montmorillonite	3.28	KOH	100	5.0	2.0
Montmorillonite	2.0	KOH	100	2.5	4.0
Montmorillonite	1.31	KOH	100	1.6	6.2
Montmorillonite	3.0	NH_4OH	150	8.0	0.5
Montmorillonite	1.0	NH_4OH	150	1.6	2.5
Montmorillonite	0.5	NH_4OH	150	8.0	5.0
Beidellite	10.0	NaOH	95	10.0	1.0
Beidellite	7.0	NaOH	95	5.5	9.0
Beidellite	11.42	KOH	95	9.0	1.1
Beidellite	4.45	KOH	95	3.5	3.0
Beidellite	1.14	KOH	95	1.0	10.0
Beidellite	8.0	NH_4OH	95	3.2	3.0
Beidellite	5.0	NH_4OH	95	1.9	5.3
Beidellite	1.0	NH_4OH	95	0.25	40.0
Illite	10.0	NaOH	35	1.4	43.0
Illite	5.0	NaOH	35	0.55	90.0
Illite	10.0	KOH	35	2.5	4.0
Illite	5.0	KOH	35	1.0	13.0
Illite	10.0	NH_4OH	35	1.0	10.0
Illite	5.0	NH_4OH	35	1.0	10.0

sible to evaluate the separate components in the first term of eq. (16) with the information so far developed. However, it may be possible to do so by carrying out appropriate calorimetric measurements.

Anion Exchange Capacity in Polyamine Resins.

—For univalent anions in the DDL equation (18) becomes

$$\left[\frac{1-\theta}{\theta} \right] A_{H^+} A_{A^-} = \frac{\gamma_3 K_2}{\gamma_1} A_{H^+} + \frac{K_3 \gamma_1 K_w}{\gamma_2 K_2} + \frac{\gamma_3 K_3}{\gamma_1 K_1} = K'_3'(\mu) a_{H^+} + K_0(\mu) K'_3'(\mu) \quad (18a)$$

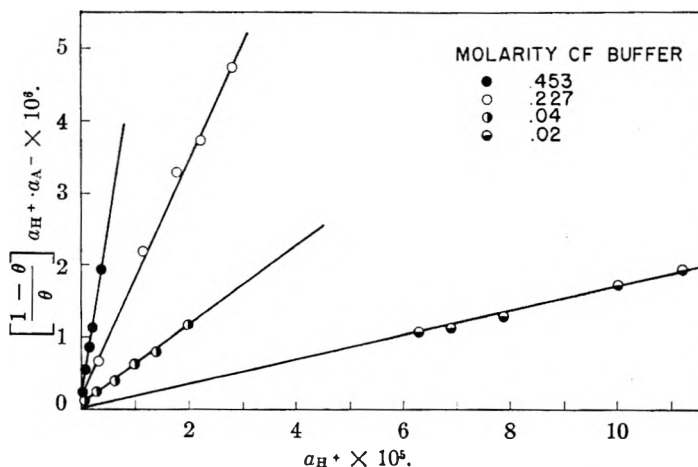


Fig. 2.—Adsorption of acetic acid on Amberlite IR-40C0 plotted according to equation (18a).

where $K'_3'(\mu) = K_3\gamma_3/\gamma_1$ and $K_0(\mu) = \gamma_1 K_w/\gamma_2 K_2 + \gamma_1/\gamma_3 K_1$. The constant $K'_3'(\mu)$ and K_0 at constant temperature are functions of the total ionic strength. Figure 2 gives plots of the data of Bishop⁹ for acetic acid on Amberlite IR-400 in buffered solutions of various ionic strengths plotted according to equation (18a) for an R_0 of 5.5 meq./g. of resin. The variation in the slope of the curves of Fig. 2 with ionic strength is shown in Fig. 3, using data of

TABLE II
EQUILIBRIUM CONSTANTS FOR AEC ON RESINS

Acid	Buffer	Resin	K_3'	K_0'	R_0 (meq./g.)
CH ₃ COOH	0.0219	Amberlite IR-400	0.017		5.5
CH ₃ COOH	.04	Amberlite IR-400	.055	1.3×10^{-6}	5.5
CH ₃ COOH	.227	Amberlite IR-400	.16	1.7×10^{-6}	5.5
CH ₃ COOH	.453	Amberlite IR-400	.53	4.1×10^{-7}	5.5
CH ₂ ClCOOH	.1	Amberlite IR-400	.11	3.0×10^{-6}	9.5
HCl	1.0	Amberlite IR-4B	.25	3.0×10^{-8}	9.2
HCl	0.1	Amberlite IR-4B	.001	9.4×10^{-8}	9.2
HCl		Amberlite IR-4	.00027		9.2
H ₂ SO ₄		Amberlite IR-4	$.0453R_0^{1/2}$		10.5

Bishop and Heymann and O'Donnell,¹⁶ in which we have plotted $\log K_3'$ vs. $\mu^{1/2}$. This result is in accord with the theory as shown below and provides evidence for the validity of the present theory.

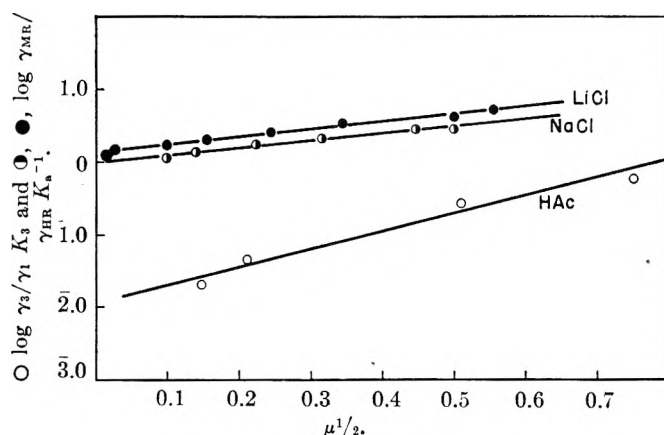


Fig. 3.—Variation of K_3' in solutions of high ionic strength.

Wadsworth and Cook¹⁶ using data of Kunin and Myers¹⁷ and Bishop⁹ for chloroacetic acid, hydrochloric and sulfuric acid on Amberlite obtained excellent correlations by means of the present theory. Table II shows values of K_3' , K_0 and R_0 found in their study. The method of evaluation of $K_0(\mu)$ employed by Wadsworth and Cook makes use of the fact that, in the region $A_{H^+} \gg K_0(\mu)$, the slope of the $\log f(\theta)$ vs. $\log A_{H^+}$ curve is constant. ($f(\theta)$ is used as an abbreviation for the left side of equation (18a).) Figure 4 exemplifies the results obtained by showing a plot of $\log f(\theta)$ vs. A_{H^+} for H₂SO₄.

Here equation (18) becomes

$$\left(\frac{1-2\theta}{\theta^{1/2}}\right) A_{H^+} A_A^{1/2} = \left(\frac{K_3(\mu)}{R_0}\right)^{1/2} A_{H^+} + \left(\frac{K_3(\mu)}{R_0}\right)^{1/2} K_0(\mu) \quad (18b)$$

In this case as in the case of HCl on Amberlite IR-4, A_{H^+} is large compared with $K_0(\mu)$ over the whole range of available data and one thus obtains a straight line on the $\log f(\theta)$ vs. $\log A_{H^+}$ plot.

(15) E. Heymann and I. J. O'Donnell, *Colloid Sci.*, **4**, 395 (1949).

(16) M. E. Wadsworth and M. A. Cook, "Theory of Adsorption on Anion Exchange Resins," presented Boston Meeting (April, 1951), American Chemical Society; *Bulletin of the Utah Engineering Experimental Station*, **51**, 41, No. 9 (1951), part II.

(17) R. K. Kunin and R. J. Myers, "Ion Exchange Resins," John Wiley and Sons, Inc., New York, N. Y., 1950.

Effect of Ionic Strength.—From equation (17) for univalent exchangeable anions one obtains

$$S = \frac{K_3 \gamma_3}{\gamma_1} = k_3 \gamma_{A^-} \quad (17a)$$

where $k_3 = (A^-) (\overline{RH^+}) / (\overline{RH^+} \dots A^-)$ is the ideal mass action constant. Since k_3 does not vary with ionic strength it is clear that K_3' should vary with ionic strength in exactly the same way as γ_{A^-} , i.e., at not too large ionic strength

$$\log K_3' = c' \mu^{1/2} + c'' \quad (20)$$

where c'' is a constant (7). This is verified by the correlation shown in Fig. 3.

Defining k_1 , k_2 and k_w in the same manner as k_3 above, i.e., as the ideal mass action constants, equation (16) may be written for the univalent exchangeable ion case as

$$I = k_3 \gamma_{A^-} \gamma_{H^+} \left(\frac{k_w}{k_2} + \frac{1}{k_1} \right) \quad (16a)$$

We see, therefore, that K_0 is given by

$$K_0(\mu) = \gamma_{H^+} \left(\frac{k_w}{k_2} + \frac{1}{k_1} \right) \quad (21)$$

K_0 should thus vary as $\mu^{1/2}$ because of γ_{H^+} . Since $I = k_3 \gamma_{A^-} K_0$, I should be a linear function of the ionic strength.

The values of I obtained in the work of Wads-

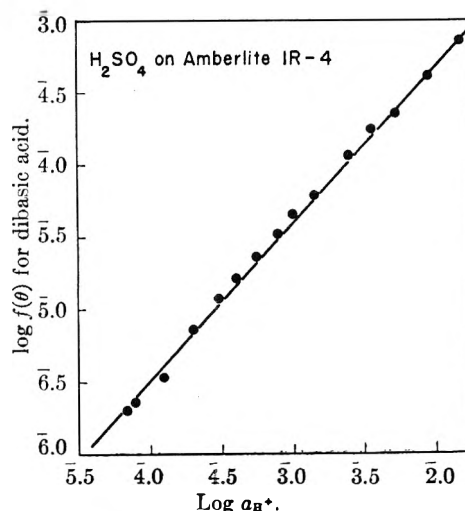


Fig. 4.—Adsorption of H₂SO₄ on Amberlite IR-4, plotted according to the logarithmic form of equation (18b).

worth and Cook are too small and the error in determining the intercept too large to allow one to determine any effects of ionic strength on the intercept of the $f(\theta)$ vs. A_{H^+} .

The effect of ionic strength on the BEC of clays is peculiar. It appears that the concentration of the clay suspension itself has a greater influence on

the value of the total BEC than the ordinary salt effect in the range of ionic strengths studied. The $\log f(\theta)$ vs. $\log A_{OH^-}$ plots for clay minerals at different suspension concentrations indicate that $K_3\gamma_3/\gamma_1$ varies directly as the percentage of the clay suspension. An explanation of this behavior was presented by Cutler and Cook.¹⁴

THE EFFECT OF EXCHANGEABLE BASES ON THE COLLOIDAL PROPERTIES OF BENTONITE¹

BY F. J. WILLIAMS, M. NEZNAYKO AND D. J. WEINTRITT

Research Laboratories, Baroid Sales Div., National Lead Co., Houston, Texas

Received July 22, 1952

Base exchange data were related to the colloidal properties of Wyoming bentonite. This involved the examination of purified clays in terms of (1) the exchangeable sodium and calcium on the clay, (2) the effects of solutions of electrolytes on the properties of bentonite and (3) field application. In the absence of excess electrolytes the viscosity and filter loss are a function of the exchangeable sodium but the relationship is not linear. For systems containing sodium and calcium salts simulating field conditions, the viscosity and gel strength passed through maxima characteristic of flocculation phenomena. This corresponds to a sodium-calcium ratio of 40/60 though high quantities of total salts may likewise cause flocculation. Filtration rate of the colloidal clay, measured under constant pressure, was an index of the stability of the system. Examination of a natural deposit on the basis of the above relationships provided a clue as to the tremendous variations in rheological properties of field samples. Practical applications of the data have been made. Through the establishment of a series of standard X-ray curves it has been found possible to estimate the per cent. of calcium and sodium of a field bentonite prepared by the described washing method. Differential thermal analysis curves of the same purified bentonites show the effect of the transition from sodium to calcium type.

I. Introduction

The deposits of bentonite found in the Wyoming-South Dakota area are generally considered to be the most abundant and the highest quality montmorillonite clays occurring in the United States. On close inspection, however, these clays have been found to vary in their colloidal properties, even within the same deposit. Experience of the authors has shown that one of the most important variables in bentonite is the make-up of the exchangeable bases. The literature shows continuous investigation of base exchange²⁻⁶ but very few papers have had direct reference to the base exchange equilibrium conditions imposed by nature on the Wyoming-type bentonites. Usually investigators have given little attention to the previous history of the sample or the make-up of the exchangeable bases and excess salt. The omission of any one of these factors can prevent a complete understanding of the causes for variation of colloidal properties.

The purpose of this investigation was to analyze the general base exchange processes which are involved in the massive sedimentary bentonite de-

posits of this area. Included was the preparation of purified homoionic clays as reference standards.

From the purified standards the effect of varying the exchangeable bases was established. The colloidal properties were determined and the purified clays were studied with X-ray and differential thermal analyses. The basic work was extended to include the effect of several electrolytes on the purified clays.

From these data the relative exchangeable base make-up of typical bentonite deposits was determined. Methods for the evaluation of those bentonites whose properties deviate from the best Wyoming-type bentonite are suggested on a more quantitative basis than in the past.

Since the interest of the authors is primarily in the field of oil well drilling fluids, the standard test methods of that industry were used throughout.

II. Materials and Experimental Methods

The bentonite samples used in this investigation were taken from known geological sections and may be described as being typical Wyoming bentonites.⁷ In the preparation of the purified bentonite samples a single batch of finely ground clay (98% through 200 mesh) was hydrated, aged and converted to the sodium type of leaching with one normal sodium chloride. The conversion technique was similar to that used by Hissink.⁸ By conversion of the natural clay to the sodium type many of the normally rejected, large clay aggregates were dispersed prior to centrifugation and as a result were available. This method, in effect, gave a more average and thereby less selective clay with respect to particle size distribution. The bulk of the excess salt retained by the clay was removed by filtration and washing, the non-clay fraction was removed by centrifugation of a 4.7% suspension and the balance of the salt was removed by five successive treatments with resinous ion exchangers.

(7) From the properties of the Baroid Sales Division, National Lead Company, Colony, Wyoming.

(8) D. J. Hissink, *Trans. Faraday Soc.*, **20**, 551 (1924).

(1) Presented before the twenty-sixth National Colloid Symposium which was held under the auspices of the Division of Colloid Chemistry of the American Chemical Society in Los Angeles, California, June 16-18, 1952.

(2) G. W. Brindley (Ed.), "X-Ray Identification and Crystal Structure of Clay Minerals," The Mineralogical Society, London, 1951

(3) C. W. Davis and H. C. Vacher, Revised by J. E. Conley, "Bentonite: Its Properties, Mining, Preparation, and Utilization," T. P. 609, U. S. Dept. of Interior, Washington, 1940.

(4) W. P. Kelley, "Cation Exchange in Soils," Reinhold Publ. Corp., New York, N. Y., 1948.

(5) C. E. Marshall, "The Colloid Chemistry of the Silicate Minerals," Academic Press, Inc., New York, N. Y., 1949.

(6) W. F. Rogers, "Composition and Properties of Oil Well Drilling Fluids," Gulf Publ. Co., Houston, Texas, 1948.

The pH was maintained between 7 and 11 throughout the process to avoid forming hydrogen bentonite.

Using the sodium bentonite prepared above, different mixed sodium-calcium bentonites were prepared by adding calcium chloride as a solution to the hydrated sodium clay in steps of 20%, on the basis of the base exchange capacity. Excess salts were removed by filtration and washing. The final percentage of exchangeable calcium and sodium in each sample was determined by base exchange methods.⁹

The homoionic clays, thus prepared, were submitted to X-ray analysis¹⁰ and showed no structural change over the original clay.

After the preparation of the purified standards, calcium sulfate and chloride were added to the sodium montmorillonite for their effect on the colloidal properties. The salt solutions were added to the aged, hydrated clays to prevent incomplete hydration.

Collection of field samples involved taking core-drill samples transversely across five deposits of bentonite of which one deposit is discussed in this paper. Geologic features such as depth of overburden, thickness of deposit, mineralogy of the bentonite bed and surrounding area were recorded.

The more important rheological properties were based on measurement of viscosity, zero and 10-minute gel strengths and filter loss.¹¹ The filter loss was determined for each suspension because the data can be used to distinguish between flocculated and non-flocculated bentonite suspensions. The methods used are in accordance with API Code 29.¹² Prepared clay suspensions were aged for 20 hours before testing except that electrolytes were added to suspensions several weeks old and aging was continued for 72 hours. Exchangeable bases and soluble salts were determined on the leachates from the base exchange determinations.

The preparation of samples for X-ray spectroscopy involved dipping a microscope slide into an aged, hydrated suspension and air drying. The dried sample was then placed in a desiccator maintained at 50% relative humidity and allowed to come to equilibrium. Samples were then run on a North American Philips High Angle Spectrometer. The (001) X-ray asymmetry values on the different bentonites were based on the Hendricks and Teller¹³ formula utilizing the technique and interpretation of Roth.¹⁴

The pH values of purified and field clays varied from 8.2 to 9.0. No attempt was made to control this value since exchangeable base make-up was the primary criterion. All sample calculations are corrected to the dry basis.

III. Experimental Results and Discussion

A. The Effect of Exchangeable Cations in the Absence of Electrolytes.—Chemicals and mineralogical analyses reported in Table I indicate that the sodium clay prepared from Wyoming bentonite was relatively pure. The base exchange capacity showed an increase from 81 to 94 meq./100 g., attributed primarily to removal of diluents identified as quartz, cristobalite and feldspar.

Figure 1 shows the effect of increasing exchangeable calcium upon the viscosity and the filter loss of a 4% suspension. These curves emphasize how dependent the rheological and structural properties are upon the relative amounts of calcium and

(9) M. Peech *Ind. Eng. Chem., Anal. Ed.*, 13, 436 (1941).

(10) Courtesy of W. F. Bradley, Illinois State Geological Survey, Urbana, Illinois.

(11) Viscosity is determined at 600 r.p.m. in a calibrated Stormer Viscometer with the center baffle removed. The gel strength is the weight in grams necessary to just move the Stormer rotor. Yield is the No. of 42 gal. bbl. of 15 cp. suspension obtainable from 1 ton of clay. Filter loss is the volume of filtrate in cc. passing a 9-cm. filter paper in 30 min. under 100 p.s.i.

(12) API Code 29: Recommended Practice for Standard Field Procedure for Testing Drilling Fluids with Appendix, Manual of Procedures for Laboratory Evaluation of Drilling Mud Materials, American Petroleum Institute, Dallas, Texas, 1950.

(13) S. B. Hendricks and E. Teller, *J. Chem. Phys.*, 10, 147 (1942).

(14) R. S. Roth, Thesis, University of Illinois, Urbana, Illinois, 1951.

TABLE I
ANALYSES OF SODIUM BENTONITE PREPARED FROM WYOMING BENTONITE

X-Ray diffraction, %	Wyoming bentonite	Centrifuged sodium bentonite
Major phase	Mont.	Mont.
Quartz	8	<0.5
Cristobalite	3	2-3 ^a
Feldspar	<3	0
Chemical analyses, %		
SiO ₂	63.20	57.86
Al ₂ O ₃	20.54	20.59
Fe ₂ O ₃	3.51	3.54
TiO ₂	0.15	0.15
R ₂ O ₃	24.20	24.68
CaO	1.30	0.39
MgO	2.49	2.66
Na ₂ O	2.16	2.72
K ₂ O	0.50	0.23
SO ₃	.53	.18
CO ₂	.30	.00
H ₂ O (110°)	7.19	7.42
H ₂ O (900°)	5.06	5.17
Base exchange analysis (meq./100 g.) ^b		
Base Exch. Cap.	81	94
Exchangeable Bases		
Ca	33	0.5
Mg	22	0.5
Na	24	93
K	2	0
Excess salts		
SO ₄	19	0
CO ₃	13	<3
Cl	0	0

^a Possible clay spacings ^b Ammonium acetate method expressed on basis of dried clay.

sodium. Generally, the sodium bentonite has high viscosity and low filter loss while the calcium bentonite has an expected low viscosity and high filter loss.

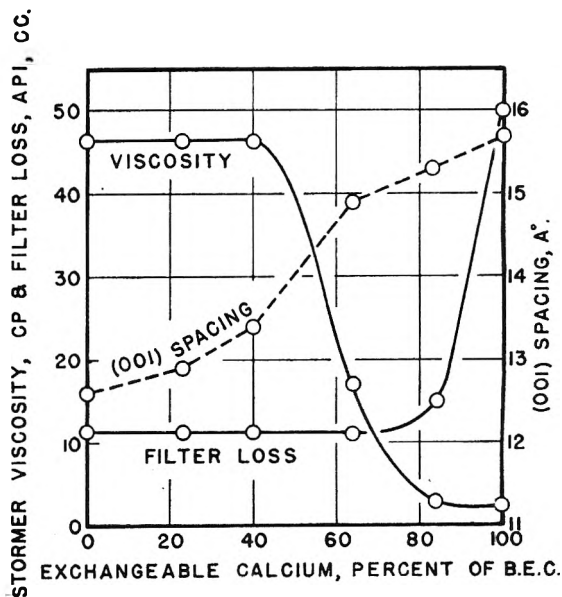


Fig. 1.—Colloidal properties at 4% clay as a function of the sodium-calcium ratio.

The sodium bentonite adsorbed 40% of the base exchange capacity as calcium before a decrease in viscosity was noted. Filter loss did not appear affected until some 70% exchangeable calcium was present.

B. The Effect of Solutions of Calcium Sulfate and Calcium Chloride.—The possibility of finding a deposit of natural clay free of electrolytes is quite small. Though bentonites show tremendous variations in their properties due to the relative amount of each ion, base exchanged on the clay, they also are influenced by the presence of electrolytes.

Figure 2 shows the effect of calcium sulfate and calcium chloride upon the colloidal properties of a 4.0% suspension of hydrated sodium bentonite. With small additions of salt the viscosity passes through a minimum, which may be due to an electroviscous effect. In natural clays this initial viscosity drop would be rarely observed since most natural clays, as indicated by the fine ruled area, have some excess salts already present. The viscosity reaches a peak with the addition of 60 meq. of excess salt per 100 g. With the addition of about 75 meq. the viscosity and gel strength begin to stabilize while the filter loss increases abruptly.

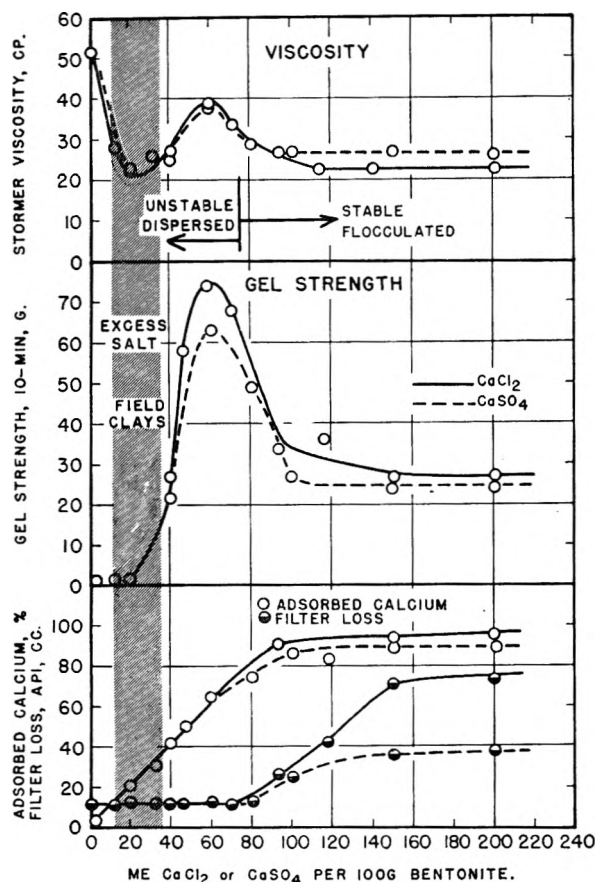


Fig. 2.—Effect of calcium salts on the properties of sodium bentonite suspensions.

This abrupt change in the bulk structure of the bentonite system as evidenced by the change from an unstable, uniformly dispersed system to a stable flocculated system has been previously noted.

Slabaugh,¹⁵ using hydrogen bentonite, showed that the point of transition from one system to the other occurs at a certain "critical salt concentration." The viscosity, gel strength and filter loss indicate that the critical salt concentration for the system is at 75 meq. per 100 g. Of interest is the apparent fact that up to 75 meq. per 100 g. of calcium replaces sodium quantitatively. At this point the almost linear relation ends and the mass action effect becomes increasingly pronounced.

Other data show that clay concentration has no appreciable effect on the completeness of the base exchange reaction.

Figure 3 is a plot of the viscosity and filter loss as a function of exchangeable calcium. In A no excess salts are present, while in B there was a continuous addition of calcium sulfate. At 65% exchangeable calcium the precipitating reaction reached a maximum as indicated by the peak in B. A manifestation of this reaction is the abrupt increase in filter loss at the same point. This indicates a disruption in the effective volume of the solvated particle.

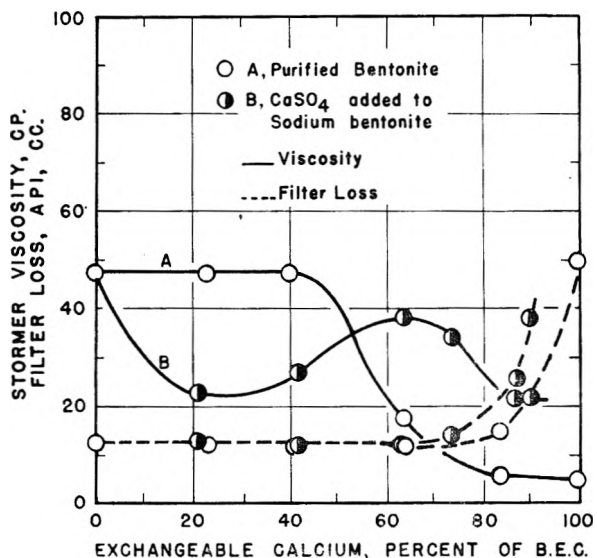


Fig. 3.—The effect of calcium sulfate on the properties of hydrated bentonite.

C. Properties of Natural Wyoming Bentonite.

—For any bentonite it has been shown that the rheological properties can be made to vary tremendously by adjustment of the ratio of exchangeable monovalent to divalent ions. And it has been further illustrated that a build-up of excess salt will have an additional effect beyond that due to the cation alone. The importance of electrolytes and their related effects on the occurrence and properties of clay are discussed by Rankama and Sahama.¹⁶

To observe the transition in physical properties with a continuous bentonite bed, five deposits were investigated. Their properties were obviously affected by the depth of "protective" overburden and they were therefore related to that dimension.

(15) W. H. Slabaugh and J. L. Culbertson, *THIS JOURNAL*, **55**, 744 (1951).

(16) K. Rankama and Th. G. Sahama, "Geochemistry," The University of Chicago Press, Chicago, Ill., 1950, Ch. 5.

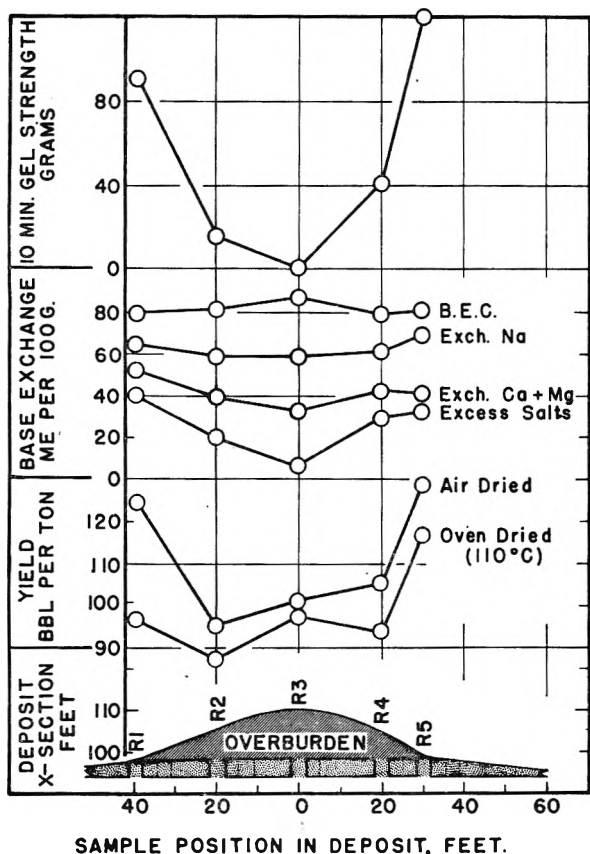


Fig. 4.—The variation in properties of a natural Wyoming bentonite as a function of overburden.

The data of Fig. 4 give some of the variations which occurred within a single deposit. The yields and gel strengths varied inversely with the overburden. The exchangeable sodium and calcium plus magnesium, and the excess salt as sulfate and carbonate vary in a similar manner. For example, there were 6 meq./100 g. of excess salt in the center of the deposit where the overburden was greatest and 38 and 31 meq./100 g. at either outcrop. The 10-min. gel strength for the same deposit was zero at the center and 90 and 110 g. at the outcrops. This is similar to the results obtained with the purified system reported in Fig. 2.

For the purpose of this investigation it has been found practical to consider the exchangeable calcium and magnesium found in the field clays as complementary to each other and of equal effectiveness.

D. Exchangeable Bases and Structural Relationships between the Purified Bentonites and the Natural Bentonites.—Twenty-seven samples were studied from five deposits and were found to have from 35 to 67% of the exchangeable bases as calcium and magnesium. In relation to the purified system these figures place the average Wyoming bentonite in the 40 to 60% exchangeable calcium range. This is the range where the purified clays show the greatest amount of instability so that small changes in the amount of calcium or sodium can induce large changes in the rheological properties.

The yield values of purified clays for the same

quantities of exchangeable calcium and sodium are considerably higher than the yield of the field clays. Much of the difference is due to weight dilution of the colloidal fraction by such minerals as quartz, feldspar, mica and gypsum. The properties are also influenced by the varying amounts of soluble salts depending on whether they are added before or after hydration of the clay. The excess salts also cause an appreciable effect on X-ray structure correlations as will be shown later.

It was observed in the yield curves of Fig. 4 that oven drying at 110° to complete dryness caused an apparently permanent decrease in yield. Unless the previous history of a sample is known the rheological properties of any given clay will not necessarily be reproducible. It has been suggested by Marshall⁵ that the various exchangeable bases become attached to the clay lattice on drying or heating but that for sodium and calcium the process is essentially reversible under the proper conditions. Air drying to the equilibrium value of about 10% moisture from an original 27% moisture apparently does not cause permanent fixation of the ions and the clays return to their former value with the 20-hour aging.

Figure 5 shows the X-ray spectrometer tracings from the series of purified montmorillonites. The corresponding numerical data are given in Table II. The progressive change as calcium is substituted for sodium is readily evident although not linear in nature. Ideally the sodium montmorillonite would

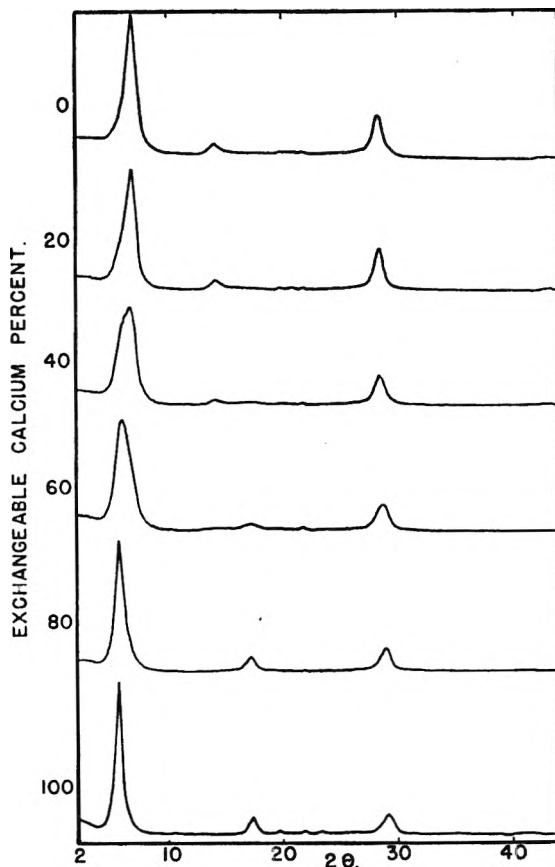


Fig. 5.—X-Ray spectrometer tracings of homoionic and di-ionic montmorillonites.

have a "single water layer" resulting in an (001) spacing of 12.4 Å. and an asymmetry of 1.0 while calcium montmorillonite would have a "double water layer" and corresponding values of 15.4 Å. and 1.0. These conditions were not achieved by aging the samples at 50% relative humidity. In the di-ionic clays the major ion predominates in influence on the (001) d value.

TABLE II
X-RAY DATA ON THE PURIFIED CLAYS

Exch. Ca % BEC	Yield, 15 cp. bbl./t.	Ratio, Ca/Na	(001) Spacing, Å.	(001) Asymmetry
0	182	0	12.6	0.63
20	182	0.25	12.9	0.33
40	182	0.67	13.4	0.57
60	152	1.50	14.9	1.44
80	88	4.10	15.3	1.50
100	42	∞	15.7	0.78

excess salt before drying. The X-ray data in Table III for field samples R3 and R5 show this to be the necessary procedure to get correlation with the corresponding data of the purified clay. The importance of this procedure can be realized upon comparison of X-ray data in the "Excess Salt Present" column and the "Salt Free" column of Table III. Note the uniformity of the X-ray data prior to washing as opposed to the actual physical properties.

These data point out that X-ray analyses of field clays can be misleading with regard to the actual calcium-sodium on the hydrated clay if an electrolyte phase is involved. The error will be equally as great if an attempt is made to correlate X-ray data from dry powder samples since rheological data are determined in relatively dilute systems and therefore the solubility of the non-clay diluents such as gypsum will affect the properties.

TABLE III
X-RAY DATA ON THE FIELD BENTONITES

Sample No.	Exch. Ca + Mg % BEC	Yield, 15 cp. bbl./t.	Excess salt present				Salt free			
			Air-dried ratio, Ca + Mg / Na	Spacing, Å.	(001) Line Asymmetry	Est. Ca, %	Air-dried ratio, Ca + Mg / Na	Spacing, Å.	(001) Line Asymmetry	Est. Ca, %
R1	67	125	0.22	12.7	0.44	10	2.01			
R2	49	95	.37	12.8	.30	20	0.96			
R3	37	101	.51	12.8	.30	20	0.59	13.8	0.69	40
R4	54	105	.30	12.8	.41	15	1.17			
R5	50	129	.18	12.7	.44	10	1.00	14.7	1.87	55

* Calculated from base exchange analysis. The Ca + Mg/Na ratios indicate probable conditions on sample used for X-ray analysis before and after washing.

In the correlation of d spacings and asymmetry values of the purified clays of known exchangeable sodium-calcium content with those of the field clays it was found that the latter clays had from 0 to 20% calcium in the exchange positions. Base exchange analyses, however, showed that the field clays were in the 40 to 60% range and that for the quantities of salt involved all of the calcium should be in exchange positions on the clay as was shown above. The cause for the high exchangeable sodium as determined by X-ray was apparently due to concentration of the excess sodium salt on drying the hydrated field clay down at 50% relative humidity. Thus, it would appear that the mass action effect of the concentrated sodium salt forced substitution of calcium by sodium in the lattice with the precipitation of CaCO₃ and CaSO₄.

To verify this effect, the ionic ratios of hydrated field clay were "fixed" by washing the clay free of

The differential thermal analysis curves for the purified clays do not show the characteristic double peak of calcium montmorillonite until 40 per cent. calcium is present. The DTA curves of the two field samples show additional influence due to magnesium and therefore do not correlate as closely with the standard curves as would be desired. More check points intermediate to the present five samples also would be desirable. The triple peak evident at 105 to 190° possibly indicates that the magnesium water is coming off at a slightly lower temperature than that of the sodium and calcium.

Acknowledgment.—The authors wish to thank the management of the Baroid Sales Division, National Lead Company, for the encouragement which made this work possible and for permission to publish these data. The help of the staff of the Baroid Research and Development Laboratories is greatly appreciated.

X-RAY DIFFRACTION STUDIES IN THE SYSTEM

 $\text{Al}_2\text{O}_3\text{-SnO}_2\text{-TiO}_2^1$

BY W. O. MILLIGAN AND B. G. HOLMES

*The Rice Institute, Houston, Texas**Received July 22, 1952*

Sixty-six gels corresponding to every ten mole per cent. in the ternary system $\text{Al}_2\text{O}_3\text{-SnO}_2\text{-TiO}_2$ were simultaneously precipitated by the addition of an excess of water to mixtures of alcoholic solutions of the appropriate amounts of aluminum, stannic and titanium alcoholates. The gels were washed free of excess alcohol, heat-treated for two-hour periods at temperature levels of 400, 600, 800 and 1000°, and examined by standard X-ray diffraction methods. In the ternary diagram corresponding to heat treatment at 400°, four principal composition regions were observed. At the vertices of the diagram the X-radiograms of $\gamma\text{-Al}_2\text{O}_3$, SnO_2 and anatase were observed, respectively. A large area of the ternary diagram corresponded to "amorphous" type X-radiograms. The composition region high in SnO_2 (and intermediate in TiO_2) yielded X-radiograms consisting of extremely broad bands, characteristic of the isomorphous $\text{SnO}_2\text{-TiO}_2$ structure. At the 600° temperature level the "crystalline" regions increased in area at the expense of the "amorphous" region. At the 800° temperature level the same trend continued and two very small amorphous regions remained. In the high titania region, mixtures of anatase and rutile were encountered, as well as mixtures of rutile and SnO_2 . On the $\text{TiO}_2\text{-SnO}_2$ leg of the ternary diagram, definite evidence of solid solution was observed. At the 1000° temperature level the samples gave sharper X-radiograms and the amorphous area completely disappeared. The phenomenon of mutual protective action against crystallization, previously observed in this Laboratory, occurs at the 400, 600 and 800° temperature levels and was especially evident in the $\text{Al}_2\text{O}_3\text{-SnO}_2$ leg in which two zones of mutual protection were very distinct at 800° in confirmation of earlier results obtained for $\text{Al}_2\text{O}_3\text{-SnO}_2$ gels prepared from inorganic reagents. In the system $\text{Al}_2\text{O}_3\text{-TiO}_2$, some extra diffraction lines were observed at the 800° temperature level, which became more prominent at 1000 and 1400° and suggested the possibility of compound formation.

Introduction

Simultaneously precipitated mixtures of two or more oxides exhibit after heat treatment several phenomena such as: (a) the product may consist of a simple mechanical mixture of the separate oxides possessing the additive properties of each constituent; (b) the presence of one or more oxides may retard or prevent the crystallization of the other, resulting in enhanced surface properties; (c) a solid solution may occur; or (d) some combination of these processes may take place. For a survey of previous work concerning hydrous oxide systems and composition zones of mutual protection, consult ref. (2). Little information is available concerning mutual protection in ternary oxide systems. In this Laboratory, 66 gels in the system $\text{NiO-Cr}_2\text{O}_3\text{-ZrO}_2$ were examined by X-ray diffraction methods at a temperature of heat treatment at 500°. In the ternary diagram, a large "amorphous" composition region was observed. It is the purpose of this present paper to extend these results to the ternary system $\text{Al}_2\text{O}_3\text{-SnO}_2\text{-TiO}_2$ at several temperature levels of heat treatment. In previous studies, the presence of inorganic impurities have led to complications and in this work the gels were prepared by hydrolysis of alcoholate solutions in order that inorganic impurities may be minimized.

Experimental

Preparation of Samples.—Sixty-six gels were prepared, corresponding to every ten mole per cent. in the ternary system $\text{Al}_2\text{O}_3\text{-SnO}_2\text{-TiO}_2$.

Solutions of aluminum isopropylate (0.0631 g. of Al_2O_3 per ml.), titanium ethylate (0.0656 g. of TiO_2 per ml.) and stannic ethylate (0.0236 g. of SnO_2 per ml.) in absolute ethyl alcohol were mixed under anhydrous conditions in one compartment of a rapid mixing device.⁴ The aluminum and

titanium alcoholates were the purest available commercial products and the stannic ethylate was prepared according to the procedure of Theissen and Koerner.⁵ An excess of distilled water was placed in the second compartment of the rapid mixing device. The solutions were then mixed as rapidly as possible and the mixed oxides were washed several times on a buchner filter with water, acetone and finally with water. This procedure removed most of the adsorbed alcohol.

The air-dried samples were ground in an agate mortar and were heat-treated for two-hour periods at temperatures of 400, 600, 800 and 1000° in a thermostatically controlled electric furnace in an atmosphere of dry nitrogen.

X-Ray Analysis.—X-Ray diffraction patterns were obtained by standard methods, using copper $K\alpha$ X-radiation. A nickel foil beta filter was employed with an exposure time of six to eight hours. Some of the results are summarized in Figs. 1-3.

Results and Conclusions

Heat Treatment at 400°.—At the temperature level of 400° the X-radiogram of pure alumina consisted of broad bands corresponding to the $\gamma\text{-Al}_2\text{O}_3$ pattern. Area A represents the composition of the system where only $\gamma\text{-Al}_2\text{O}_3$ patterns were detected. Both stannic oxide and titania exhibited mutual protective action with the alumina. However, stannic oxide inhibited the crystallization of alumina more than it did the titania.

Area B corresponded to the samples which were amorphous to X-rays. In this region alumina inhibited the degree of crystallization of anatase much more than it did the stannic oxide. When stannic oxide was mixed with approximately equimolar amounts of titania and alumina, crystallinity increased; whereas stannic oxide mixed with only 30% alumina did not crystallize as well.

Area C consisted of samples which gave X-ray patterns corresponding to the anatase form of titania. It was observed that as little as 10% stannic oxide favored the rutile form of titania and at the approximate composition of 80% titania and 20% stannic oxide the anatase pattern disappeared and the stannic oxide or rutile pattern appeared.

(1) Presented before the twenty-sixth National Colloid Symposium which was held under the auspices of the Division of Colloid Chemistry of the American Chemical Society in Los Angeles, California, June 16-18, 1952.

(2) H. B. Weiser, W. O. Milligan and G. A. Mills, *This Journal*, **52**, 942 (1948).

(3) W. O. Milligan and L. M. Watt, *ibid.*, **52**, 230 (1948).

(4) H. B. Weiser and W. O. Milligan, *ibid.*, **40**, 1071 (1936).

(5) P. A. Theissen and O. Koerner, *Z. anorg. allgem. Chem.*, **195**, 83 (1931).

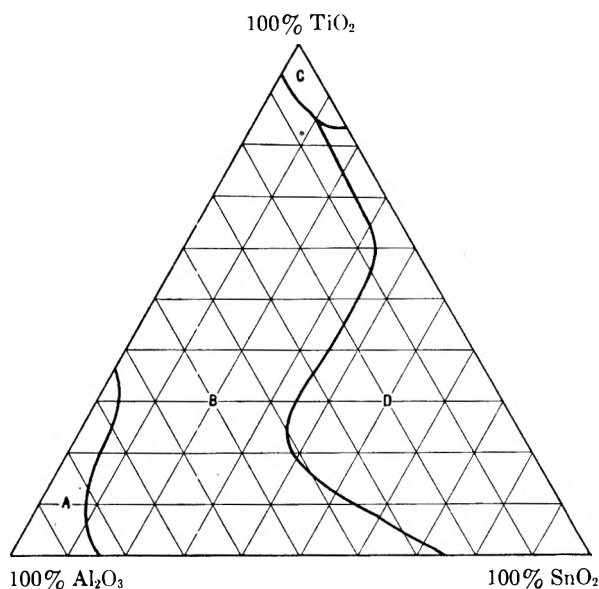


Fig. 1.—The Al_2O_3 - TiO_2 - SnO_2 system heat treated at 400° . The areas correspond to: A, γ -alumina; B, amorphous; C, anatase; D, stannic oxide-titania.

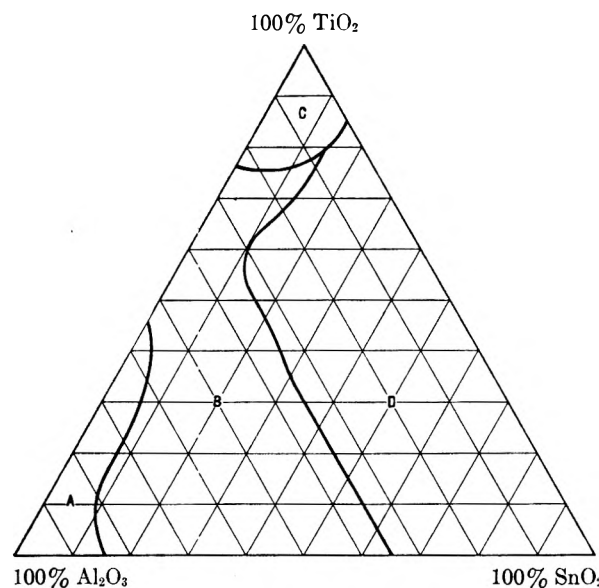


Fig. 2.—The Al_2O_3 - TiO_2 - SnO_2 system heat treated at 600° . The areas correspond to: A, γ -alumina; B, amorphous; C, anatase; D, stannic oxide-titania.

Alumina greatly inhibited the crystallization of anatase inasmuch as no bands of anatase or γ - Al_2O_3 could be detected at a composition of 90% titania and 10% alumina.

The samples corresponding to the composition illustrated in area D gave the stannic oxide pattern. It was observed that a composition of 90% stannic oxide and 10% titania had a tendency to be amorphous whereas throughout the remaining area the patterns of stannic oxide were relatively sharp. In the area corresponding to the range of composition of 10% titania and 90% stannic oxide to approximately 80% titania and 20% stannic oxide slightly shifted diffraction lines of stannic oxide were found. This indicated the possible formation of a solid solution of titania and stannic oxide. It was noted that the SnO_2 - TiO_2 system possessed

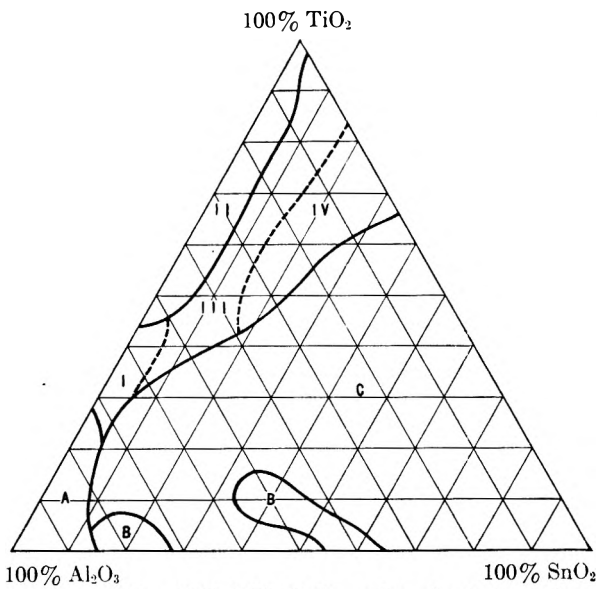


Fig. 3.—The Al_2O_3 - TiO_2 - SnO_2 system heat treated at 800° . The areas correspond to: A, γ -alumina; B, amorphous; C, stannic oxide-titania; I, γ -alumina + anatase; II, rutile + anatase; III, rutile; IV, rutile + stannic oxide.

properties similar to those of the dual oxide systems investigated by Passerini⁶ in which he reported solid solution formation. This phenomenon was further investigated and will be described below.

Heat Treatment at 600° .—It was found that area A had increased slightly on heating to 600° . The γ - Al_2O_3 patterns were sharper and no lines of stannic oxide or titania were detected superimposed in the γ - Al_2O_3 patterns.

Area B, the amorphous area, had decreased considerably with increased heating. Alumina exerted a greater influence on the crystallization of titania than it did on the crystallization of stannic oxide. Approximately equimolar amounts of stannic oxide, titania and alumina crystallized as readily as the dual oxide composition of 30% alumina and 70% stannic oxide; these results differ greatly from the results obtained from the 400° heat-treatment.

Area C corresponding to the anatase form of titania became considerably larger on increased heating at the expense of the amorphous area. In this case, the influence exerted on the crystallization of anatase by alumina was markedly different than in the 400° case. The alumina did not inhibit the crystallization of anatase appreciably until a composition of approximately 80% titania and 20% alumina was reached. The transition point between the anatase pattern and the rutile or stannic oxide pattern remained essentially unchanged on increased heating.

Area D became larger on increased heating and the same mutual protection which was observed earlier at the composition of 90% titania and 10% stannic oxide was noted. The stannic oxide pattern clearly indicated a shift in lattice constants in the composition range of 90% titania and 10% stannic oxide to 90% stannic oxide and 10% titania.

An interesting phenomenon was observed in Area D with respect to the dual oxide system Al_2O_3 - TiO_2 . When 10% alumina was added to 90%

(6) L. Passerini, *Gazz. chim. ital.*, 60, 535 (1930)

stannic oxide only weak broad bands of stannic oxide were detected; however, superimposed in the broad bands were spots which indicated the presence of larger crystals of stannic oxide. The appearance of larger crystals mixed with the smaller crystals of SnO_2 was observed throughout the range of composition of 90% stannic oxide and 10% alumina to 70% stannic oxide and 30% alumina. A further study of this phenomenon and the formation of the solid solution of $\text{TiO}_2\text{-SnO}_2$ was made after heat treatment at 800° .

Heat Treatment at 800° .—On heating to 800° , the area corresponding to γ -alumina had become smaller with the γ -alumina patterns becoming much sharper. However, γ -alumina bands were observed superimposed with rutile bands throughout the range of composition from approximately 25% titania and 75% alumina to 45% titania and 55% alumina. No mixed patterns of γ -alumina and stannic oxide were detected.

At 800° the anatase form of pure titania is transformed to the rutile form which is isomorphous with stannic oxide. In the area corresponding to rutile + anatase, mixed patterns of rutile and anatase were observed. Alumina apparently exerted enough influence on the titania to stabilize the anatase form to a greater extent than was indicated in the pure titania, even though the strongest line of anatase was present in the pure titania sample. This and the possible formation of a compound is elaborated on further in the discussion of Fig. 1.

The area corresponding to rutile can be subdivided into four areas: (I) the area corresponding to the mixed patterns of γ -alumina and rutile, (II) the area corresponding to the mixed patterns of anatase and rutile, (III) the area corresponding to the pure rutile pattern and, (IV) the area corresponding to the mixed isomorphous patterns of stannic oxide and rutile. It was noted that in area (III) the rutile form of titania was greatly favored by the presence of small amounts of stannic oxide.

The area corresponding to the samples which gave the stannic oxide pattern had greatly increased on heating and were interrupted by two small zones of composition in which the samples were essentially amorphous to X-rays. The amorphous areas and the solid solution phenomenon are discussed along with Figs. 2 and 3.

Figure 1 illustrates the dual oxide system $\text{SnO}_2\text{-TiO}_2$. The compositions 80% titania and 20% stannic oxide and 70% titania and 30% stannic oxide gave mixed patterns of stannic oxide and rutile. At compositions 60% titania and 40% stannic oxide, and 50% titania and 50% stannic oxide mutual protection was at a maximum. These patterns were broad bands corresponding to the stannic oxide pattern. Mutual protection was not observed again until a composition of 90% stannic oxide was reached.

In the range of composition from 60% titania and 40% stannic oxide to 10% titania and 90% stannic oxide solid solution was found which gave an X-ray pattern corresponding to the stannic oxide structure. Rutile and stannic oxide are isomorphous structures which crystallize in the tetragonal

system. Figure 4 represents the lattice constants plotted against the composition of the solid solution. In determining these lattice constants Cohen's⁷ method was used.

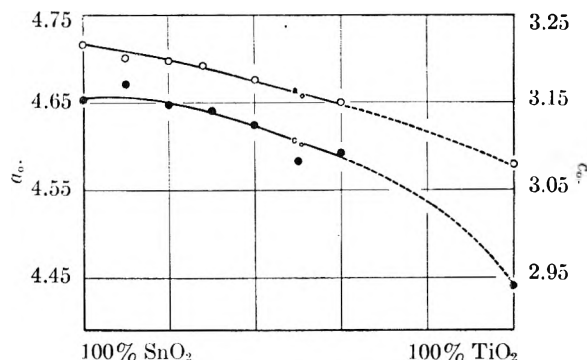


Fig. 4.—Lattice constants of rutile and stannic oxide plotted against mole per cent.

The dotted portion of Fig. 4 indicates how the curves would appear if the dual oxide system $\text{SnO}_2\text{-TiO}_2$ was completely miscible throughout its entire range of composition. However, at a composition of approximately 40% stannic oxide and 60% titania two phases appear with X-ray patterns corresponding to the ($\text{TiO}_2\text{-SnO}_2$) pattern and the pure rutile pattern.

Figure 2 illustrates the dual oxide system $\text{Al}_2\text{O}_3\text{-TiO}_2$, in which two zones of mutual protection were observed. The first zone detected was in the range of composition from 80% alumina and 20% titania to 50% alumina and 50% titania. The second zone of mutual protection was noted at the composition of 20% alumina and 80% titania.

It was observed that X-ray patterns of 40% alumina and 60% titania, and 30% alumina and 70% titania consisted of lines of rutile and anatase plus some extra lines of unknown origin. These two samples were later heated to 1400° for two hours under nitrogen. On further heating the anatase-rutile mixed pattern disappeared and no $\alpha\text{-Al}_2\text{O}_3$ lines were detected; however, a sharp pattern of the unknown compound was found which is not listed in the A.S.T.M. X-ray index file. Identification of this new phase must await further studies.

An illustration of the dual oxide system $\text{Al}_2\text{O}_3\text{-SnO}_2$ is given in Fig. 3. A study of this system was made earlier by Weiser, Milligan and Mills.² The earlier samples were prepared from inorganic salts and heated to 565° . It was noted in the samples prepared from metallic alcoholates and heated to 600° only one amorphous zone, which occurred between the approximate compositions 85% alumina and 15% stannic oxide, and 35% alumina and 65% stannic oxide, was detected. On increased heating to 800° the oxide system prepared from the alcoholates behaved very similarly to the system described by Weiser, Milligan and Mills in that two zones of maximum mutual protection were detected. One zone occurred at the composition of 40% alumina and 60% stannic oxide and the other zone occurred at a composition of 80% alumina and 20% stannic oxide.

It was noted that when the oxides were prepared

(7) M. U. Cohen, *Rev. Sci. Instruments*, 6, 68 (1935).

from their metallic alcoholates two stannic oxide crystal sizes were detected at the compositions of 10% alumina and 90% stannic oxide, 20% alumina and 80% stannic oxide, and 30% alumina and 70% stannic oxide. The sample 20% alumina and 80% stannic oxide, contained the maximum amount of the larger type crystals indicating that 20% alumina had a markedly enhancing effect on the growth of larger stannic oxide crystals. This phenomenon was not observed in the work of Weiser, Milligan and Mills.

Heat Treatment at 1000°.—A preliminary study was made on the system heated to 1000°. The results were very similar to the results obtained after the 800° heat treatment with the following exceptions: (a) the amorphous area had completely disappeared; (b) all the samples gave much sharper X-radiograms; (c) titania was completely transformed to its most stable form, rutile; (d) the zones of mutual protection previously observed at the lower temperature levels were not detectable.

The results obtained in the ternary system Al_2O_3 - SnO_2 - TiO_2 are in agreement with the general conclusions concerning the existence of multiple composition zones of mutual protection against crystallization which have been set forth in earlier papers.

DISCUSSION

ANON.—Did you make any particle size measurements in the amorphous regions?

W. O. MILLIGAN.—We made no attempt to do so. We were working with nearly 300 samples and could not study extensively each individual one. Such measurements would be of value. The question as to whether these materials are poorly crystalline or truly amorphous would

have to be considered. Some of our patterns did appear to be of the truly amorphous type.

ANON.—I am on your side! I believe you do have amorphous regions.

W. O. MILLIGAN.—I have been on both sides at different times.

ANON.—When you hydrolyzed the alcoholates did you proceed next merely to heat the wet oxide sample mixtures?

W. O. MILLIGAN.—No. The samples were washed successively with water and acetone and finally with water, and were then air-dried, prior to heat treatment at elevated temperatures.

ANON.—Did the nature of this treatment, and other factors, such as pH value, affect the location of the zones of mutual protection?

W. O. MILLIGAN.—Although such systematic studies have not been made, we would expect all such factors to influence the results.

ANON.—Is there any evidence of a relation between the zones of mutual protection and stoichiometric ratios of the oxides?

W. O. MILLIGAN.—Certainly no simple relation exists.

A. I. McCLELLAN.—Why are two amorphous zones observed in the Al_2O_3 - SnO_2 leg of the triangle and not in the other two legs?

W. O. MILLIGAN.—At 800° temperature level, two amorphous zones were found in the Al_2O_3 - SnO_2 leg, whereas in the other two legs, all of the samples were crystalline, at least in part, and two zones of mutual protection were detected, in which the degree of crystallinity was markedly decreased.

R. D. VOLD.—Did you carry out any studies of the effect of different rates of cooling on the properties of these materials?

W. O. MILLIGAN.—In our work, all such variables were held strictly constant. However studies of the type you mention would be of great interest.

SPECIFIC HEAT OF SYNTHETIC HIGH POLYMERS.

II. POLYHEXAMETHYLENE ADIPAMIDE AND SEBACAMIDE¹

By R. C. WILHOIT² AND MALCOLM DOLE

The Chemical Laboratory of Northwestern University, Evanston, Illinois

Received July 22, 1952

Data are given for the specific heat of ribbons and of undrawn and drawn filaments of 6-6 Nylon as well as of annealed 6-6 Nylon from room temperature to 280°. The results of a similar study of 6-10 Nylon in ribbon form are also included as well as data for three monomeric analogs of Nylon. No heats of transition can be detected at the temperature of the second-order transition, 47°, but a slight heat of transition of the order of 1 cal. g.⁻¹ has been observed for the crystal structure change at 165°. By estimating the heat of fusion of perfectly crystalline Nylon from the data on the monomeric analogs, it was possible to calculate the degree of crystallinity of the different forms of Nylon over the whole temperature range. The undrawn filaments were the least crystalline and the annealed Nylon the most crystalline at room temperature, but at 220°, the drawn filaments were more crystalline than annealed Nylon. The crystallinity increases from about 160 to 220° at which temperature it passes through a maximum.

Introduction

The data on two polyamides and three monomeric analogs contained in this paper represent the second contribution in a series devoted to the measurement and interpretation of specific heat data on synthetic high polymers. The first paper,³ on

polyethylene, contained in addition to the thermal measurements, calculations of the degree of crystallinity and a statistical theory of crystallite length.

Magne, Portas and Wakeham⁴ determined the average specific heat of Nylon over the temperature range -4.5 to +28.5° with an estimated average error of about 1% (actual fluctuations in several cases amounted to 3 to 5% from the mean). These authors also refer to an average value of 0.555 for the specific heat over the temperature range 20 to

(1) Presented before the twenty-sixth National Colloid Symposium which was held under the auspices of the Division of Colloid Chemistry of the American Chemical Society in Los Angeles, California, June 16-18, 1952.

(2) A. E. C. Predoctoral Fellow, 1949-1951.

(3) M. Dole, W. P. Fetting, Jr., N. Larson and J. A. Wethington, Jr., *J. Chem. Phys.*, **20**, 781 (1952).

(4) F. C. Magne, H. J. Portas and H. Wakeham, *J. Am. Chem. Soc.*, **69**, 1896 (1947).

250°. None of these results shows in detail how the specific heat changes with change of temperature. The time-temperature cooling curves of a number of polyamides were studied by Baker and Fuller⁵ but such measurements are too crude to calculate from the data the finer details of changes in the specific heat. Furthermore, super-cooling enters in to complicate any attempted interpretation of the results. It was to fill a significant gap in knowledge of the thermodynamics of Nylon that this research was undertaken.

Experimental

Materials.—The various samples of 6-6 and 6-10 nylon, polyhexamethylene adipamide and polyhexamethylene sebacamide, in the form of ribbons, undrawn and drawn filaments were kindly supplied to us by Dr. C. E. Black of the Rayon Technical Division, E. I. du Pont de Nemours and Company in 1947. The following information accompanied the samples.

6-6	Nylon, batch V-432	
	Relative viscosity, poises	25.1
	NH ₂ ends/10 ⁶ g.	24.0
	COOH ends/10 ⁶ g.	113.1
	Number av. mol. wt.	11,000
	Stabilizer	1 mole % acetic acid
6-10	Nylon, batch V-431	
	Absolute viscosity (phenol), poises	141
	NH ₂ ends/10 ⁶ g.	21.0
	COOH ends/10 ⁶ g.	159.6
	Number av. mol. wt.	9,250
	Stabilizer	1 mole % acetic acid.

6-6 Nylon undrawn filaments. Batch V-432 rapidly extruded from the melt and cooled in the order of one second. Each yarn contains 23 filaments and weight is 400 denier.

6-6 Nylon drawn filaments. The above undrawn yarn was hot-drawn. Weight of yarn produced 80 denier, tensile strength was 6.5 g. per denier and elongation at break 14.3%.

The nylon samples were used as received except for drying. They were stored in a desiccator before use and after placing in the calorimeter, the samples were evacuated for several hours before filling the void spaces of the calorimeters with helium.

Considerable difficulty was experienced with thermal decomposition of 6-6 nylon at temperatures above the melting point. Pockets of gas formed which caused the nylon to swell and to spill over into the calorimeter which after cooling and solidification produced a hard mass which led to much damage to the calorimeter in taking it apart. Annealed nylon could not, therefore, be prepared in the calorimeter. It was made by heating the 6-6 nylon in a purified nitrogen atmosphere in a glass flask until the nylon melted and then by cooling it slowly during 8 hours from 270 to 200° and during 120 hours from 200° to room temperature. After breaking the glass, the nylon was removed from the flask and broken up into lumps for insertion into the trays of the calorimeter.

Three monomeric analogs of the polyamides N,N'-di-*n*-hexyladipamide, N,N'-di-*n*-hexylsebacamide and N,N'-di-*n*-propyladipamide, were also studied in the hope of obtaining information on the specific heat and heat of fusion of the 100% crystalline polymer. The first two monomers were kindly made for us by Dr. J. G. VanOot of the Carothers Research Laboratory, E. I. du Pont de Nemours and Company while the third was synthesized by us by first preparing adipyl chloride from adipic acid and thionyl chloride, then making the propylamine hydrochloride and finally converting to the amine by treatment with potassium hydroxide. We are indebted to Professor C. D. Hurd for suggesting the use of this compound as an analog and for preparative details. The product was recrystallized from a solvent containing 80% and 20% alcohol, maximum melting point 178.5°, melting range 173-179°. The maximum

melting points and melting ranges of the N,N'-di-*n*-hexyladipamide and sebacamide were, respectively, 159°, 145-159° and 142°, 115-142°. These melting ranges were estimated from plots of the enthalpy as a function of temperature; the visual melting ranges were only about two degrees.

Measurement of the Specific Heat.—The apparatus used for the measurements has been described in detail elsewhere,⁶ but modifications in operating procedures had to be introduced because of the higher temperatures required for the nylon measurements as compared to those on polythene. A very careful and detailed study was made of the temperature distribution about the inner surface of the adiabatic jacket and methods and equations developed for keeping heat exchange to a minimum and calculating thermal losses. We shall not describe these methods *in extenso* as we are now in the process of building a new and more symmetrically designed calorimeter and adiabatic jacket in which temperature inequalities during the heating should be considerably reduced. It is sufficient to say that every attempt was made to adjust the temperature controls, the heating currents and the air-cooling rates, to values such that heat transfer was reduced to a minimum. More thermocouple systems were installed so that a record could be made of temperature differences between the center of one side, the center of the bottom, the edge of the top of the adiabatic jacket and the center of the bottom of the calorimeter. Corrections due to heat transfer between these points were applied to the data, as well as the corrections described in our previous papers.⁶ The total corrections in any one specific heat measurement amounted to about 1-2% of the heat added on the average. Table I gives a list of the average fluctuations of the specific heat data from a smooth curve.

TABLE I

AVERAGE DEVIATION OF THE OBSERVED SPECIFIC HEAT DATA FROM SMOOTH CURVES, CAL. G.⁻¹

6-6 Nylon annealed	0.002
6-6 Nylon drawn	.004
6-6 Nylon ribbon	.004
6-6 Nylon undrawn filament	.009
6-10 Nylon ribbon	.004
N,N'-Di- <i>n</i> -hexyladipamide	.001 ₇
N,N'-Di- <i>n</i> -hexylsebacamide	.001 ₂
N,N'-Di- <i>n</i> -propyladipamide	.003 ₆

In the case of the crystalline monomers which exhibit no peculiarities in their thermal behavior and which melt at lower temperatures than the polymers, the fluctuations are less. It is apparent that some of the observed deviations result from the non-crystalline and fluctuating properties of the polymers themselves. Although we are currently attempting to improve our experimental accuracy by the construction of a new calorimeter and adiabatic jacket, it would appear that the very nature of the polymer is such that a limit to the significant accuracy of the work will soon be reached—unless, of course, the study of the fluctuations becomes important.

Experimental Results

There are three temperature regions of especial interest in the case of 6-6 nylon, 40-50° where at 47 to 49° nylon is said to pass through a second-order transition point,⁷ in the neighborhood of 165° where the crystal structure of nylon changes from triclinic to a pseudohexagonal close packed system and the region of the melting point, 263°. Specific heats of 6-6 nylon in the form of ribbons, undrawn filaments, drawn filaments and of annealed nylon

(6)(a) M. Dole, W. P. Hettinger, Jr., N. R. Larson, J. A. Wethington, Jr., and A. E. Worthington, *Rev. Sci. Instruments*, **22**, 812 (1951); (b) M. Dole, N. R. Larson, J. A. Wethington, Jr., and R. C. Wilhoit, *ibid.*, **22**, 818 (1951).

(7) R. F. Boyer and R. S. Spencer, *J. Applied Phys.*, **15**, 398 (1944). "Advances in Colloid Science," Vol. II, Interscience Publishers, Inc., New York, N. Y., 1946, p. 1.

(5) W. O. Baker and C. S. Fuller, *Ind. Eng. Chem.*, **38**, 272 (1946).

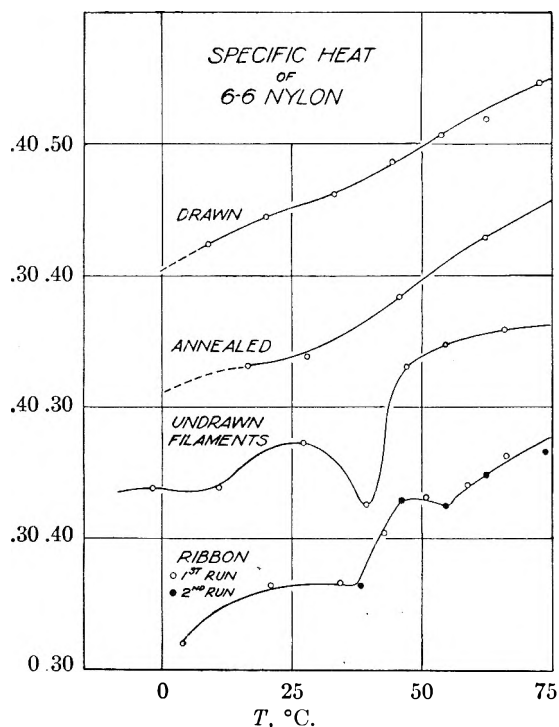


Fig. 1.—Specific heat of polyhexamethylenedipamide.

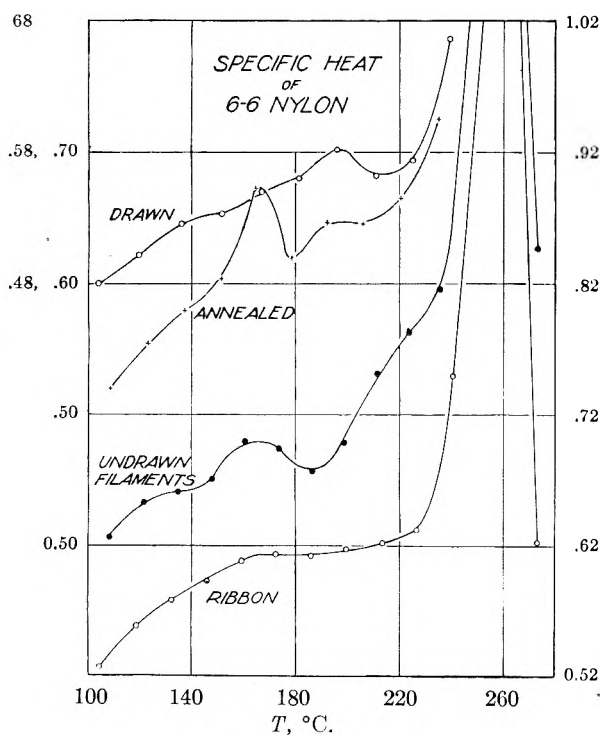


Fig. 2.—Specific heat of polyhexamethylenedipamide.

in these three temperature ranges are illustrated in Figs. 1, 2 and 3. As the curves for the drawn and annealed nylon are the most regular and as these are the two most interesting forms of nylon, specific heat values for the drawn and annealed nylon at rounded-off values of the temperature are given in Table II. Data for 6-10 nylon ribbon are also included as this was the only form of 6-10 nylon studied.

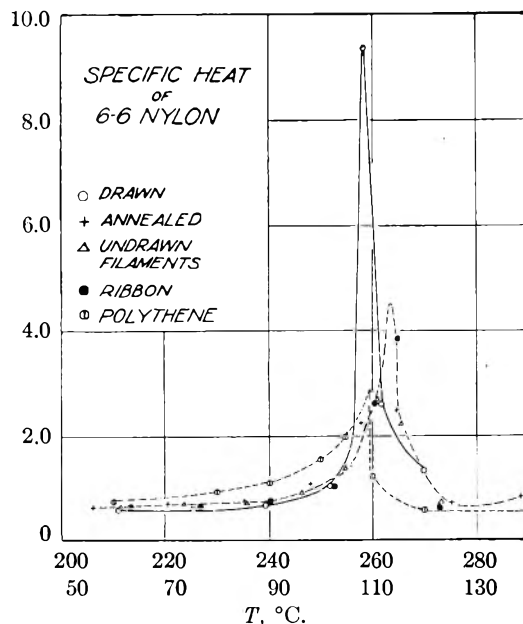


Fig. 3.—Specific heat of polyhexamethylenedipamide.

TABLE II
SMOOTHED VALUES OF THE SPECIFIC HEAT OF ANNEALED
AND DRAWN 6-6 NYLON AND 6-10 NYLON RIBBONS

Temp., °C.	6-6 Nylon		6-10 Nylon ribbons
	Annealed	Drawn	
0	0.311	0.302	0.327
20	.333	.345	.373
40	.367	.376	.420
60	.424	.420	.486
80	.468	.458	.512
100	.505	.479	.518
120	.548	.503	.531
140	.583 ₆	.528	.561
160	.642	.542	.592
180	.620	.560	.588
200	.646	.582	.686
220	.664	.567	1.95
240	.80	.676	0.737
250	1.13	1.55	.639
260	2.75	6.5	.627
270	1.30	1.35	.632
280	0.75	0.75	.639

Table III includes smoothed specific heat values for three monomeric analogs of 6-6 and 6-10 nylon as well as the heats of fusion of each of these substances as determined from an enthalpy plot.

Interpretation of the Data

Heats of Transition.—Possibly the most interesting question which comes to mind with respect to the thermal behavior of nylon is, can a latent heat or heat of transition at 47 or 165° be observed? In Fig. 4 we have plotted the enthalpy of the four forms of nylon for both of these temperatures. It readily can be seen that no break in the enthalpy corresponding to a latent heat exists at 47°. On the contrary, in the case of the undrawn filaments, the break, if any does occur, seems to be in the negative direction; that is, if the enthalpy below 40° is extrapolated to temperatures above 40°, the extrapolated values lie slightly above the enthalpy

TABLE III
SPECIFIC HEATS AND HEAT OF FUSION OF MONOMERIC
ANALOGS OF NYLON
Specific heats, cal. g.⁻¹ T⁻¹

Temp., °C.	N,N'-n- Hexyl- adipamide	N,N'-n- Hexyl- sebacamide	N,N'-n- Propyl- adipamide
60		0.69	
80		.596	
100	0.493	.524	
120	.523	.634	0.490
130	.542	.812	.501
140	.610	Melting	.505
150	.79	0.68	.504
160	Melting	.641	.511
170	0.658	.646	.63
180	.640	.652	Melting
190	.642	.657	0.642
200	.642	.663	.656
210	.642	.669	.657
Heats of fusion, cal. g. ⁻¹			
	31.2	34.8	37.8
Max. m.p., °C.	159	142	179

observed, but by less than 1 cal. g.⁻¹. The undrawn filaments were cooled more rapidly from the melt than any of the other forms and contain in all probability a greater fraction of amorphous nylon. Langkammerer and Catlin⁸ in their study of spherulite formation in 6-6 nylon demonstrated that transparent filaments of nylon containing no spherulites could be formed by rapidly quenching molten nylon. They could detect no formation of spherulites by annealing in the solid phase. However, there is no evidence that formation of spherulites influences the specific heat, the lack of spherulites suggests only that such nylon would probably be less crystalline than nylon containing spherulites. If a very small fraction of the amorphous content of the undrawn filaments, say 1 to 2%, should crystallize in the neighborhood of 40°, the enthalpy above 40° would be less by the latent heat of crystallization of this amount of the nylon. Fuller, Baker and Pape⁹ made a comprehensive study of the effect of heat treatment on 6-6 and 6-10 nylon, using X-ray diffraction measurements and observing changes in Young's modulus and shrinkage in length as indications of the structural changes occurring during the heat treatment. In brief they found that the crystallinity of the solid polymer depended most critically on the rate of cooling from the melt and to a lesser extent on annealing at 200° after solidification at a lower temperature. A sample of 6-10 nylon, about 0.5 mm. thick, quenched at 20° on a metal plate did not crystallize on annealing at 200° to the same extent as a sample originally cooled slowly to 200° (over about 40 minutes) from the melt. Some crystallization did

(8) C. M. Langkammerer and W. E. Catlin, *J. Polymer Sci.*, **3**, 305 (1948).

(9) C. S. Fuller, W. O. Baker and N. R. Pape, *J. Am. Chem. Soc.*, **62**, 3275 (1940).

occur, however, on annealing at 200°. Unfortunately, no quantitative estimates of the extent of crystallinity were given by Fuller, Baker and Pape. Other studies of the effect of temperature on polyamides are those of Clark, Mueller and Stott¹⁰ who studied nylon in bulk form; Brill¹¹ who discovered the crystal structure change of nylon at 165° and the effect of water vapor on promoting crystallization at 100°; Hess and Kiessig¹² who studied the change with temperature of the long period in nylon; and Wallner¹³ who discussed methods of determining crystallite dimensions from the X-ray data.

Turning now to the enthalpy effects in the neighborhood of 165°, it can be seen that a slight latent heat probably does exist here, particularly in the case of annealed nylon, but the latent heat is extremely small, of the order of 1 cal. g.⁻¹, or about one-thirtieth of the heat of fusion actually observed over the melting range. It is uncertain from the specific heat data whether a transition has occurred in the case of the drawn nylon; there is a maximum at 195° and a dip in the curve at 210° but this may be due to crystallization occurring during the measurement.¹⁴ Transition heat effects in un-

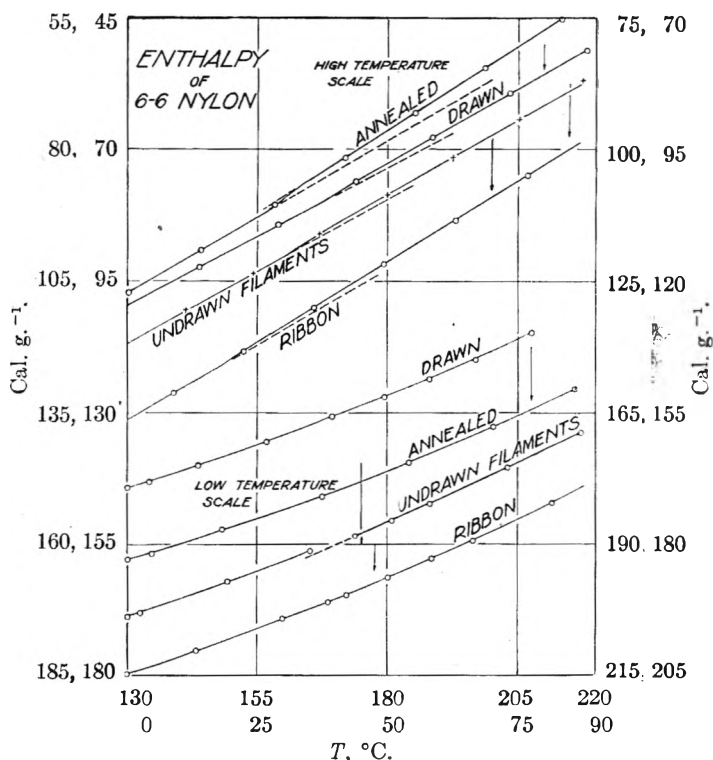


Fig. 4.—Enthalpy of polyhexamethylenadipamide. The lower set of four curves covers the temperature range 0 to 90°; the upper set 130 to 220°. The numbers on the ordinates give the enthalpy values for the different curves; the arrows between curves show how much the scale is changed. The scale for the undrawn filaments should have 4.2 cal. g.⁻¹ added to it.

drawn and ribbon nylon are barely perceptible;

(10) G. L. Clark, M. H. Mueller and L. L. Stott, *Ind. Eng. Chem.*, **42**, 831 (1950).

(11) R. Brill, *J. prakt. Chem.*, **161**, 49 (1942).

(12) K. Hess and H. Kiessig, *Z. physik. Chem.*, **193A**, 196 (1944).

(13) L. G. Wallner, *Monatsh.*, **79**, 86 (1948).

(14) According to unpublished studies of Dr. C. E. Black of the du Pont Company, no transition in nylon has been detected above a temperature of 165°.

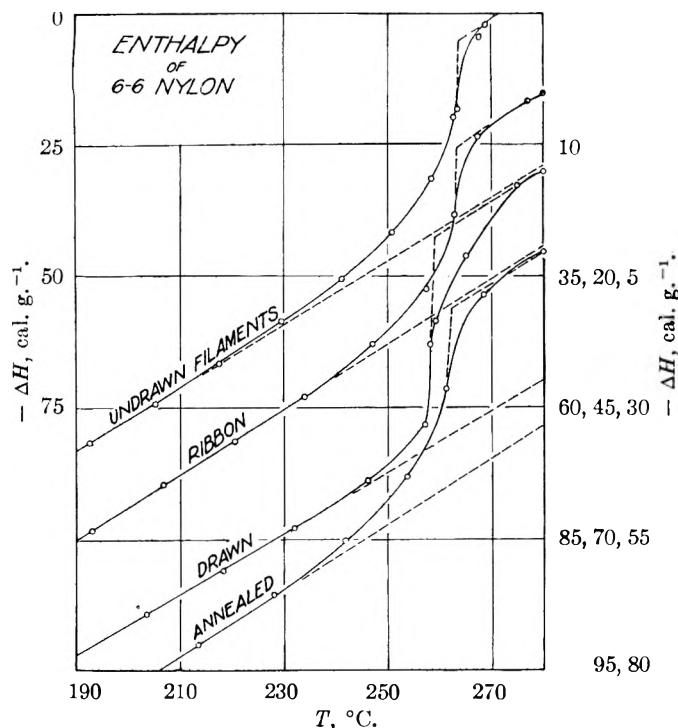


Fig. 5.—Enthalpy of polyhexamethylenedipamide. The scale for the undrawn filaments should be increased by 4.2 cal. g.⁻¹; otherwise the scales for all curves have been displaced by an equal amount between curves.

in fact, from Fig. 2 only a break at 165° can be seen in the specific heat curve of ribbon nylon in contrast to the curves for the other forms which all suggest a latent heat of transition at or near 165°. The specific heat data for 6-10 nylon indicate a possible transition at or near 165°. This is in agreement with X-ray evidence.¹⁵

The conclusion to be reached from a study of Fig. 4 is that the enthalpy of crystalline nylon is largely independent of the crystal form. Our data do not, of course, allow us to compare the enthalpy of the α and β forms of nylon discovered by Bunn and Garner¹⁶ because we do not have available pure samples of these forms for study. Bunn and Garner state that the β -form is usually present in very small percentage.

Melting Behavior of Nylon.—With respect to the phenomena associated with the melting of nylon, it would appear that as slightly suggested by the data on polythene, the drawing of nylon produces a greater degree of crystallinity as compared to the annealed in the neighborhood of the melting point. This seems to be clear from the greater rise in the enthalpy of the drawn nylon at the melting point than the rise of any of the other forms of nylon, Fig. 5. In Fig. 5 the zero of the enthalpy is taken at 280° and each zero is displaced downward to the same extent from the curve above it for the different samples studied except for the undrawn filament whose zero is 4.26 cal. g.⁻¹ above the top axis. The estimated enthalpy increase on melting, as well as estimates of the melting point (defined as the temperature where the specific heat passes

through a maximum) and of the melting range are given in Table IV.

The shapes of the specific heat and enthalpy curves are such as to suggest that in the case of drawn 6-6 nylon and 6-10 nylon (ribbon form) part of the nylon if not all of it melts and then perhaps recrystallizes and melts again, or that a considerable fraction melts at one temperature and a significant fraction at a higher temperature. The width of the specific heat curve at half the estimated maximum in the specific heat is 31° in the case of 6-10 nylon, 11° for the annealed 6-6 nylon and 4° for drawn nylon as compared to 20° for polythene. Although the half width for drawn nylon indicates a relatively sharp melting point, the base of the hump of the specific heat curve unexpectedly broadens out, suggesting either the phenomenon of recrystallization mentioned above, or the possibility that there are some crystallites that melt slightly above the point at which most of the drawn material melts. Evans, Mighton and Flory¹⁷ describe some experiments on decamethylene sebacate in which crystals formed by rapidly cooling the melt to 55° melted at 75° despite the fact that 75° is about 5° below the maximum melting temperature. The 70:30 copolyester of decamethylene adipate with decamethylene isophthalate seemed to recrystallize between 56 and 60° as judged from a

decrease in specific volume with rise of temperature in this range.

TABLE IV
HEATS REQUIRED FOR FUSION, MELTING POINTS AND MELTING RANGES OF 6-6 AND 6-10 NYLON

	6-6 Nylon			An- nealed	6-10 Nylon ribbon
	Ribbon	Undrawn fila- ments	Drawn fila- ments		
M.p., °C.	263	264	259	262	225?
Melting range, °C.	25	40	18	30	30-40
Half width melt- ing range, °C.	7	12	4	11	31
H_f , cal. g. ⁻¹	29.0		39.5	33.3	26.3

On the basis of modern theories of crystallization in linear high polymers¹⁸ we should expect the specific heat to rise smoothly to a maximum and then to drop sharply at the temperatures above which the longest crystallites in the solid melt. Such a behavior is exhibited by polythene, all forms of 6-6 nylon, except the drawn form, but not by 6-10 nylon. In fact, the specific heat curve of this last substance seems to "tail off" toward temperatures above the melting point rather than toward temperatures below it.

The Crystallinity of Nylon.—To calculate the fraction of crystallinity in the different forms of nylon by the methods used for polythene it is necessary to know the heat of fusion of perfectly crystalline nylon as well as the enthalpy of amorphous nylon below the melting point. Because of

(15) Unpublished observation of Dr. C. E. Black.

(16) C. W. Bunn and E. V. Garner, *Proc. Roy. Soc. (London)*, **189A**, 39 (1947).

(17) R. D. Evans, H. R. Mighton and P. J. Flory, *J. Am. Chem. Soc.*, **72**, 2018 (1950).

(18) These theories are reviewed in paper I of this series.

the vast amount of research done on hydrocarbons, it was possible to estimate rather accurately the expected heat of fusion of perfectly crystalline polythene by extrapolating to large molecular weights the known heats of fusion of the crystalline lower molecular weight hydrocarbons. However, in the case of nylon there are no similar data. As a start on the task of adding to our knowledge along this line we have measured the heats of fusion of three monomeric analogs of nylon given in Table III. We need to know in addition to the values of Table III the heats of fusion of crystalline compounds containing two and more of the nylon repeating units so that an extrapolation of the heat of fusion per gram could be made to infinite molecular weight.

Another difficulty in applying the data of Table III results from the large difference of temperature between the melting points of the monomers and nylon, an extrapolation of nearly 100° being required to make use of the monomeric heats of fusion in estimating the crystallinity of nylon. If the specific heats of liquid and crystalline nylon were known accurately, the variation of the heat of fusion of crystalline nylon with temperature could be calculated, but we can only estimate the specific heat of liquid nylon because of the difficulties of making accurate specific heat measurements at high temperatures (300°) and because of the decomposition of 6-6 nylon in the molten state; furthermore, there is no direct method of determining the specific heat of crystalline nylon.

A third uncertainty in the determination of the fraction of crystallinity involves our ignorance concerning the crystal structure of the monomeric analogs of nylon. Presumably they should have the same crystal structure as the crystalline polymers if these heats of fusion are to be used in the estimation of the heat of fusion of nylon. The fact that the heat of transition at 165° for 6-6 nylon is small suggests that the heats of fusion may not change appreciably with change of structure, at least if the structural changes are no more pronounced than they are for 6-6 nylon at 165°.

As a consequence of the difficulties and uncertainties listed above, only the roughest estimates of the crystallinity of the different forms of nylon can be made.

Qualitatively, from a study of the enthalpy curves it would appear that annealed nylon is more crystalline than drawn over the temperature range 0-165° but less crystalline above this range. Such an effect was suggested by the measurements on polythene but the difference between the drawn and the annealed forms is much more marked in the case of nylon. The undrawn filaments are the least crystalline at room temperature as would be expected from the rapid rate at which they were quenched from the melt.

Black and Dole¹⁹ could detect no difference between the density of drawn and undrawn fibers after annealing to temperatures above 200°. It would be interesting to have density measurements of the different forms of nylon at 220°, the temperature of maximum crystallinity.

For a rough quantitative estimate of the crystal-

linity we shall make the following assumptions: First, that the specific heat of liquid nylon has a temperature coefficient equal to that of the monomeric analog, N,N'-di-*n*-hexylsebacamide and a specific heat of 0.71 at 275°. This yields the equation for the specific heat

$$C_p(\text{liquid}) = 0.71 + 0.0006(T - 275^\circ) \quad (1)$$

where T is in degrees centigrade. From Table III it will be noted that the three liquid monomeric analogs of nylon all have about the same specific heat. Equation (1) yields specific heat values slightly lower than those adopted for liquid polythene.

Second, that the heat of fusion of crystalline 6-6 nylon is given by equation (2) where 43 is the heat

$$H_f = 43 + 0.07(T - 179^\circ) \quad (2)$$

of fusion of N,N'-di-*n*-propyladipamide corrected for the end effect and T is in degrees centigrade.

From a study of the heats of fusion of straight chain hydrocarbons it was found that the methyl groups on the two ends of the chain contributed -2.5 kcal./mole to the heat of fusion; this result was obtained by extrapolating the curve of the molal heat of fusion as a function of the number of carbon atoms in the chain back to zero number of carbon atoms. The molal heat of fusion of N,N'-di-*n*-propyladipamide is 8.6 kcal.; adding 2.5 we obtain 11.1 kcal. which divided by the molecular weight of the adipamide gives 48.6 cal./g. There is the possibility that the end effect would not be as pronounced in the case of the adipamide as in the case of the straight chain hydrocarbons; hence we have decided to adopt a value for the heat of fusion of the adipamide intermediate between the observed value and that corrected completely for the end effect.

Evans, Mighton and Flory¹⁷ calculated the heat of fusion of 6-10 nylon from the slope of the linear plot of the reciprocal of the absolute temperature of melting *versus* the mole fraction of the 6-10 nylon in various copolymers of this substance; the equation is

$$\frac{1}{T_m} - \frac{1}{T_m^0} = -\frac{R}{h_u} \ln X_A \quad (3)$$

where T_m^0 and T_m are the melting temperatures of pure polymer and copolymer, respectively. X_A is the mole fraction of the unit capable of crystallizing, the 6-10 nylon in the samples studied, and h_u is the heat of fusion per repeating unit. They found 25.9 cal./g., a result obviously too low as judged from our observations (we found 26.3 cal./g., for the heat of fusion of the partially crystalline 6-10 ribbon). In the case of polyesters, Evans, Mighton and Flory obtained much higher heats of fusion calculated from the equations

$$\frac{1}{T_m} - \frac{1}{T_m^0} = -\frac{2R}{h_u z_n} \quad (4)$$

and

$$\frac{1}{T_m} - \frac{1}{T_m^0} = \frac{R}{h_u} \left[\left(\frac{z}{z_n} \right) (1 - v_2) - \mu (1 - v_2)^2 \right] \quad (5)$$

than from eq. (3). Equation (4) expresses the lowering of the melting point as a function of the number average of the number of repeating units per molecule while eq. (5) gives the lowering of the

melting point as the result of dilution with a monomeric substance of volume fraction v_1 . In eq. (5) z/z_s is the ratio of the molar volumes of the repeating unit and diluent and μ is the energy of mixing parameter. Our data for the heats of fusion of the monomeric analogs of nylon suggest that the heats of fusion calculated from eqs. (4) and (5) are more valid than those from eq. (3).

The temperature coefficient of the heat of fusion was estimated by adopting the values 0.65 and 0.57 for the specific heat of liquid and solid N,N'-di-*n*-propyladipamide at 179°. The specific heat of the solid, crystalline nylon is possibly of the order

$$C_p(\text{solid}) = 0.31 + 0.0020(T - 0^\circ) \quad (6)$$

The validity of eq. (1), (2) and (6) undoubtedly diminishes the greater the difference between T and the constant temperature of the equation. In fact, if eq. (1) is integrated between 280 and 0° the change in enthalpy is 176 cal. g.⁻¹, about the value actually observed for the different forms of nylon. Hence, if eq. (1) were used in the crystallinity calculations, unreasonably low values of the crystallinity would be obtained. Nevertheless, it was a help in mapping out the enthalpy curve for amorphous nylon in the neighborhood of the melting point.

From the enthalpy change of annealed nylon due to melting given in Table IV and from the heat of fusion at 263° calculated by eq. (2) we estimate that annealed nylon has a crystallinity of about 70% at 220°. If we make the assumption that the percentage crystallinity of annealed nylon does not change with temperature below 220°, then the equation for the enthalpy of the amorphous nylon, H_L , becomes

$$H_L = 0.7H_t + H_{\text{annealed}} \quad (7)$$

Similarly, the equation for the enthalpy of the completely crystalline nylon, H_c , would be

$$H_c = H_L - H_t \quad (8)$$

The crystallinity of the other forms of nylon can

now be calculated up to 220° from the expression (θ is the fraction of amorphous nylon present).

$$100(1 - \theta) = 100 \times \frac{H_L - H_{\text{sample}}}{H_t} \quad (9)$$

or

$$100(1 - \theta) = 100 \left\{ 0.7 + \frac{H_{\text{annealed}} - H_{\text{sample}}}{H_t} \right\} \quad (10)$$

Equation (9) is a general expression for the percentage of crystallinity; eq. (10) is restricted to the special conditions assumed. Above 220°, the liquid enthalpy of 6-6 nylon can be extrapolated below the melting point using the integrated form of eq. (1) and taking the enthalpy of all the nylon samples to be -12 cal. g.⁻¹ at 263° as compared to zero at 280°. Equation (9) can then be used directly.

The results of the crystallinity calculations based on these assumptions are shown in Fig. 6. It is interesting to note that the percentage of crystallinity of the different samples of 6-6 nylon does not change much beyond a few percentage units, which are probably within the experimental error, up to about 160°. At this point the crystallinity of all the forms of 6-6 nylon begins to increase with temperature as compared to the annealed nylon. This is reasonable, inasmuch as Fuller, Baker and Pape⁹ demonstrated by X-ray studies that rapidly quenched polyamides partially crystallized when annealed at 200°. This was true of the specimens oriented by cold drawing as well as of the unoriented specimens. All forms of nylon begin to melt as the temperature is raised above 220°; in other words this temperature seems to yield the maximum percentage of crystallinity.

At this point it is interesting to point out that in contrast to polythene whose drawn fibers had a slightly greater density but smaller crystallinity than the annealed material, the density of drawn nylon fibers before annealing is less than the density of annealed undrawn filaments if the data obtained by Black and Dole¹⁹ can be assumed to be valid for the samples studied in this research. In other words, the density and crystallinity both increase in the order, undrawn filaments, drawn filaments, annealed nylon.

The increase in crystallinity of the drawn material with temperature finds possible confirmation in the work of Hess and Kiessig,¹² who estimated from their X-ray data that the long period, the presumed length of the crystallites, increased from 74 to 85 Å. on heating from 20 to 220°. However, the long period for undrawn filaments was greater than for the drawn according to Hess and Kiessig despite the smaller degree of crystallinity. As was found in the case of polythene, conclusions regarding changes in the crystallinity as deduced from X-ray measurements do not always agree with conclusions derived from the thermal studies.

Turning now to the 6-10 nylon ribbon, we can estimate rather crudely its crystallinity by adopting the following equation for the enthalpy of liquid 6-10 nylon and by assuming that the heat of fusion of perfectly crystalline 6-10 nylon is 3.6 cal. g.⁻¹ greater than that of 6-6 nylon (the heat of fusion of the dihexylsebacamide was 3.6 cal. g.⁻¹

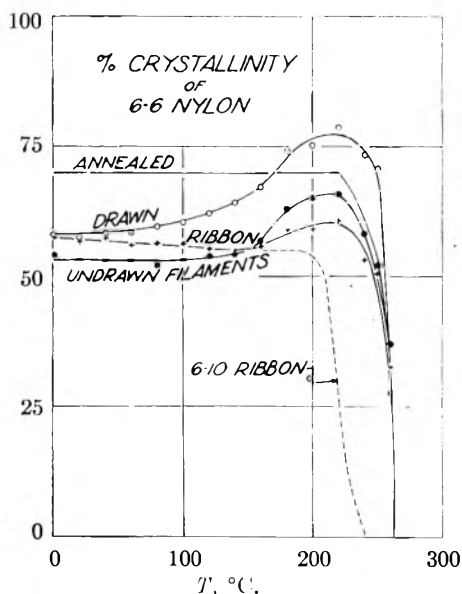


Fig. 6.—Crystallinity estimates for polyhexamethyleneadipamide (four forms) and sebaccamide (ribbon form) as a function of temperature.

greater than that of the dihexyladipamide).

$$H_L = -176 + 0.629T \quad (11)$$

Equation (11) was estimated from a plot of the enthalpy of 6-10 nylon as a function of temperature; as we would expect H_L to be a quadratic function of T , it is obvious that (11) cannot be valid much below the melting point. Crystallinity calculations based on these assumptions are shown in Fig. 6. The value of 54% at 200° may be assumed to be approximately the crystallinity at room temperature by analogy with the 6-6 nylon ribbon whose crystallinity did not change much between 200° and room temperature. Hermans and Weidinger²⁰ estimated the per cent. crystallinity of quenched and annealed 6-10 nylon from X-ray intensity measurements and found 50 and 60%, respectively. These estimates agree approximately with that of ours.

Acknowledgments.—Grateful acknowledgment is made of funds donated for this research from the Rayon Technical Division of E. I. du Pont de Nemours and Company, the Visking Corporation of Chicago and the Research Corporation (Frederick Gardner Cottrell Grant). We are particularly indebted to Dr. C. E. Black of the du Pont Company for helpful cooperation.

DISCUSSION

M. J. VOLD.—My question relates to how degree of crystallinity is best defined. Your definition appears to be an experimental one, in terms of heat contents. Do you think it can be interpreted as showing the existence of regions in which only a very small number of molecules or segments are regularly aligned and how extensive must such regions be to show up?

MALCOLM DOLE.—I think that in our thermal method we measure all degrees of order either a few molecules or hundreds of molecules crystallized together. To answer your question as to how we should define crystallinity, I believe that the best definition is in terms of the structural entropy of the material as compared with the entropy of

(20) P. H. Hermans and A. Weidinger, *J. Polymer Sci.*, **4**, 709 (1947).

a perfect crystal. However, I know of no way of calculating the structural entropy. But from the theoretical standpoint this is the soundest definition of crystallinity.

R. B. DEAN.—It seems to me that heat measurements could conceivably lead to negative crystallinity; for example with a high polymer with lots of holes in it and with less than the number of contacts that a liquid has.

MALCOLM DOLE.—I suppose that if we made some measurements in the liquid range and then extrapolated those measurements down below the melting point and if these extrapolated enthalpy values were below the actually measured ones, we would get a negative crystallinity. But, I have never heard of such a system, which would, in fact, approach that of a gas.

R. D. VOLD.—May you not get into a semantic difficulty with crystallinity itself, if the thermal measurements measure short range order as well as long range order, and if crystallinity is defined by the X-ray method in terms of a longer range extension of ordered regions in space? The X-ray definition is not the same as the thermal definition.

MALCOLM DOLE.—It can be called "crystallinity as measured by the thermal method!" As I have already mentioned, the best definition is that in terms of structural entropy. This definition will take into account all degrees of order.

S. W. BENSON.—Another trouble with the definition is that you might have strains locked into the liquid or disorganized solid, with no crystals present. This effect would show up in thermal measurements as some kind of crystallinity.

MALCOLM DOLE.—When you have a long chain polymer whose segments are randomly disposed and partial crystallization occurs, the amorphous regions in between the crystalline regions are constricted or strained. In our thermal measurements, on the complete melting of the polymer, the "heat of relaxation" of this strain shows up in our results.

ANON.—Has not a good bit of work of this kind also been done on the study of metals?

MALCOLM DOLE.—Many specific heat measurements have been made on metals and alloys but I do not feel qualified to comment on them.

ANON.—Ordinarily we consider a copper wire to be crystalline. I wonder if by your thermal method some of the copper may not be amorphous?

MALCOLM DOLE.—This question could be answered by measuring the specific heat of a single crystal of copper and comparing such data with data obtained on polycrystalline copper.

X-RAY STUDIES OF CRYSTALLINE AND AMORPHOUS ORDER IN HIGH POLYMERS¹

By SAMUEL KRIMM²

Textile Research Institute and Frick Chemical Laboratory, Princeton University, Princeton, N. J.

Received July 22, 1952

A Geiger counter X-ray spectrometer has been applied to the study of problems associated with the order in crystalline and amorphous polymers. Two investigations are dealt with, the study of the percentage of crystallinity in polyethylene as a function of temperature and stress, and the changes in the scattering pattern of polystyrene as a function of temperature. In connection with the first of these problems, the method which was developed to determine crystallinity is discussed and the results of the determination in unstressed polyethylene of crystallinity as a function of temperature are compared with those obtained by other methods. The crystallinity and orientation studies on stressed polyethylene are discussed in terms of previous stress-birefringence results. The study of the scattering from polystyrene as a function of temperature has revealed a change in the pattern in the vicinity of the second-order transition temperature. It is shown that this can be interpreted in terms of changes in configuration of the polymeric chains, and the bearing of these results on the nature of the glass transition is discussed.

Introduction

The study of polymer structure by means of X-ray diffraction methods has furnished much information about the arrangements of atoms and molecules in these materials. In addition to straightforward structure determination, however, the X-ray method can be utilized to investigate various problems concerned with the over-all type and degree of order present in these materials. This paper is concerned with two such problems: (a) the determination of the degree of crystallinity in polyethylene as a function of temperature and stress, and (b) the changes in the scattering pattern of polystyrene as a function of temperature.

In the usual experimental technique, the recording of the diffraction pattern on a photographic film is adequate for a structure determination. In the present case, however, a more accurate measure of the diffracted intensities was necessary than could be attained with the photographic film and for this purpose a Geiger counter spectrometer was devised to detect the diffracted radiation.³ A brief description follows of the spectrometer and pertinent techniques used.

Experimental

Copper radiation, monochromatized by reflection from a pentaerythritol crystal, was used to obtain the diffraction patterns. In order to permit more accurate compensation for variations in the X-ray tube output than was possible with the regulated voltage input, the beam issuing from the opposite port of the X-ray tube was monitored with a second pentaerythritol crystal and another Geiger counter. By using the ratio of diffracted beam count to monitor count, intensity fluctuations were effectively kept down to 0.5 to 1.0%. Collimation of the beam was accomplished by Soller slits in front of the sample and the scanning Geiger counter, these slits permitting larger specimen areas to be irradiated and thus increasing the intensity of the diffracted beam. As a result of the geometry of the slit system, the angular width of radiation intercepted by the Geiger counter was 0.15°; the diffracted line width at half maximum intensity for the crystalline materials studied was about 0.80°. Between the first Soller slit and the sample, provision was made for the accurate insertion into the beam of a set of nickel filters and a fine pinhole collimator. These were used to get a measure of the incident beam intensity and of absorption by the sample. This X-ray method for deter-

mining thickness from absorption was shown to be accurate to within 1%.

The sample was mounted inside a temperature-controlled oven (controlled to within about $\pm 0.5^\circ$) on an orientation jig of such design that the sample could be elongated as well as rotated in a plane perpendicular to the incident X-ray beam from outside the oven. This enabled determination of the density distribution around the Debye-Scherrer diffraction rings and hence provided a measure of crystallite orientation. The scanning counter was mounted so that it could be moved in a horizontal plane along a graduated circle, the axis of rotation being the sample position. This circle was calibrated by means of the strong diffraction lines of a number of standard materials, the calibration indicating that the circle readings were accurate to within the error in setting the Geiger counter on the circle, which was $\pm 0.05^\circ$. The outputs of the scanning and monitoring counters were each fed into a commercial decimal scaling unit. A relay circuit and electrical timer permitted both scalars to be started and stopped simultaneously. The counting period used at each circle setting was 1 minute.

The readings thus obtained were corrected in the following way before being used to plot the diffraction curve. After correction for the normal background count of the Geiger tubes, the diffraction reading was divided by that of the monitor. This result was divided by the corresponding ratio for the pinhole-collimated transmitted beam, thus giving a ratio proportional to that of the diffracted beam to the transmitted beam. From this value the air scattering was subtracted, since it had been related to the same transmitted beam intensity. The values thus obtained were then corrected for relative absorption by the sample and by the exit cellophane window on the oven, which included correction for coincidence losses due to relatively high counting rates on the transmitted beam. Correction was also made for polarization of the beam by the monochromatizing crystal and by the sample, as well as for incoherent scattering.⁴ These results represent the corrected diffraction readings used, $I_{2\theta}/I_{2\theta=0}$, and were plotted to give the diffraction curve.

In cases where different masses of a given material were in the same X-ray beam and it was desired to base the resulting diffraction curves on the same scattering mass, the above diffraction readings were corrected by means of the ratio of ρt values of the samples, determined from the X-ray absorption measurements made at the beginning and end of each run (ρ is the density and t the thickness of the sample, the product being determined from the absorption law $I = I_0 \exp(-\mu_m \rho t)$, where μ_m is the mass absorption coefficient of the material).

X-Ray Determination of Crystallinity in Polyethylene.—The basis for the X-ray determination of crystallinity in polymers is a comparison between the integrated intensities scattered by the amorphous regions in a completely and in a partly amorphous sample. It was shown^{4,5} that this is a

(1) Presented before the twenty-sixth National Colloid Symposium which was held under the auspices of the Division of Colloid Chemistry of the American Chemical Society in Los Angeles, California, June 16-18, 1952.

(2) Department of Physics, University of Michigan, Ann Arbor, Michigan.

(3) S. Krimm and R. B. Stein, *Rev. Sci. Instruments*, **22**, 920 (1951).

(4) S. Krimm and A. V. Tobolsky, *J. Polymer Sci.*, **7**, 57 (1951).

(5) S. Krimm and A. V. Tobolsky, *Textile Research J.*, **21**, 806 (1951).

more valid procedure than one in which the intensities at a given angle are compared. In the case of polyethylene, the samples were compared at constant scattering mass with a completely amorphous sample, which was obtained by heating the polymer to just above its melting point. The use of various assumptions involved in this procedure has been justified.⁴

The technique of the method is illustrated in the determination of crystallinity as a function of temperature in unoriented polyethylene. Diffraction patterns were obtained at 27, 60, 90, 100 and 120, some of which are shown in Figs. 1 and 2. The broken lines in the patterns indicate the separation of the total scattering into components due to the amorphous and to the crystalline regions; the lower solid line in each curve is the incoherent scattering. The following assumptions were made in separating the amorphous and crystalline parts of the scattering: (1) The diffraction curves of the amorphous and crystalline components were assumed to be symmetrical in the immediate vicinity of the maximum. (2) No influence of crystalline interferences is present at angles lower than $2\theta = 18.0^\circ$. (3) The ratio of the amorphous peak intensity at $2\theta =$

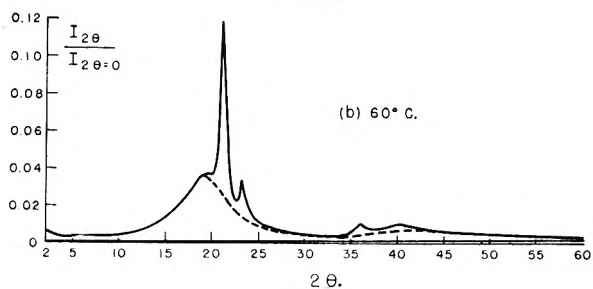
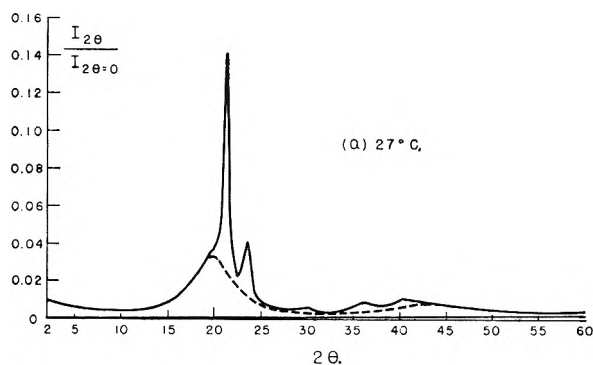


Fig. 1.—Radial scattering from unoriented polyethylene, at 27 and 60°.

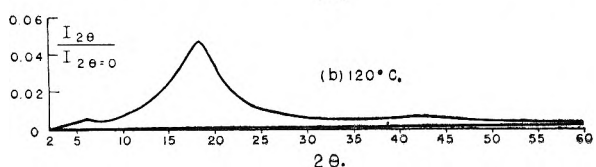
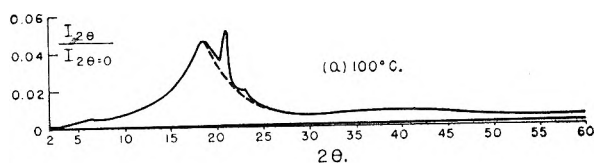


Fig. 2.—Radial scattering from unoriented polyethylene, at 100 and 120°.

19° to that at $2\theta = 42^\circ$ is about 5.1. (4) The approximate position of the maximum of the amorphous scattering in the 27° pattern can be obtained from the variation of the peak position with temperature. These assumptions were usually more than sufficient to resolve the experimental curves.

By comparing the coherent amorphous scattering between $2\theta = 2^\circ$ and 30° at a given temperature with that for the sample at 120° it was possible to obtain the percentage of amorphous material and therefore the quantity of crystalline component. The crystallinity values calculated in this way are shown in Fig. 3. Also shown is the variation of crystallinity with temperature as determined (a) from density measurements, (b) by comparing the intensities of the amorphous halo maxima and (c) by comparing the intensities at an angle other than that of the peak. It can be seen that the latter two methods give results which differ from the method of integrated intensities and also which differ greatly from each other. This is to be expected, since the position of the amorphous peak changes with temperature and the selection of an arbitrary 2θ value at which to measure the intensity therefore results in the comparison of quantities which are not equivalent in their measure of the amount of amorphous material. Similarly, the peak intensity of the amorphous halo does not necessarily reflect the amount of scattering material if different structures are compared. This is clearly brought out in the comparison of the scattering from equal masses of octacosane at 65 and 150° ,⁵ where the integrated intensities were found to be the same but the heights of the amorphous peaks to be different. These results further confirm the necessity of using an integrated scattering intensity as a measure of the amount of scattering material.

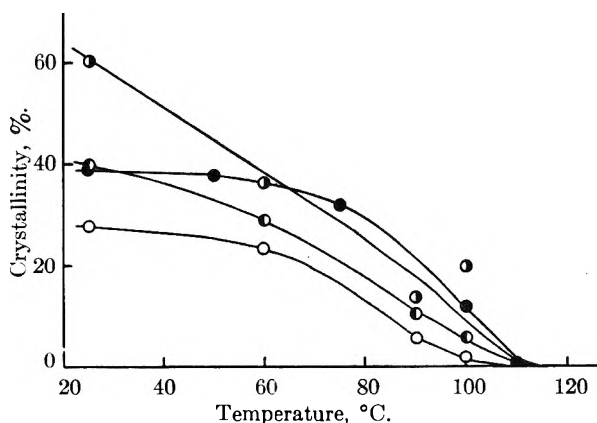


Fig. 3.—Crystallinity in unoriented polyethylene as a function of temperature: ●, density; ○, amorphous area; ○, amorphous peak; ●, $2\theta = 16.0^\circ$ intensity.

It is to be noted that the variation of crystallinity with temperature as determined by the X-ray method is somewhat different from the variation determined from density measurements: the X-ray values are generally lower, especially at temperatures just below the melting point. It seems likely that this is due to the presence of regions in the vicinity of the melting crystallites which, though amorphous in nature and therefore contributing to the amorphous scattering, are of slightly

higher density than that to be expected by extrapolation of the liquid density curve to the temperature in question. This could result from the ordering effect of the existing crystallites on those chains which have just been "melted" into amorphous regions. Studies on the formation of nuclei in polyethylene cooled from the molten state would seem to confirm this idea.⁶

By means of the above method, the crystallinity changes in stressed polyethylene were investigated in a series of experiments similar to previous stress-birefringence studies.⁷ The samples were elongated 20% and any relaxation was allowed to take place. After relaxation the temperature was varied both below and above the temperature at which elongation originally took place. At each temperature a diffraction curve was obtained and the radial scan resolved into amorphous and crystalline components as described previously. Comparison of the equatorial with the meridional scans at various temperatures showed that no orientation of the amorphous halo is obtained at this elongation, therefore, justifying the above procedure for determining crystallinity. The crystallinity values were determined in the manner described above and are shown in Fig. 4. The arrows on the lines connecting crystallinity values indicate the sequence of heating and cooling, which was always such that the specimen was cooled below the temperature of elongation before being heated above it.

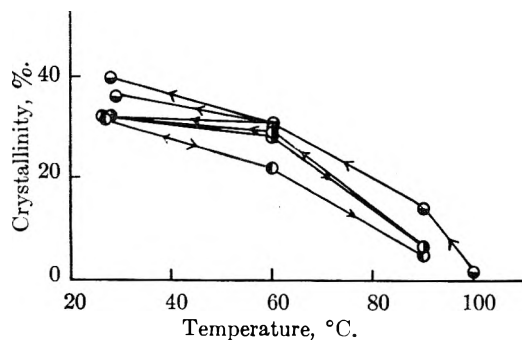


Fig. 4.—Crystallinity in polyethylene stretched 20% at various temperatures, as a function of temperature. Stretched 20% at: ○, 27°; ●, 60°; ●, 90°.

The orientation of crystallites in the stretched samples was estimated from the intensity distribution around the Debye-Scherrer diffraction ring. In the case of a specimen containing randomly oriented crystallites, the intensity is uniform around the ring. When the crystallites become preferentially oriented the rings break up into arcs, which manifest themselves as peaks in the Geiger counter scan around the ring. The degree of orientation was taken as proportional to the width of this peak at half maximum intensity and defined as $\Theta = (180^\circ - \beta)/180^\circ$, where β is the half width in degrees. The orientation determined in this manner is shown in Fig. 5. The numbers beside each point relate to the extent to which the preferred direction of the axes of the crystallites deviates from the direction of stretching.⁴

(6) S. W. Hawkins and R. B. Richards, *Textile Research J.*, **4**, 515 (1949).

(7) R. S. Stein, S. Krimm and A. V. Tobolsky, *Textile Research J.*, **19**, 8 (1949).

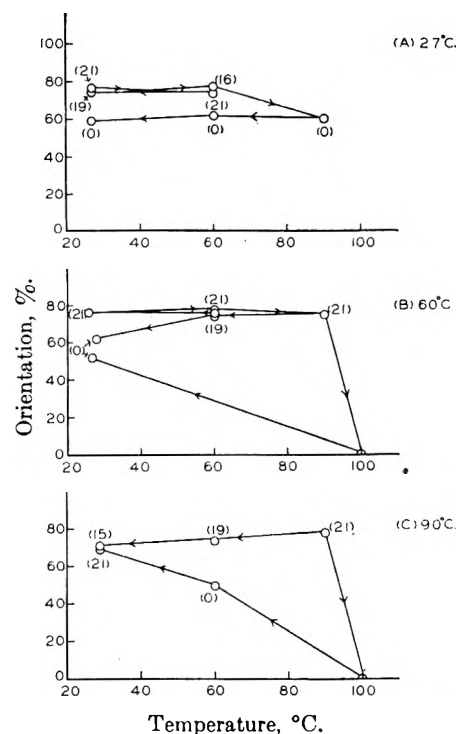


Fig. 5.—Orientation as a function of temperature for samples of polyethylene elongated 20% at various temperatures.

It is interesting to compare these results with previous work on the stress and birefringence behavior of polyethylene carried through the same stress-temperature cycles.⁷ The crystallinity-temperature curves for the elongated samples follow in general form the birefringence-temperature curves, thus confirming the original hypothesis that the amount of oriented crystalline material is a function of temperature only. It is seen from the X-ray data that the temperature cycles are responsible for changes in orientation of the crystallites, these changes being generally reproducible over the temperature range extending below the original temperature of elongation but irreversible when this temperature is exceeded. The orientation curves also show that a sufficient amount of incipient chain order is maintained at 100° (the sample was kept there for about 1.5 hours) to give an oriented crystallization when the sample is cooled. If the material is not heated much above the original elongation temperature, the retained order is high enough so that the material crystallizes with approximately the same degree, and direction, of orientation as was produced by the original elongation. This order is undoubtedly partly that of chains of newly melted crystallites, since the percentage of crystalline material is practically zero at this high temperature. It seems likely that the major part of the stress-temperature behavior in polyethylene is a result of the amount and type of orientation of the crystallites rather than the percentage of crystalline material.

Studies of crystallinity in more highly elongated specimens could not be undertaken by the above methods, since it was shown⁴ that orientation of the amorphous regions occurs.

Scattering from Polystyrene as a Function of Temperature.—The X-ray diffraction pattern obtained from a specimen of polystyrene is characteristic of that of an amorphous material, *viz.*, it consists of broad and diffuse halos. In the radial Geiger counter scan of polystyrene there are two broad peaks, with spacings, determined in the present work, of 8.84 and 4.67 Å. (applying Bragg's law to the angular positions of the peak maxima). At room temperature the 4.67 Å. peak is about twice as intense as the 8.84 Å. The origins of these two peaks have been elucidated by a study of samples of oriented polystyrene, for which it has been possible to show X-ray evidence of orientation by means of the Geiger counter scans.⁵ These show a concentration of scattering at the equator for the 8.84 Å. peak and at the meridian for the 4.67 Å. peak. It appears that the 8.84 Å. peak arises from interferences between atoms in neighboring main chains, which are about 9–10 Å. apart. The 4.67 Å. peak seems to be due to at least two different types of interatomic spacings: those between atoms in alternate phenyl groups in the same chain and those between atoms in phenyl groups and main chain atoms in neighboring chains.

The scattering pattern of unoriented polystyrene was studied as a function of temperature between room temperature and 200°. At temperatures above 90° the sample was enclosed in a mica window cell in order to eliminate any possible flow or orientation effects, correction being made for the scattering due to the mica. Equilibrium was established at each temperature before a scattering curve was obtained. It was noted that at temperatures above about 90° the relative intensities of the two peaks were different from that at the lower temperatures. The ratio of the intensity of the 4.67 Å. peak to that of the 8.84 Å. peak as a function of temperature is shown in Fig. 6. It can be seen that this ratio is fairly constant up to about 90°, at which point it falls linearly to a lower value which is then constant above about 160°. It was observed that the positions of the two peaks remain practically constant until about 160°, above which the spacings increase. The changes are shown in the following table.

Temp., °C.	Bragg spacing, Å.		Temp., °C.	Bragg spacing, Å.	
26	8.84	4.67	135	8.84	4.67
70	8.84	4.67	170	9.03	4.77
90	8.84	4.67	200	9.50	4.92

It thus appears that a definite structural change takes place in polystyrene within the temperature range of about 90 to 160°, a change which is not en-

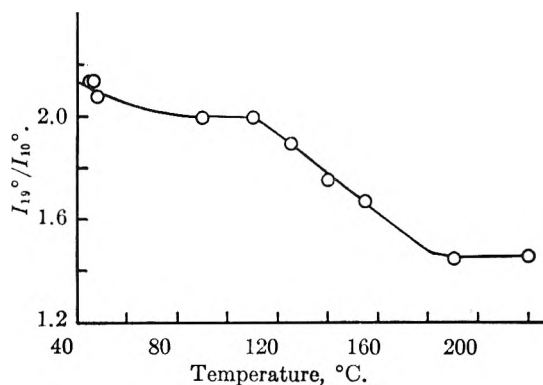


Fig. 6.—Ratio of intensities of two halos as a function of temperature for unoriented polystyrene.

tirely explained by the thermal expansion of the material. Then the increase in the intensity of the 8.84 Å. peak would indicate the presence of a larger number of such interatomic units contributing to the 4.67 Å. peak, on a relative basis, although the exact extent of such a change would require a Fourier analysis of the scattering curve. This might arise as a result of a change in configuration of the chain with increase in temperature (perhaps due to increased rotational freedom) such that neighboring chains are able, on the average, to maintain a more regular distance of separation from one another over a longer length of chain. Further increase in temperature then would result in expansion by means of increased separation of chains, as is indicated by the data in the previous table. The fact that the increase in the 8.84 Å. spacing is relatively greater than that of the 4.67 Å. spacing would seem to substantiate the belief that the latter spacing arises from both inter- and intramolecular distances. It is significant that a change in slope of the specific volume-temperature curves for polystyrene fractions has been reported⁸ at about 160°, in addition to the more abrupt change at the transition point. This coincides with the present findings that the mechanism of expansion of the material is different above and below 160°.

The scattering curves of polystyrene as a function of temperature indicate that the material is passing through various equilibrium configurational structures in the temperature range of about 90 to 160°. If the above interpretation of this phenomenon is correct, *viz.*, its connection with increased rotational freedom at higher temperatures, it would suggest that the glass transition in polystyrene is associated with the temperature at which the barriers to rotational freedom are overcome and therefore that the transition is at least partly of the equilibrium type.

(8) T. G. Fox and P. J. Flory, *J. Applied Phys.*, 21, 581 (1950).

PACKING ORIENTATION OF SOAP CRYSTALLITES¹BY MARJORIE J. VOLD²*Department of Chemistry, University of Southern California, Los Angeles, California**Received July 22, 1952*

The distribution of crystallite orientations in compacted powders has been examined for zeta and delta sodium palmitate and two forms of calcium stearate monohydrate. Crystallite orientation is determined from the dependence of the intensities of lines in the X-ray diffraction pattern on the disposition of the sample to the incident beam. In all four soaps crystallites set their (00*l*) planes preferentially parallel to the sample surface. Pastes in *n*-hexadecane, which appears to act as a lubricant, are even more readily oriented. In addition to having (00*l*) planes parallel to the surface of the sample, the crystallites are also oriented in the rubbing direction. Soap crystals in gels of calcium stearate with *n*-hexadecane (and small amounts of water) are not readily oriented by the same mechanical forces effective with pastes or powders. This fact suggests that inter-particle cohesion occurs in the gels. An anomaly occurs in that low and (presumed) high orders of the (00*l*) series show different dependence of intensity on sample disposition to the X-ray beam.

This paper is part of a continuing series of investigations in which it is sought to elucidate the structure of gels consisting of a matrix of interlocked and grown together crystallites with liquid retained in the pore space, particularly soap gels. These gels possess a number of physical properties such as yield value, texture, syneresis, liquid loss under pressure, cohesiveness, flow properties, etc., which must ultimately be interpretable in terms of the behavior of aggregates of soap crystallites of defined distribution as to size, shape and manner of cohesion one to another. The size and shape of soap particles recovered from such gels could be studied and indeed very interesting results have been obtained in correlating changes in consistency of lubricating greases during working, with changes in fiber dimensions as seen with the electron microscope.³ However, whether the original gel is a mechanical dispersion of the observed particles or possesses a more elaborate structure built from them as suggested by electron micrographs of sodium laurate fibers prepared from aqueous solution⁴ is not easy to determine. Application of electron microscopy⁵ to thin slices of gels of calcium stearate hydrate in *n*-hexadecane shows the existence of a coherent soap structure but still leaves to inference the relation of the structure to that of the original gel.

The present work is based on the supposition that if inter-particle cohesion is a factor in the structure of soap gels, the extent to which the individual crystallites are oriented by mechanical forces will be affected. Detailed prediction of the distribution of orientations to be expected from various model structures has not been attempted. Rather, the present work is essentially qualitative, exploring to see whether the phenomenon gives any promise of utility for the study of gel structure or indeed even exists. Variation of intensity of the various peaks in the diffraction pattern of the soap as a function of disposition of the sample to the incident beam was chosen as a method of determining the distribution of crystallite orientations.

(1) Presented before the twenty-sixth National Colloid Symposium which was held under the auspices of the Division of Colloid Chemistry of the American Chemical Society in Los Angeles, California, June 16-18, 1952.

(2) National Lubricating Grease Institute Fellow, 1951-1952.

(3) A. Bondi, A. M. Cravath, R. J. Moore and W. H. Peterson, *Inst. Spokesman*, 13, No. 12, 12 (1950).

(4) L. Marton, J. W. McBain and R. D. Vold, *J. Am. Chem. Soc.*, 63, 1990 (1941).

(5) R. D. Vold, H. F. Coffey and R. F. Baker, *Inst. Spokesman*, 15, No. 10, 8 (1952).

Determination of Non-random Orientation.—A North American Phillips X-ray Spectrometer was used for this work, following the procedure described by Schulz.⁶ The samples were prepared for X-ray examination as flat disks mounted so that any direction with respect to surface of the sample could be brought into the plane of the incident and recorded diffracted beam bisecting the angle between them. With appropriate precautions, the intensity of the diffracted beam is directly proportional to the volume fraction of soap crystals oriented with the corresponding crystal plane perpendicular to this direction. The orientation of a set of parallel diffracting planes is defined by two coordinates, the angle between the outward normals to the planes and the sample surface (σ), and the angle between the intersection of the planes with the sample surface and a reference direction in the surface parallel to the direction in which the sample was rubbed or stroked during the preparation (ρ). Two mounts are required to explore all orientations in order to ensure that variations in intensity are due to non-random orientation rather than to variation in the volume of sample illuminated by the incident beam and varying absorption. Each is valid over a range which could be calculated from Schulz's equations but requires also independent experimental verification since the range depends in part on the perfection of the mechanical arrangements.

The sample mounts used are shown in Fig. 1. Each consists of a brass ring 2.5" o.d. which fits into a similar brass ring 2.5" i.d. fixed on the axis of the sample mount. The inner ring can be rotated (angle ϕ). In the R mount the sample is contained in a cup 0.625" i.d. and 0.375" deep with its surface plane containing the ring axis. The cup can be rotated in its own plane (angle Δ). The incident beam is "reflected" from the surface and underlying layers. The incident beam is defined by two horizontal slits 1.5" apart, the first 0.08" high and 0.04" wide and the second 0.04" high and unrestricted in width. A third slit, 0.08" high and 0.04" wide, is placed at the counter entrance. Under these conditions a randomly oriented powder (-100 mesh $\text{Na}_4\text{P}_2\text{O}_7$) gave intensities independent of sample orientation for $0 \leq \sigma \leq 45^\circ$ and all ρ . In the T mount the sample is contained in an open hole 0.375" in diameter in a brass slide 0.04" thick. The slide can be turned about its own axis (angle α). A single slit 0.01" wide and 3 mm. high defines the incident beam; the counter slit is made 0.02" wide and also 3 mm. high. For calibration with $\text{Na}_4\text{P}_2\text{O}_7$ a thinner slide was used so that the absorption by the salt was comparable to that by soap gels and in accord with the value ($\mu T = 0.3-0.5$) recommended by Schulz. Results are valid for $45^\circ \leq \sigma \leq 90^\circ$ within 5% for all ρ at $\sigma = 90^\circ$ but only for $\rho \sim 0^\circ$ at other values of σ .

To explore the total accessible range of crystallite orientations, samples are run in both mounts at $\sigma = 45^\circ$, $\rho = 0$ where the valid ranges overlap and a conversion factor obtained to permit expression of the intensities on the same scale. This factor varies with the Bragg angle since reflection measurements weaken lines at small Bragg angles relatively more than those at high angles while the reverse is true for transmission measurements.

Materials.—The sodium palmitate was prepared in 1942 from Eastman palmitic acid (I.V. 0.0, eq. wt. 257). Analysis showed that it had not acquired any acidity on storage. It was dried to constant weight at 110° before use. A

(6) L. G. Schulz, *J. Applied Phys.*, 20, 1030 (1949).

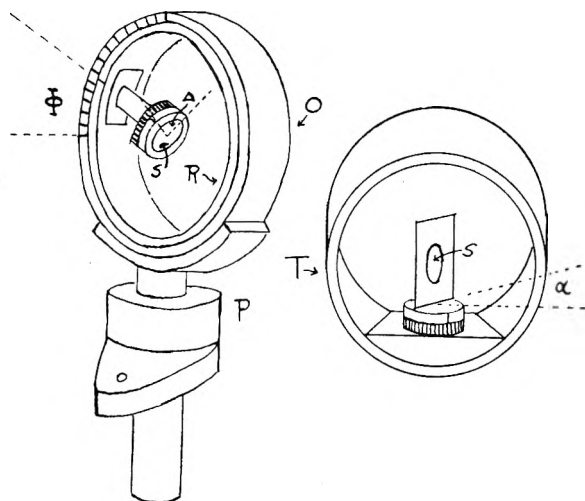


Fig. 1.—Sample mounts for orientation analysis. Inner rings R and T are interchangeable on the post P which stands perpendicular to the plane of incident and diffracted beam. In R, X-rays are "reflected" from the sample while in T they are "transmitted" through the sample which is at S in both cases. In R the experimental angles ϕ and Δ are respectively equal to the angles σ and ρ of crystallite orientation relative to the sample surface. In T the relation is $\cos \sigma = \sin \alpha \sin \phi$; $\cos \rho = \cos \phi / \sin \sigma$.

preparation in the zeta form was obtained by heating a sample with 40% soap and 60% water in a sealed tube to the isotropic liquid state and then allowing it to stand several days at 65°. A portion of this material was converted to the delta form by mechanical agitation at 40° as described by Vold, Grandine and Schott.⁷ The samples were allowed to dry in laboratory air resulting in a final water content of ca. 3%.

The calcium stearate monohydrate was prepared from a stearic acid of m.p. 69.2–69.7, eq. wt. 286, I.V. 0.3, purified from Armour's Neofat 65 by 3 recrystallizations from acetonitrile. After metathesis in aqueous alcohol between calcium chloride and the stearic acid neutralized with carbonate free sodium hydroxide, the precipitated calcium soap was extracted in a Soxhlet extractor with water at 100° for several hours after the last detectable chloride ion had been washed out. The monohydrate was in the VI-H form as prepared and yielded calcium stearate in the VI-A form upon dehydration. The water content of the hydrate determined by loss of weight at 110° was 2.89%. The VI-S form was obtained by dispersing 30% of the soap with 65% *n*-hexadecane and 5% water in a sealed tube at 155° and cooling slowly to room temperature. Solvent-free material was obtained by extraction with a light petroleum solvent boiling initially at 50°.

The crystallographic state of the materials was checked in all four cases by determining their X-ray diffraction patterns which corresponded exactly to those found for the respective forms by Vold, Grandine and Schott⁷ for the sodium soaps and Vold and Smith³ for the calcium soaps.

du Pont *n*-hexadecane (cetane) was used directly except for sweeping with nitrogen to remove dissolved oxygen. It had n_D^{20} 1.4345 compared to the literature value n_D^{20} 1.43449.

Gels of calcium stearate in *n*-hexadecane and water were prepared from a sample of the soap which had been dried to constant weight at 115°, by dispersing weighed amounts of soap and solvents at 155° in a sealed tube, equilibrating at this temperature for two hours or more and "quenching" in a freezing mixture of solid CO₂ and acetone.

Samples for X-ray study were prepared by piling the powder or gel loosely in the sample cup, compacting with vertical pressure under a glass plate and sliding off the glass plate in a fixed direction, vertical in the sample mounts at $\phi = 0$,

$\Delta = 0$ or $\alpha = 0$, $\phi = 90^\circ$, respectively. The intensities of diffraction peaks from duplicate surfaces were generally reproducible within 5–10%, but if the vigor of directional rubbing was purposely varied the extent of non-random orientation varied also, and to different extents with different samples so that a necessary further development is the definition and control of shearing motions during sample preparation.

Experimental Results and Interpretation

Solvent-free Soaps.—Results obtained for the dependence of intensity of reflections indexed as low orders (003–005) of the (00*l*) planes for the four soaps upon the angle σ are shown in Fig. 2. For the two sodium palmitate samples the results are for an arbitrary (but constant) value of ρ ; for calcium stearate hydrate VI-H they have been shown experimentally to be independent of ρ . The results plotted for calcium stearate VI-S were obtained for a paste of solvent-free soap in an approximately equal weight of *n*-hexadecane prepared at room temperature.

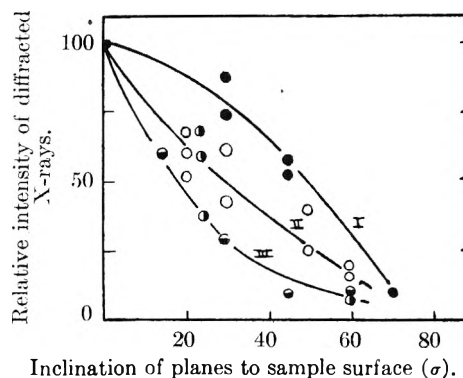


Fig. 2.—Preferred orientation in solvent-free soap powders; low orders of the (00*l*) spacing: I, ●, delta sodium palmitate; II, ○, zeta sodium palmitate; III, ●, calcium stearate hydrate VI-H; IV, ● (no curve) calcium stearate hydrate VI-S as a paste in *n*-hexadecane.

In all four cases the intensity is maximal near $\sigma = 0$, which means that most of the crystallites in the sample lie with their (00*l*) planes parallel to the sample surface. This is a behavior which would be expected for plate-like or ribbon-like crystals whose (00*l*) planes are parallel to the plate surface or ribbon surface, respectively. The extent of the orientation differs with the different samples. Many factors are involved including particle asymmetry, whether the oriented units are individual crystals or partly ordered aggregates, the method of sample preparation, inter-particle friction, etc. It is tempting to conclude that the delta sodium palmitate contains the least asymmetric particles and to cite this "fact" in interpretation of the observation that in aqueous gels (ca. 30% water) this modification is far more friable than the zeta form, but in view of the many other variables such a conclusion is not presently justified.

Following Stosick,⁹ Vold and co-workers^{7,8} have attempted to interpret the crystal modifications of some of the soap forms in terms of two dimensional slabs with stacking disorder and accordingly indexed a number of reflections as high orders of the (00*l*) spacing. The orientation dependence of the intensities of some of these reflections is shown in

(7) R. D. Vold, J. D. Grandine, 2nd, and H. Schott, *THIS JOURNAL*, **56**, 128 (1952).

(8) R. D. Vold and T. D. Smith, *J. Am. Chem. Soc.*, **73**, 2006 (1951).

(9) A. J. Stosick, *J. Chem. Phys.*, **18**, 1035 (1950).

Fig. 3. They all appear to tend toward maximum intensity at high angles of inclination to the sample surface almost exactly contrary to the behavior of the low orders. Since all (00 l) planes in a single crystallite should be parallel, this result stands as an anomaly for which no truly convincing explanation can be given.

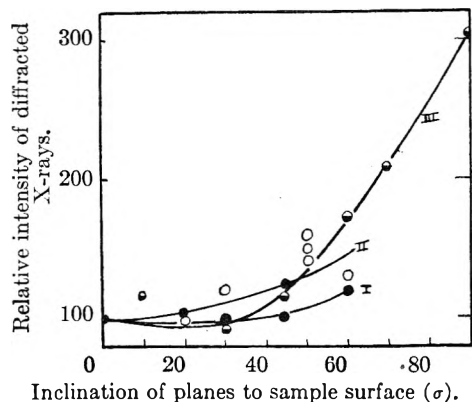


Fig. 3.—Preferred orientation in solvent-free soap powders; empirical high orders of the (00 l) spacing: I, ●, delta sodium palmitate, 8th and 9th orders; II, ○, zeta sodium palmitate, 10th, 12th and 15th orders; III, ●, calcium stearate hydrate VI-H, 13th order.

As many as ten different modifications of sodium soaps have been reported, on the basis of differences in X-ray diffraction pattern, but the question had been raised as to whether any of these distinct patterns could arise from reproducible non-random orientation of particles of the same crystal form subjected to different mechanical treatment. However, none of the variations in relative intensity of lines for either delta sodium palmitate or zeta sodium palmitate which are found when the X-rays are incident at different angles, leads to a pattern resembling any other reported soap modification.

For calcium stearate hydrate VI-H as a dry powder no variation of any of the intensities occurred as the sample surface was turned in its own plane. Peaks at d/n equal to 4.4, 4.15 and 3.4 Å., designated by Vold and Smith⁸ as ($hk\zeta$) bands showed essentially the same dependence on inclination to the sample surface shown in curve III of Fig. 3. This type of packing suggests the dominant occurrence of thin crystallites for which these planes lie perpendicular to the plate or ribbon surface.

Pastes of Calcium Stearate Hydrate in *n*-Hexadecane.—A paste of 45% calcium stearate VI-H was prepared in *n*-hexadecane at room temperature and the dependence of the intensity of the 003 reflections on both tip (σ) and turning motions (ρ) of the sample surface investigated in the range from $\sigma = 0$ to $\sigma = 45^\circ$. The results are shown in Fig. 4. At $\sigma = 0$ no dependence should occur since the plane normals being observed all stand perpendicular to the sample surface and along the rotation axis. For increasing angles of tip (σ) concentration of intensity occurs for planes whose normals lie in the rubbing direction. The directional stroking or rubbing conceivably exerts a torque tending to turn particles so that their long dimension is in the rubbing direction. Resistance to such a torque should increase with decreasing length-width ratio. Thus

the occurrence of the preferred orientation suggests high length-width ratios (*i.e.* "ribbons"). Failure to observe the same effect with the dry powder is ascribed to inter-particle friction since it is unlikely that the dispersion process used could itself have had any gross effect on particle shape.

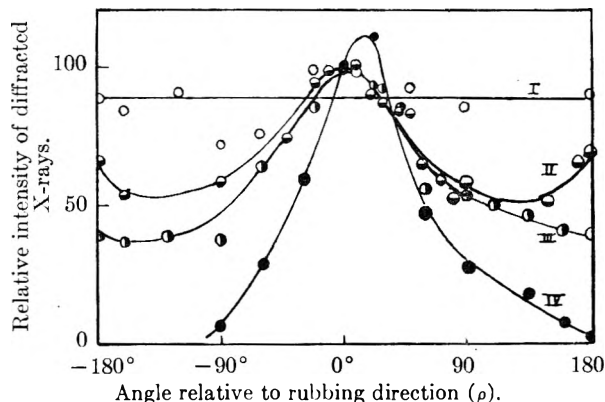


Fig. 4.—Preferred orientation in pastes of calcium stearate VI-H in *n*-hexadecane: I, ○, $\sigma = 0$; II, ○, $\sigma = 5^\circ$; III, ○, $\sigma = 10^\circ$; IV, ●, $\sigma = 45^\circ$. Intensity is taken as 100 in the rubbing direction at each value of σ .

The same kind of result was obtained for pastes of calcium stearate hydrate VI-S in *n*-hexadecane. For this sample, orientation dependence was studied for the peaks at d/n of 4.55 Å. (S peak) and 3.85 Å. (C peak) both of which are empirically high orders of the 00 l spacing, 11 and 13, respectively.⁸ The results are shown in Fig. 5. The planes responsible for the "S" peak are aligned preferentially close to the rubbing direction (plane normal at 110° to rubbing direction) while for the "C" peak little orientation is observed. This difference in preferred direction of presumably parallel crystal planes in the same crystallites is similar to that also encountered for the sodium palmitate samples and for calcium stearate hydrate VI-H. It constitutes a very real and serious objection to the index assignments previously suggested⁸ despite the numerical coincidences and other supporting data in favor of the assignment.

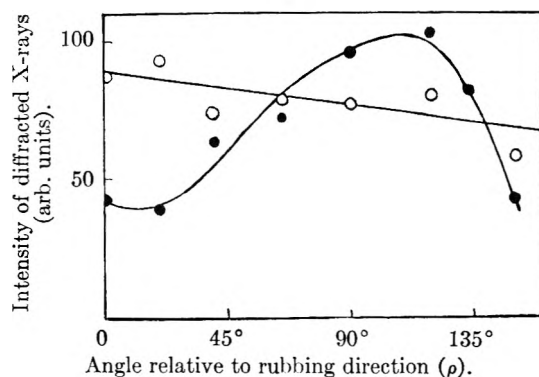


Fig. 5.—Preferred orientation in a paste of calcium stearate VI-S in *n*-hexadecane (at $\sigma = 60^\circ$): ○, "C" peak at $d/n = 3.85$ Å.; ●, "S" peak at $d/n = 4.55$ Å.

Gels of Hydrated Calcium Stearate with *n*-Hexadecane.—Samples of calcium stearate in *n*-hexadecane with water present in varying amounts up to one mole per mole of soap, prepared by dis-

persing the materials in a sealed tube at 155° and quick cooling yield mixtures of calcium stearate hydrate and a poorly crystallized form of anhydrous soap (VI-N) which shows only a single broad halo (at d/n 4.2 Å.) besides very weak (003) and sometimes (005) spacings. Two samples prepared with excess water (2 moles per mole soap and 19 moles per mole soap, respectively) displayed diffraction patterns corresponding to mixed VI-H and VI-S forms of calcium stearate hydrate. This was unexpected since heretofore calcium hydrate VI-S had been realized only in samples cooled slowly. The (003) spacing in the set of samples (measured at $\sigma = 0$, $\rho = 0$) showed progressively increasing intensity with increasing water content. These results are shown in Fig. 6.

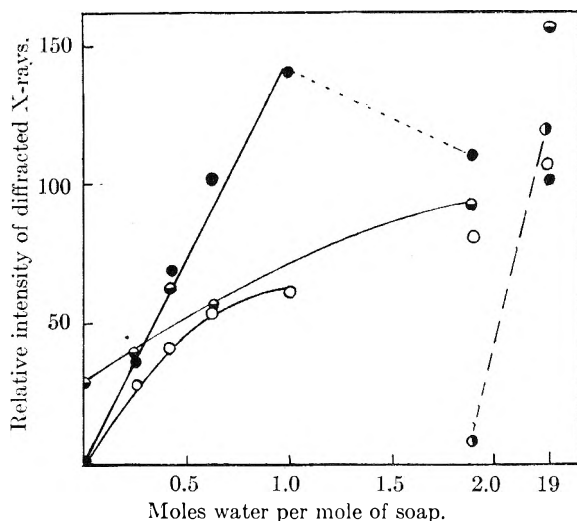


Fig. 6.—Diffraction behavior of gels of calcium stearate (45%) in *n*-hexadecane as a function of water content. The patterns were taken at $\sigma = 0$, $\rho = 0$. Relative intensities are adjusted to give the "B" peak at 4.15 Å. an intensity of 100 in all cases. The B peak occurs with nearly the same intensity in all four forms of calcium stearate and its hydrate. ●, "A" peak, $d/n = 4.4$ Å., occurs only for calcium stearate monohydrate VI-H (and anhydrous calcium stearate in which the transformation to form VI-A is inhibited). ○, "C" peak, $d/n = 3.85$ Å., occurs for both the VI-H and VI-S forms of calcium stearate monohydrate; ○, "S" peak, $d/n = 4.55$ Å., characteristic of calcium stearate monohydrate VI-S form; ○, 003 spacing (d/n ca. 16.7 Å., varying by ± 0.7 Å. for the different forms).

The determination of a distribution of crystallite orientations with more than one species of crystal present and virtually identical (00 l) spacings presents a complication which, however, did not have to be considered in detail because the major phenomenon encountered is the resistance of the gels to orientation at all under the mild stresses employed. No preferred orientation was detected for any of the diffraction peaks other than the low orders of the (00 l) spacing, nor was any preferred orientation established with reference to a rubbing direction in the sample surface. Dependence of the intensities of the (003) peaks on the angle of tip (σ) is shown in Fig. 7. The anhydrous sample and both of those with excess water tend to have their (003) planes somewhat oriented in a preferred direction slightly inclined to the sample surface. With intermediate

water contents systematic orientation does not occur but very extensive fluctuations are found as a function of angle. The fluctuations suggest the occurrence of sizeable regions of gel within which the soap particles are preferentially disposed to each other, but with such regions not broken down by the relatively mild stresses of forming the sample for X-ray examination.

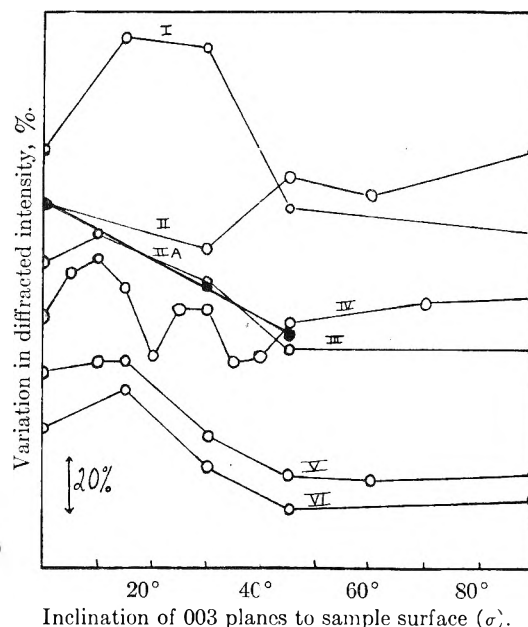


Fig. 7.—Preferred orientation of (003) planes in gels of calcium stearate in *n*-hexadecane (45% soap, varying water content). The intensity is taken as 100 at $\sigma = 0$ for each sample. The water contents in moles per mole of soap are I, 0.0; II, 0.27; III, 0.42; IV, 0.61; V, 1.9; VI, 19.0. II-A, ●, sample II after removal of most of the *n*-hexadecane.

In an isolated experiment, most of the solvent was removed from the gel with 0.27 mole of water per mole of soap, by dilution with pentane and filtering to leave a somewhat waxy, exceedingly triboelectric powder. This sample (II-A of Fig. 7) showed maximal intensity of its (003) planes parallel to the sample surface in common with the solvent-free soaps and with mechanically prepared pastes in *n*-hexadecane. This is taken as confirmatory evidence that the behavior of the gels is due to interparticle structure rather than solely to smaller particle size or more nearly isometric ultimate particles.

Conclusions and Prognosis.—It has been shown that reproducible non-random packing of asymmetric soap particles does occur. The phenomenon has been used to test and cast doubt upon the interpretation of diffraction patterns of soap crystals solely in terms of stacking disorder of otherwise perfect crystallites. Further, it has been shown that orientation of the constituent particles in gels can be made to occur but differs from that encountered for solvent-free soaps or mechanical pastes. The approach is thus presented as one which may, with further refinement, be capable of yielding useful results in at least two directions, *viz.*, shape distribution and packing characteristics of particles in polycrystalline systems and interparticle structure in gels.

A STUDY OF SOAP AEROGELS FROM LUBRICATING GREASES¹

BY W. H. PETERSON AND A. BONDI

*Shell Development Company, Emeryville, California**Received July 22, 1952*

For a more complete understanding of lubricating greases, a precise knowledge of the nature of the soap structure and its interaction with the oil component was desired. Therefore, the unchanged soap skeleton of a grease was isolated using Kistler's technique of obtaining aerogels. This technique involves removal of the fluid after the system has been heated above the fluids critical temperature. In the present case the operation should be performed at a temperature safely below the first transition point of the soap. Accordingly, the oil phase must be replaced by a sufficiently volatile medium without however, forming a fluid interface which would lead to the collapse of the soap structure. These requirements were met by displacing the oil from the grease gel by liquid butylene and the latter by liquid ethylene in a pressure bomb. The porous soap skeleton obtained after release of the ethylene has the dimensions of the original grease gel, the volume shrinkage being of the order of only 2% and a surface of approximately 80 sq. m./g. (nitrogen adsorption). Most of the experiments with the skeleton were designed to test the mechanical properties of reconstituted grease gels in a variety of oils. Use of the aerogel eliminated the influence of the oil properties on the growth of the soap fibers which ordinarily interferes with such interaction studies. Reconstitution, *i.e.*, replacement of the original oil into the skeleton, led to a grease which closely duplicated the properties of the original, thus indicating the reversibility of the system. Reconstitution with other oils showed grease consistency to depend upon the viscosity and the purity of the oil used. Consistency was found to increase linearly with the logarithm of the oil viscosity, but decreased as the oil contained larger amounts of adsorbable impurities.

One of the primary purposes of recent investigations of lubricating greases has been to determine the extent of interaction between soap and oil. X-Ray examination^{2a} and thermal differential analysis^{2b} suggest that up to about 100° there is little if any interaction between alkali or calcium soap and oil. The oil apparently is held by capillary action in the interstices of the soap-fiber tangle which the electron microscope has made visible.³ Transplantation of the gel structure from one oil to another without grossly affecting the nature of the gel has lent additional support to the concept of the two-phase nature of greases.⁴

At the outset of the work to be reported here, which paralleled in time many of the quoted studies, the question was not only to find a way to ascertain in a qualitative manner the independence of soap gel structure and oil, but also to obtain some quantitative information regarding the relationship between oil properties and grease properties. Previous work in this Laboratory had shown that oil viscosity has a profound influence on the dimensions of the soap fibers which are formed by affecting the diffusional processes operative in crystal nucleation and growth.⁵ To complete the picture, it was desirable to determine the effect—if any—of oil properties on the properties of greases gelled by soap fibers of fixed dimensions, which earlier studies did not control.³ For this purpose the soap fiber-tangle was isolated in unchanged form from a grease by the elimination of the liquid in the absence of a

meniscus—*i.e.*, at or above its critical temperature—to form an aerogel,⁷ and this soap aerogel was reconstituted with various fluids so that the properties of the resulting greases could be related to those of the fluid vehicle.

Experimental

Grease Composition and Manufacture.—The soda-base grease used contained approximately 91% refined mineral oil and 9% soda soap. The soda soap was made by saponifying a mixture composed of hydrogenated fish-oil fatty acids and a minor amount of 12-hydroxystearic acid⁸ after they had been melted in part of the oil. After dehydration, the balance of the oil was added and heating continued until solution of the soap in oil was accomplished. This solution was allowed to cool slowly without stirring and then yielded a gel which required milling to form a grease.

Preparation of Soap Aerogel from Grease.—Aerogels were made of both the gel⁹ and grease. Measured sections of gel (approx. $\frac{1}{4}$ " \times $\frac{1}{4}$ " \times 4") were used to detect any dimensional or volume change resulting from the oil removal. The volumes calculated from measured dimensions were checked by oil displacement.

Grease was used to obtain a large amount of gel since it could be easily packed into 60-mesh screen holders (18" \times 3 $\frac{3}{4}$ " \times $\frac{1}{4}$ "). The layers were relatively thin ($\frac{3}{8}$ " to $\frac{1}{4}$ "). Four screen containers were placed in a pressure vessel, separation between the screens being maintained by glass rods. The fluent flow was from top to bottom and parallel to the axis of the screens. Petroleum C₄ fraction was first used to remove the oil and subsequently displaced by an equal amount of ethylene. The charge of butylene or ethylene was completely renewed each day. This recharging took about four hours. The oil was recovered from the butylene by passing through a hot water heat exchanger to flash off the light solvent. The volume of butylene was measured by a gas meter and the oil weighed. When all (99%) of the oil in the grease had been recovered, ethylene was interchanged with the butylene in the same fashion and for the same number of cycles. During the ethylene interchange the bomb was kept in an ice-bath and the pressure maintained above 500 p.s.i. Before releasing the ethylene the bath was warmed to 30°. During the warming, the pressure was allowed to rise to above critical (750 p.s.i.) and maintained between 800 and 1000 p.s.i. by release of some of the ethylene. At 30° the remaining ethylene was slowly released. The bomb was then opened and the soap aerogel weighed and stored in closed cans.

Reconstitution of Grease from the Aerogel.—Reconstitution of the grease from the aerogel was usually effected by adding the required weight of oil to the soap aerogel chunks

(1) Presented before the twenty-sixth National Colloid Symposium which was held under the auspices of the Division of Colloid Chemistry of the American Chemical Society in Los Angeles, California, June 16–18, 1952.

(2)(a) M. J. Vold, G. S. Hattiangdi, and R. D. Vold, *Ind. Eng. Chem.*, **41**, 2311 (1949); (b) R. D. Vold, *et al.*, *ibid.*, **41**, 2539 (1949); F. H. Stross and S. Abrams, *J. Am. Chem. Soc.*, **73**, 2825 (1951).

(3) B. B. Farrington, *Ann. N. Y. Acad. Sci.*, **53**, 979 (1951).

(4) G. V. Browning, "New Approach to Lubricating Grease Structure," paper presented at 17th Annual Meeting of the N.L.G.I., New Orleans, Oct. 3, 1949.

(5) A. Bondi, J. P. Caruso, H. M. Fraser, J. D. Smith, S. T. Abrams, A. M. Cravath, R. J. Moore, W. H. Peterson, A. E. Smith, F. H. Stross, E. R. White and J. N. Wilson, "Developments in the Field of Soda Base Grease," Proceedings of the Third World Petroleum Congress, Section VII, 380–385, 1951.

(6) C. J. Boner, "Influence of Chemical Structure of Lube Oil on the Manufacture of Lubricating Grease," paper presented at N.L.G.I. 18th annual meeting, Chicago, October, 1950.

(7) S. S. Kistler, U. S. Patent 2,249,767.

(8) U. S. Patents 2,308,599; 2,380,960; 2,445,935; 2,445,589 and 2,588,556.

(9) The hard mass obtained from slow cooling of the soda grease prior to milling, is here designated as "gel."

TABLE I
PROPERTIES OF LUBRICANTS USED TO RECONSTITUTE AEROGEL

Lubricant	77°F.	Viscosity, cs. at 100°F.	210°F.	Viscosity index	Specific gravity d_{4}^{20}	Refractive index, n_D^{20}	Average molecular weight	Aniline point, °C.
A (Distillate)	3200	1008	34	50
Treated A	1600	566	26	62	0.9092	1.5020	565	108.4
B (Distillate)	880	325	18.6	61	.9005	1.4940	530	109
Turbine oil	245	108.1	9.32	56	.8950	1.4898	418	99.9
Distilled medicinal white oil	165	80.1	9.25	99	.8660	1.4767	489	119.3
Spray oil	37.5	20.9	3.65	36	.8819	1.4815	312	88.7
Light medicinal white oil	12.5	8.24	2.27	93
Cetane	3.97	3.05	1.26	133	.7739	1.4352	233	...
Dow Corning fluid 200	242	193.2	77.5	138	.9711	1.4059	3600	...

and evacuating the system to remove entrapped air. To observe dimensional changes during reconstitution, measured gel pieces were immersed in excess oil and the gel recovered and measured after draining off the free oil. Otherwise, with aerogel from grease the gel-like soap-oil chunks which resulted were stirred and mashed into a grease to incorporate any oil not soaked up by the gel. This mixture was then homogenized by working lightly with a spatula on a steel plate.

Oils.—The properties of the fluid lubricants used are listed in Table I. Some of the oils used were further refined in the laboratory either by passing through silica-gel columns or by vacuum distillation using conventional techniques.

Test Methods Used for the Grease.—The grease properties examined were consistent, as measured by the micro-cone penetrometer and the mechanical stability, as measured by the Shell Roll Test.

The micro-cone penetrometer¹⁰ consists of the Standard ASTM penetrometer with a small aluminum cone of 74° angle and 21 mm. high replacing the ASTM cone. The total plunger and cone assembly weighs 58.3 g. A standard 5 cm. diameter and 3.4 cm. deep cup was used to hold the grease. The sample was worked lightly (to break any thixotropic hardening) on a steel plate immediately before testing by means of a flexible steel spatula. The standard procedure of taking penetration by bringing the tip of the cone to the surface of the grease and releasing the cone assembly for five seconds was used. The depth of penetration of the cone was measured in dmm. For convenience consistency is expressed as 1000/penetration.

The Shell Roll Test¹¹ apparatus consists of a rotating iron cylinder, 180 mm. long and 90 mm. i.d., in which courses a free roller 176 mm. long and 60 mm. o.d. filled with lead to weigh 5 kg. \pm 100 g. The cylinder, closed at one end and fitted at the other with a threaded cap, revolves at 160 \pm 5 r.p.m.; 75 g. of grease is charged and at convenient intervals the grease is removed from the cylinder and penetration values obtained. The grease, immediately after removal, is brought to 25 \pm 0.2° by placing on a cooling plate maintained at temperature by circulating water. The grease is then loaded into the test cup and promptly tested to avoid variation in the results due to thixotropic hardening. Repeat penetrations are usually taken. The sample is then reloaded to the cylinder and the test continued. For comparative purposes the initial penetration was obtained by extrapolating the roll-life curve back to the first 0.1 hr.

Results and Discussion

If a grease structure formed by the solid gel agent were self-supporting and not interacting with the environment, its shape should be independent of the fluid contained in it. Upon re-embodiment with the original fluid, the gel should have the same properties as the original gel. Interchange of grease from one fluid to another can be effected without damage to the structure,⁴ but the removal of the fluid from a gel usually results in its collapse due to

contracting forces exerted by the surface tension of the receding fluid meniscus. Such gels cannot be reincorporated into the oil except by molecular dispersion at high temperatures. The use of a technique developed by Kistler⁷ some years ago avoids a receding meniscus by heating the gel system above the critical temperature of the liquid before its release.

Extraction.—Removal of the oil from a grease above its critical temperature is clearly pointless since the soap structure would be dissolved in the oil at a far lower temperature. In fact, in order to obtain the soap structure wholly intact and representative, the temperature should not exceed the lowest phase transition temperature of the soap—in this case about 80°—during the entire isolation process. It was therefore decided to displace the oil by low boiling hydrocarbons with critical temperatures below 80°.

This requirement restricted the choice of oil displacement fluids, and ethylene ($t_c = 9.8^\circ$) which happened to be readily available was used. A section of measured dimensions cut from unmilled soda-base grease gel was placed in a Jerguson sight-glass gage and was extracted with liquid ethylene at 0° and ca. 500 p.s.i. After no more oil was obtained in the separator of the system (see Experimental Section for details of the method), the temperature was raised to 30° and the ethylene released. During extraction the gel was observed to shrink slightly and the recovered aerogel had indeed lost 20% in volume. It was considered possible that the oil and the liquid ethylene might not have been entirely miscible and that the receding menisci of the interface between the two liquids might have developed sufficient interfacial tension to collapse the weakest components of the structure. Separate experiments on the oil-ethylene system showed that indeed the two liquids are only partially miscible and that, especially at high ethylene ratios, two phases are in equilibrium over a fair range of concentrations. As the interfacial tension between these two hydrocarbon liquids is probably only of the order of a few dynes/cm. the partial collapse of the soap structure indicates the delicacy of this isolation process.

To avoid even partial collapse of the gel structure, a two-stage process was adopted. The oil was first displaced by liquid butylene ($t_c = 160^\circ$) with which it is completely miscible at room temperature; then the butylene was displaced by ethylene which in turn was released above its critical tem-

(10) Shell Method Series, No. 479/48, Shell Development Company, Emeryville, California, 1948.

(11) R. P. McFarlane, *Inst. Spokesman*, 6, No. 12 (1943).

perature. A summary of a typical aerogel preparation is given in Table II. The resulting aerogel (sometimes called the "soap-skeleton" of the grease) had maintained the volume of the original grease lump within 1% and therefore exhibited a bulk density equal to the soap concentration in the grease, *viz.*, 0.08 g./cm.³. The aerogel appeared as a pithy, chalky, rather brittle, opaque, white, porous solid. Soxhlet extraction of the same grease with pentane and subsequent evaporation of the solvent, on the other hand, resulted in a horny piece of soda soap which was slightly heavier than water (see Table III).

TABLE II

AEROGEL PREPARATION FROM GREASE

A. Replacement of oil by butylene in grease skeleton

Interchange number	Period between interchanges, days	Vol. liquid C ₄ to vol. free space used in interchange	Wt. oil in sample at start of interchange, g.	Remaining oil displaced, %	Total oil displaced, %	Total soap in displaced oil, %
1	0.25	1	1385	68.8	69.8	0.18
2	2.75	1	431	64.3	90.2	.015
3	1	1.1	154	61.5	97.0	.002
4	1	1	60	55.0	99.4	.001
5	1	4.9	27	70.5	100.7	...
6	1	1	8	37.5	101.0	...
7 ^a	3	4.5	5	100.0	101.2	...

^a Interchange with ethylene follows.

B. Material Balance

	Charged	Recovered
Soap, g.	132	130
Oil, g.	1373	1385
Total, g.	1505	1515
% Gain	...	0.7
% Soap in total	8.78	8.64

gel structure when stereoscopic views are made.

Reconstitution.—Reconstitution of lubricating greases by reincorporation of oil into the aerogel had yet to be proved possible. Since the reconstitution was not carried out in a truly reversible manner, the advancing meniscus of the oil might collapse the structure during its penetration into the pores. A 15 to 20% shrinkage of the gel did occur during the reincorporation process, which—in order to prevent entrapment of air—was carried out *in vacuo*. However, electron micrographs of the reconstituted grease showed no collapse or breakdown of structural elements (Fig. 1).

The mechanical properties of the grease reconstituted with the original oil and soap aerogel derived from the unworked grease gel are nearly identical with those of the product from the gel prior to extraction (Table IV). The visual appearance of the reconstituted gel before working into grease was, except for the shrinkage mentioned above, the same as that of the original gel. However, the aerogel from the grease (worked gel) gave a gel-like solid upon reconstitution which required milling (as did the original gel) to yield a grease again. The "set" of the structure may result from increased interaction (perhaps cementation) of the soap fibers at their contact points during the period in which the oil is removed or from local compression of the structure by capillary forces during reconstitution. The consistency and mechanical stability of the worked samples were very nearly alike before and after processing, (Table IV), but the pattern of the breakdown curve was different as shown in Fig. 2. The lack of a hump in the curve for the reconstituted grease is interpreted to mean that some

TABLE III

LOSS IN SOAP STRUCTURE VOLUME DUE TO LIQUID INTERFACE

Method of recovering soap structure	Nature of interface	Per cent. of original after			
		Extraction Wt.	Vol.	Reconstitution ^a Wt.	Vol.
Soxhlet extraction with isopentane of oil followed by room-temperature evaporation of the pentane	Liquid C ₅ to C ₅ vapor	9.6 ^b	10.8	10.8	10.8
Ethylene extraction of oil. Ethylene then removed after heating system above 30°	Liquid ethylene to oil	9.6 ^b	80	77	81
Butylene extraction of oil followed by ethylene exchange with butylene. Ethylene then removed after heating system above 30°	None	8.85 ^c	99	88.5	87.5

^a Method of reconstitution always led to oil-air interface.

^b 8.65% soap in original gel. ^c 8.78% soap in original gel.

The surface area of the soap aerogel as determined by nitrogen adsorption¹² was about 80 to 100 m.²/g. (Certain irreversible phenomena taking place during the nitrogen adsorption process precluded more accurate determination of the surface area.) This area corresponds to an average fiber diameter of 500 to 600 Å., in agreement with electron microscope observation, suggesting that the visible geometric area of the soap fibers represents their entire area, *i.e.*, the absence of pores in or on the fibers. Carrying out the Kistler process on a grease specimen mounted on the electron microscope screen provides a clear picture of a relatively undisturbed

(12) Kindly carried out by Dr. Harold T. Byck and Dr. E. E. Roper.

TABLE IV

MECHANICAL PROPERTIES OF GREASE BEFORE AND AFTER AEROGEL PROCESS

Type of aerogel	Micropenetration		Roll life, hr.	
	Worked, original	Worked, reconstituted aerogel	Original	Reconstituted aerogel
Unworked gel	160	163	4.5 ^a	4.5 ^a
Worked gel (grease)	100	115	145 ^b	165 ^b

^a Hours to 290 micropen. (No protection against oxidation during gel preparation.) ^b Hours to 180 micropen. (Grease protected against oxidation during preparation before extraction.)

breakdown of large fibers may have occurred in the process. The changes wrought by the process cy-



A. Grease before treatment.



B. Grease after extraction with butylene and ethylene, release of ethylene after heating to 30° C., and reconstitution with oil.

Fig. 1.—Effect of Kistler's aerogel technique on soap fibers of a grease.

cle are, however, not very serious, since the roll lives (as indicated in the curve) closely coincide after 70 hours.

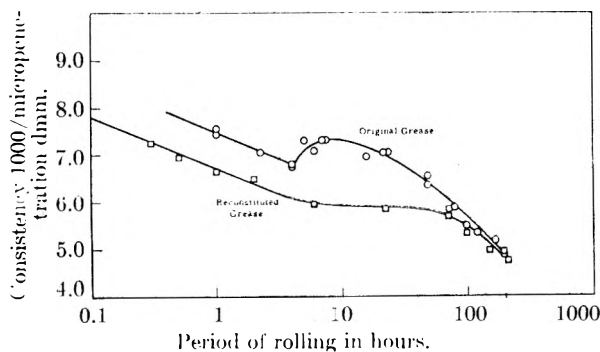


Fig. 2.—Shear stability of reconstituted grease.

Effect of Oil Viscosity and Composition on Grease Properties.—While, as shown above, reconstitution with the original oil produces a grease of nearly the same “worked consistency” as the starting material, reconstitution with other oils often gives greases which differ in consistency from the grease from which the soap aerogel had been derived. In the absence of surface-active substances from the oils, the grease consistency appears to be unaffected by the chemical composition of the mineral oils and depends only on the viscosity in the manner shown in Fig. 3. The curve does not continue to fall toward lower values of viscosity but goes through a minimum and increases again for very thin liquids. The soap aerogel imparts to silicone polymer fluids a higher consistency than to the equiviscous petroleum oil, possibly because of the more pronounced flocculation of soap particles in these fluids, a similar effect is also obtained with carbon black.¹³

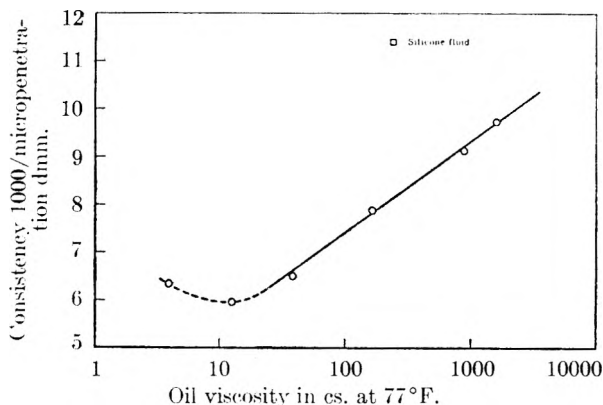


Fig. 3.—Relation of oil viscosity to grease consistency.

The presence of adsorbable components in the oil, as in the case of unrefined or residual oil fractions, leads to noticeable reduction in consistency as shown in Table V. This effect is believed to be due to the reduced interaction (friction) between soap fibers as a result of their having been covered with a layer of adsorbed polar material which may screen off the mainstay of interaction, namely, the planes normal to the dipole sheets.

TABLE V
INCREASE IN GREASE CONSISTENCY WITH HIGHLY REFINED OILS

Lubricant type	Oil viscosity, cs. at 77°F.	Consistency, 1000/micropenetration, dmm.
Distilled medicinal white oil	165	7.82
Turbine oil	218	7.70
Treated A	1600	9.7
A (Distillate)	3200	8.3

If one considers the consistency, as determined by the cone penetration method, to be a measure of the yield strength of the gel structure, then only the effect of adsorbable impurities on consistency is understandable. There is no *a priori* principle which could explain the effect of oil viscosity upon consistency. One might perhaps have expected more

(13) M. J. Forester and D. J. Mead, *J. Applied Phys.*, **22**, 705 (1951); A. Bondi and C. J. Pentler, *THIS JOURNAL*, **57**, 72 (1953).

rapid flocculation and therefore a harder grease with lower viscosity oils in contrast to most of the observed curve. The approximately linear relation between consistency and the logarithm of the oil viscosity also does not suggest any simple physical picture for the nature of this effect. It may perhaps be that the commonly used drop-cone penetration measures not only the yield stress of the grease but contains also a viscous component, especially in the range of relatively soft greases which have been examined. This problem is the subject of a separate investigation.

The shear stability of greases—as measured by the rate of consistency loss in the Shell Roll Tester—decreases as the oil viscosity increases (Table VI), probably owing to the larger shear stress which acts on the fibers to break them as the viscosity is higher. This effect is well known from pigment

TABLE VI
OIL VISCOSITY RELATED TO GREASE CONSISTENCY AND SHEAR STABILITY

Lubricant	Lubricant treatment	Viscosity, cs. at 77°F.	Consistency ^a after 0.1 hr. working in roll test	Rate of breakdown in roll test
Treated A	Acid washed and clay treated	1600	9.71	1.76
B	None	880	9.11	1.37
Distilled medicinal white oil	Clay treated and distilled	165	7.88	1.06
Spray oil	Acid washed and clay treated	38.0	6.50	0.65
Light medicinal white oil	None	12.5	5.95	0.50
Cetane	Acid and caustic washed	3.97	6.36	0.81
Silicone DC 200	None	242	11.4	2.4

^a Consistency, 1000/micropenetration in dmm.

grinding (Fig. 4) where the rate of particle size reduction is likewise proportional to the oil viscosity.¹⁴ In grease manufacture this effect of viscosity is entirely overshadowed by the beneficial effect of increased oil viscosity on fiber growth¹⁵ and thus on

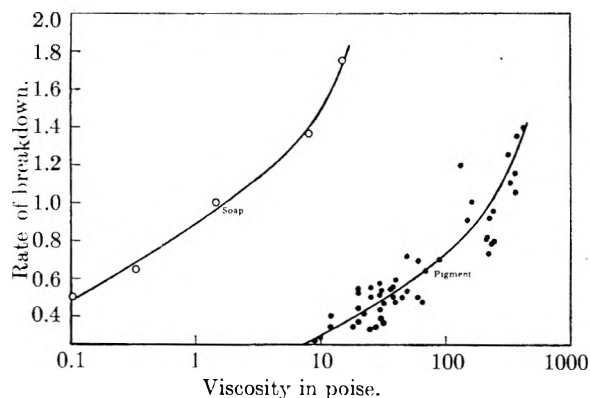


Fig. 4.—Relation of viscosity to shear stability.

(14) E. Fisher and D. Gaus, in Alexander's "Colloid Chemistry," Vol. VI, 1946, p. 300.

(15) R. J. Moore and A. M. Cravath, *Ind. Eng. Chem.*, 43, 2892 (1951).

the shear stability of the type of soda soap grease discussed in this paper.

Conclusions

(1) By means of the Kistler aerogel technique, authentic soap structures can be recovered from lubricating greases. These soap aerogels occupy within 1 or 2% the same volume as did the starting material. Electron micrographs also showed the absence of any significant changes in the processed soap structure. (2) Reincorporation of the original oil into the aerogel leads to a product which differs only slightly in its mechanical properties from those of the starting material. (3) The consistency of greases made by incorporation of the soap aerogel into other oils increases with the viscosity of the oils over a wide range, nearly independent of the oil composition, but their shear stability decreases. (4) Specific effects were noted with a silicone oil, which was gelled to higher consistency than the equiviscous hydrocarbon oil, and with oils containing adsorbable impurities, which depressed the consistency presumably by reducing the adhesion between soap fibers.

DISCUSSION

ANON.—Do I understand that by this technique you can replace the oil with water?

W. H. PETERSON.—Unfortunately soda soap is soluble in water and the fibers would possibly be somewhat changed. In water insoluble soaps it should be possible.

ANON.—What happens to aluminum soap?

W. H. PETERSON.—The method appears applicable to all kinds of greases.

A. L. McCLELLAN.—What explanation do you propose to offer for the fact that the reconstituted soap fibers do not seem to split lengthwise and cause the increase in penetration you have observed in the original greases?

W. H. PETERSON.—The fibers still do to some degree, as is evidenced by the flattening of the shear-breakdown curve in that region in which a hump occurs in the curve of the original grease. It depends on the rate and degree at which the process of splitting lengthwise goes on as opposed to the rate of breakage to shorten the fiber. These rates must become similar, otherwise we would not parallel the original curve toward the end of the 70-hour roll period. However some changes in the soap structure probably occur due either to compression or interaction of the soap with itself, while the soap aerogel is being formed or reconstituted. This is shown by the set exhibited when soap aerogel derived from grease in reconstitution, indicating some interaction between the soap fibers at their points of contact.

ANON.—Do you have any direct evidence for the fibering of the soap and the effect of the axial ratio on grease consistency?

W. H. PETERSON.—The evidence for this was published in *Ind. Eng. Chem.*, 43, 2892 (1951). The electron micrographs show this effect very nicely when samples are taken at different stages during the roll test.

R. D. VOLD.—I should like to refer to the paper just mentioned. I have the impression that you then attempted to account quantitatively for the consistency in terms of the length-width ratio of the fibers and that now you are postulating a three-dimensional structure with elastic properties, which presumably will resist rupture, and thus contribute an important component to the consistency as determined by penetration method.

W. H. Peterson.—I think you have two means of gelling oil at work here. One extreme is the brush-pile analogy in which interaction between fibers is of minor importance. The other extreme would be isometric shapes held together by flocculation forces. There is evidence that the soap

fibers do interact. So, therefore, part of the contribution to their consistency is that interaction. But you can, if you hold the interaction constant, relate consistency to the length-width ratio. If you vary the interaction, as we did by adding the impure oil, then the consistency again is interfered with, and can be related to that interaction.

M. J. VOLD.—When the original oil is extracted is it not

possible that some of the polar bodies may remain sorbed on the soap fibers and thus contribute to the apparent effect of the nature of the oil used in reconstituting the grease on its final consistency?

W. H. PETERSON.—The oils used were for the most part mineral oils selected without regards to composition except that they be free of polar bodies.

A NEW APPROACH TO GAS FLOW IN CAPILLARY SYSTEMS¹

BY R. M. BARRER

Chemistry Dept., Aberdeen University, Aberdeen, Scotland

Received July 22, 1952

An account has been given of some results obtained using the time lag method for the investigation of porosity, tortuosity factor, mean capillary radius, r , and internal area, A , of porous media. This method leads to results for r and A which differ characteristically from these quantities obtained by the steady state methods due to Adzumi or Arnell. There are reasons for believing that the time lag method measures true internal areas more exactly than steady state methods. The time lag method has been extended to investigations of adsorption and surface diffusion for gases adsorbed according to Henry's law. Surface diffusion in "Vycor" porous glass (where a high surface:volume ratio is combined with fine capillaries) was at room temperatures and above comparable with volume diffusion along the capillaries in the gas phase in a number of instances (O_2 , N_2 , A , Kr , CH_4 , C_2H_6). During the transient state of flow the separation factor for mixed gases diffusing through a septum can be greatly enhanced. Thus in a N_2 : C_2H_6 mixture, where in the steady state there is little separation, one may have large transient state separation factors. Enhanced transient state separation factors may also arise with isotopic species such as H_2 , HD and D_2 .

Problems connected with transport of fluids in porous media occur in considerable numbers. Capillary rise of liquids, wetting processes, flow of underground water or petroleum, resistance to flow due to porous beds in combustion chambers, catalyst reactors, fluid catalysts, and in filtration processes provide just a few examples of technically important fluid transport problems.

Parallel with the practical aspects of such processes come fundamental researches into kinetic molecular and quasi-thermodynamic treatments of flow. Many studies of this kind have been made, under a wide variety of conditions.² Gas flow in single capillaries provides a simple means whereby several types of flow may be identified and their characteristics defined. These are: molecular streaming (Knudsen flow); streamline (or Poiseuille) flow; turbulent flow; and orifice flow. To these flow mechanisms should be added surface transport, where molecules move within the influence of the force field of the solid.

In recent years considerable experience has been gained of diffusion in channels so restricted as to be no more than an average sized molecule in diameter.³ Such channels are provided by certain types of aluminosilicate mineral (zeolites like chabazite, mordenite, levynite, gmelinite, harmotome and several others). Attention has also been paid by us to the flow of gases in beds of small spheroidal particles (crystals of synthetic analcite) under conditions where diffusion into the crystals did not occur

but where flow was comparatively rapid between and around the individual crystallites in the bed.⁴ In the beds of analcite particles the surface to volume ratio was not large. More recently gas flow and sorption in a "Vycor" porous glass has been investigated.⁵ In this medium the surface to volume ratio is very high and a state of affairs can be achieved where all molecules spend a substantial fraction of their lifetime inside the porous medium directly within the range of surface forces from the medium. This case is intermediate between flow almost entirely confined to the gas phase and intracrystalline diffusion in zeolite crystals where the diffusing molecules are wholly within the influence of the force field of the crystals. It thus permits the interplay of gaseous and surface flow to be studied.

One object of the investigations in analcite beds and in porous glass has been to develop a method of approach^{2c,4,5} which differs from and is in some ways complementary to the traditional steady state procedures of Kozeny,⁶ Carman,⁷ Adzumi,⁸ and others.⁹ These approaches have shown that information can be obtained from the steady state of flow as to the average capillary size in the porous medium, the number of capillaries per unit volume and the internal surface of the porous medium. A second and independent flow method of determining such properties provides a valuable check on the results of the first method and thereby helps to show what are the limitations of such methods and of the physical model of the capillary system which

(1) Presented before the twenty-sixth National Colloid Symposium which was held under the auspices of the Division of Colloid Chemistry of the American Chemical Society in Los Angeles, California, June 16-18, 1952.

(2) *E.g.*, (a) K. Herzfeld and H. Smallwood in Taylor's "Treatise on Physical Chemistry," The Macmillan Co., Inc., New York, N. Y., 1931, p. 73. (b) R. M. Barrer, "Diffusion in and Through Solids," Cambridge University Press, Cambridge, England, 1941, chap. 2. (c) R. M. Barrer, *Faraday Soc. Discussion*, No. 3, 51 (1948).

(3) *E.g.*, R. M. Barrer, *Ann. Repts. of the Chem. Soc.*, **41**, 32 (1944). R. M. Barrer, *Quart. Rev.*, Vol. 111, 1949, No. 4, p. 293.

(4) R. M. Barrer and D. M. Grove, *Trans. Faraday Soc.*, **47**, 826, 837 (1951).

(5) R. M. Barrer and J. A. Barrie, *Proc. Roy. Soc.*, **A213**, 250 (1952).

(6) J. Kozeny, *Sitzber. Akad. Wien.*, **136**, [IIa] 271 (1927).

(7) P. Carman, *Faraday Soc. Discussion*, No. 3, 72 (1948).

(8) H. Adzumi, *Bull. Chem. Soc. Japan*, **12**, 304 (1937); also G. Lochmann, *Angew. Chem.*, **53**, 565 (1940), and ref. 4.

(9) J. C. Arnell, *Can. J. Research*, **A24**, 103 (1946); *ibid.*, **A25**, 191 (1947); P. Carman and J. C. Arnell, *ibid.*, **A26**, 129 (1948).

they involve. In this communication the procedure we are developing has been outlined and some of its results indicated.

The Model for the Capillary Structure of the Medium.—The pore geometry of beds of irregular particles is so complex that the capillary network is usually idealized as a set of parallel uniform capillaries running through the medium in the direction of flow. Some shortcomings of this simple picture are inevitable and instances revealed by our experiments will be given later; its advantage is that in terms of the model it permits the flow processes to be clearly and quantitatively formulated. Thus, the actual bed of thickness l , bounded by the planes $x = 0$ and $x = l$, in which flow occurs in the $+x$ direction, is replaced by a bed of identical permeability, of thickness l_1 and comprising a set of parallel capillaries all of radius r . In such a bed, $l_1 = k_2 l$ where k_2 denotes the tortuosity factor.

For molecular streaming the general differential equation of flow in such a medium is¹⁰

$$\frac{\partial c}{\partial t} = D \frac{\partial^2 c}{\partial x^2} \quad (1)$$

where C denotes the concentration at time t and point x and where D is the diffusion coefficient of gas in

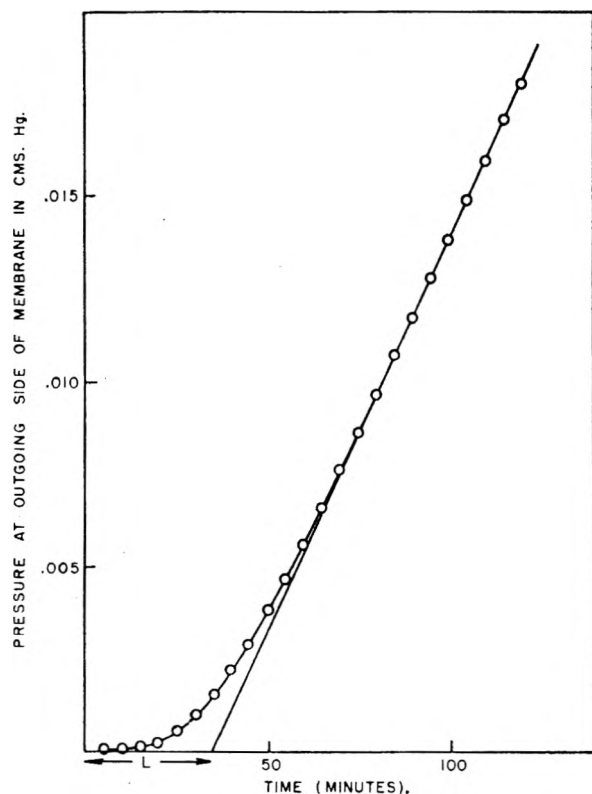


Fig. 1.—Time lag, L , for SO_2 gas at 5° , flowing through a column of analcite spheroids. Ingoing pressure = 0.374 cm. Hg (ref. 4).

(10) In terms of the model, D is the diffusion coefficient in any of the capillaries of which the idealized medium is composed. It is of course true that equation 1 can be written without reference to any model and the modified diffusion coefficient D^* can still be obtained from $L = \frac{l^2}{6D^*}$ (eq. 5). Thus $D^* = k_2^2 D$ where k_2 is the tortuosity factor (l.c.).

the porous medium. For streamline flow, the corresponding equation is

$$\frac{\partial c}{\partial t} = D' \frac{\partial^2 c^2}{\partial x^2} \quad (2)$$

and it can be seen that while eq. (1) is capable of explicit solution, eq. (2) being non-linear is not. Particular attention has therefore been given to the molecular streaming flow range.

Basis of a New Procedure for Investigating Surface and Pore Properties.—The solution of eq. (1) can readily be obtained for transient flow in the capillary system for the boundary conditions

$$\begin{aligned} C &= C_0 \text{ at } x = 0 \text{ for all } t \\ C &= 0 \text{ at } t = 0 \text{ for } 0 < x < l_1 \\ C &\approx 0 \text{ at } x = l_1 \text{ for all } t \end{aligned}$$

The solution is^{2c}

$$C = C_0 \left(1 - \frac{x}{l_1}\right) - \frac{2C_0}{\pi} \sum_{n=1}^{\infty} \frac{1}{n} \sin \frac{n\pi x}{l_1} \exp - \frac{Dn^2\pi^2 t}{l_1^2} \quad (3)$$

Experimental measurements to correspond to the above boundary conditions can easily be made^{4,5}; in practice it is sufficient if during the run the concentration at the outgoing surface should always be much less than that at the ingoing surface of the porous bed.

The quantity Q which has diffused through unit cross section after a time t is

$$Q = -D \int_0^t \left(\frac{\partial c}{\partial x}\right)_{x=l_1} dt = \frac{DC_0}{l_1} \left[t - \frac{l_1^2}{6D} + \frac{2l_1^2}{\pi^2 D} \sum_{n=1}^{\infty} \frac{(-1)^{n+1}}{n^2} \exp - \frac{Dn^2\pi^2 t}{l_1^2} \right] \quad (4)$$

Thus, as t increases, Q approaches the asymptote

$$Q = \frac{DC_0}{l_1} \left[t - \frac{l_1^2}{6D} \right] \quad (5)$$

Accordingly this asymptote makes an intercept

$$L = \frac{l_1^2}{6D} = \frac{k_2^2 l^2}{6D} \quad (6)$$

upon the axis of t . Figure 1 shows the approach to the steady state of flow,⁴ and the time lag L , for SO_2 at 5° and with C_0 corresponding to 0.374 cm. of Hg. The porous medium was a 94-cm. column of analcite spheroids of mean radius 5×10^{-3} cm. The total cross-section of the column was $A_c = 0.0962$ cm.² and the porosity was 0.50 cc./cc. It is clear from Fig. 1 that L can be determined with accuracy. From the value of L the ratio k_2^2/D follows at once.

For a gas showing negligible adsorption and flowing in a capillary (or system of parallel capillaries) of radius r , the diffusion coefficient D is given by^{2c, 4, 1}

$$D = \frac{4r}{3} \sqrt{\frac{2RT}{\pi M}} \quad (7)$$

Thus the time lags for a group of such gases should be proportional to \sqrt{M} ; or the products $D\sqrt{M}$ should be constant. The correctness of this view is indicated in Table I for a variety of gases in the analcite column.⁴ Variations in the product $D\sqrt{M}$ are at least in part the result of a tendency of the unconsolidated medium to settle during the course

of the experiments. In the last column of Table I are given the mean pore radii according to eq. (7) and the parallel capillary model.

TABLE I
TRANSIENT FLOW IN ANALCITE BEDS AT 25°

Gas	L_c^a min.	D_c^b cm. ² sec. ⁻¹	$D\sqrt{M}$	$r \times 10^4$ cm.
He	4.9	10.9	21.8	1.30
Ne	9.8	5.46	24.5	1.46
A	14.7	3.64	23.0	1.37
Kr	21.7	2.46	22.6	1.34
H ₂	3.0	17.7	25.2	1.51
N ₂	11.0	4.84	25.6	1.53
O ₂	12.5	4.26	24.2	1.44

^a Length of column of analcite = 98 cm. ^b k_2 is taken in this calculation to be $\sqrt{2}$.

The values of r in Table I may be compared with values obtained from steady state flow measurements through the same column¹ (Table II). The pore radii in column four in Table II have been derived by the method of Adzumi^{2c,8} from a combined study of Knudsen and Poiseuille flow (assuming as before that $k_2 = \sqrt{2}$). These radii are much larger than are those in Table I derived using the time lag method. The reason for this is discussed later in this paper.

TABLE II
STEADY STATE FLOW DATA IN ANALCITE BEDS AT 25°

Gas	Knudsen permeability, K_k , cm. ² sec. ⁻¹	$10^4 \times$ Poiseuille permeability, K_p , cm. ³ sec. g. ⁻¹	$10^4 \times r$, cm.
He	11.5	9.3	9.6 ₄
Ne	6.0	4.4	6.0 _h
A	3.7	6.2	7.0 ₉
Kr	2.9	5.8	6.4 ₉
H ₂	15.6	14.5	7.1 _h
N ₂	4.65	7.0	5.4 ₃
O ₂	4.45	5.6	6.0 ₂

Independent Measurement of k_2 and of r .—The mean capillary radius r can be determined by an independent method, from sorption measurements. These following the B.E.T. or analogous procedures give A the surface area of the porous medium in cm.²/cm.³. Next the porosity ϵ can be measured in cm.³/cm.³, and the ratio $2\epsilon/A = r$ may be derived (eq. (7)) and then from eq. 6 one obtains k_2 .

Barrer and Barrie⁵ made a close study of flow and sorption in "Vycor" porous glass. Figure 2 gives typical sorption isotherms obtained in this medium. These are of Type IV in Brunauer's classification¹¹ and therefore give both ϵ ¹² and A . The value of $r = 2\epsilon/A$ can be further checked in this system by using Kelvin's equation¹³ applied to the desorption branch of the isotherm. In most porous media a distribution of values of r is obtained by this method.¹⁴ In the case of porous glass however the desorption branch of the hystere-

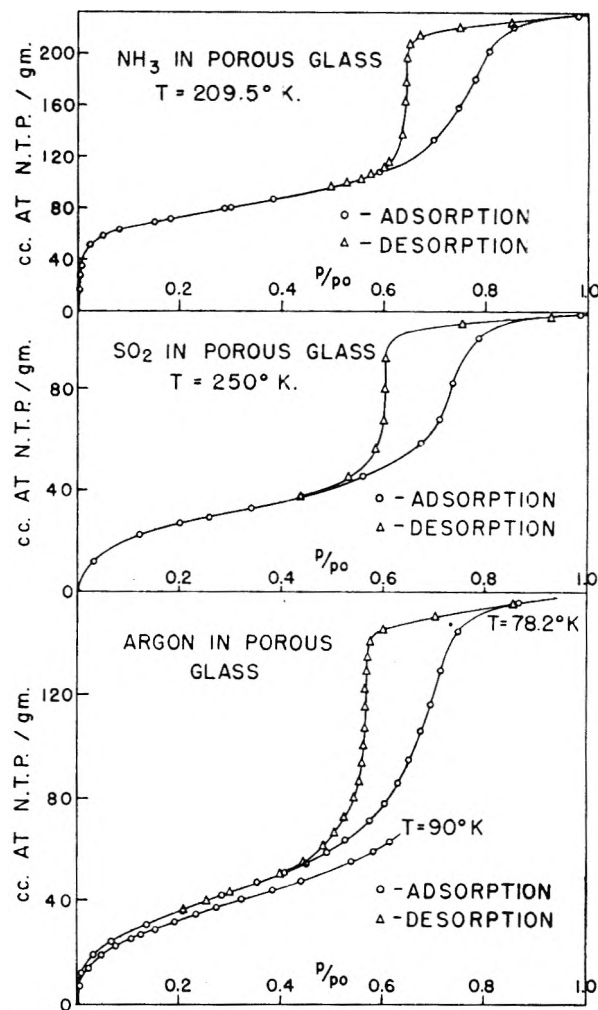


Fig. 2.—Typical sorption isotherms in porous glass (ref. 5).

sis loop was nearly vertical, showing that evaporation occurred from menisci which nearly all have the same radius of curvature. The value of r obtained from Kelvin's equation was corrected according to the suggestion of Foster¹⁴ for the presence of an adsorbed film about two molecules thick, which persists just after the liquid meniscus has disappeared.

In porous glass the two methods agreed excellently and gave $r = 30 \times 10^{-8}$ cm. In the same medium k_2 was then derived as 2.56 and 2.51, using time lag data for the non-sorbed gases He and Ne, respectively. As soon as k_2 is known, D for many gases in the porous medium followed (cf. ref. 5 and see also Table I).

Wyllie and Rose¹⁵ suggest that k_2 can be derived from the ratio R of the specific resistance of a porous medium saturated with a conducting fluid to the specific resistance of the fluid itself. They give for this ratio $R = \epsilon/k_2$, and from their results values of k_2 may be calculated in the range 3.53 to 1.65 for various media, the majority giving values around 2.5. This method can be used independently of the sorption procedure used by us.

In some media of particularly simple structure estimates of the tortuosity factor have been made.

(11) S. Brunauer, "Physical Adsorption of Gases and Vapors," Oxford University Press, New York, N. Y., 1944, chap. 6.

(12) See eq. 10 for another method of obtaining ϵ .

(13) $RT \ln p/p_0 = -2\sigma V/r$ (8)

where p/p_0 is the relative pressure of sorbate vapor, and σ is the surface tension of liquid sorbate of molecular volume V .

(14) A. G. Foster, *Paraday Soc. Discussion*, No. 3, 41 (1948).

(15) M. Wyllie and W. Rose, *Nature*, 165, 972 (1950).

In beds of spheres k_2 has been alternately given^{16,17} as $\pi/2$ and $\sqrt{2}$. Carman¹⁷ has indeed suggested that $k_2 = \sqrt{2}$ for a variety of porous media, but this estimate now appears too low. If k_2 is not known, a reasonable estimate would on present evidence be ~ 2.5 .

Pore Properties by the Time Lag Method.—The steady state flux dn/dt of non-sorbed molecules in Knudsen flow through unit cross section of a porous bed is, in terms of the parallel capillary model, where N capillaries traverse unit cross section of the bed

$$\frac{dn}{dt} = \frac{N\pi r^2 DC_0}{k_2 l} \quad (9)$$

Substituting from eq. (6) ($L = k_2^2 l^2 / 6D$) and recalling that $N\pi r^2 k_2 l = \epsilon l$ (where ϵ is in cc./cc. of porous medium) one has

$$\frac{dn}{dt} = \frac{\epsilon l}{6L} \times C_0 \quad (10)$$

This simple equation can sometimes give a good estimate of the porosity. Thus in porous glass the sorption method gave $\epsilon = 0.30$ cc./cc. while eq. (10) gives $\epsilon = 0.33_6$ and 0.32_8 using Ne and He, respectively.

When the tortuosity factor k_2 has been determined (or is assumed) the time lag method readily gives the internal area A of the solid, for it leads to a value for $r = 2\epsilon/A$, whence A is obtained.

Barrer and Grove⁴ determined the surface area of analcite spherulites by three flow methods: the time lag procedure; and the steady state procedures of Adzumi⁸ and of Arnell.⁹ In order these methods gave $A = 7100$, 1500 and 1260 cm.²/cm.³, respectively. The time lag method gives a much larger value, parallel to the notably smaller value of r , pointed out earlier in comparing Tables I and II. The difference is related to limitations of the parallel capillary model.

Thus before the steady state is established (*i.e.*, during the time lag period) the penetration of gas involves every part of the surface and pore structure of the medium. In the steady state however blind or *cul-de-sac* pores contribute little to the rate of flow. Accordingly the surface area derived from steady state data should be too small and the average pore radii are correspondingly too large. On the other hand the time lag method should give a good measure of the total surface area and a better idea of the average pore radius.

Adsorption and Surface Flow Processes by the Time Lag Method.—An important field of application of the new procedure lies in the investigation of adsorption, surface flow and gas fractionation through septa. Surface flow has been considered to occur on a variety of surfaces, but adequate methods of investigation have not been developed until recently. Early transient investigations by Wicke¹⁸ and others¹⁹ do not carry much conviction because the mathematical analysis of the results is unavoidably crude. Steady state investigations by Flood

and Tomlinson²⁰ and by Carman, *et al.*,^{21,22} appear to have placed the reality of surface flow in porous media such as finely divided carbon, silica and other powders beyond reasonable doubt, and Carman and Raal²² have recently summarized a number of surface diffusion coefficients of sorbed vapors on such media. Their analysis refers only to surface flow in adsorbed films at higher relative pressures where dense monolayer or multilayer films and even capillary condensation occur. The data establish that surface mobility increases rapidly, the greater the amount sorbed. This means that, if surface flow can still be treated as a diffusion, the equation of transient flow must be

$$\frac{\partial c_s}{\partial t} = \frac{\partial}{\partial x} \left(D_s \frac{\partial c_s}{\partial x} \right) \quad (11)$$

with D_s a function of C_s . The analysis used by Carman and Raal for the steady state gives merely an average D_s over a considerable interval of surface concentration. Moreover their method does not appear suitable for measuring surface diffusion in the most dilute films, where Henry's law governs the sorption equilibria. It is here that the time lag method is particularly useful. In these most dilute films the equation of surface flow in a capillary is

$$\frac{\partial c_s}{\partial t} = D_s \frac{\partial^2 c_s}{\partial x^2} \quad (12)$$

where C_s denotes the number of adsorbed molecules per cm. length of capillary, while at the same time Knudsen flow in the gas phase is governed by

$$\frac{\partial c_g}{\partial t} = D \frac{\partial^2 c_g}{\partial x^2} \quad (13)$$

In eq. (13) C_g denotes the number of gas phase molecules per cm. length of the capillary. Provided adsorption equilibrium is maintained between flowing gas and the adsorbed film, the total flow is represented by the sum of the above equations, where the relation between C_g and C_s follows Henry's law. Thus considering a capillary, at a point x one has

$$2\pi r C'_s = C'_g; \quad \pi r^2 C = C_g$$

where C'_s and C denote the number of molecules per cm.² of surface and per cc. of gas phase, respectively, at x . Thus

$$\frac{C'_s}{C_g} = \frac{C'_s}{C} \times \frac{2}{r} = \frac{2k_s}{r} \quad (14)$$

where k_s denotes the Henry's law sorption constant. Adding (12) and (13) and substituting from 14 gives

$$\frac{\partial C'_g}{\partial t} = \left(\frac{D + \frac{2k_s}{r} D_s}{1 + \frac{2k_s}{r}} \right) \frac{\partial^2 C'_g}{\partial x^2} = D_1 \frac{\partial^2 C'_g}{\partial x^2} \quad (15)$$

Thus the growth of concentration in the gas phase follows Fick's law with a modified diffusion coefficient.

(20) A. E. Flood and R. H. Tomlinson, *Can. J. Research*, **B26**, 38 (1948).

(21) P. Carman and P. le Malherbe, *Proc. Roy. Soc. (London)*, **A203**, 55 (1950).

(22) P. Carman and F. A. Raal, *ibid.*, **A209**, 38 (1951).

(16) D. Hitchcock, *J. Gen. Physiol.*, **9**, 755 (1926).

(17) P. Carman, *Trans. Inst. Chem. Engrs.*, **15**, 150 (1937).

(18) E. Wicke and R. Kallenbach, *Kolloid Z.*, **97**, 135 (1941).

(19) R. Haul, *Angew. Chem.*, **62**, 10 (1950).

In the steady state the flux under the same conditions is obtained from

$$D \frac{\partial^2 C_g}{\partial x^2} + D_s \frac{\partial^2 C_s}{\partial x^2} = 0 \quad (16)$$

which gives for the flux dn/dt per unit area of cross section

$$\frac{dn}{dt} = -N \left(D + D_s \frac{2k_s}{r} \right) \frac{\partial C_g}{\partial x} = -N D_s \frac{\partial C_g}{\partial x} \quad (17)$$

(cf. eq. 9 and note that $\pi r^2 c = c_g$)

Surface Diffusion Coefficients.—The relations 6 and 7 ($L = k_2 l^2 / 6 D_1$ where D_1 is given by eq. (15) with $D = \frac{4r}{3} \sqrt{\frac{2RT}{\pi M}}$) leads after suitable rearrangement to⁵

$$D_s = D_1 \left\{ 1 - \frac{r}{2k_s} \left(\frac{L_1}{L_{He}} \sqrt{\frac{M_{He}}{M}} - 1 \right) \right\} \quad (18)$$

where L_{He} is the time lag for a non-sorbed gas such as helium (or neon) and M_{He} and M are the molecular weights of helium and of the sorbed gas, respectively. Accordingly, from k_2 , k_s , r , L_1 and L_{He} (or L_{Ne}) all of which quantities are accessible to direct measurement, the surface diffusion coefficients can be obtained. A careful study⁵ of the flow of H_2 , He, Ne, A, Kr, N_2 , O_2 , CH_4 and C_2H_6 , together with adsorption measurements, led to consistent values of D_s , and to the conclusion that in a "Vycor" porous glass membrane for which $r = 30 \times 10^{-8}$ cm. surface flow is comparable with gas phase diffusion for all the gases save H_2 , He and Ne.²³

A distinction was once more observed between the results derived from the time lag method above, and conclusions drawn from the steady state of flow. In the latter case the relative permeation velocities were very nearly always in the ratio of $1/\sqrt{M}$ where M denotes the molecular weight (Table III). This behavior is to be expected for pure gas phase diffusion, but not for surface and gas phase diffusion combined. The distinction arises from the limitation of the parallel capillary model which has been outlined earlier. Thus in building up the steady state there is creep of molecules into every crevice and blind pore in the system and it is this process which reveals surface diffusion. The total surface of the solid is involved during this stage in the flow and sorption processes. In the steady state permeation velocity on the other hand the crevices and blind pores play little or no part; moreover the bulk of the fluid is transported in the steady state by the comparatively few capillaries of greatest diameter provided these are continuous through the medium. For such capillaries surface diffusion will clearly be less important, compared with gas phase diffusion. In the steady state therefore surface flow may be obscured unless this flow is relatively great. A further example of the same distinction between the transient and the steady state of flow is given in the next section.

Separation of Mixtures.—Equation (15) can be integrated with the boundary conditions used for eq. (3). The quantity Q which has diffused through unit area of the bed in time t is then

(23) Since an account of this work is available elsewhere its fuller discussion will not be given here (Barrer and Barrie⁵).

$$Q = \frac{C_0 N \pi r^2 D_2}{k_2 l} \left(t - L_1 + \frac{12 L_1}{\pi} \sum_{n=1}^{\infty} \frac{(-1)^{n+1}}{n^2} \exp - \frac{D_1 n^2 \pi^2 t}{k_2^2 l^2} \right) \quad (19)$$

where $L_1 = k_2^2 l^2 / 6 D_1$ and D_1 and D_2 are defined by eq. (15) and (17). At any time $t = k L_1$ substitution in eq. (19) gives

$$Q = \frac{C_0 N \pi r^2 k_2 l}{6} \left(1 + \frac{2k_s}{r} \right) \left\{ k - 1 + \frac{12}{\pi^2} \sum_{n=1}^{\infty} \frac{(-1)^{n+1}}{n^2} \exp - \frac{n^2 \pi^2 k}{6} \right\} \quad (20)$$

The separation factor during the transient state of flow for two gases sorbed according to Henry's law is then

$$\rho = \left(\frac{Q}{C_0} \right)_1 / \left(\frac{Q}{C_0} \right)_2 = \frac{1 + \frac{2k_{s1}}{r}}{1 + \frac{2k_{s2}}{r}} \left\{ \frac{(k-1) + \frac{12}{\pi^2} \sum_{n=1}^{\infty} \frac{(-1)^{n+1}}{n^2} \exp - \frac{n^2 \pi^2 k}{6}}{\left(\frac{k L_1}{L_2} - 1 \right) + \frac{12}{\pi^2} \sum_{n=1}^{\infty} \frac{(-1)^{n+1}}{n^2} \exp - \frac{n^2 \pi^2 k L_1}{6 L_2}} \right\} \quad (21)$$

and L_2 now denotes the time lags for species 1 and 2 and k_{s1} and k_{s2} are the corresponding Henry's law sorption constants. For sufficiently large values of $t = k L_1$

$$\rho = \frac{\left(1 + \frac{2k_{s1}}{r} \right) L_2}{\left(1 + \frac{2k_{s2}}{r} \right) L_1} \quad (22)$$

However for the reason noted in the previous section surface diffusion tends to become more and more obscured as the steady state is approached, and so we would anticipate that eq. (21) will define the separation factors over the earlier transient stage, but that by the time the steady state is reached ρ is not given by eq. (22), but by $\sqrt{\frac{M_2}{M_1}}$.

This latter prediction is borne out by the experiments of Barrer and Barrie⁵ summarized in Table III.

TABLE III

Gas pair	Relative permeation rate (obsd at 292° K.)	Relative rate according to eq. (22)	Relative rate according to $\sqrt{M_2/M_1}$
He:Ne	2.29	2.33	2.25
CH ₄ :Ne	1.08	1.70	1.12
N ₂ :Ne	0.86	1.36	0.85
O ₂ :Ne	.77	1.25	.79
C ₂ H ₆ :Ne	.92	1.65	.82
Kr:Ne	.50	0.77	.49
H ₂ :Ne	2.85	2.83	3.17

The separation factors defined by eq. (21) suggest that over the early transient stage of Knudsen flow very marked fractionations of mixtures might occur. This is true of pairs of molecules of the same or nearly the same molecular weight, provided they are sorbed to different extents. The sorption and flow data of Barrer and Barrie for C_2H_6 and N_2 when applied to eq. (21) give the calculated separation factors of Table III over a

range of values of $t = kL_1$. The molecular weights are such that in absence of sorption effects there would be little fractionation of the gas mixture, but because of the differing sorptions marked transient state separations are in fact possible.

The separation of isotopic species can also be enhanced in the transient state, even where the adsorption of these species is identical. In absence of sorption effects one has

$$L_{H_2}:L_{HD}:L_{D_2} = 1.414:1.732:2.00$$

and in Table IV are given the separation factors in mixtures of $H_2 + HD$ and of $H_2 + D_2$. These are initially appreciably larger than is anticipated from the ratios $\sqrt{M_{HD}/M_{H_2}}$ or $\sqrt{M_{D_2}/M_{H_2}}$, but slowly approach these ratios as k increases. It should be noted however that the total amount of gas transmitted during the period of enhanced separation may be quite small.

The data for the system $O_2:CH_4$ are of interest, because the time lags for each gas are nearly the same (see below). According to eq. (21) therefore neither in transient nor in steady state will there be an appreciable change in the fractionation factor. The time lags and the Henry's law adsorption constants at 292°K., for the several gases referred to in Table IV diffusing in the "Vycor" porous glass membrane used²⁴ are given.⁵

TABLE IV
SEPARATION FACTORS ρ ACCORDING TO EQ. 21 FOR SEVERAL MIXTURES AT 292°K.

$N_2:C_2H_6$		$O_2:CH_4$		$H_2:HD$		$H_2:D_2$	
$k =$ t/LN_2	ρ	$k =$ t/LO_2	ρ	$k =$ t/LH_2	ρ	$k =$ t/LD_2	ρ
2.0	35.9	0.6	0.66	0.8	1.91	0.8	3.13
3.0	14.6	0.8	.66	0.9	1.84	0.9	3.12
4.0	7.32	1.0	.66	1.00	1.80	1.00	2.82
5.0	4.60	1.6	.66	1.10	1.74	1.10	2.66
6.0	3.37	1.8	.67	1.20	1.67	1.20	2.49
8.0	2.27	2.4	.67	1.30	1.63	1.30	2.41
10.0	1.78	5.0	.67	1.40	1.60	1.40	2.31
12.0	1.53	10.0	.69	1.50	1.56	1.50	2.21
14.0	1.37	15.0	.69	1.60	1.53	1.60	2.09
16.0	1.27	20.0	.69				
20.0	1.14	100	.69				
200	0.83	200	.69				

I am indebted to Dr. J. Barrie, for the calculations in Table IV.

(24) This membrane was 2.69 cm. thick and of 0.924 cm.² cross section.

	N_2	C_2H_6	O_2	CH_4	H_2	HD	D_2
Time lag, min.	39.5	260	44.7	43.7	4.2	5.15 ²⁴	5.93 ²⁴
Adsorption constant $\times 10^7$	5.04	52.5	5.16	7.94

(25) Calculated value assuming negligible sorption, from measured value for H_2 .

THE PERMEATION OF WATER AND ISOÖCTANE THROUGH PLUGS OF MICROSCOPIC PARTICLES OF CRUSHED QUARTZ¹

By R. T. JOHANSEN, P. B. LORENZ, C. G. DODD,² FRANCES D. PIDGEON AND J. W. DAVIS

Surface Chemistry Laboratory, Petroleum Experiment Station, U. S. Bureau of Mines, Bartlesville, Oklahoma

Received July 22, 1952

Some previous tests of the Kozeny-Carman equation have suggested that permeation of different liquids through the same porous medium follows different flow mechanisms. These anomalies often have been ascribed to the operation of "surface forces." The purpose of this work was to investigate the observed discrepancies by comparing specific surface areas calculated from different liquid permeability measurements, from gas adsorption and from microscopy. Four quartz-powder samples, sized to fall within particle-size ranges of 1 to 4 μ , 3 to 13 μ , 7 to 35 μ and 22 to 57 μ , respectively, were used in the experiments. The specific surface areas calculated from gas adsorption, water permeability and isoöctane permeability results decreased in the order given and differed by a nearly constant percentage for all powders. The difference between water and isoöctane results could be attributed largely to porosity differences. High porosities in isoöctane were produced by flocculation caused by the presence of a film of adsorbed water. Flocculation may alter the value of the Kozeny constant k_1 and since it makes porosity microscopically non-uniform, the Kozeny porosity function may be inapplicable. There is no evidence for a continuous immobile layer of the flowing liquid.

The nature of fluid flow through a porous solid medium has long been the subject of investigation³ and speculation, but the problem has not been satisfactorily solved. One particular difficulty, the role of special forces, often referred to as "surface forces," at the solid-liquid interface is incompletely understood. This paper describes an investigation of the nature of surface forces that affect the flow of water and isoöctane through compacted

beds of crushed quartz. Measurements of solid surface area presented to the flowing liquid have been employed as a tool to study flow mechanisms.

The Kozeny equation, as modified by Carman,^{3a} is widely used to predict the relation between permeability, porosity and the surface area of a porous medium. The equation is based on three separate assumptions, each of which is valid only within certain limits.

The first assumption is Darcy's law, which can be written in the simplest form³ as

$$V = KP \quad (1)$$

in which V is the volume rate of flow across a porous medium under a driving pressure P , and K is the permeability. It is recognized that this law is valid only in the range of viscous flow. The

(1) Presented before the twenty-sixth National Colloid Symposium which was held under the auspices of the Division of Colloid Chemistry of the American Chemical Society in Los Angeles, California, June 16-18, 1952.

(2) Continental Oil Co., Ponca City, Okla.

(3) (a) P. C. Carman, *Trans. Inst. Chem. Engrs. (London)*, **15**, 150 (1937); (b) R. R. Sullivan and K. L. Hertel, in "Advances in Colloid Science," E. O. Kraemer, Ed., Vol. 1, Interscience Publishers, Inc., New York, N. Y., 1942, p. 37.

criterion of viscous flow is Reynolds' number, which for porous media takes the form^{3a}

$$R = \rho V / \eta AS \quad (2)$$

where ρ and η are the density and viscosity of the liquid, and S is the surface area per unit bulk volume of the porous medium. It is found that equation (1) is obeyed when $R < 1$. The permeability shows an apparent decrease at higher values of R . A decrease has been reported¹ also for low values of R , supposedly because there are stagnant layers of liquid near the solid surface which are set in motion only at higher pressure gradients. However, the range of the reported measurements did not extend below about $R = 10^{-1}$, while other workers⁵⁻⁸ have extended the range down to $R = 10^{-6}$ without finding deviations from equation (1). Measurements are reported here which extend the range down to $R = 10^{-8}$.

The second assumption in the Kozeny-Carman equation is that the permeability can be separated into two factors, one depending only on the solid and one depending only on the fluid

$$K = \frac{K_0 A}{L} \times \frac{1}{\eta} \quad (3)$$

where K_0 is the "specific permeability" of the porous medium, A is the cross sectional area and L is the length. This relation has been tested and verified by permeation of fluids of different viscosities through the same porous medium.^{6,8,9-12} However, notable exceptions have been reported.^{5,11-14} Some anomalies have been shown to disappear when beds are thoroughly packed¹⁵ and when slip corrections are made for gas permeability.^{11,12} Other explanations have been: an immobile layer of liquid,¹⁶ slippage of liquids,¹⁷ swelling of the solid surface,^{18,19} and an electrokinetic effect.²⁰ Direct measurements of the electrokinetic effect²¹ indicate that it is too small to explain the discrepancies. The energy of inter-

action between liquid and solid would influence the other three suggested phenomena. In the present work, water and isoctane were selected as liquids having different viscosities and different energies of interaction with the quartz which was employed as the solid.²²

The third assumption of the Kozeny-Carman equation is

$$K_0 = \epsilon^3 / k S_0^2 = \frac{1}{k S_0^2} \frac{\epsilon^3}{(1 - \epsilon)^2} \quad (4)$$

where ϵ is the fractional porosity of the porous medium, S_0 is the surface area per unit volume of the solid phase and k is the Kozeny constant. We used the value 5.00 for the latter.² Equation 4 has been justified in many cases by studying K_0 as a function of ϵ when S_0 is constant,² or by using K_0 and ϵ to calculate S_0 and comparing with surface areas measured in other ways.^{3,23,24} However, when equation (4) is applied to irregular fine particles in beds of high ϵ , low values of S_0 are obtained²⁵ which increase systematically with decreasing porosity.^{26,27} Lea and Nurse discuss three possible reasons for this behavior: non-uniform packing, inadequacy of the porosity function, and variations in k . However, they note that results after different packing techniques are nearly the same.

We have tested equation (4) by measuring surface area by gas adsorption and particle counts under the light microscope and comparing with permeability areas. Permeability was measured while varying both S_0 and ϵ in turn, by using four different size fractions of powder, and by packing the finest powder fraction to several different degrees of compaction.

Experimental

Materials.—The quartz powders used were sized carefully by meshing, elutriation or sedimentation from commercially available crushed quartz powder. Table I gives the "mean projected diameters" and the ranges of size of the powder fractions.²⁸ After sizing, the powders were cleaned with hot chromic acid, rinsed copiously with deionized water, rinsed with reagent grade acetone and dried in an oven at 110°. The powders were reheated and cooled in a desiccator immediately before use.

TABLE I

MICROSCOPIC PARTICLE SIZE MEASUREMENTS

Powder designation	M-1	E-1	S-2	S-1
Mean projected diam., μ	43	24	7.9	2.3
Size range, μ	22-57	7-35	3-13	0.7-4.1

The water was distilled first from alkaline KMnO_4 . Just before use, this product was redistilled, which elimi-

(22) Cf. F. L. Howard and J. L. Culbertson, *J. m. Chem. Soc.*, **72**, 1185 (1950).

(23) J. C. Arnell, *Can. J. Research*, **24A**, 103 (1946); *ibid.*, **25A**, 191 (1947); J. C. Arnell and G. O. Henneberry, *ibid.*, **26A**, 29 (1948).

(24) C. G. Dodd, J. W. Davis and F. D. Pidgeon, *THIS JOURNAL*, **55**, 684 (1951).

(25) P. C. Carman, in "Symposium on New Methods for Particle Size Determinations in the Subsieve Range," American Society for Testing Materials, Philadelphia, Pa., 1941, p. 24.

(26) F. M. Lea and R. W. Nurse, *Trans. Inst. Chem. Engrs. (London)*, **25**, Supplement, "Symposium on Particle Size Analysis," p. 47 (1947).

(27) P. C. Carman and P. le R. Malherbe, *J. Soc. Chem. Ind. (London)*, **69**, 134 (1950); *J. Applied Chem. (London)*, **1**, 105 (1951).

(28) Complete size distributions and statistical calculations on the powder fractions are presented elsewhere.²⁹

(29) F. D. Pidgeon and C. G. Dodd, to be published.

(4) W. Siegel, Chap. XI of "Der Chemie Ingenieur," A. Eucken and M. Jacobs, Eds., Vol. I, Part II, Akademische Verlagsgesellschaft m.b.H., Leipzig, 1933.

(5) G. Bozza and I. Secchi, *Giorn. chim. ind. applicata*, **11**, 443, 487 (1929).

(6) G. H. Fancher, J. A. Lewis and K. B. Barnes, *Mineral Industries Exp. Sta. Bull.*, Penn. State College, **12**, 1933.

(7) O. E. Meinzer and V. C. Fishel, *Trans. Am. Geophys. Union*, **15**, Part II, 405 (1934).

(8) M. R. Hatfield, *Ind. Eng. Chem.*, **31**, 1419 (1939).

(9) E. Manegold, *Kolloid-Z.*, **81**, 269 (1937).

(10) P. C. Carman, *J. Soc. Chem. Ind.*, **57**, 225 (1938).

(11) L. J. Klinkenberg, in "Drilling and Production Practice 1941," American Petroleum Institute, New York, N. Y., 1942, p. 200.

(12) J. C. Calhoun and S. T. Yuster, in "Drilling and Production Practice 1946," American Petroleum Institute, New York, N. Y., 1947.

(13) H. B. Bull and J. P. Wronski, *THIS JOURNAL*, **41**, 463 (1937).

(14) L. Grunberg and A. H. Nissan, *J. Inst. Petroleum*, **29**, 193 (1943).

(15) P. J. Rigden, *J. Soc. Chem. Ind.*, **66**, 130 (1947).

(16) J. C. Henniker, *Revs. Modern Phys.*, **21**, 322 (1949).

(17) E. C. Bingham, "Fluidity and Plasticity," McGraw-Hill Book Co., Inc., New York, N. Y., 1929, p. 29.

(18) F. Fairbrother and H. Varley, *J. Chem. Soc.*, 1584 (1927); H. C. Hepburn, *ibid.*, 3163 (1927); D. Hubbard, E. H. Hamilton and A. N. Finn, *J. Research Natl. Bur. Standards*, **22**, 339 (1934).

(19) K. Mysels and J. W. McBain, *J. Colloid Sci.*, **3**, 45 (1948).

(20) G. H. Bishop, F. Urban and H. L. White, *THIS JOURNAL*, **35**, 137 (1931); H. L. White, B. Monaghan and F. Urban, *J. Gen. Physiol.*, **18**, 515 (1935); B. F. Ruth, *Ind. Eng. Chem.*, **38**, 564 (1946).

(21) P. B. Lorenz, to be published.

nated dissolved air that might form bubbles in the plug. The freshly distilled water had a pH of 7.1. After the water had passed through the plug, its pH had decreased to a value between 6.5 and 4.9, probably because acidic salts from the chromic acid treatment were being removed slowly. It was found that water permeability measured more than 5 days after distillation was not reproducible but became progressively lower. Such slow plugging with water has been noticed previously.¹⁹ It may be due to the growth of microorganisms not removed by prefiltration.

The "isoöctane" (2,2,4-trimethylpentane) was the purest grade obtainable from the Rohm & Haas Co. It was passed through a 3-foot column of commercial activated silica gel and distilled over sodium under an atmosphere of helium. The purified isoöctane was stored at 2 to 4° in tightly sealed glass jugs. Physical constants were determined after standing and compared with values reported by the National Bureau of Standards:²⁰ density at 25.00°, 0.6880 g./ml. (N.B.S., 0.68781 g./ml.); n_D^{20} 1.3914 (N.B.S., 1.39145).

Apparatus.—Figure 1 is a diagram of the apparatus. It was patterned after the design of Dodd, Davis and Pidgeon,²⁴ and improved for greater flexibility, precision and convenience. A wide range of pressures could be attained by using either mercury or the permeating liquid in the U-tube manometer. To avoid evaporation losses and meniscus corrections in the latter case, the overflow device was enclosed, and a manometer tube was attached on the low pressure side with the same diameter as the manometer tube on the high pressure side. The attachments on the overflow device were removable so that the cell could be safely vibrated.

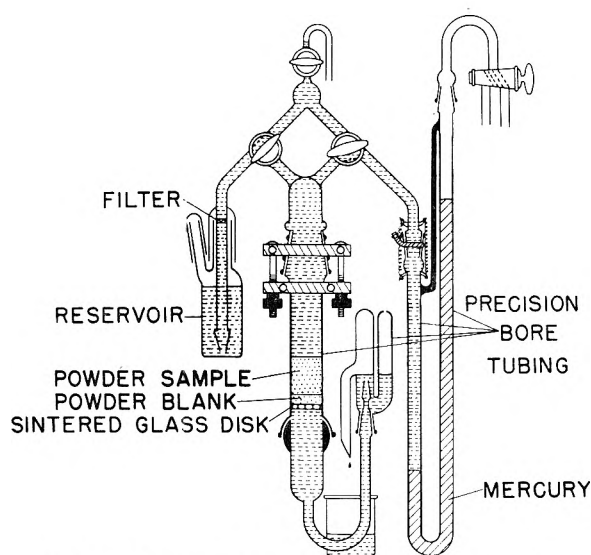


Fig. 1.—Apparatus for permeability measurements.

Danger of contamination and leakage was minimized by reducing the number of stopcocks and joints. They were lubricated with Apiezon M grease for water runs, with polyethylene glycol for isoöctane runs. Neither exhibited any detectable solubility in the liquid with which it was used.

The sintered-glass supporting disk was cemented with water glass, directly into the precision-bore tubing so that it was possible to measure the bottom of the plug accurately.

Formation of Plugs.—Using the vibrational method of Bartell and Albaugh,³¹ the powder plugs were formed in the cell which had been partly filled with liquid. An improved vibrator was designed,³² with belt drive and quality bearings mounted on a massive frame, so that extraneous vibrations were absent. The metering funnel was mounted directly on the shaker and modified, according to the size of the par-

ticles, to deliver the powder continuously over a period of 1 to 2 hours. With the finer powders a funnel with an annular opening formed by a round knob in the stem broke up agglomerates. The cell was turned in the shaker until the top of the bed was smooth and level. Obtaining a level top on the powder bed was not difficult when the plugs were packed in water, but in the case of the two finer-size fractions packed in isoöctane, it was necessary to level the tops of the beds with a flat metal plunger. The length of the packed plug was measured with a cathetometer at nine places around the cell to cancel out any slight irregularities or any deviation of the top of the plug from a plane parallel to the surface of the sintered disk. An arithmetical average of these measurements was used.

With the above procedure there was no difficulty in obtaining plugs of reproducible porosity in either water or isoöctane. However, ϵ became higher as the fineness of the powder increased, especially in isoöctane, where $\epsilon \approx 0.73$ for S-1. Also in isoöctane there was additional packing of the two finer powders during the initial stages of permeation with a mercury head. In this way S-1 powder could be packed to $\epsilon = 0.65$ and S-2 to $\epsilon = 0.60$. After this, plugs of the S-2 powder remained constant, but further high-pressure permeation of plugs of S-1 powder caused formation of channels. This was first indicated by an increase of permeability. Later the channels became large enough to be visible. It was found that plugs of the S-1 powder could be packed to porosities as low as 0.58 by pressing on the metal plunger. Permeabilities could be measured at any value of ϵ if very low driving pressures were used. High pressures caused channeling within the porosity range 0.60 to 0.68, but this was not observed with high pressures on either side of this range.

Permeability Measurements.—These were made according to formula 7 or formula 12 of Dodd, Davis and Pidgeon.²¹ Mercury was used in all water runs and in the isoöctane runs on S-2 powder. Isoöctane itself was the manometric liquid when it permeated the other powders. Three or more separate plugs of each powder were made successively and several determinations were made on each plug. When measurements had been completed on a plug the powder was carefully removed and a blank run was made on the disk alone. A blank run made before the plug had been formed was inaccurate because some powder always penetrated the disk and increased its resistance to flow.

Precision Analysis.—Combining formulas 1, 3 and 4

$$S_0 = \left[\frac{1}{k} \frac{A}{\eta K L} \frac{\epsilon^3}{(1 - \epsilon)^2} \right]^{1/2} \quad (5)$$

The formula for K has the form

$$K = \frac{\text{const.}}{t} \ln \frac{h_0}{h} \quad (6)$$

in which t is time, h is fluid head across the plug and $h = h_0$ at $t = 0$. Porosity is calculated from

$$1 - \epsilon = W/DAL \quad (7)$$

where W is the weight of the powder and D is the density of the solid. From these formulas we find

$$\frac{W}{S_0} \times \frac{\partial S_0}{\partial W} = -\frac{3 - \epsilon}{2\epsilon} \quad (8)$$

$$\frac{A}{S_0} \times \frac{\partial S_0}{\partial A} = \frac{3 - \epsilon}{4\epsilon} + \frac{1}{2} \quad (9)$$

$$\frac{L}{S_0} \times \frac{\partial S_0}{\partial L} = \frac{3 - \epsilon}{4\epsilon} - \frac{1}{2} \quad (10)$$

$$\frac{D}{S_0} \times \frac{\partial S_0}{\partial D} = \frac{3 - \epsilon}{4\epsilon} \quad (11)$$

$$\frac{1}{S_0} \times \frac{\partial S_0}{\partial h} = -\frac{1}{2h \ln(h_0/h)} \approx -\frac{e}{2h_0} \quad (12)$$

The second of equation (12) is based on the fact that the constant of equation (6) is most accurately determined when $h_0/h = e$ (base of natural logarithm). Using $\ln \eta = C/T$, where T is absolute temperature

$$\frac{1}{S_0} \frac{\partial S_0}{\partial T} = \frac{C}{2T^2} \quad (13)$$

Table II gives the per cent. error in S_0 caused by estimated errors in individual measurements, using formulas (8) to (13).

(30) F. D. Rossini, K. S. Pitzer, W. J. Taylor, J. P. Ebert, J. E. Kilpatrick, C. W. Beckett, M. G. Williams and H. G. Werner, *Natl. Bur. Standards (U.S.), Circ.*, C461, 40 (1947).

(31) F. E. Bartell and F. W. Albaugh, in "Fundamental Research on Occurrence and Recovery of Petroleum, 1946-47," American Petroleum Institute, New York, N. Y., 1949, p. 81.

(32) The authors are grateful to Mr. H. C. Hamontre of this station for valuable advice in redesigning the vibrator.

TABLE II
PRECISION ANALYSIS OF PERMEABILITY METHOD

	Maximum error in measurement	Per cent. error in S_0	
		Water and $\epsilon = 0.40$	Isoöctane and $\epsilon = 0.60$
W , %	0.15	0.5	0.3
A , %	0.4	0.8	6
L , %	1	1.1	5
D , %	2	3	
h , cm.	0.01	0.07	0.7
T , °C.	0.2°	0.2	1

W was obtained from the loss in weight of the metering funnel. The largest error was the weight of the unused powder, which gained weight from atmospheric moisture. In control measurements on the S-1 powder, the gain was less than 0.5% of the remaining powder. The plug was formed in precision bore tubing, $A = 5.067 \text{ cm.}^2 \pm 0.4\%$. The variation of A for different plugs was virtually zero. The uncertainty in L was about 0.04 cm., so all plugs were made at least 4 cm. long to reduce the relative error. The value of D for quartz at 25° is 2.649 g./cc.³³ The possibility of swelling, mentioned earlier, probably does not occur in isoöctane,³⁴ but it may occur in water. The 2% error in the table is estimated for the S-1 powder and corresponds with a layer 100 Å. thick with density intermediate between quartz and water. Fluid head was measured with the cathetometer. The error in Table II is calculated for $h_0 = 20 \text{ cm.}$, which was the smallest initial fluid head. The temperature was measured with a calibrated thermometer and maintained at $25 \pm 0.2^\circ$ by means of an air thermostat. Values of η for isoöctane were interpolated from values³⁵ at 20 and 30°.

Gas Adsorption Measurements.—Specific surface areas of the S-1 and S-2 powders were measured by the BET method, using nitrogen at 78 to 82°K.³⁶ and an apparatus designed and calibrated for precise volumetric and manometric measurements.³⁷ Surface areas of the E-1 and M-1 powders were measured by the adsorption of krypton³⁸ in a low pressure apparatus incorporating a calibrated multiple range McLeod gage. Comparison of nitrogen and krypton measured areas on the S-1 and S-2 powders justified the use of 19.5 Å.² as the cross-sectional area of the adsorbed krypton molecule.

Microscopic Measurements.—Microscopic surface area measurements were made by the improved projected area method of Pidgeon and Dodd²⁹ employing Fairs comparison eye-piece graticules,³⁹ and the relation between particle surface area and the projected area of randomly mounted particles.⁴⁰⁻⁴²

Results

As in previous work using the pressure decline technique,²⁴ the slopes of the plots, which were proportional to the permeability, were constant within 1%, even though the Reynolds number, R , declined during a single run by a factor as high as 10, as shown in Table III. The table also gives average values of K_0 , ϵ , "mean hydraulic radius"¹²

(33) R. B. Sosman, "The Properties of Silica," Chemical Catalog Co. (Reinhold Publ. Co.), New York, N. Y., 1927, chap. 18.

(34) W. R. Ruby and R. P. Loveland, *THIS JOURNAL*, **50**, 345 (1946).

(35) E. B. Evans, *J. Inst. Petroleum Tech.*, **24**, 321 (1938).

(36) S. Brunauer, P. H. Emmett and E. Teller, *J. Am. Chem. Soc.*, **60**, 309 (1938); P. H. Emmett, in "Advances in Colloid Science," E. O. Kraemer, Ed., Interscience Publishers, Inc., New York, N. Y., 1942, p. 1.

(37) W. E. Barr and V. J. Anhorn, "Scientific and Industrial Glass Blowing and Laboratory Techniques," Instruments Publishing Co., Pittsburgh, Pa., 1949, chap. XII.

(38) R. A. Beebe, J. B. Beckwith and J. M. Honig, *J. Am. Chem. Soc.*, **67**, 1554 (1945).

(39) G. L. Fairs, *Chemistry and Industry*, **62**, 374 (1943).

(40) F. B. Kenrick, *J. Am. Chem. Soc.*, **62**, 2838 (1940).

(41) F. V. Tooley and C. W. Parmelee, *J. Am. Ceram. Soc.*, **23**, 304 (1940).

(42) V. Vouk, *Nature*, **162**, 329 (1948).

of the pores, $\epsilon^2[S_0(1 - \epsilon)]$, and S_0 for each liquid and from gas adsorption and microscopy. Figure 2 shows the relation between the four measurements of S_0 by plotting each against the gas-adsorption area. It is seen that S_0 determined by the graticule, projected area method becomes unreliable for the S-1 powder, because of technical difficulties.²⁹ The plots of water and isoöctane areas are strikingly linear, which indicates that, for any given liquid, surface areas measured by the permeability method are quite as self-consistent as those obtained by gas adsorption.

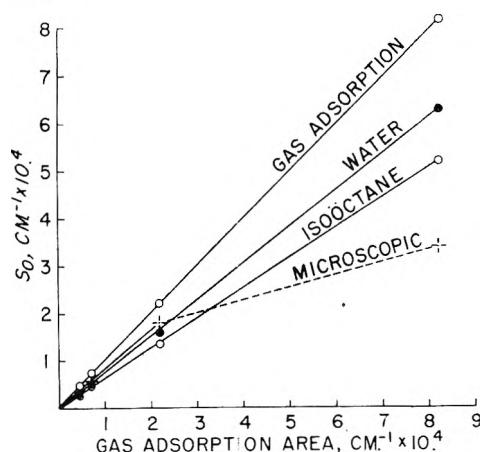


Fig. 2.—Comparison of surface areas.

Nevertheless, there is an absolute difference between gas adsorption, water and isoöctane areas that should be examined. Higher values of S_0 from gas adsorption may be expected, since gas molecules can penetrate blind surface cracks inaccessible to flowing liquid. The difference between surface areas measured by water and by isoöctane, which might appear to contradict the second assumption of the Kozeny-Carman equation (equation (3)) depends somewhat on the fact that eq. (4) does not completely account for the effect of changes in porosity on permeability. In Fig. 3 the calculated surface area of S-1 powder is plotted as determined at various values of ϵ . The relation between calculated S_0 and ϵ is similar to that found for *air* permeabilities by Carman and Malherbe, some of whose data are plotted on the same scale for comparison. If the plot obtained with isoöctane is extrapolated to the porosity at-

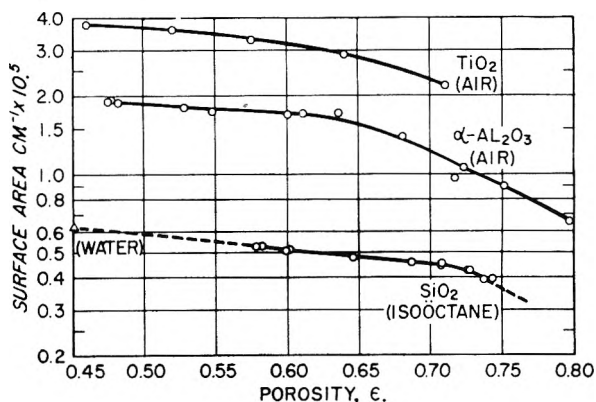


Fig. 3.—Apparent surface areas at different porosities.

TABLE III
 SUMMARY OF EXPERIMENTAL RESULTS

		Reynolds number $k \times 10^6$		Specific permeability, millidarcys ⁴³	Porosity	Mean hydraulic radius, μ	Specific surface area, m. ² /cm. ³		Microscopy
		Min.	Max.				Perm.	Gas adsn.	
M-1	H ₂ O	20	200	458	0.41	2.3	0.296 ± 0.010	0.47	0.32
	C ₈ H ₁₈	6	30	542	.42	2.7	.272 ± .003		
E-1	H ₂ O	6	20	112	.38	1.2	.508 ± .010	0.73	0.55
	C ₈ H ₁₈	6	10	266	.44	1.7	.454 ± .001		
S-2	H ₂ O	0.1	1	17	.40	0.4	1.58 ± .03	2.24 ± 0.02	1.9
	C ₈ H ₁₈	10	90	150	.60	1.1	1.35 ± .02		
S-1	H ₂ O	0.002	0.006	1.5	.45	0.13	6.30 ± .01	8.22 ± .08	3.4
	C ₈ H ₁₈	0.05	0.06	8.3	.59	.28	5.21 ± .01		

tained with water, the "isoöctane area" is found to be identical with the "water area."

No systematic comparison of S_0 at various ϵ 's was made for the coarser powders. It is found that when surface areas of the S-2 and E-1 powders are plotted against the porosities on the coordinates of Fig. 3, the lines connecting water and isoöctane points have approximately the slope of the straight part of the plot for the S-1 powder. With M-1 powder the porosities were not very different when permeability was measured with water and with isoöctane, yet there is still a difference of 5% in the calculated surface areas "corrected" to the same porosity.

Discussion

Our results support previous observations that equation (4) is inadequate. Beds of our finer powders in isoöctane with large ϵ and low S_0 had all the properties of flocculated sediments listed by workers who have studied the variations of sedimentation volumes of particles in different liquids.⁴⁴ The major factor that causes variations is the presence of surface active impurities.⁴⁵ In dealing with non-polar liquids and hydrophilic solids, water is a surface active impurity. It causes large ϵ by binding the particles together in relatively large flocs and may exclude isoöctane from contact with some of the surface, making the measured values of S_0 low. If the flow is mostly around a floc rather than through its pores, flocculation effectively produces large irregular "particles" and probably would cause variations in the Kozeny constant, k , as the porosity changed.

Rapid flow in flocculated beds probably displaces whole flocs, which causes compression by allowing them to pack more efficiently, or causes channeling by leaving holes.

Rigden has emphasized that, in beds of flocculated powders, ϵ is microscopically non-uniform. In this case the experimentally determined ϵ lacks physical significance and the porosity function, $\epsilon^3/(1 - \epsilon)^2$, is inapplicable. When the flocs are so closely packed by manual compression that

the pore space within the flocs and the space between the flocs are equal, the liquid probably flows past all of the particles and gives the most accurate value for the surface area. This technique was used by Rigden,¹⁵ and Carman and Malherbe,²⁷ who state that "permeabilities should give a low value of S_0 at high porosities, but should give correct values if the plug is compressed into the normal range, . . . and S_0 showed a strong tendency to become constant for $\epsilon < 0.6$." Although constant values of S_0 were never reached with the S-1 powder, Carman and Malherbe show curves for some carbon blacks which do level off and give constant values of S_0 . This means that eq. (4) is valid within the "normal range" of porosities.

Nevertheless, it is probable that no packing technique can eliminate the influence of flocculation on bed structure and on k . This factor is probably responsible for the difference at identical ϵ between water and isoöctane areas. Our results support this conclusion in several ways. The flow mechanism remains unaltered down to the lowest values of Reynolds' number for each liquid. Either swelling of quartz in water, or a continuous immobile film of liquid near the solid surface would give high apparent S_0 (cf. equations (5) and (11)). But permeability areas are lower than gas adsorption areas. Considering the probable accuracy of our results, any immobile film cannot be thicker than a few per cent. of the mean hydraulic radius of our finest pores (0.13 micron for water and 0.26 micron for isoöctane). These results agree with precise measurements of other workers,⁴⁶ who concluded that no such immobile layer exists thicker than about 0.02 to 0.1 micron. Of course, it must be concluded that there is stagnant liquid in minute surface cracks in the quartz particles if the difference between areas by gas adsorption and water permeability is real, and not due to an unfortunate choice of assumed values for k and the area of the adsorbed nitrogen molecule. Table II also indicates that any swelling of quartz cannot exceed 0.02 micron. If there were any slippage of either liquid at the interface with quartz, it would give low apparent S_0 . The agreement between permeability and microscopy for areas of the coarser powders, for which the latter measurements are probably accurate, indicates that slippage is also negligible, as previously concluded by Bingham.¹⁷ Evidently

(43) M. Muskat, "Physical Principles of Oil Production," McGraw-Hill Book Co., Inc., New York, N. Y., 1949, p. 130.

(44) W. D. Harkins and D. M. Gans, *THIS JOURNAL*, **36**, 86 (1932); C. R. Bloomquist and R. S. Shutt, *Ind. Eng. Chem.*, **32**, 827 (1940); W. Gallay and I. E. Puddington, *Can. J. Research*, **21B**, 171 (1943).

(45) H. J. Dawe, Thesis, University of Michigan (1941); P. Tanamushi and S. Tomatsu, *Bull. Chem. Soc. Japan*, **17**, 23 (1942); K. L. Wolf and D. Kuhn, *Angew. Chem.*, **63**, 277 (1951); cf. E. K. Fischer and D. M. Gans, in Vol. VI of Alexander's "Colloid Chemistry," Reinhold Publ. Corp., New York, N. Y., 1946, p. 310.

(46) R. Bulkley, *J. Research Natl. Bur. Standards*, **6**, 89 (1931); S. H. Bastow and F. P. Bowden, *Proc. Roy. Soc. (London)*, **A151**, 220 (1935).

surface forces have a negligible influence on permeability and equations 1 and 3 are justified.

It should be pointed out that our results on permeability to water and a hydrocarbon contradict those of Bozza and Secchi,⁵ which are often quoted to illustrate that surface forces influence permeability. Since they measured ϵ only in water, a porosity correction is impossible.

For dimensionally stable and chemically inert systems, such as water or isoöctane and quartz, permeation follows the Kozeny-Carman law when the porosity of the packed bed is uniform enough to result in liquid flow over all the particle surface.

This condition might have been achieved had it been possible to produce beds formed in isoöctane without flocculation. The condition apparently was realized in the water permeability results described above.

DISCUSSION

A. L. McCLELLAN.—I wonder if it would be possible to run one of these permeations using liquid nitrogen?

R. T. JOHANSEN.—I don't know! We had enough trouble using water and isoöctane.

A. L. McCLELLAN.—I wonder if nitrogen were used, would the areas be more comparable to the BET areas?

R. T. JOHANSEN.—I don't feel qualified to answer this.

CAPILLARY RISE OF WATER IN SOILS UNDER FIELD CONDITIONS¹

BY GEORGE JOHN BOUYOUCOS

Soil Science Department, Michigan State College, East Lansing, Michigan²

Received July 22, 1952

A new electrical resistance method was developed which makes possible a continuous measurement of the soil moisture content of soils under field conditions. This method was applied to the study of the capillary rise of water in soils under controlled field conditions. It proved to be very successful and practical. The results obtained show that where excessive rainfall did not cause the water tables to rise to wet the soil by close proximity, there was practically no capillary rise from the water tables to the upper soil horizons which had a high moisture gradient and a tension gradient. There was also very little movement of water from the wetter to the drier soil layers above. It is concluded that capillary movement of water from the water tables supplies little, if any, water to the plants during a season of growth. The roots of plants, accordingly, have to go to the water, which they accomplish with greater ease and rapidity than capillarity can bring it to them. Capillarity is important in supplying plants with water only through very short distances.

Introduction

Capillary rise of water in soils has received a great deal of study on the part of soil investigators. It can probably be said, that this study has been motivated principally by two practical objectives: (1) to determine the role of capillarity in lifting and supplying water to the growing plants; and (2) to determine the role of capillarity in the loss of soil water by evaporation. The primary practical issues involved have been: (1) under what soil conditions does capillarity lift water to the root zones, or to the surface soil; (2) from what probable depths; (3) at what rate; and (4) in what quantity.

Theoretically, it can be readily demonstrated that, given unlimited time, capillarity can lift water to great heights. For example, Keen,³ using the well known equation for height of capillary rise ($h = 2T/gDr$), calculated the following theoretical heights of rise of water in ideal soils: fine gravel, $\frac{1}{3}$ foot; coarse sand, 1.5 feet; fine sand, 7.5 feet; coarse silt, 31.25 feet; fine silt, 150 feet; and clay, over 150 feet. In practice, however, the larger magnitudes of capillary rise have never been observed, either in the laboratory or in the field.

It can also be readily demonstrated that, having a constant water table and short columns of soil with continuous water films, very large amounts of

water can be pumped to the surface by capillarity.⁴

Under actual field conditions, however, it has not been as easily and generally demonstrated that there is a significant capillary rise of water either from the water tables, or from the wetter soil horizons to the drier surface soil horizons. As a result, there has been considerable difference of opinion as to the practical importance of capillary rise of water in field soils. For example, the earlier soil investigators, who leaned heavily on the capillary tube hypothesis (which emphasizes distance rather than rate) attributed great importance to the capillary rise of water in field soils.

This view is typically illustrated by McGee⁵ who estimated that in the great plains 6 inches of water annually are brought to the surface by capillarity from a depth of 10 feet. On the other hand, Alway and McDole,⁶ Moore,⁷ Bodman and Colman,⁸ and the Rothamsted Experiment Station in England,⁹ found that the upward movement of water, caused by capillarity after the water content of soils falls below field capacity, is of no practical significance. Romistroff,¹⁰ of Russia, states that water which penetrates beyond 16 to 20 inches does not return to the surface except by the way of the plant roots. Results obtained by the Roth-

(4) F. H. King, *U. S. Geol. Surv. Ann. Rpt.* 19, Part 2, 92 (1897-1898).

(5) W. J. McGee, *U. S. Dept. Agr. Bur. Soils Bull.*, 93 (1913).

(6) F. J. Alway and G. R. McDole, *J. Agr. Research*, 9, 27 (1917).

(7) R. E. Moore, *Hilgardia*, 12, 383 (1939).

(8) G. B. Bodman and E. A. Colman, *Soil Sci. Soc. Am. Proc.*, 8, 116 (1943).

(9) Rothamsted Expt. Sta., *J. Agr. Soc.*, 31, 454 (1941).

(10) W. G. Romistroff, "Das Wesen der Dürre," *Steinkopf, Dresden*, 1926.

(1) Presented before the twenty-sixth National Colloid Symposium which was held under the auspices of the Division of Colloid Chemistry of the American Chemical Society in Los Angeles, California, June 16-18, 1952.

(2) Contribution from the Soil Science Department of the Michigan Agricultural Experiment Station, East Lansing, Michigan. Authorized for publication by the Director as Journal article No. 1371.

(3) B. A. Keen, *Trans. Faraday Soc.*, 17, 228 (1922).

amsted Experiment Station,⁹ tend to substantiate Romistoff's claim.

A serious handicap in the study of capillary rise or movement of water in soils under field conditions, has been the lack of a suitable method. Until a few years ago, the only method that was available, was the conventional oven dry method, which consisted of taking a soil sample, drying it, and calculating its moisture content. This method not only consumed time and energy but was also misleading in studying soil movement in soil of non-uniform texture. For example, if soil samples were collected at different dates from the same field and if the samples varied in texture, any difference in moisture content noted, would more likely be due to differences in texture than to movement of moisture.

In an effort (at the Michigan State College) to find a more suitable method to measure soil moisture in the field, the plaster of Paris electrical resistance method was devised.¹¹ This method makes it possible to take a continuous measurement of soil moisture electrically. It utilizes two units, a small porous absorbent block made of plaster of Paris¹² and a modified Wheatstone bridge or ohmmeter. Inside the block are two parallel electrodes with leads. Such a block, when buried in the soil becomes part of the soil. It absorbs moisture from the soil and gives it up to the soil very readily, so that its moisture content tends to stay in constant equilibrium with the moisture content of the soil. In fact, this block involves

the principle of capillarity. The electrical resistance of the block varies with its moisture content and that in turn varies with the moisture content of the soil in which it is buried. Therefore, by calibration, the moisture content of the soil may be determined by measuring the electrical resistance of the block. Figure 1 shows the relationship between the electrical resistance of the block and the total moisture content of the soil.

The key to the success of this block lies in the fact that the electrodes are covered or imbedded in the plaster of Paris. This gives the block a constant environment so that errors arising from differences in soil compaction, texture, structure, soil type and electrical lines of force, are eliminated or minimized. Only units with such internal electrodes have been successful in measuring soil moisture under field conditions. Units with external electrodes have proven unsuccessful. This accounts for the unsuccessful attempts that have been made in the past, to apply the electrical resistance principle to soil moisture measurements.

A very important aspect of this electrical resistance method is that it actually measures moisture tension. Its effective range is from field capacity, or 500 ohms, to approximately 2,000,000 ohms. In the soil moisture free energy concept, this represents the equivalent range of tension from 0.3 atmosphere of pressure to 20 atmospheres of pressure. On the basis of this free energy concept, different soils at any given electrical resistance level hold their water with the same force or tension. For example, at 3,000 ohms resistance a clay and a sandy soil hold their respective water with the same force or tension. This means, then, that a sandy soil containing 8% of water at 3,000 ohms is just as wet as a clay soil containing 30% of water at the same electrical resistance level.

This being the case, the electrical resistance method is able to detect movements of moisture in field soils, even though the soils are heterogeneous and not uniform in texture. This represents a marked advantage over the gravimetric method, whose accuracy is greatly affected by soil textural differences.

Referring again to Fig. 1 there are two soil moisture constants illustrated. These constants are important in a discussion of capillarity. The first, is the permanent wilting point. This constant falls on the curve at about 100,000 ohms resistance. The permanent wilting point represents the moisture content in soils at which plants wilt and die. The tension with which the water is held at the wilting point is equivalent to about 16 atmospheres of pressure.

The second soil moisture constant is field capacity. It falls on the curve at 500 ohms resistance. Field capacity is the moisture a field soil contains about 3 days after it has been soaked by rain or irrigation, the excess water has drained away and evaporation has been prevented. Field capacity is the maximum amount of water a soil can retain under normal field conditions. At field capacity the water is held by the soil with a tension equivalent to 0.3 atmosphere of pressure.

It is of interest to note that the water which

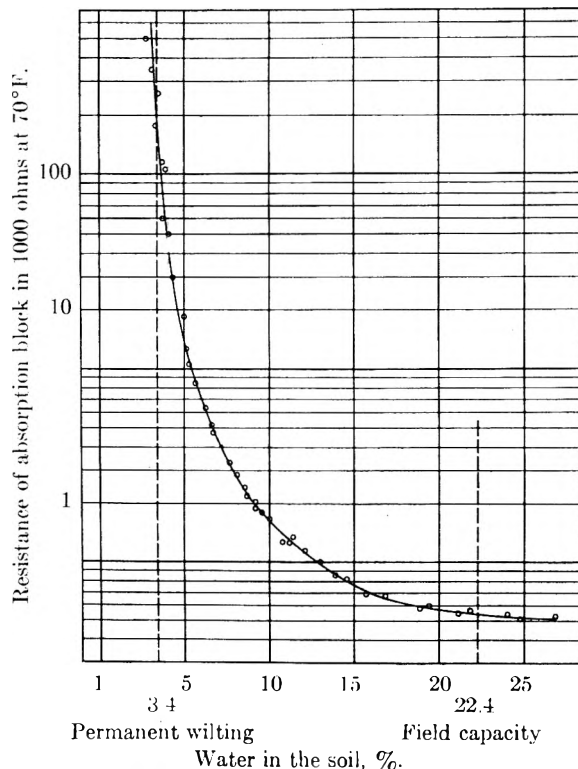


Fig. 1.—Relationship between block resistance and soil moisture content.

(11) G. J. Bouyoucos and A. H. Mick, *Soil Sci.*, 63, 455 (1947).

(12) A nylon unit also has been developed. Its principle is the same as that of the plaster of Paris block, but it lasts much longer in the soil, is more sensitive and measures a greater range of soil moisture.

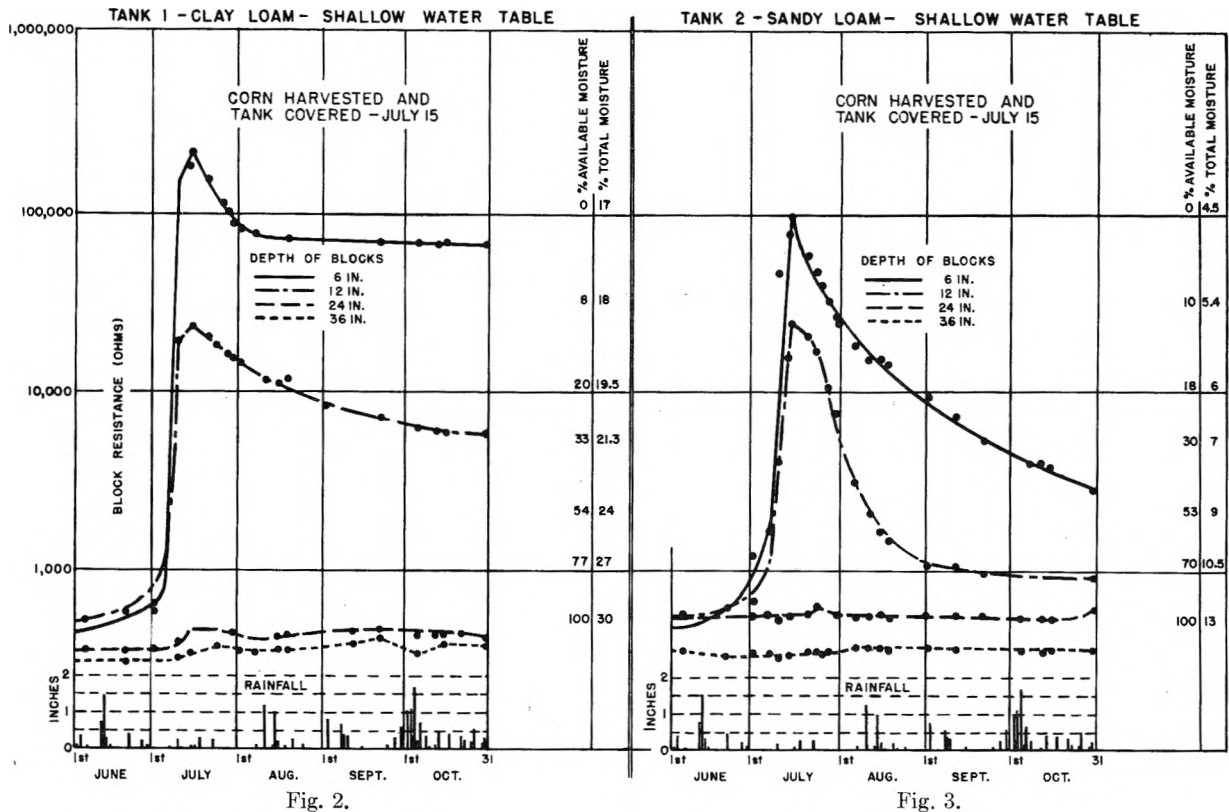


Fig. 2.

Fig. 3.

the plants use for their growth is that which falls in the range between the field capacity and the wilting point. This range is called the capillary water available for plants.

Procedure.—It was realized from the outset that the plaster of Paris electrical resistance method provided an improved means of studying the capillary rise of water in soils. Accordingly, the method was applied to the study of the problem.¹³

The general procedure was: (1) grow corn in the soil to reduce its moisture content to different values at the various depths and thus create a moisture gradient, and consequently a tension gradient from the surface to a depth of 36 inches; (2) harvest the corn; (3) cover the soil to protect it from rainfall and prevent loss of moisture by evaporation; and (4) study the movement of moisture by the plaster of Paris electrical resistance method. The plaster of Paris blocks were placed in the soil at 6, 12, 24 and 36 inches depth and left there permanently. The soil had previously been screened and mixed and was, therefore, very uniform in texture. There were three different types of soil used. Each soil was contained in metal tanks 3 by 3 feet without bottom or top, but having water-tight sides. The tanks were sunk in different fields, or locations, having shallow to very deep water tables.

Experimental Results

The experiment was continued over a period of six years. In this paper, the results of only one year are presented. However, they are typical. They are shown in Figs. 2 to 7. These figures also show the rainfall and the calibration of the soils in terms of per cent. of available water and total water.

It is readily seen from these graphs that, by the time the corn was harvested, a very marked and variable moisture gradient had been created at the various depths in practically all soils. Remembering that 100,000 ohms resistance represents the wilting point, it will be noted that the moisture

content was reduced in some soils, from the wilting point at 6-inch depth to field capacity at 36 inches; while in other soils, it was reduced from beyond the wilting point at 6 inches to the wilting point at 36 inches. In other words, the maximum range of electrical resistance varied from 500 ohms to about 1,000,000 ohms. In terms of the soil moisture free energy concept, this represented a tension gradient equivalent from 0.3 atmosphere of pressure to 18 atmospheres of pressure. This was a very marked tension gradient and provided a wide range to show the movement of moisture from one level to another.

However, an examination of the moisture curves reveals that, with the exception of one case (Fig. 3, sandy loam, shallow water table), there was no appreciable capillary rise of water from the water tables to the upper drier layers of soil, even though the 36 inches depth of some soils was at field capacity or higher. Consider for example Fig. 6: the soil at 36 inches remained at field capacity or higher, and yet no water rose to wet even the neighboring 24 inches depth, during a period extending from July 15 to October 31.

Not only was there no appreciable upward capillary rise of water from the water tables, but there was also no significant movement of water from the wetter soil layers to the drier layers above. For example, the 24 inch depth was nearly always wetter than the 6 and 12 inch depths, and yet there is hardly any indication that water moved from the 24 inch to the 6 and 12 inch layers above.

The sandy loam in Fig. 3 shows that an upward capillary rise of water did take place in this soil. It must be stated here, that in sandy loams there was a strong tendency for capillary rise to take place

(13) G. J. Bouyoucos, *Soil Sci.*, 64, 71 (1947).

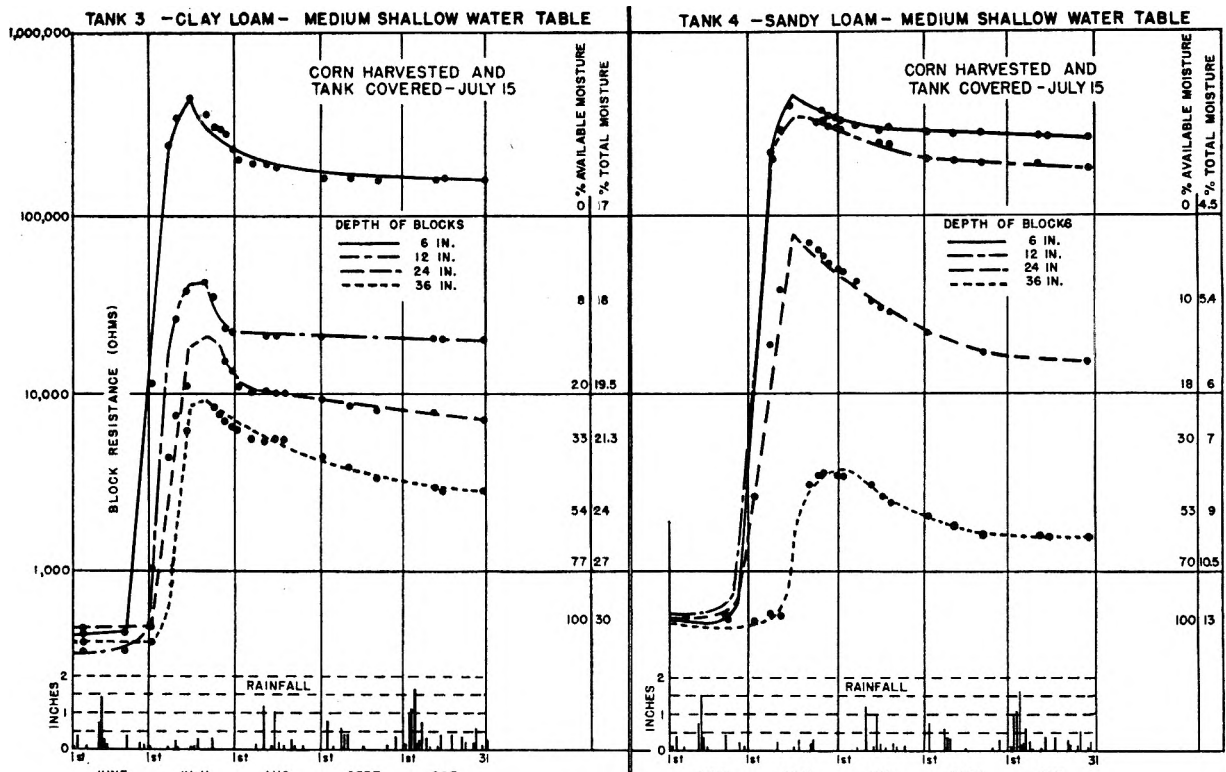


Fig. 4.

Fig. 5.

when the water table was shallow. This is to be expected in view of the less friction capillary rise encounters in coarser textured soils.

The results of this investigation point to the conclusion, therefore, that where excessive rainfall did not cause the water table to rise to wet the soil

by close proximity, there was practically no capillary rise from the water tables to the upper horizons of soil which had a high moisture gradient and tension gradient. The only evidence that there was a capillary rise was in the case of sandy loam with shallow water table.

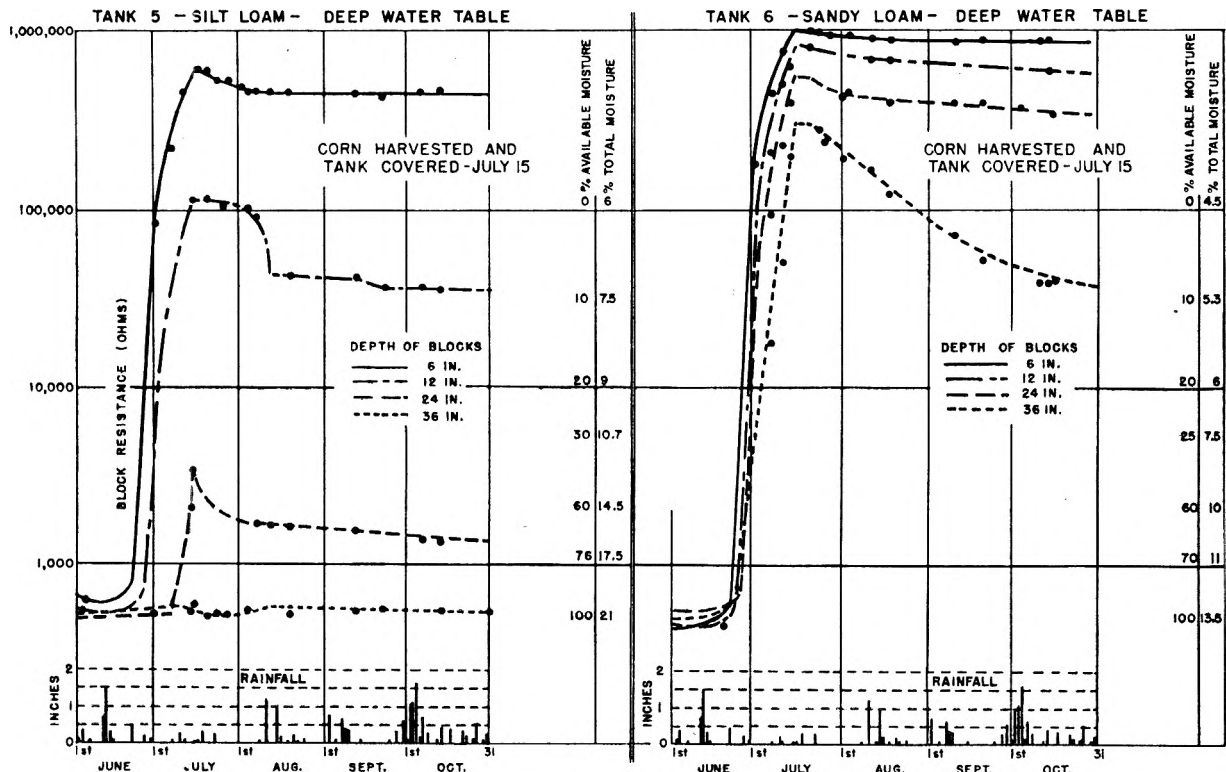


Fig. 6.

Fig. 7.

Discussion

The results obtained in this investigation on the capillary rise of water in soils appear quite logical in the light of our present knowledge of soil moisture relationships.

Capillary conductivity is fundamentally controlled by the tension gradient which acts as the driving force in the movement of water. In actual practice, however, and especially under field conditions, this tension gradient is beset with many difficulties and its force may be opposed or counterbalanced by various soil factors. Among the most important of these factors are the following.

(1) The tenacity with which the water is held by the soil increases with an increase in the moisture tension. This increase of tenacity and tension begins to operate from as high a moisture content as field capacity, which is the maximum amount of water soils can retain under normal field conditions. Movement of water as free energy increases is bound to become extremely slow or non-operative.

(2) Even where there is free water, as is the case in a water table, capillary rise of water can be tremendously impeded by: (1) the friction of the capillaries to the passage of water; (2) the translocation and swelling of soil colloids with the consequent clogging of the capillary pores; (3) the water films and capillary pores becoming dis-

continuous; and (4) capillary pores becoming filled with entrapped air.

From the standpoint of the plants, rate of movement is more important than distance of movement. This is because the water requirements of plants are immediate, large and continuous. While in time, water may rise to considerable distances in the soil, the rate of rise is too slow to benefit the immediate and large demands of the plants for water. The conclusion is, therefore, that capillary movement of water, especially from the deeper water tables, supplies little, if any, water to the growing plants during the short season of growth. Actually, the water that is the greatest determining factor in plant growth, is that which the soil is able to retain from rainfall and irrigation, or the available capillary water. The roots of plants, therefore, search for this water, which they find with ease and rapidity. In this connection it is of interest to note the astounding rate and extent of root growth that plants make in a single season. Dittmer¹⁴ has estimated that a single rye plant under favorable conditions develops as a seasonal total, a root surface, including root hairs, of 6875 square feet and a total root length of 387 miles, carrying 6603 miles of root hairs. The average daily increase of root lengths alone was estimated at more than 3 miles. Capillarity is of importance in supplying plants with water only through very short distances and in small amounts.

(14) H. J. Dittmer, *Am. J. Botany*, 24, 417 (1927).

WETTING CHARACTERISTICS OF CELLULOSE DERIVATIVES.

II. INTERRELATIONS OF CONTACT ANGLES^{1,2}

By B. ROGER RAY³ AND F. E. BARTELL

Contribution from the Department of Chemistry, University of Michigan, Ann Arbor, Michigan

Received July 22, 1952

The wetting characteristics of several cellulose derivatives were determined by measuring the advancing and receding angles of contact formed upon them by each of four different water-organic liquid pairs. In general, the angle of contact measured through the water phase was found to increase as the length and number of substituted side chains increase in the cellulose derivatives. Hysteresis of contact angle of considerable magnitude was shown to occur in all systems studied. Calculations based upon contact angle equations taking into account this hysteresis effect indicate (1) that the water advancing contact angle of a given solid-water-organic liquid system, θ_{sw}^* , is closely related to the water advancing contact angle, θ_{swa}^* , of the corresponding solid-water-air system and to the organic liquid receding contact angle, θ_{soa}^* , of the corresponding solid-organic liquid-air system; and (2) that the factors responsible for hysteresis effects in the two solid-liquid-air systems appear to continue to be operative in the solid-liquid-liquid system, so that equations can be combined in such a way as to cancel out these factors. Consequently, one can postulate modified Bartell-Osterhof equations as follows: $\gamma_{wa} \cos \theta_{swa}^* - \gamma_{oa} \cos \theta_{soa}^* = \gamma_{wo} \cos \theta_{swo}^*$ and similarly $\gamma_{wa} \cos \theta_{swa}^* - \gamma_{oa} \cos \theta_{soa}^* = \gamma_{wo} \cos \theta_{lwo}^*$. When these formulations were applied to each of the fairly large number of systems studied, it was found that the observed and the calculated interfacial contact angles were in good agreement.

Many of the substituted derivatives of cellulose have properties particularly suited for wetting studies. They can be obtained in satisfactory purity and can be formed into smooth films, foils

and fibers which have readily reproducible and stable surface properties. They have low free surface energies and can be classed as typical soft solids; that is, adsorptive effects appear to be at a minimum and finite and measurable contact angles in air are produced on them with several organic liquids as well as with water. Although several of these polymers are of great technical interest, there is scant information available on their wetting characteristics.

It was deemed worthwhile to make a study of each of the three systems of contact angles, solid-water-air, solid-organic liquid-air, and solid-

(1) Presented before the twenty-sixth National Colloid Symposium which was held under the auspices of the Division of Colloid Chemistry of the American Chemical Society in Los Angeles, California, June 16-18, 1952.

(2) The data in this paper were taken from a portion of a thesis of B. Roger Ray, submitted to the School of Graduate Studies of the University of Michigan in partial fulfillment of the requirements for the Ph.D. degree, December, 1945.

(3) Minnesota Mining and Manufacturing Co. Fellow, 1943-1945. Present address: Chemistry Department, University of Illinois, Urbana.

water-organic liquid, on the surfaces of each of a number of cellulose derivatives, using derivatives of known composition with surfaces prepared in known and reproducible manners. In addition to establishing correlations between wetting behavior and the physical and chemical characteristics, it was hoped that quantitative interrelationships could be shown among the three contact angle systems. Significant hysteresis effects were found to occur on these solids, *i.e.*, two characteristic contact angles were found for each system depending upon whether, in the formation of the angle, a given liquid phase had been caused to advance or to recede over the solid surface.

The first contribution⁴ of this series presented the results pertaining to the contact angles of water and of several different organic liquids upon the solids in air. Correlations were found between wetting and chemical properties (degree of substitution and nature of substituent group) and also between wetting and the physical properties (degree of polymerization, density, tensile strength and mode of formation of the surface). The present contribution gives the results obtained with the interfacial contact angles of water against organic liquids upon portions of the same samples of derivatives.

Experimental Details

Measurement of Contact Angles.—The interfacial contact angles were measured by the vertical-rod, the vertical-plate, the tilting-plate or the controlled-drop-volume method depending upon the form of the solid surface under study. Details of these methods, as well as other details of measurements, have previously been given.

All the solid-water-organic liquid systems studied gave finite and reproducible angles except systems in which the particular organic liquid caused swelling or a partial dissolving of the solid. The initially formed angles quickly reached constant values which remained unaltered for the observation period of 10 to 30 minutes. The reproducibility was good, the average deviation of the individual measurements being about $\pm 1^\circ$. Each solid was placed in contact with the first liquid, *i.e.*, the liquid which was to be receded, two minutes before the angle was formed by displacing this liquid with the second liquid. The surface properties of a sample appeared to be the same whether the sample was freshly prepared or had been subjected to two years of exposure to laboratory air.

The contact angles, both the angles in air and the interfacial angles, were usually found to be significantly different on the opposite sides of foils of the derivatives. These foils had been cast from concentrated solutions spread on metal plates then later stripped after evaporation of the solvent. It was necessary, therefore, to distinguish between the data obtained on each of the two sides of a foil.

Mutually saturated pairs of liquids were used for the contact angle measurements. Water had a negligible solubility and a negligible effect upon the surface tensions of the organic liquids used. Likewise, these organic liquids had little effect upon the surface tension of water, as can be seen from Table I. As reported previously⁴ the various solid-water-air contact angles were the same, within the accuracy of the measurements, for pure water as for water saturated with any one of the organic liquids.

Materials.—As has been stated, for the interfacial measurements reported herein portions of the same samples of the cellulose derivatives were used as were used for the previously reported measurements in air.⁴ Information was given in the previous report as to the sources, methods of synthesis and compositions of the solid materials.

The carefully purified liquids were stored in dark bottles over activated silica gel. The methylene iodide discolored slightly when exposed to light and the last traces of surface-

active contaminants could be removed from the bromobenzene only by repeated treatments with silica gel. The water used was freshly redistilled. It was stored in Pyrex bottles and was delivered by siphon from the interior of the liquid. The surface and interfacial tension values of the liquids are given in Table I. The values shown in columns 2 and 4 were used in the calculations to follow.

TABLE I
SURFACE TENSIONS OF PURE LIQUIDS AND OF WATER SATURATED WITH ORGANIC LIQUIDS; INTERFACIAL TENSIONS OF WATER AND ORGANIC LIQUIDS
Temperature $25 \pm 0.1^\circ$

Liquids	Surface tension of liquid, γ_{la}^a , dynes/cm.	Surface tension of water satd. with org. liquid, $\gamma_{w'a}^a$, dynes/cm.	Interfacial tension, γ_{wo} , dynes/cm.
Water	72.1		
Methylene iodide	50.2	71.6"	48.0
α -Bromonaphthalene	44.0	70.6"	41.6
α -Chloronaphthalene	41.9"		40.5"
Heptane	19.8	70.2"	50.8"
Bromobenzene	35.9	71.3"	38.4

^a Values are from the literature

Results

Experimental Data.—In Table II are given the observed values of the interfacial contact angles formed on surfaces of the derivatives by several water-organic liquid pairs. For each system the advancing angle, θ_{swo}^a , and the receding angle, θ_{swo}^r , are given, as well as the hysteresis effect, $\Delta\theta$.⁵ Values enclosed in parentheses indicate systems in which swelling effects were observed but in which the angles did not change appreciably with time. Values enclosed in parentheses and with an arrow, designate cases of swelling or softening in which the angles did change more or less slowly with time, finally reaching the stable values recorded in Table II.

Each of the four derivatives studied in the form of a foil had been produced on commercial equipment by flowing a 20% solution onto a metal roll and evaporating the mixed solvents.⁴ It cannot be said with certainty which side in each case had solidified in contact with air. The two sides are therefore distinguished in the tables merely as sides A and B. For comparison a film of Acetate-FM2 was formed on a glass rod from a 20% solution in acetone-ethanol-chloroform. The "air-side" of this film was found to have wetting characteristics more like side A of the foil than of side B, but significantly different than either.

The films of the fatty acid triesters were formed by coating glass rods from 10% chloroform solutions. The evaporation rate and humidity were controlled and finally the coated rods were heated at 70° for three hours.

Both the advancing and receding interfacial angles increased in magnitude with increase in the organophilic character of the derivatives, *i.e.*, water wet the solids progressively less as the

(5) The subscripts s, l, a, w and o stand for solid, liquid, air, water and organic liquid, respectively. γ represents tension values and θ the contact angle. All contact angles were measured through the water phase. The superscript a or r is used with θ to denote an advancing or receding condition, again with respect to the water phase for interfacial systems.

TABLE II
INTERFACIAL CONTACT ANGLES OF WATER AND ORGANIC LIQUIDS ON SURFACES OF CELLULOSE DERIVATIVES

Cellulose derivative	Methylene iodide			α -Bromonaphthalene			Bromobenzene			Heptane		
	θ_{sw}^a	θ_{sw}^r degrees	$\Delta\theta$	θ_{sw}^a	θ_{sw}^r degrees	$\Delta\theta$	θ_{sw}^a	θ_{sw}^r degrees	$\Delta\theta$	θ_{sw}^a	θ_{sw}^r degrees	$\Delta\theta$
Acetate-FM2												
Foil, Side A ^a	111	67	44	106	69	37	119.5	64.5	55	105	50	55
Foil, Side B ^a	105	59	46	105	55	50	115	46	69	104	44	60
Film	103	70	33									
Triacetate												
Film	101.5	81	20.5	106	82	24	113	81	32			
Acetopropionate-II												
Foil, Side A	119	77.5	41.5	128	80	48	122.5	75	57.5	114	75	39
Foil, Side B	116	69	47	124.5	65	59.5	123	56	67	110	53	57
Tripropionate												
Film	120	84.5	35.5	(180)	(120)		(180)	(180)		154	133.5	20.5
Acetobutyrate-II												
Foil, Side A	127	83	44	131	86	45		79		112	70	42
Foil, Side B	128	80	48	128	74	54	141.5	72.5	69	110	67.5	42.5
Tributyrate												
Film	138	100	38									
Tricaprate												
Film	(145)	(123.5)	21.5									
Ethyl cellulose-II												
Foil, Side A	121	65.5	55.5	(180)	(105)			(71.5)		129.5	67.5	62
Foil, Side B	118	58	60				(180)	(68.5)		123	65	58

^a The system cellulose acetate-water- α -chloronaphthalene gave angles of 110° and 67.5° for side A and 104.5° and 54° for side B. The $\Delta\theta$ values were then 42.5 and 50.5°, respectively.

length and number of substituted side chains increased. Although there were large individual deviations, the contact angles increased in the approximate order of acetate, triacetate, acetopropionate, ethyl cellulose, acetobutyrate, tripropionate, tributryate and tricaproate. The solid-water-air contact angles measured in the earlier work were found to increase approximately in this same order.

Theoretical Considerations

When a liquid drop rests upon a solid surface there will exist about the line of intersection a balance of interfacial tension forces resulting in a definite angle of contact. The relative magnitudes of these different tensions determine the magnitude of the angle of contact of the liquid. For an ideal case the interrelationships can be expressed by the Young equation which for a solid-liquid-air (or vapor) system is

$$\gamma_{sa} - \gamma_{sl} = \gamma_{la} \cos \theta_{sla} \quad (1)$$

This equation holds for a system in true equilibrium and can be applied with assurance only to a system in which the surface of the solid is perfectly plane and homogeneous in character and in which the tension (or the free surface energy) of each interface remains constant. Very few, if any, systems have been studied which were of certainty in a condition of true equilibrium, unique for the system.

For practically every system studied including solid-liquid-air (or vapor) and solid-liquid-liquid systems two characteristic angles, an advancing angle and a receding angle, were obtained. Moreover, angles (at least temporarily stable) of any value between these limiting values could have been obtained. Such effects have been referred to as "hysteresis" effects and the actual difference in

the measured angles themselves has been called "hysteresis of the contact angle."

Two factors most generally responsible for "hysteresis of the contact angle" are: (1) surface roughness and (2) changes in the interfacial tension relationships.

(1) **Surface Roughness.**—If a surface is not perfectly plane and homogeneous hysteresis effects of considerable magnitude may be obtained. For rough surfaces the magnitude of the apparent hysteresis appears to be largely dependent upon the slopes of the sides of the asperities on the surface which cause the roughness.^{6,7} The cellulose derivatives studied had very smooth surfaces and possible roughness effects have not been considered.

(2) **Changes in Interfacial Tension Relationships.**—Consider the case of a liquid drop, say water, on a solid with a second fluid phase present. The interfacial tension between water and the other fluid phase will at all times remain constant. Nevertheless, the contact angle, measured through water, is larger when the water drop is caused to advance than when the water drop is caused to recede. This difference in angle value can be explained by assuming that the tension of water against solid or the tension of the other fluid against solid, or both, do not remain the same for a receding drop as for an advancing drop. One or both of the solid-fluid interfacial tensions must have become altered by movement of the drop. Perhaps this alteration may have occurred only in the area immediately adjacent to the drop periphery where water advances over a solid previously in contact with organic liquid but recedes over solid previously in contact with water. The distance over

(6) B. Roger Ray and F. E. Bartell, *J. Colloid Sci.*, in press.

(7) F. E. Bartell and J. W. Shepard, *This Journal*, **57**, Feb. (1953).

No Hysteresis—Ideal System

Solid-liquid-air systems

$$\begin{aligned} \gamma_{sa} - \gamma_{sw} &= \gamma_{wa} \cos \theta_{s'wa} = A_{s'wa} \\ \gamma_{sa} - \gamma_{so} &= \gamma_{oa} \cos \theta_{s'oa} = A_{s'oa} \end{aligned}$$

Subtracting (3) from (2)

$$\gamma_{so} - \gamma_{sw} = A_{s'wa} - A_{s'oa}$$

Solid-liquid-liquid system

$$\gamma_{so} - \gamma_{sw} = \gamma_{wo} \cos \theta_{s'wo} = A_{s'wo}$$

Therefore, from (4) and (5)

$$A_{s'wa} - A_{s'oa} = A_{s'wo}$$

also

$$\gamma_{wa} \cos \theta_{s'wa} - \gamma_{oa} \cos \theta_{s'oa} = \gamma_{wo} \cos \theta_{s'wo}$$

Water Advancing

Case I. Hysteresis—Simplified Actual System^a

Solid-liquid-air system

$$\begin{aligned} \gamma_{sa} - \gamma_{sw} &= \gamma_{wa} \cos \theta_{s'wa} = A_{s'wa}^a \\ \gamma_{sa} - \gamma_{so} &= \gamma_{oa} \cos \theta_{s'oa} = A_{s'oa}^a \end{aligned}$$

(3a) from (2a)

$$\gamma_{so} - \gamma_{sw} + (\gamma_{sa} - \gamma_{sa}^a) = A_{s'wa}^a - A_{s'oa}^a$$

Solid-liquid-liquid systems

$$\gamma_{so} - \gamma_{s'w} = \gamma_{wo} \cos \theta_{s'wo} = A_{s'wo}^a$$

or, adding and subtracting γ_{sw}

$$\gamma_{so} - \gamma_{sw} + (\gamma_{s'w} - \gamma_{s'w}^a) = A_{s'wo}^a$$

from (4a) and (5a')

$$A_{s'wa}^a - A_{s'oa}^a - (\gamma_{sa} - \gamma_{sa}^a) = A_{s'wo}^a - (\gamma_{s'w} - \gamma_{s'w}^a)$$

(6)

(7)

Water Receding

Solid-liquid-air systems

$$\begin{aligned} \gamma_{sa}^r - \gamma_{s'w}^r &= \gamma_{wa} \cos \theta_{s'wa}^r = A_{s'wa}^r \\ \gamma_{sa}^r - \gamma_{so}^r &= \gamma_{oa} \cos \theta_{s'oa}^r = A_{s'oa}^r \end{aligned}$$

(3r) from (2r)

$$\gamma_{so}^r - \gamma_{s'w}^r + (\gamma_{sa}^r - \gamma_{sa}^r) = A_{s'wa}^r - A_{s'oa}^r$$

Solid-liquid-liquid systems

$$\gamma_{so}^r - \gamma_{s'w}^r = \gamma_{wo} \cos \theta_{s'wo}^r = A_{s'wo}^r$$

or, adding and subtracting γ_{so}

$$\gamma_{so}^r - \gamma_{s'w}^r + (\gamma_{so}^r - \gamma_{so}^r) = A_{s'wo}^r$$

from (4r) and (5r')

$$A_{s'wa}^r - A_{s'oa}^r - (\gamma_{sa}^r - \gamma_{sa}^r) = A_{s'wo}^r - (\gamma_{so}^r - \gamma_{so}^r)$$

(6r)

Case II. Hysteresis—Actual System^a

Solid-liquid-air systems

$$\begin{aligned} \gamma_{sa} - \gamma_{s'w}^a &= \gamma_{wa} \cos \theta_{s'wa}^a = A_{s'wa}^a \\ \gamma_{sa}^a - \gamma_{so} &= \gamma_{oa} \cos \theta_{s'oa}^a = A_{s'oa}^a \end{aligned}$$

(11a) from (10a)

$$(\gamma_{so} - \gamma_{s'w}^a) + (\gamma_{sa} - \gamma_{sa}^a) = A_{s'wa}^a - A_{s'oa}^a$$

or

$$(\gamma_{so} - \gamma_{sw}) + (\gamma_{s'w} - \gamma_{s'w}^a) + (\gamma_{sa} - \gamma_{sa}^a) = A_{s'wa}^a - A_{s'oa}^a$$

(12a')

Solid-liquid-liquid system

Same as (5a')

From (12a') and (5a')

$$A_{s'wa}^a - A_{s'oa}^a - (\gamma_{s'w} - \gamma_{s'w}^a) - (\gamma_{sa} - \gamma_{sa}^a) = A_{s'wo}^a - (\gamma_{s'w} - \gamma_{s'w}^a)$$

(13a)

^a s'^w represents solid-water interface, solid previously in contact with air. s'^o represents solid-organic liquid interface, solid previously in contact with water. s'^a represents solid-air interface, solid previously in contact with organic liquid. s'^w represents solid-water interface, solid previously in contact with organic liquid.

$$\begin{aligned} \gamma_{sa} - \gamma_{s'w} &= \gamma_{wa} \cos \theta_{s'wa} = A_{s'wa}^r \\ \gamma_{sa} - \gamma_{so} &= \gamma_{oa} \cos \theta_{s'oa} = A_{s'oa}^r \end{aligned}$$

(11r) from (10r)

$$(\gamma_{s'o} - \gamma_{s'w}) + (\gamma_{sa} - \gamma_{sa}^r) = A_{s'wa}^r - A_{s'oa}^r$$

or

$$(\gamma_{s'o} - \gamma_{sw}) + (\gamma_{s'o} - \gamma_{so}) + (\gamma_{sa}^r - \gamma_{sa}^r) = A_{s'wa}^r - A_{s'oa}^r$$

(12r')

Solid-liquid-liquid system

Same as (5r')

From (12r') and (5r')

$$A_{s'wa}^r - A_{s'oa}^r - (\gamma_{s'o} - \gamma_{s'o} - \gamma_{so}) - (\gamma_{sa}^r - \gamma_{sa}^r) = A_{s'wo}^r - (\gamma_{s'o} - \gamma_{so})$$

(13r)

which alteration occurred would be relatively unimportant. The alteration may be caused by sorption or by layer formation effects. In the present investigation the cellulose derivatives used were chosen because they had low free surface energies and were not expected to exhibit marked sorptive or layer formation effects. Nevertheless, since hysteresis of contact angle of considerable magnitude occurred on the surface of each cellulose derivative, possible sorption and layer effects cannot be disregarded.

Calculations.—If no hysteresis of contact angle occurred at a given solid surface, the three Young equations for the solid-water-air, solid-organic liquid-air and solid-water-organic liquid systems could be used without modification. It has been shown⁸ that these unmodified equations can be combined into a single expression containing only directly measurable quantities for systems in which all three contact angles are finite and measurable. Where hysteresis does occur it is necessary to take into consideration both advancing and receding angles and any alteration of surface and interfacial tensions which may occur as the various liquids advance or recede. Combination of these three more complicated equations gives a complicated equation containing unmeasurable quantities. Nevertheless, the development outlined below, together with the data obtained, will show factors operating to cause hysteresis in the solid-liquid-air systems appear to remain operative in the corresponding solid-liquid-liquid system and to cancel out in the combined equation. Therefore, even in the case of the complicated actual system the simple combined equation can be used to calculate from two measured angles the remaining unmeasured angle of the system and this calculation will be in good agreement with an actual measurement of this third angle.

In the parallel table columns are given the related Young equations shown with advancing and receding angle symbols and with primes and ⁺s denoting probable modification of tensions caused by liquid action on the solid in the actual system. In order to demonstrate the development as clearly as possible a simplified actual system, case I, is first considered, followed by a consideration of the more complicated actual case II. In both cases I and II, no alterations are indicated in the surface or interfacial tensions of the liquids since for the liquids used those tensions were shown to remain practically unaltered during the experiments.

In case I it is postulated that there is no alteration in the interfacial tension solid-liquid for liquid drops on the solid in air whether the drop is advanced or receded. The forces causing hysteresis in the solid-liquid-air systems are considered to be due solely to the alteration of the solid-air tension in the area of solid just uncovered by a receding liquid.

In the actual systems measured, as will be shown by the data given below, it was found that in fact

$$A_{swa}^a - A_{soa}^a = A_{swo}^a \quad (6a')$$

(8) F. E. Bartell and H. J. Osterhof, *Colloid Symposium Monograph*, 5, 113 (1927).

also

$$A_{swa}^r - A_{soa}^a = A_{swo}^r \quad (6r')$$

and also, therefore, that

$$\gamma_{wa} \cos \theta_{swa}^a - \gamma_{oa} \cos \theta_{soa}^a = \gamma_{wo} \cos \theta_{swo}^a \quad (7a)$$

and

$$\gamma_{wa} \cos \theta_{swa}^r - \gamma_{oa} \cos \theta_{soa}^a = \gamma_{wo} \cos \theta_{swo}^r \quad (7r)$$

That is, there is in fact, in the actual systems, a correlation between the three angles of contact.

If the equations (6a) and (6r) for Case I, the simplified actual system, could be considered to be correct, it would mean that

$$\gamma_{sa} - \gamma_{sa}'' = \gamma_{sw} - \gamma_{sw}'' \quad (8)$$

and also that

$$\gamma_{sa}' - \gamma_{sa} = \gamma_{sa}' - \gamma_{sa} \quad (9)$$

That is, the modification of tension at the solid surface caused by recession of a given organic liquid or of water on a given low surface tension solid in air is practically the same as the modification caused by recession of the same liquid on the same solid in the corresponding two-liquid system.

The greatest difficulty encountered in any attempt to explain modification of the solid surface by recession of a liquid in a simplified system such as that postulated in Case I is that the effect would often be to raise the tension at the surface rather than to lower it. The adhesion tension of water advancing on acetate FM2, foil side B (see Table III) is 34.9 dynes/cm., while the adhesion tension of water receding on this solid is 62.3 dynes/cm. From equations (2a) and (2r) we would have $\gamma_{sa} - \gamma_{sw} = A_{swa}^a = 34.9$ dynes/cm., and $\gamma_{sa}' - \gamma_{sw} = A_{swa}^r = 62.3$ dynes/cm. Since in our simplified system we have postulated that in the area under the drop the tension, γ_{sw} , does not change, and that the difference in the systems shall be considered to be due entirely to the difference between the tension at the unmodified solid surface in air, γ_{sa} , and the tension at the surface in air modified by having been previously covered by water, γ_{sa}' , it follows in this case that

$$\gamma_{sa} - \gamma_{sa}' = -27.4 \text{ dynes/cm.}$$

which means that the water in receding has left a surface with a tension 27.4 dynes/cm. higher than that of the original unmodified surface.

It seems quite likely that in the actual solid-liquid-air system the interfacial tension solid-liquid would be different for water advancing over a solid previously covered by air and for water receding over a solid previously covered by water. Therefore, it seems likely that the more complicated equations of Case II more nearly represent the facts. Using equations (10a) and (10r) of Case II and the data for water advancing and receding on acetate FM2, foil side B, we would have

$$\gamma_{sa} - \gamma_{sa}' = A_{swa}^a = 34.9 \text{ dynes/cm.}$$

and

$$\gamma_{sa}' - \gamma_{sa} = A_{swa}^r = 62.3 \text{ dynes/cm.}$$

or

$$(\gamma_{sa} - \gamma_{sa}') - (\gamma_{sa}' - \gamma_{sa}) = -27.4 \text{ dynes/cm.}$$

In this case we would not have to postulate a rise in any tension when water receded. Both changes

TABLE III
EXPERIMENTAL AND CALCULATED VALUES OF THE INTERFACIAL ADHESION TENSIONS FOR WATER AND ORGANIC LIQUIDS
ON CELLULOSE DERIVATIVES

System	System in air				Interfacial system (water advanced) adhesion tension, dynes/cm.		Interfacial system (water receded) adhesion tension, dynes/cm.	
	Contact angle, degrees		Adhesion tension, dynes/cm.		Exper., A_{swo}^a	Calcd., A_{swo}^a	Exper., A_{swo}^r	Calc., A_{swo}^r
	θ_{s1a}^a	θ_{s1a}^r	$(\gamma_{1a} \cos \theta_{s1a}^a)$	$(\gamma_{1a} \cos \theta_{s1a}^r)$	$(\gamma_{wo} \cos \theta_{swo}^a)$	$(A_{swo}^a - A_{s1a}^a)$	$(\gamma_{wo} \cos \theta_{swo}^r)$	$(A_{swo}^r - A_{s1a}^r)$
Acetate-FM2, foil, side A								
Water	64	40	31.5	55.1				
Methylene iodide	40	18	38.4	47.6	-17.2	-16.1	18.7	16.7
α -Bromonaphthalene	28	6	39.1	43.8	-11.6	-12.3	14.9	16.0
α -Chloronaphthalene	25	0	37.9		-13.8		15.5	17.2
Bromobenzene	11	0	35.2		-18.9		16.6	19.9
Acetate-FM2, foil, side B								
Water	61	30	34.9	62.3				
Methylene iodide	42	20	37.2	47.2	-12.4	-12.3	24.7	25.1
α -Bromonaphthalene	28	6	39.1	43.8	-10.8	-8.9	23.8	23.2
α -Chloronaphthalene	26.5	0	37.5		-11.1		23.8	24.8
Bromobenzene	12.5	0	35.0		-16.2		26.7	27.3
Acetate-FM2, film								
Water	64	42	31.5	53.5				
Methylene iodide	44	33	36.5	42.2	-10.8	-10.7	16.4	17.0
Triacetate, film								
Water	67.5	52	27.6	44.4				
Methylene iodide	47	39.5	34.2	38.7	-9.6	-11.1	7.4	10.2
α -Bromonaphthalene	33.5	24	36.7	40.2	-11.4	-12.6	5.8	7.7
Bromobenzene	7	0	35.3		-15.0		6.0	9.1
Acetopropionate-H, foil, side A								
Water	74	53	19.9	43.3				
Methylene iodide	49	31	32.9	43.0	-23.2	-23.1	10.4	10.4
α -Bromonaphthalene	34	20	36.5	41.4	-25.6	-21.5	7.2	6.8
Bromobenzene	17	0	34.1		-25.9		9.9	9.2
Acetopropionate-H, foil, side B								
Water	72	40	22.3	55.2				
Methylene iodide	46	25	34.8	45.0	-21.0	-22.7	17.2	20.4
α -Bromonaphthalene	28	6	38.9	43.8	-23.6	-21.5	17.6	16.3
Bromobenzene	8	0	35.4		-20.9		21.5	19.8
Tripropionate, film								
Water	79	69.5	13.8	25.2				
Methylene iodide	65	41.5	21.2	37.6	-24.0	-23.8	4.6	4.0
Acetobutyrate-H, foil, side A								
Water	76	53.5	17.4	42.8				
Methylene iodide	46	21	34.8	46.8	-28.9	-29.4	5.7	8.0
α -Bromonaphthalene	32	8	37.3	43.6	-27.3	-26.2	2.9	5.5
Bromobenzene	13	0	35.1				7.4	7.7
Acetobutyrate-H, foil, side B								
Water	75.5	48.5	18.0	47.7				
Methylene iodide	43	17	36.6	47.9	-29.5	-29.9	8.4	11.1
α -Bromonaphthalene	23.5	11	40.3	43.2	-25.6	-25.2	11.5	7.4
Bromobenzene	14	0	34.6		-30.0		11.5	13.1
Tributyrate, film								
Water	87	74	3.7	19.9				
Methylene iodide	60	37.5	25.1	39.8	-35.6	-36.1	-8.4	-5.2
Ethyl cellulose-H, foil, side A								
Water	80	47	12.6	49.1				
Methylene iodide	57	37	27.3	40.2	-24.7	-27.6	19.9	21.8
Ethyl cellulose-H, foil, side B								
Water	74	44	19.9	51.8				
Methylene iodide	59	30	26.3	43.5	-22.5	-23.6	25.4	25.5

could represent a lowering of tensions, the lowering at the solid-water interface being more pronounced than the lowering at the solid-air interface, so that the resultant tension at the solid-air interface would be the greater when the water receded, and consequently, since the tension water-air remains unchanged, the receding solid-water-air angle would be smaller than the advancing solid-water-air angle.

In spite of the complications and the at present unmeasurable quantities introduced into equations (13a) and (13r) of Case II, the fact remains that experimental evidence indicates that equations (6a') and (6r'), and (7a) and (7r) do hold. Therefore, it would still be indicated that the complicated factors responsible for hysteresis in the three separate angle systems do cancel out in the combined equation. That is, it is indicated that

$$[(\gamma_{sw} - \gamma_{s'w}) + (\gamma_{sa} - \gamma_{s'a})] = (\gamma_{sw} - \gamma_{s'w}) \quad (14)$$

$$[(\gamma_{s'o} - \gamma_{s'o'}) + (\gamma_{s'a} - \gamma_{s'a'})] = (\gamma_{s'o} - \gamma_{s'o'}) \quad (15)$$

Differences in solid-water-organic liquid angles obtained on different cellulose derivatives reflect variations in the energy terms. On cellulose acetate (and triacetate) the solid-water-organic liquid angles of the four water-organic liquid combinations were not greatly different from one another. On the tripropionate the water-methylene iodide angles were much lower than the water-heptane angles, while on the more polar esters (acetate, acetopropionate and acetobutyrate) the water-methylene iodide angles were somewhat higher than the water-heptane angles. An interpretation of these trends in terms of the interfacial energies of the systems would be as follows: As the hydrocarbon character of a derivative becomes dominant, the interfacial energy of the solid-water interface becomes relatively higher while the interfacial energy of the solid-heptane interface becomes relatively lower, and the interfacial contact angle (measured through water) tends, therefore, to become greater. Because of the polar nature of the methylene iodide the comparable solid-methylene iodide interface will be at a higher energy level and the interfacial angle will in this case tend to be smaller than for the heptane system.

Experimental Verification of Interrelationship of Contact Angles.—In Table III are given both advancing and receding contact angle values for water and for certain organic liquids in air against different cellulose derivatives together with their calculated adhesion tension values. In Table II are given both advancing and receding interfacial contact angle values obtained with water and the different organic liquids against these same solids.

In columns 6 and 8 of Table III are given the data obtained from application of the equations (5a) and (5r), respectively, using solid-water-organic liquid contact angle values in the calculations.

In columns 7 and 9 of the table are given data for corresponding systems using A_{swa}^a , A_{swa}^r , A_{soa}^a and A_{soa}^r , the experimental adhesion tension values for advancing and receding contact angles for solid-water-air and for solid-organic liquid-air systems, respectively. The tabulated values were calculated according to equations (6a') and (6r').

TABLE IV
COMPARISON BETWEEN OBSERVED AND CALCULATED INTERFACIAL CONTACT ANGLES ON CELLULOSE DERIVATIVES

System	Contact angles, degrees			
	Advancing, θ^a		Receding, θ^r	
	Obsd.	Calcd.	Obsd.	Calcd.
Acetate-FM2, foil, side A				
Methylene iodide	111	109.5	67	69.5
α -Bromonaphthalene	106	107	69	67
α -Chloronaphthalene	110		67.5	65
Bromobenzene	119.5		64.5	59
Acetate-FM2, foil, side B				
Methylene iodide	105	104.5	59	58.5
α -Bromonaphthalene	105	102	55	55.5
α -Chloronaphthalene	104.5		54	52.5
Bromobenzene	115		46	45
Acetate-FM2, film				
Methylene iodide	103	103	70	69
Triacetate, film				
Methylene iodide	101.5	103	81	78
α -Bromonaphthalene	106	107	82	79.5
Bromobenzene	113		81	77
Acetopropionate-H, foil, side A				
Methylene iodide	119	119	77.5	77.5
α -Bromonaphthalene	128	121	80	81
Bromobenzene	132.5		75	76
Acetopropionate-H, foil, side B				
Methylene iodide	116	118	69	65
α -Bromonaphthalene	124.5	121.5	65	66.5
Bromobenzene	123		56	59
Tripropionate, film				
Methylene iodide	120	119.5	84.5	85
Acetobutyrate-H, foil, side A				
Methylene iodide	127	127.5	83	80
α -Bromonaphthalene	131	129	86	82
Bromobenzene			79	78.5
Acetobutyrate-H, foil, side B				
Methylene iodide	128	128.5	80	76.5
α -Bromonaphthalene	128	127	74	79
Bromobenzene	141.5		72.5	70.5
Tributyrate, film				
Methylene iodide	138	138.5	100	96
Ethyl cellulose-H, foil, side A				
methylene iodide	121	124	65.5	63
Ethyl cellulose-H, foil, side B				
Methylene iodide	118	118.5	58	58

It is to be noted that good agreement is obtained for the interfacial or solid-water-organic liquid adhesion tensions when calculations are based upon use of either the interfacial contact angle values according to equations (5a) and (5r) or upon adhesion tension values obtained by using solid-liquid-air angles based upon equation (6a') and its counterpart equation (6r'). This experimentally obtained agreement tends to validate the use of equations (6a') and (6r'), and (7a) and (7r). As discussed above, this agreement indicates also that the factors responsible for hysteresis effects in solid-liquid-air systems are very closely related to those responsible for hysteresis effects in corresponding solid-liquid-liquid systems and in com-

bined equations appear to cancel out. That is, it is shown that even in those systems in which hysteresis occurs the correlation between the three contact angles continues to exist. Combined equations by means of which the third angle can be calculated from two measured angles appear still to be valid.

The agreement between calculated and experimentally determined interfacial angles is shown in Table IV. The agreement of the angle values in the majority of the systems was well within the limits of experimental error.

DISCUSSION

ANON.—In regard to which side of a plastic foil had been formed in contact with a metal plate, I can mention some electron microscope work done at Brooklyn Polytech.

and which has never been published. It is quite easy to decide between which side was on the machine and which side was in the air, because the side that was on the machine has in it ridges, so if you rub the two sides together the "metal sides" will stick, whereas the "air sides" will slide past each other easily.

B. R. RAY.—I wish we had known that. It was very confusing at the initial stages of research. We appreciate knowing this point.

ANON.—What effect does annealing have upon these two faces?

B. R. RAY.—We did not investigate the possible effects of various conditionings of these films and foils. The films produced in the laboratory were all made in the same way, *i.e.*, the evaporation was allowed to take place slowly in a desiccator and then the films were heated at 70° in an oven for three hours, and then stood in a desiccator in air. We used this procedure consistently and did not study the effect of various conditionings and treatments.

PROPERTIES OF CAPILLARY-HELD LIQUIDS¹

By P. C. CARMAN

National Chemical Research Laboratory, South African Council for Scientific and Industrial Research, Pretoria, South Africa

Received July 22, 1952

This paper reviews some recent advances in the study of capillary-held liquids. Evidence is given that capillary condensation in micropores is separate and additional to formation of multilayers, though the two processes may influence one another. It is then shown that, though experimental methods for their study are different, capillary condensate and liquid retained in macropores show similar characteristics, and that their properties differ only in so far as they are affected by capillary radius. Attention is directed to the meaning of capillary radius in a pore-space and to the mode of retention of capillary-held liquids; and then the influence of capillary radius on density, surface tension, freezing point and heat of condensation of capillary condensates is discussed. Recent work on the flow of capillary condensate is summarized. Hysteresis is considered and it is shown that the views of Haines, based on macropore systems, not only antedate the theories on hysteresis in micropore systems which are at present in vogue, but also represent a considerable advance on them.

Physical adsorption on microporous adsorbents such as silica gel is generally considered to be characterized by the Type IV and Type V isotherms of Brunauer, Emmett and Teller,² since these lead to a finite limit of adsorption at the saturation vapor pressure, p_0 , of the adsorbate in the liquid state. Earlier theories, as summarized by Brunauer,³ attributed adsorption wholly to capillary condensation; while a later tendency, following on the successful application of multilayer adsorption to the external surface of non-porous adsorbents, was to discard capillary condensation altogether.⁴ The first part of this paper presents direct evidence that formation of multilayer films and capillary condensation both play a part.

Capillary condensation arises from the action of surface tension at a curved meniscus. If it is accepted as occurring in microporous adsorbents, there is no sharp distinction between capillary condensate and capillary-held liquid in a macroporous system, *e.g.*, moisture in a damp bed of sand. The present tendency is to treat these separately, partly because their study requires different tech-

niques; but it is desirable to treat them as a whole. Macropore systems afford a clearer view of the mechanism by which capillary liquid is held in a pore-space; micropore systems show more clearly how properties alter from those of bulk liquid as a result of increasing curvature of the meniscus, *i.e.*, decreasing pore radius. In the present paper, an attempt to review some of the physical properties of capillary condensates has been hampered by absence of reliable data. The conclusion cannot be avoided that this is a field which is being unnecessarily neglected, particularly in comparison with the wealth of experimental measurements on monolayer and multilayer adsorbed films.

Relationship between Adsorbed Films and Capillary Condensate.—Capillary condensation takes place because, at a curved meniscus, surface tension reduces the equilibrium vapor pressure p below that of bulk liquid p_0 , in accord with the Kelvin equation

$$\ln \frac{p_0}{p} = \frac{2\sigma M}{\rho a RT} \quad (1)$$

where σ = surface tension, ρ = density, M = molecular weight, T = absolute temperature and a is the harmonic mean of the two principal radii of curvature, a_1 and a_2 , *i.e.*

$$\frac{2}{a} = \frac{1}{a_1} + \frac{1}{a_2} \quad (2)$$

This is general for any curved liquid-vapor interface, with the signs of a_1 and a_2 positive if the

(1) Presented before the twenty-sixth National Colloid Symposium which was held under the auspices of the Division of Colloid Chemistry of the American Chemical Society in Los Angeles, California, June 16-18, 1952.

(2) S. Brunauer, P. H. Emmett and E. Teller, *J. Am. Chem. Soc.*, **60**, 309 (1938).

(3) S. Brunauer, "The Adsorption of Gases and Vapours. Physical Adsorption," 1943, p. 120.

(4) S. Brunauer, L. S. Deming, W. E. Deming and E. Teller, *J. Am. Chem. Soc.*, **62**, 1723 (1940).

surface is convex to the liquid and negative if concave to the liquid. Thus, for a spherical droplet, $p > p_0$. In a circular capillary, radius r , we can put

$$a = a_1 = a_2 = r \cos \theta \quad (3)$$

where θ is the contact angle, thereby relating the relative pressure, p/p_0 , to the capillary radius.

In contrast to the mechanism of capillary condensation, adsorbed films arise from van der Waals interactions between adsorbent and adsorbate. On an open surface, multilayer films are formed and increase indefinitely in thickness as the relative pressure increases toward unity. On the inner wall of a capillary, such layers could increase in thickness till they filled the capillary, after which adsorption would cease. Theories attributing adsorption in micropores solely to limited multilayer adsorption have been advanced,⁴⁻⁶ but, as conditions are also suitable for capillary condensation, it seems probable that it must also play some part. Recently, direct evidence of this has appeared⁷ and is illustrated by Fig. 1. In this, a loose powder with a surface of 300 m.²/g. is compared to a plug formed by compressing the same powder to a porosity of about 0.5. Capillary condensation should be absent from the powder. If physical adsorption in the plug took place only by multilayer formation, the adsorption isotherm should lie below that for the powder, since restriction of the pore-space limits the thickness of multilayer films. That the converse is true is strong evidence that an additional contribution is being made by capillary condensation.

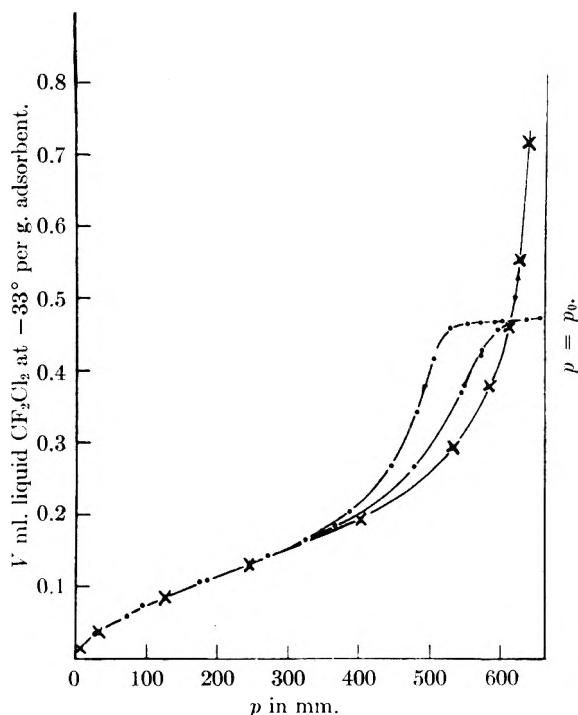


Fig. 1.—Adsorption CF_2Cl_2 on Linde silica at -33.1° : X, loose powder; ●, plug porosity 0.506.

(5) (a) R. B. Anderson, *J. Am. Chem. Soc.*, **68**, 686 (1946); (b) R. B. Anderson and W. K. Hall, *ibid.*, **70**, 1727 (1948).

(6) G. Pickett, *ibid.*, **67**, 1958 (1947).

(7) P. C. Carman and F. A. Raal, *Proc. Roy. Soc. (London)*, **209A**, 59 (1951).

It is to be noted that the isotherm also acquires a feature considered to be characteristic of capillary condensation, namely, hysteresis on desorption. In fact, it is frequently considered that the lower limit of the hysteresis loop is also the lower limit of capillary condensation; but it is evident in Fig. 1 that the effect of capillary condensation extends below this point. Indeed, it is probable that it extends even into the region where the isotherms for powder and plug coincide, as this can result from a balance between an increase of adsorption due to condensation and a decrease of multilayer sorption due to loss of the surface of filled capillaries. Stronger evidence of the latter effect is shown in Fig. 2 for a finer powder, with a surface 960 m.²/g., at two porosities. The isotherm for the higher porosity plug falls below that for the powder before it rises above, while, for the lower porosity, it always remains below.

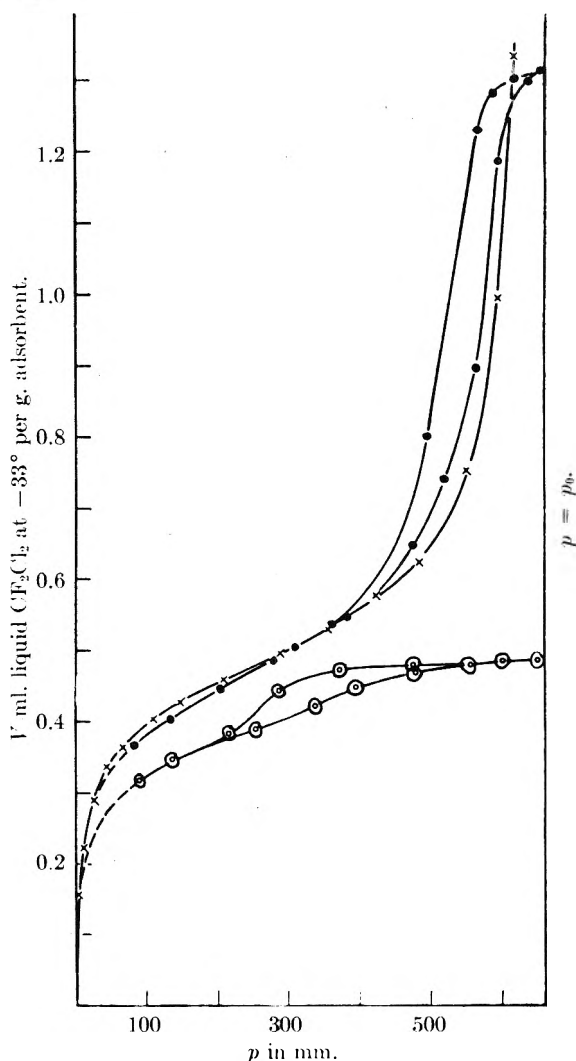


Fig. 2.—Adsorption of CF_2Cl_2 on Carbolac I at -33.1° : X, loose powder; ●, plug porosity 0.739; ○, plug porosity 0.496.

It may therefore be accepted that film formation and capillary condensation take place simultaneously in micropore systems, and, to some extent, influence one another to a degree which it is rather

difficult to define. Thus, experimentally, we measure the quantity of adsorbate per unit weight of adsorbent. From the viewpoint of capillary condensation, it is most convenient to assume the adsorbate has the same density as bulk liquid and to express it as a volume v per unit weight of adsorbent, since, in this form, it is at once possible to assess how completely the total pore volume is filled. This has been done in Figs. 1 and 2. A difficult problem is presented when we attempt to divide a volume v of adsorbate at relative pressure p/p_0 quantitatively into capillary condensate and adsorbed films. This is further complicated by the fact that the presence of adsorbed films decreases effective capillary radii, so that, though the maximum radius of capillaries filled by condensation at a given p/p_0 should be given by equations (1) and (3), the actual maximum radius of filled capillaries is somewhat larger. Attempts to solve these difficulties and hence to arrive at pore size distributions have been made with considerable success in recent years,^{8,9} but it cannot be claimed that finality has been reached.

Capillary-held Liquid in Macropores.—If pore radii exceed a few hundred Ångström units, the vapor pressure of capillary condensate as given in equation (1) differs so little from p_0 that it is difficult or impossible to measure it experimentally. Consequently, adsorption takes place in pores of this size essentially as a multilayer film on a free surface. The ability to detect capillary condensation by measurements of vapor pressure will be used here as the criterion between "micropores" and "macropores." In the intermediate range, capillary condensation is evidenced only as an extremely rapid rise of the curve of v vs. p in the vicinity of p_0 and a very narrow hysteresis loop.

The fact must be pointed out, however, that, though capillary condensation apparently ceases to play a part in adsorption, a larger pore radius means a smaller surface per unit pore volume, so that the proportion of the total pore volume which can be occupied by multilayer films in macropores becomes negligibly small. Theoretically, when $p = p_0$, we must expect the pore-space to be full, so that, in effect, almost the whole pore-space is available for capillary-held liquid. It emerges therefore that, in macropore systems, adsorption of films and retention of capillary-held liquid take place under conditions such that neither influences the other.

A great deal of work on capillary-held water in macropores has been carried out by soil physicists,¹⁰⁻¹⁵ since soils are normally macroporous systems, and a problem of vital importance is

drainage of moisture from a soil pore-space initially saturated with water. This work is based upon the fundamental fact that, owing to the action of surface tension, a curved surface causes a change in the state of tension or of compression of the liquid below that surface. Thus, in a capillary wetted by the liquid, a curved meniscus is formed which is concave on the vapor side and this produces a state of tension in the capillary-held liquid, compared to bulk liquid. As a tensile stress has the dimensions of a pressure, this is commonly called a "pressure deficiency" or "suction pressure," P , and its relationship to the curvature of the surface is given by the thermodynamic relationship

$$P = \frac{2\sigma}{a} \quad (4)$$

where a is the harmonic mean radius of curvature of the surface as defined in equation (2). Now, if a liquid is placed under tension or compression, its vapor pressure is changed according to the thermodynamic relationship

$$\ln \frac{p_0}{p} = \frac{MP}{\rho RT} \quad (5)$$

Equations (4) and (5) lead to the Kelvin equation (1), and it is thus clear that, for capillary-held liquids, lowering of vapor pressure may be regarded as a secondary property resulting from the state of tension induced by a curved meniscus.

It follows that it is more natural to plot the proportion of capillary-held liquid in a porous solid against P than against p/p_0 . In the case of macropore systems, this has the further advantage that P and not p/p_0 is the quantity which can be measured experimentally. Details of the measurement need not be given, as they have frequently been described and reviewed.¹⁰⁻¹⁵

It is sufficient to note here that, for water at about 25°, measurement at P directly is not feasible above about 5×10^7 dynes/cm.², at which point p/p_0 is approximately 0.99. Higher values of P , i.e., lower values of p/p_0 , can be obtained by measuring p and applying equation (5). The most convenient way to express concentration of liquid for comparing one system with another is "degree of saturation," S , i.e., filled pore-volume per unit of total pore-volume, assuming capillary-held liquid has the density of normal liquid.

Actually, a plot of degree of saturation versus a linear scale of P is not wholly satisfactory, particularly when a visual comparison of different pore-systems is desired, so that it has become a regular practice to plot P on a logarithmic scale. In Fig. 3, it has in this way become possible to compare a micropore system (data of Fig. 1), a fairly fine macropore system (water in plaster of paris)¹⁵ and a coarse macropore system (water in 80-100 mesh sand)¹⁶; and it becomes clear how closely similar all of these are in their general features. In particular, all show well-marked hysteresis loops, all of which, under careful experimental conditions, are highly reproducible and so not due to impurities. If the process of removal or addition of liquid is reversed in the middle of a

(8) E. P. Barrett, L. G. Joyner and P. P. Halenda, *J. Am. Chem. Soc.*, **73**, 373 (1951).

(9) P. C. Carman, *Proc. Roy. Soc. (London)*, **209A**, 69 (1951).

(10) W. B. Haines, *J. Agr. Sci.*, **17**, 264 (1927).

(11) W. B. Haines, *ibid.*, **20**, 97 (1930).

(12) G. W. Robinson, "Soils: Their Origin, Constitution and Classification," 3rd edition, 1949, p. 277.

(13) L. D. Baver, "Soil Physics," 1946, p. 204; A. N. Puri, "Soils, Their Physics and Chemistry," 1949, p. 337.

(14) L. A. Richards, *Soil Sci.*, **53**, 241 (1942). L. A. Richards and M. Fineman, *ibid.*, **56**, 395 (1943). L. A. Richards and L. R. Warner, *J. Agr. Research*, **69**, 215 (1944).

(15) D. Croney, J. D. Coleman and E. W. H. Curren, *Brit. J. App. Phys.*, **2**, 85 (1951).

(16) M. C. Leverett, *Trans. Am. Inst. Mining Met. Engrs.*, **142**, 152 (1941).

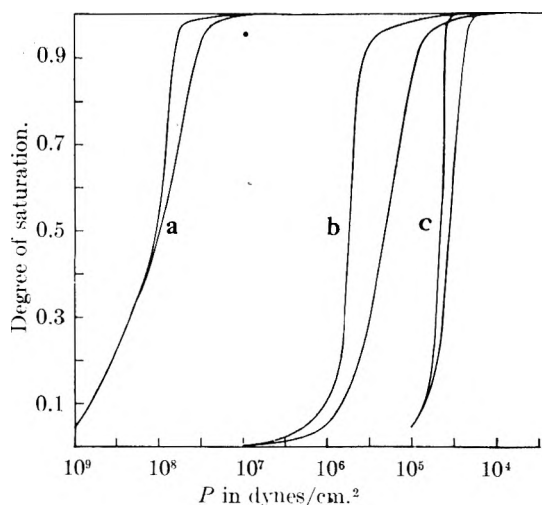


Fig. 3.—Curves of P versus degree of saturation for various porous media: a, from Fig. 1; b, water in plaster of paris; c, water in sand-bed.

loop, "scansion curves" which cross the loop are obtained. These are familiar in capillary condensation, a recent very detailed study of them being given by Emmett and Cines¹⁷ for argon on porous glass. Exactly similar scansion lines appear in all macropore systems and a detailed study of them was given by Haines¹¹ in 1930 for water in a bed of spherical glass particles of radius 0.19 mm.

In Fig. 3 for both micropores and macropores, the two branches of the hysteresis loop level off fairly sharply near complete saturation. This denotes uniform pores, which fill or empty simultaneously at a fairly definite value of P or p/p_0 and it becomes less well-defined when pores are non-uniform.

In macropore systems, there is lower limit to the hysteresis loop, but liquid contents below this limit must still be retained by capillary forces. This confirms the point made previously that reversible capillary condensation in micropore systems should be expected, and does actually take place, below the hysteresis loop.

Significance of Capillary Radius.—Data such as presented in Figs. 1, 2 and 3 are used to obtain pore size distributions by application of equations (1) or (4), by assuming that $\theta = 0$ and that capillaries are circular, so that $a = r$. The assumption that the pore-space is equivalent to a bundle of circular capillaries of varying radii is highly artificial and it is desirable to understand more clearly the relationship of a to the real pore-space.

As a real pore-space is completely interconnected, consider a bundle of interconnected capillaries, all partly filled. As the vapor pressure in the large capillaries is larger, distillation will take place until the largest capillaries are empty and the smallest ones filled, the only partially empty capillaries being an intermediate group with equal radii. Similarly, the tension or suction pressure in the smaller capillaries is greater, so that liquid will flow from larger to smaller capillaries to produce the same end results. This means that, in a real pore-space, capillary-held liquid will redistribute

itself until the curvature of the meniscus is uniform at all points, accompanied by a corresponding uniformity of P and p/p_0 . Such redistribution takes place by two mechanisms, namely, distillation through the empty part of the pore-space and flow of liquid through the filled part. Whether liquid is removed by evaporation, or by drainage, the remaining part re-adjusts itself by either or both mechanisms until a new, uniform curvature of meniscus is attained.

One of the most important ways by which capillary liquid is retained is illustrated in Fig. 4. This shows a point of contact between two particles, in this case, spheres. At this, an annular ring of liquid can be held by surface tension, acting at the curved meniscus. The principal radii of curvature are shown as r_1 and r_2 , but are in opposite senses, so that the value of a is given by

$$\frac{2}{a} = \frac{1}{r_1} - \frac{1}{r_2}$$

If the ring grows in size, both r_1 and r_2 increase, but not at the same rate, so that a also increases. An increase of p or a decrease of P therefore allows the annular ring to grow and *vice versa*. If values of a are interpreted as radii of circular capillaries, therefore, it is seen that these are larger than either r_1 or r_2 , and that a single annulus corresponds to a group of capillaries varying from zero radius upwards.

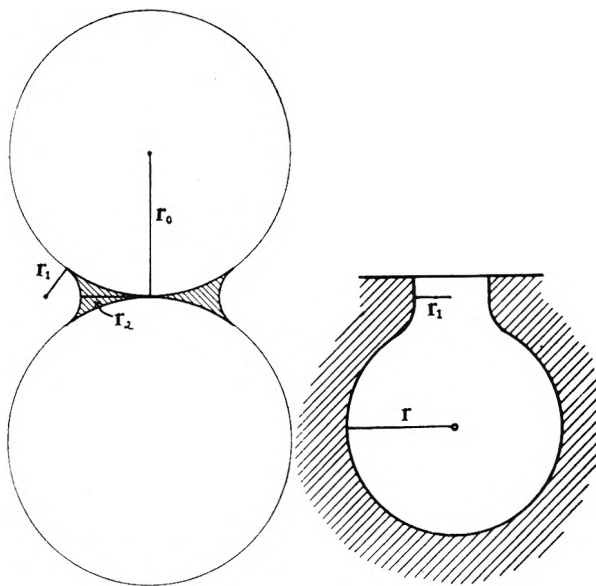


Fig. 4.—Annular ring retained at point of contact. Fig. 6.—"Ink-bottle" pore at point of contact.

If we start from a filled pore-space, and remove liquid, by, say, evaporation, formation of annuli at points of contact only takes place in the last stages. In order to understand more clearly the behavior in the earlier stages, consider a short, open-ended capillary with a cross section formed by circular cylinders, as shown in Fig. 5(a) or 5(b). This provides a reasonable two-dimensional analog to the pore-space in a bed of spheres. If r_3 is the radius of the inscribed circle, the capillary will empty when a hemispherical meniscus of this radius can be formed, *i.e.*, at a constant value of

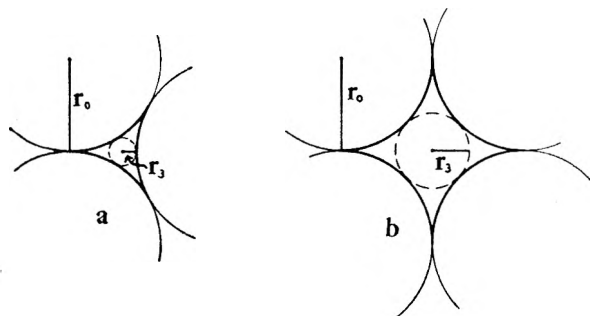


Fig. 5.—Cross sections of pore-space formed between cylinders in two modes of packing. r_3 = radius of inscribed circle.

p/p_0 or P corresponding to $a = r_3$. Emptying, however, will not be complete, as the wedge-shaped corners of the cross section will still contain liquid, corresponding to the formation of annular rings at points of contact between particles. Thereafter, as p decreases, the wedge-shaped portions gradually evaporate. Clearly, two stages of emptying can be traced. In the first, the main part of the capillary-held liquid is removed and the constant value of $a = r_3$ can be reasonably regarded as the "pore radius." In the second stage, corresponding to evaporation from annuli, interpretation of a as a "pore radius" is more or less meaningless. In real pore systems, the two stages overlap, as pores vary in size, so that, before the smaller pores have emptied, annuli have formed at the larger pores. Further discussion of these points with respect to hysteresis will be undertaken later.

Effect of Capillary Condensation on Adsorbent.

—The main effects arise from the state of tension in the capillary liquid. In macropore systems, it is familiar in the increased cohesion shown by clays and fine sands when slightly moistened. If moisture is gradually removed from any originally full pore-space, the increase of cohesion and strength passes through a maximum, since capillary forces must increase when P increases from zero, but their effectiveness for cohesion must decrease to zero when the capillary held liquid is completely removed.

In micropore systems, P attains values large enough to produce a mechanical effect on rigid adsorbents. It has been shown by Wiig and Juhola¹⁸ that, when capillary condensation of water commenced on charcoal, a well-defined contraction in the volume of the adsorbent was observed. This reached a maximum at $p/p_0 \simeq 0.7$, corresponding to nearly complete filling of the pores, and then decreased as p/p_0 increased further, i.e., as P decreased. On desorption, owing to hysteresis, pores remained full to $p/p_0 \simeq 0.5$ and thereafter emptied more rapidly. In accord with this, the maximum contraction was also reached at $p/p_0 \simeq 0.5$, and fell off more sharply. Further, the maximum contraction was larger, as the lower value of p/p_0 corresponds to a larger value of P .

Properties of Capillary Condensate.—If a capillary-held liquid differs from bulk liquid only by virtue of the presence of a curved meniscus, it should be possible to predict its properties. As

differences are only likely to be appreciable in micropores, this range of pore sizes is generally most suitable for experimental study of properties; but it should be essential that: (i) properties of capillary condensate are measured and that the effect of multilayer films is avoided or at least corrected for; (ii) pore radii are several times larger than the diameters of adsorbate molecules, say, at least 10 Å.

Data which conform to these requirements are practically non-existent. The most obvious property to consider is *density*. If the relative pressure of the capillary condensate is given, the tension to which it is subjected is calculable by equation (5), and, from this, using the compressibility coefficient, a decrease of density can be estimated quantitatively. There seems, however, to be no suitable data to test this. A great deal of evidence confirms that the limiting volume of adsorbate at $p = p_0$ equals the volume of the pore-space or that different liquids give consistent saturated volumes. Exceptions, such as mentioned by Broad and Foster,¹⁹ appear only when pores are present which cannot be entered by adsorbate molecules. The above observation, however, is not surprising, since, at $p = p_0$, the capillary condensate is not under tension and so should have the normal density. The values required are densities of capillary condensates at relative pressures below unity. Unfortunately, the only accurate measurements, using the helium displacement method, of adsorbate densities over a wide range of relative pressure, have been carried out on charcoals. This is an undesirable choice of adsorbent from the viewpoint of capillary condensation, since adsorption isotherms with liquids such as carbon tetrachloride, acetone and ether^{20,21} approach a limit and are classified as Type I or "Langmuir" isotherms by Brunauer, Emmett and Teller. This infers that the pores are so narrow that only a single layer of molecules can be accommodated on their internal surface. Such an interpretation is not beyond question, and recently Pierce, Wiley and Smith²² have cited strong arguments that Type I isotherms must involve at least some degree of capillary condensation. The correct view is more probably that, in capillaries approaching molecular dimensions, both film formation and capillary condensation are so profoundly modified that the adsorbate is in a state intermediate between normal types of adsorption on the one hand and interstitial solid solution on the other. In any case, the experimental data cannot be considered to be fully satisfactory with respect to ordinary capillary condensation.

Adsorption of water vapor on charcoals gives Type V isotherms, with well-marked hysteresis, and so appears more closely similar to ordinary capillary condensation; but the behavior of the same adsorbents to organic adsorbates makes it

(19) D. Broad and A. G. Foster, *J. Chem. Soc.*, 366 (1945).

(20) J. D. Danforth and T. de Vries, *J. Am. Chem. Soc.*, **55**, 2792 (1933).

(21) N. G. M. Tuck, R. L. McIntosh and O. Maass, *Can. J. Research*, **26B**, 20 (1948).

(22) C. Pierce, J. W. Wiley and R. N. Smith, *THIS JOURNAL*, **53**, 669 (1949).

(18) E. O. Wiig and A. J. Juhola, *J. Am. Chem. Soc.*, **71**, 561 (1949).

difficult to place full confidence in the results. Two accurate investigations have been reported^{18,23} and the results obtained are illustrated in Table I, together with calculated values. The difference from the normal value at saturation can be attributed to pores which are too small for water molecules to enter and which become blocked to access of helium. Assuming this is the case and paying attention only to variation from the value at $p/p_0 = 1$, we see that results vary in fair agreement with one another and with theoretical values.

TABLE I
DENSITIES OF WATER ADSORBED ON CHARCOAL

	$p/p_0 = 1$	$p/p_0 = 0.9$	$p/p_0 = 0.5$
Theoretical	1.0	0.994	0.955
Juhola and Wiig ¹⁸	0.93	.93	.85
McDermot and Tuck ²³	.955	.95	.91

Surface tension is the property which, acting at a curved surface, is responsible for the decrease of vapor pressure and the state of tension in capillary-held liquids. The possibility of its variation in small pores is thus one which must be carefully considered, since, if this takes place, calculation of pore radii from p by equation (1) ceases to be valid. For capillary radii approaching molecular diameters, equation (1) should be expected to fail, since it is a thermodynamic relationship and so depends on a surface containing very large numbers of atoms. The failure of equation (1) as a relation between σ , p and a and variations in σ need not be considered separately, since, if p and a are known, equation (1) can be used to define σ , and values so obtained can be compared with those for bulk liquid. Equation (4) is affected to the same degree as equation (1), and equation (5) is unaffected.

Direct experiments on variation of σ in micropores are not very feasible, so that we have to rely on (i) theoretical calculations, (ii) comparison of pore radii calculated by equation (1) using normal values of σ with values calculated by other methods.

Theoretical calculations are not likely to reach finality until the theory of liquids is more complete than it is at present. In papers by Tolman²⁴ and by Kirkwood and Buff,²⁵ a rather rapid decrease of σ with decreasing radius is envisaged, e.g., for argon at 90°K., the calculations lead to a decrease of about 40% for a radius of 20 Å. A more recent paper by Hill,²⁶ however, while agreeing that σ decreases, estimates a very much smaller decrease. Thus, defining σ by equation (1), he calculates that the decrease is 9.7% for $a = 15$ Å. and falls off very rapidly for larger radii, e.g., 5.5% for $a = 20$ Å. The calculations have no validity for radii much under 15 Å.

A direct check on equation (1) could be made if pore radii were measurable by an independent method, but this is not practicable. It has, however, been shown^{8,9} that, if some suitable

allowance is made for presence of adsorbed films, equation (1) leads to a reasonable estimate of the total pore surface, even when the calculations include pores under 10 Å. radius.

On the freezing point of capillary condensate, there is a considerable amount of experimental work. Earlier work has been summarized by Brunauer²⁷ and provides ample evidence that capillary condensates can remain liquid to temperatures as much as 100° below the normal freezing point. Jones and Gortner,²⁸ using a dilatometer method, observed freezing of water in a saturated silica gel. This commenced a little below 0°, but 33% was still liquid at -48°, as would be expected for a distribution of pore sizes. If we assume the vapor pressure of crystalline solid phase is the same in capillaries as in bulk solid, the depression of freezing point can be easily calculated. Evidence in accord with this has recently been reported by Iwakami,²⁹ who used heat capacity measurements to detect the freezing point of CCl₄ on silica gel, and by Higuti and Shimizu,³⁰ who employed measurements of dielectric polarization to detect the freezing point of *o*-nitrophenol adsorbed on silica gel. The latter followed the decrease in freezing point with decrease in saturation with capillary condensate, i.e., with decreasing capillary radius, down to 35° below the normal freezing point.

Batchelor and Foster,³¹ for dioxane on ferric oxide gel and, more recently, Brown and Foster,³² for ethylenediamine on silica gel, detected freezing point depression by vapor pressure measurements. Their results indicate that the vapor pressure of capillary-held solid is less than that of bulk solid. As it is difficult to visualize formation of a meniscus by a solid, capillary forces would not be expected to alter its properties, so that this observation indicates that further work is required.

The latent heat of vaporization of capillary condensate is an important property which appears to have been almost completely neglected. There is an abundance of work on heats of adsorption when formation of monolayer or multilayer films is predominant, but this does not seem to have been extended to capillary condensation. In a paper by Gleysteen and Deitz,³³ some calculations are reported on data of Lambert and Clark³⁴ for adsorption of benzene on ferric oxide gel, a system which showed capillary condensation with a well-marked hysteresis loop. Isothermic heats of adsorption, calculated by the Clausius-Clapeyron equation, at the widest part of the hysteresis loop showed 8660 cal./mole on the adsorption branch and 9420 cal./mole on the desorption branch, compared with about 8000 cal./mole (isothermic) for liquid

(27) S. Brunauer, as ref. 2, p. 444.

(28) I. D. Jones and R. A. Gortner, *This Journal*, **36**, 387 (1932).

(29) Y. Iwakami, *J. Chem. Soc. (Japan), Pure Chem. Section*, **72**, 707 (1951).

(30) I. Higuti and M. Shimizu, *J. Am. Chem. Soc.*, **74**, 198 (1952).

(31) R. W. Batchelor and A. C. Foster, *Trans. Faraday Soc.*, **40**, 301 (1944).

(32) M. J. Brown and A. G. Foster, *Nature*, **169**, 37 (1951).

(33) I. F. Gleysteen and V. R. Deitz, *J. Research Natl. Bur. Standards*, **35**, 285 (1945).

(34) B. Lambert and A. M. Clark, *Proc. Roy. Soc. (London)*, **122A**, 497 (1929).

(23) H. L. McDermot and N. G. M. Tuck, *Can. J. Res.*, **28B**, 292 (1950).

(24) R. C. Tolman, *J. Chem. Phys.*, **17**, 332 (1949).

(25) J. G. Kirkwood and F. P. Buff, *ibid.*, **17**, 338 (1949).

(26) T. L. Hill, *J. Am. Chem. Soc.*, **72**, 3923 (1950).

benzene. The "heats of vaporization" of capillary condensate thus exceeded that of bulk liquid, but, more important, there was a distinct difference between adsorption and desorption. A similar, but smaller, result, namely, 200 cal./mole difference between the two branches, was shown by Joyner and Emmett³⁵ for adsorption of nitrogen on porous glass.

Flow of Capillary Condensate.—The flow of capillary-held liquids in macropore systems is well understood and is described adequately in text-books on soil physics.^{12,13} The force which produces flow is a difference in capillary tension, *i.e.*, movement takes place from a region of low tension to a region of high tension. The rate of flow is limited by the viscosity of the liquid and by the permeability of the porous medium, a factor which is determined by its pore size distribution. In a partly saturated medium, flow can take place only through the filled part of the pore-space, so that the permeability is less than for a saturated medium, the ratio of the unsaturated permeability to saturated permeability being called the relative permeability.

In recent experiments,³⁶ the writer has shown that capillary condensate in micropores follows the same laws. Using the porous plug discussed in Fig. 1, constant vapor pressures, p_1 and p_2 , of CF_2Cl_2 were maintained at the two ends. Capillary condensation took place, but, owing to vapor pressure difference, $\Delta p = p_1 - p_2$, different tensions, P_1 and P_2 , were produced at the two ends, and this caused a flow to take place from P_1 to P_2 . The value of ΔP is readily calculated from Δp by use of equation (5). Since p_1 and p_2 were kept constant, a steady state flow was produced in which condensation took place at p_1 and evaporation at p_2 , and the rate of this could be measured. From these data, an experimental value of the permeability was arrived at. In order to obtain a "calculated" value, the permeability of the plug to air, which is neither adsorbed nor condensed, was measured, and this could then be used to calculate the permeability toward liquid CF_2Cl_2 , assuming the viscosity of bulk liquid at the temperature of the experiment.

For a saturated plug, the "observed" permeability was 15–20% below the "calculated" permeability, for each of two adsorbates, CF_2Cl_2 and SO_2 . This might perhaps be cited as evidence that viscosities were somewhat higher than for bulk liquid; but there is sufficient uncertainty in the calculation from air permeability to liquid permeability to cover this difference. The results can certainly be considered to show that no profound change takes place in either the mechanism of flow or in viscosity for micropore systems.

Saturation permeabilities correspond to the saturation pressure, p_0 , and are obtained by extrapolation. In an actual experiment, p_1 and p_2 are both below p_0 , so that the observed rate of flow corresponds to a value of v which is less than the saturation value and which is the average of

values for p_1 and p_2 . Now, values of v are obtained from Fig. 1 and, owing to the hysteresis loop, it is necessary to know how p_1 and p_2 have been set up if v is to have definite values. Thus, if the whole plug is originally at p_0 and p_1 and p_2 have been obtained by decreasing from p_0 , then v must be obtained from the desorption branch of the isotherm. If p_1 and p_2 have been obtained from an initial zero pressure, the adsorption branch must be used. If p_1 and p_2 are first increased and then decreased without proceeding to p_0 , a "scansion" curve in the hysteresis loop is followed and, as the course of this is normally unknown, no determinate value of v can be arrived at. The latter type of measurements were avoided. The interesting fact found was that a given value of v gave the same permeability, whether obtained by adsorption or desorption.

Furthermore, the variation of permeability with the degree of saturation was almost the same as curves obtained for sand-beds, thereby affording further evidence for similarity in the mechanism of flow.

Hysteresis.—Though the hysteresis loop shows that condensation in capillaries is irreversible, it has been repeatedly shown to be highly reproducible on a well-cleaned adsorbent, and is therefore due neither to impurities nor to slow rates of equilibration. Theories to explain hysteresis fall into three categories. The first due to Gleysteen and Deitz,³³ is the extension of the Brunauer, Deming, Deming and Teller³ theory that multilayer adsorption alone is sufficient to account for adsorption in micropores. The experiments of Carman and Raal,⁷ discussed earlier, are adverse to this viewpoint.

Other theories assume capillary condensation. The second type of theory, originally advanced by Zsigmondy,³⁷ attributes hysteresis to the difference between advancing and receding contact angles of a liquid on a solid surface. Originally attributed to strongly adsorbed impurities, this theory would fail for hysteresis on well-cleaned surfaces, but it is given a stronger foundation by experimental studies of MacDougall and Ockrent,³⁸ and theoretical arguments by Cassie,³⁹ which indicate that advancing angles and receding angles may both give reproducible values on perfectly clean solid surfaces. The main objection to the theory is then the necessity to assume contact angles. In many cases of strong hysteresis, there is every reason to assume good wetting of the solid surface by condensate, *i.e.*, a "contact angle of zero." Indeed, as noted by Gans,⁴⁰ most systems which are conventionally stated to possess a "zero contact angle" are more correctly described as possessing "no contact angle," so that the difference between advancing and receding angles becomes meaningless.

We shall therefore consider in detail only the third possibility, namely, theories based upon "delayed formation of a meniscus." Consider a pore represented by a short, uniform, circular capillary, open at both ends. Assuming $\theta = 0$,

(37) R. Zsigmondy, *Z. anorg. allgem. Chem.*, **71**, 356 (1911).

(38) G. MacDougall and C. Ockrent, *Proc. Roy. Soc. (London)* **180A**, 151 (1942).

(39) A. B. D. Cassie, *Discussion Farad. Soc.*, **3**, 11 (1948).

(40) D. M. Gans, *This Journal*, **49**, 165 (1945).

(35) L. G. Joyner and P. H. Emmett, *J. Am. Chem. Soc.*, **70**, 2359 (1948).

(36) P. C. Carman, *Proc. Roy. Soc. (London)*, **180A**, 151 (1942).

and that it is originally full of condensate, then evaporation will occur when p/p_0 is reduced to a value corresponding to $a = r$ in equation (1), as a hemispherical meniscus with this radius is formed. In the empty capillary, condensation cannot take place at the same value of p/p_0 , since there is no mechanism by which a meniscus can be created in empty space. Thus, according to Foster,⁴¹ hysteresis arises from this "delay" in formation of a meniscus and occurs in the adsorption condensation portion of the hysteresis loop. It follows that only the desorption branch should be used to calculate pore size distributions by the Kelvin equation. Cohan^{42,43} elaborated this theory by pointing out that condensation on the wall of the capillary gives a film with a cylindrical curvature, so that $2/a = 1/r$. Thus, condensation should proceed spontaneously when p/p_0 is increased to a value corresponding to $a = 2r$.

In strong contrast to the "open pore" type of theory is the "closed pore" or "ink-bottle" theory.⁴⁴⁻⁴⁷ Suppose we consider a spherical pore with radius r as shown in Fig. 6, connected to the rest of the pore-space by a narrow neck of radius r_1 . If the pore is full, the body of the pore should empty when p/p_0 corresponds to $a = r$, but, once again, a meniscus cannot form because its formation requires a bubble to appear in the condensate filled interior of the pore. As the bubble must grow from a small nucleus, requiring a very low value of p/p_0 to appear spontaneously, this is not possible. Evaporation therefore can only occur when p/p_0 corresponds to $a = r_1$, *i.e.*, to the curvature of the meniscus in the neck. On adsorption, no condensation occurs for p/p_0 corresponding to $a = r_1$, as a meniscus cannot form in the neck, so that we should expect condensation to appear when p/p_0 corresponds to $a = r$. In this case, it is the adsorption or condensation branch of the hysteresis loop which gives the correct pore radius by application of the Kelvin equation. This is not quite true, since, if r_1 is less than $1/2r$, condensation will commence on the walls of the neck instead of in the interior of the capillary.

It is probable that both "open pore" and "closed pore" theories have some elements of truth, but the difficulty in assessing their relative merits resides in the highly simplified models of the pore-space which they present. A very comprehensive study of conditions in an actual pore-space was made by Haines,^{10,11} before any of the "open pore" or "closed pore" theories, but, as it was applied to capillary-held moisture in sands and soils, it has been neglected in the literature on adsorption. Though Haines mainly considered the pore-space between uniform spheres of radius r_0 in close-packing, the principles are sufficiently illustrated by spheres in simple cubic packing. The pore-space is divided into "cubic voids" in which can be in-

scribed spheres with a radius $0.73 r_0$. We might expect the voids to empty, therefore, when p/p_0 is decreased to a value corresponding to $a = 0.73 r_0$. But the voids are interconnected by passages such as shown in Fig. 5(b), assuming the circles represent spheres instead of cylinders, in which the radius of the inscribed circle is $0.41 r_0$. For a meniscus to be able to enter the void, therefore, p/p_0 must decrease to correspond to $a = 0.41 r_0$. The "ink-bottle" theory thus has some validity. Once the voids empty, isolated annuli are left at points of contact and evaporation from these has already been considered. Suppose next we consider condensation. Each wedge-shaped corner in Fig. 5(b) corresponds to an annulus as in Fig. 4. As p/p_0 increases, the annuli grow in size, but no new meniscus should form until they make contact with one another. At this point, $r_1 = 0.41 r_0$, but $r_2 = -0.59 r_0$, so that $2/a = (1/r_1) + (1/r_2)$, *i.e.*, $a = 2.82 r_0$. Consequently, the pore-space does not fill till p/p_0 corresponds to this value of a , which must be contrasted to the "pore-radius," $0.73 r_0$.

It is clear from this that delay in formation, of a meniscus is very much more marked on condensation than on evaporation, *i.e.*, ink-bottle effects are relatively unimportant. This view is reinforced if we bear in mind that, even for uniform spheres, packing in a real bed is always of random type and, in addition, particles are seldom either spherical or uniform in size. The "cubic pores" just considered are "ink-bottles" with no fewer than six identical, constricted openings. In random packing, such a situation is impossible. For any voids, one or more connecting channels will be wide enough to allow a meniscus to enter easily. Indeed, both "voids" and "entry passages" will cover a range of over-lapping sizes and will appear merely during evaporation or desorption as a continuous "pore size distribution" over a fairly wide range. On condensation, growth of annuli till they make contact will be little affected by the above factors, so that this remains the main cause of hysteresis. Calculation of pore size distributions from the desorption branch of a hysteresis loop is thus well justified.

It will be noted that, from the point where isolated annuli are formed on evaporation, the processes of evaporation and condensation are reversible. This has been confirmed by Haines and others for macropores, and, as shown experimentally in Fig. 1, closure of the hysteresis loop for micropores does not mean that capillary condensation is absent below this point. It does mean, however, that all pores or voids are empty and that the remaining capillary condensate is retained solely as annuli at points of contact.

In micropore systems, the simultaneous formation of adsorbed films must exert some effect upon hysteresis. This has been considered by Foster^{41,48,49} and also by Cohan,⁴³ and the qualitative conclusion to be drawn is that presence of adsorbed films assists formation of a meniscus, and hence tends to reduce hysteresis. As experimental evi-

(41) A. G. Foster, *Trans. Faraday Soc.*, **28**, 645 (1932).

(42) L. H. Cohan, *J. Am. Chem. Soc.*, **60**, 433 (1938).

(43) L. H. Cohan, *ibid.*, **66**, 98 (1944).

(44) E. O. Kraemer in H. S. Taylor's "A Treatise of Physical Chemistry," 1931, p. 1661.

(45) J. W. McBain, *J. Am. Chem. Soc.*, **57**, 699 (1935).

(46) K. S. Rao, *This Journal*, **45**, 506 (1941).

(47) S. M. Katz, *ibid.*, **53**, 1166 (1949).

(48) M. J. Brown and A. G. Foster, *Research*, **3**, 97 (1950).

(49) A. G. Foster, *This Journal*, **55**, 638 (1951).

dence in favor of this, Foster has shown that, on a given adsorbent, an increase in size of adsorbate molecules decreases the size of the hysteresis loop, and can cause it to disappear altogether. We should thus expect hysteresis to be more marked in macropore systems than in micropore systems and, on the whole, this appears to be the case, provided a suitable scale of plotting, as in Fig. 3, is chosen.

Thus far, we have accepted that evaporation and condensation, though highly reproducible, are not reversible processes, and it would appear from this that one or both of the branches of the hysteresis loop must be thermodynamically unstable. This is not quite the correct way to view the phenomenon. In plotting p/p_0 as a function of v , the volume of condensate per unit weight of adsorbent, we are dealing with a specific property of the capillary condensate, but are leaving out of account the extent of the surface, and the surface energy associ-

ated with this. According to the hysteresis loop, a given quantity of condensate per unit weight of adsorbent can exist in equilibrium with widely different pressures of vapor. This is because the given volume of condensate can be distributed in different ways, producing different curvatures of the meniscus. Concomitant with this, however, the distribution of adsorbent surface area between the liquid-solid and vapor-solid interfaces and also the extent of the liquid-vapor interface undergo change, and it is this change in surface energy which causes the change in free energy shown by the change of p/p_0 . We should thus regard the hysteresis loop obtained on plotting p/p_0 vs. v as the projection of a surface on a three-dimensional plot such as p/p_0 vs. both v and, say, the area of the liquid-vapor interface per g. of adsorbent.

Acknowledgment.—This paper is published with the permission of the South African Council for Scientific and Industrial Research.

ADSORPTION IN CAPILLARIES¹

By CONWAY PIERCE AND R. NELSON SMITH

Department of Chemistry, Pomona College, Claremont, California

Received July 22, 1952

The properties of porous solids are reviewed and compared with those of plane surfaces. Two types of capillaries are indicated, those that show desorption hysteresis and those that do not. The difference is ascribed to the method by which adsorption occurs. Methods are described for computing capillary sizes from the desorption isotherm. These computations are not valid for pore radii below about 20 Å. and for the pores whose isotherms are the Langmuir type. Brief discussions are given of the adsorption of water by carbon, surface mobility in relation to filling of capillaries, adsorption from solution and the effects of external capillaries on adsorption.

In practical applications of adsorption a porous solid is almost always used, because of the higher surface development. Theoretically, however, the process of adsorption in pores is not nearly so well understood as is adsorption on a non-porous surface. The purpose of this paper is to examine and review various aspects of adsorption in capillaries and to suggest tentative explanations for some of the phenomena.

Criteria for Recognition of Capillaries.—The presence of capillaries is recognized by the deviations of the adsorption isotherm from the S-shaped isotherm of non-porous solids. When capillaries become filled the isotherm flattens out because the inner surfaces are no longer accessible for the growth of a multilayer film. In typical cases this leads to Brunauer's Type I, IV and V isotherms.

If a sample contains some capillaries along with a large "free" surface the isotherm may be S-shaped and at a superficial glance it will seem that the surface is non-porous. In this case the presence of capillaries can be detected by quantitatively comparing the isotherm with true non-porous isotherms. This is done by means of the n -values of Table I, which are composite values for the number of layers adsorbed as a function of relative

pressure, when the surface is non-porous. To compare these with an experimental isotherm one constructs n -values from the isotherm, taking the adsorption at the inflection "point B" as the monolayer value.

TABLE I
STATISTICAL NUMBER OF LAYERS ADSORBED AT VARIOUS RELATIVE PRESSURES²

p/p_0	Number of layers n	p/p_0	Number of layers n
0.250	1.29	0.600	2.08
.300	1.38	.700	2.50
.400	1.56	.800	3.5
.500	1.78	.900	5.6

The eventual effect of capillaries is to depress the isotherm below the non-porous isotherm, but an initial effect may be to increase adsorption at the point where capillary condensation sets in. Both effects are shown in isotherms obtained by Carman and Raal³ for loose powder and plugs made by compressing the powders.

Types of Capillaries.—It is well recognized that in their adsorption behavior there are two different types of capillaries, (1) those that fill at low relative pressure and (2) those that fill at relative pressure of 0.5 to 1.0. The former show no hys-

(1) (a) Presented before the twenty-sixth National Colloid Symposium which was held under the auspices of the Division of Colloid Chemistry of the American Chemical Society in Los Angeles, California, June 16-18, 1952. (b) This is a report of work conducted under contract N8onr 54700 with the Office of Naval Research.

(2) C. Pierce, *This Journal*, **57**, Feb. (1953).

(3) P. C. Carman and F. A. Raal, *Proc. Roy. Soc. (London)*, **A209**, 59 (1951).

teresis on desorption, the latter do. The designations of class I and class II have been proposed by the writers⁴ for the two types. As discussed later the two types appear to fill by different mechanisms.

Examples of isotherms for the two types of capillaries are shown in Fig. 1. A and E represent extreme cases for class I capillaries whose isotherms are of the Langmuir type. B shows the S-shaped isotherm of a non-porous solid and C an isotherm for class II capillaries. A typical water isotherm for an activated charcoal D also illustrates class II capillaries.

Adsorption of Water by Carbon.—The peculiar properties associated with the adsorption of water by clean carbon surfaces have proved useful in studies of charcoal capillaries. When a non-porous carbon surface is free of oxygen, sulfur or halogens it has little tendency to adsorb water. This is shown in the water isotherm of Graphon, a graphitized carbon black.⁵ There is little adsorption below $0.95 p_0$ and a relative pressure of 0.99 is needed to adsorb a statistical monolayer (an amount of vapor sufficient to cover the surface with a monolayer if uniformly spread over the surface). At saturation only two statistical layers are adsorbed. By contrast, the ethyl chloride isotherm of Fig. 1 shows a monolayer completed at about $0.15 p_0$ and at saturation the adsorption of some 30 statistical layers.

When the carbon sample has capillaries the adsorption of water takes place as in Fig. 1D. The saturation adsorption is now almost as large a liquid volume of water as of other adsorbates. A sharp rise in the water isotherm at pressures below $0.95 p_0$ is therefore taken as indication for the presence of capillaries in a carbon sample.

Capillary Condensation.—Filling of capillaries can occur by two distinct processes (1) condensation of vapor at a meniscus which bridges the walls of the pore or (2) by the building up of a multi-molecular film on the capillary walls until the space is filled. There can, of course, be a combination of the two, starting with a wall film and ending up with a meniscus after the films on opposite walls merge. The term "capillary condensation" should strictly speaking be applied only to the first process, condensation of vapor at a meniscus.

The size and shape of a capillary determine which one of the two processes is effective in adsorption. Condensation cannot occur until a meniscus bridges the pore. If the pore is sufficiently narrow to be bridged by a single molecule or by a uni-molecular layer on each wall, condensation sets in with the start of adsorption. This appears to be the case for charcoal S600H of Fig. 1, whose pores are all filled at a relative pressure near 0.05. The isotherm for non-porous Graphon in Fig. 1 shows that at 0.05 less than half the first layer is completed on a plane surface. It must be then that after the first molecules have bridged the pore and formed a meniscus the two walls exert sufficient force on the surface molecules to cause con-

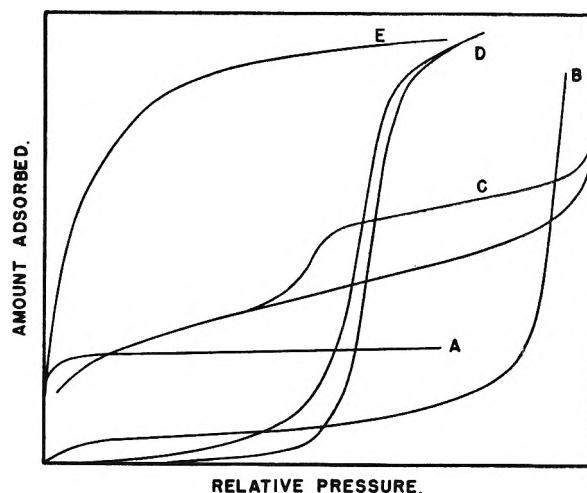


Fig. 1.—Typical isotherms: A, ethyl chloride on activated charcoal, S600H, prepared by carbonization of Saran plastic; B, ethyl chloride on Graphon; C, nitrogen on catalyst isotherm of Oulton; D, water isotherm for S600H; E, ethyl chloride on activated charcoal S84 showing large pores.

densation more readily or at a lower pressure than on a plane surface.

If a pore is too wide to be bridged by a uni-molecular layer on each wall the first adsorption must be in a wall film, just as on a plane surface. In this case the start of the isotherm is just like that for a non-porous solid and the isotherm will agree with the n -values of Table I up to the point that the wall films meet and merge, capillary condensation starts, and surface begins to disappear because of filling of pores. This is apparently the mechanism for the adsorption of the catalyst whose isotherm is shown in Fig. 1. The isotherm follows the n -values up to a relative pressure of about 0.6, corresponding to some 2 molecular layers in the wall film, before it begins to show effects of capillary condensation.

According to this view the essential difference between class I and class II capillaries is in their method of filling. Class I fill by immediate capillary condensation at the start of adsorption, class II by a combination of wall film adsorption and capillary condensation after the wall films meet.

Adsorption isotherms show that wall forces can extend into an adsorbed liquid layer up to distances of several molecular diameters, since the vapor pressure of adsorbed molecules is less than that of bulk liquid up to saturation, where the film is some 20–30 molecules in thickness. The exact nature of these forces is not known; perhaps they are related to a polarization of the molecules starting with the first layer and extending throughout the liquid film with constantly diminishing effect until the outer layer has the vapor pressure of bulk liquid.

Wall effects are greater in a liquid held in a capillary than for a film of the same thickness held on a plane surface because of the greater wall area within given radial distance of film molecules. It is this effect that accounts for the filling of the pores of S600H at lower relative pressure than is needed to form a first layer on a plane surface.

The augmentation of wall forces in pores pro-

(4) C. Pierce and R. N. Smith, *THIS JOURNAL*, **54**, 784 (1950).

(5) C. Pierce, R. N. Smith, J. W. Wiley and H. Cordes, *J. Am. Chem. Soc.*, **73**, 4551 (1951)

vides a plausible explanation for the desorption hysteresis found with Class II capillaries. In the initial stages of adsorption there are single wall films. Later these meet and merge. When this occurs all molecules of the combined film are now held on two walls and are therefore more tightly bound than before the films merged. Consequently desorption from the meniscus occurs at lower pressure than the original adsorption in a single wall film. There is no hysteresis for class I capillaries since their adsorption and desorption occur in the same manner, both from a meniscus.

External Capillaries.—In a powdered sample the spaces between the particles have some capillary properties. Such capillaries differ however from ordinary pores in solids, in that the boundary walls are not rigidly connected and an adsorbed film may push the particles apart. In samples with areas of the order of 100 sq. m. per g. the particle diameters are of the order of 300 Å. When spheres of this diameter are packed only a small fraction of the void space is in the usual capillary size range. Consequently the low pressure adsorption is not markedly affected. At pressures near p_0 however there may be considerable condensation in the external pores and the total adsorption greater than would be the case for an equivalent area of plane surface. Because of this capillary condensation near p_0 , there is considerable uncertainty in the choice of n values for the statistical number of layers near saturation and as previously discussed² the n values of Table I were rather arbitrarily selected in the higher pressure region.

Experimentally it is observed that when a powdered sample has adsorbed at high relative pressure the film cements the particles together, the entire powder mass forming a single lump.

When particles are very small they crowd more closely together and the external capillaries may be sufficiently narrow to affect the low pressure adsorption. In this event the capillaries behave as Class I and the isotherm may appear to be a normal one for a non-porous surface. A case in point is that of Carbolæ I, a Cabot ink black of specific area near 1000 sq. m. per g. The nitrogen area corresponds to particles near 26 Å. in diameter but the electron microscope diameter is near 100 Å. The unusual roughness factor of 4 must be due either to large pits which act as Class I capillaries or to external capillaries which augment the low pressure adsorption. The water isotherm⁵ confirms the existence of capillarity since it shows a pronounced adsorption starting at about 0.5 p_0 .

Size of Capillaries.—The Kelvin equation has for years been used to compute the radius of cylindrical capillaries, by measurement of the relative pressure at which they are emptied. Recently Shull,⁶ Oulton,⁷ Barrett, Joyner and Halenda,⁸ Carman⁹ and the writer² have revised the computation by taking into account the thickness of the wall film which remains when a pore is

emptied at a given relative pressure. These computations are all based on the assumptions that: (1) capillaries may be represented by an equivalent system of circular pores; (2) the Kelvin equation holds at all relative pressures; (3) the wall film at a given relative pressure has the same thickness as the film on a plane surface at that pressure.

Pore size distributions computed in this way are self consistent in that the summations of the pore volumes and areas are in good agreement with the total volumes and areas as measured from the isotherms. Since the computation can be made² without use of any arbitrary constants except as implied in the assumptions above and since the inner capillary volume is not the total pore volume, the agreement in volumes and areas leads to the conclusion that the distributions so obtained are sound. Further, when a sample has a narrow range of pore sizes the Kelvin radii are in agreement with those computed from the surface-volume ratio.

There are, however limitations to the application of this method: (1) The computation is based on cylindrical capillaries. The self consistent results obtained neither prove nor disprove that the capillaries are round. We have also made the computation for flat-walled pores and obtain essentially the same agreement, except that now the width of the pore is about the same as the radius computed on the round pore basis.

Actually, if one considers the formation of capillaries, which usually occurs by release of volatile matter from a plastic mass, a very irregular pore shape is expected. Possibly the best capillary model would be a random mixture of black and white balls from which one imagines one kind removed without collapse of the structure. This model shows a continuum of interlacing pores varying in width from one to several molecular diameters.

(2) The calculation seems to break down for pores below 20–25 Å. in radius. Samples with small pores show poor agreement between the summation of individual pore volumes and the total pore volume as taken from the saturation adsorption. There are two reasons for non-applicability of the method to small pores. As pressure approaches zero the Kelvin equation is no longer valid. It is derived on the assumption that the surface energy in the wall film in a capillary is the same as that of bulk liquid. This is not even approximately true as the film thickness falls below two molecular diameters. At present we have no method for computing the surface energy of film molecules, so that the Kelvin equation can be applied for smaller pores. Another cause for the failure of the calculations for small pores is the non-applicability of statistical n -values when the film gets below two molecules in thickness. In the computation one uses the statistical value, but actually in this region the thickness must be either one or two molecular layers, not some intermediate value as used in the computation.

Size of Class I Capillaries.—For the reasons discussed above, one cannot apply the Kelvin equa-

(6) C. G. Shull, *J. Am. Chem. Soc.*, **70**, 1405 (1948).

(7) T. D. Oulton, *This Journal*, **52**, 1206 (1948).

(8) E. P. Barrett, L. G. Joyner and P. P. Halenda, *J. Am. Chem. Soc.*, **73**, 373 (1951).

(9) P. C. Carman, *Proc. Roy. Soc. (London)*, **A209**, 69 (1951).

tion for relative pressures below about 0.5. Class I capillaries empty at relative pressures between 0 and 0.4. Estimates of their size must therefore be based on other considerations than the Kelvin equation. Two points of view have been advanced.

The usual interpretation of a Type I or Langmuir isotherm is that the pores are filled by a unimolecular layer on each wall. The basis for this view is that adsorption occurs in the pressure range normally associated with formation of the first layer and that since the isotherm is flat after point B is passed the pores are filled by the first layer. According to this view the pore width is only two molecular diameters and the adsorption at point B is the amount required for a monolayer.

For reasons previously discussed¹⁰ the writers cannot accept this interpretation. Our arguments may be summarized.

(1) Surface areas of charcoals computed on this basis are unrealistic. For S84, whose isotherm is shown in Fig. 1 the point B area is near 3000 sq. m. per g. Such an area requires that each carbon atom contribute some 6 square ångström units to the area.

(2) Liquid volumes of various adsorbates held in a given charcoal at saturation are essentially constant. If pores were as small as two molecular diameters in width one would expect steric effects for packing of various kinds of molecules into the narrow capillaries and would therefore not anticipate anything like constant liquid volumes.

(3) As discussed above, class I capillaries seem to adsorb by capillary condensation rather than formation of a single layer in the wall. One does not need to assume monolayer adsorption to account for filling of the pores at low relative pressure.

(4) Type I isotherms may show wide variations in the relative pressures at which the pores are filled. This is illustrated in the isotherms for S600H and S84 in Fig. 1. S84 was prepared by steam activation of S600H. Presumably the effect of such treatment is to widen the pores some threefold since after activation the pore volume per gram is more than three times as great as before. Yet both isotherms are type I. If the point B adsorption denotes a monolayer for S600H it cannot also denote a monolayer for S84 unless the only effect of the steam activation has been to create new pores.

(5) The initial heats of adsorption for porous carbons are much higher¹⁰ than for non-porous. This indicates a cooperation of adjacent walls in the adsorption process.

An interpretation of Type I isotherms is that adsorption occurs by capillary condensation, as discussed above, and that capillaries up to several molecular diameters may fill at low relative pressure provided there is a narrow place at which a meniscus can start. The narrower the capillary the lower the pressure at which it is completely filled. Conversely, if pores are wide a higher pressure is needed, as is the case for S84.

According to this model, a class I capillary such as those of S84, might be wider than the Class II capillaries of isotherm C in Fig. 1, the different adsorption behavior depending upon the width of pores at constrictions rather than the maximum width. There is, however, no method at this time for evaluating the width of class I capillaries. Consequently, there is no method for measuring the surface areas in porous bodies with class I capillaries since we do not know how wide the pores are which fill at point B. There is therefore no need to assume that charcoals have such a structure that every carbon atom lies in the surface, a structure that is difficult to reconcile with the rigidity of particles.

Actually, the concept of an average width for class I capillaries is somewhat meaningless. As we visualize the formation of such capillaries they are highly irregular both as to form and width and could better be represented as cone shaped than by equivalent cylindrical pores. Many class II capillaries, on the contrary, seem to be uniform in size, as shown by the steepness of the desorption isotherm.

Surface Mobility.—Several lines of evidence give indications that adsorbed molecules can move about freely on a uniform surface. If the surface is not uniform but can hold adsorbate molecules at all sites, then the molecule will come to rest at the site which holds it most firmly. Thus, on charcoal the first adsorbed molecules tend to flow to the region of the capillary where the binding is tightest, *i.e.*, to the region where the two walls can contribute to the binding. It is because of this mobility that a charcoal bed removes vapors so rapidly. The limiting rate factor in the adsorption of vapors from an air stream is the speed of diffusion of vapor to the *external* surface of the adsorbent granule. If it were not for surface mobility the surface of the granule would become saturated while the inner surface had no adsorbate.

Adsorption of most vapors by charcoal is almost instantaneous when the vapor is admitted to the adsorbent. This is not true for water vapor; hours of contact may be needed before equilibrium is reached. This fact suggests that water vapor may not be mobile on a carbon surface or that it is not held by all surface sites. It must therefore reach the ultimate site of tightest binding in the capillaries by gaseous diffusion to the inside of the capillary, which requires a long time interval for final equilibrium. Equilibration of a charcoal bed with water vapor is for the same reason a slow process. Saturated air must be passed through the bed for many hours before water equilibrium is established. Other vapors set up equilibrium as rapidly as the vapor is let into the charcoal bed.

Adsorption from Solution.—When a solid can hold solute molecules much more tightly than solvent molecules we may remove solute from solution by adsorption. A very favorable case is adsorption of organic molecules from aqueous solution by charcoal, which is a poor adsorbent for water molecules.

Capillaries appear to hold solute molecules just as they condense vapor molecules. An activated

(10) C. Pierce, J. W. Wiley and R. N. Smith, *THIS JOURNAL*, **53**, 669 (1949).

charcoal of pore volume 0.35 ml./g. was found to adsorb 3.2 mmoles benzoic acid or a volume of 0.31 ml. (computed from density of solid benzoic acid). Although this amount of acid was held by 530 ml. of solution the adsorption was nearly complete after shaking for an hour. This again points to surface mobility. A benzoic acid molecule striking the surface is held as a two dimensional gas on the surface. It then migrates to the point of tightest binding, or into the capillaries. Insofar as the charcoal is concerned it makes no difference whether the adsorbate molecule comes from the vapor phase or from solution; in any event the final state of adsorbate is that of a condensed film in the capillaries of the solid.

Non-rigid Systems.—In all the discussions of this paper it is assumed that the adsorbent is a rigid body which does not greatly alter its size or shape

when saturated with adsorbate. Isotherms of non-rigid systems, such as adsorption of benzene by rubber or water by proteins, bear superficial resemblances to isotherms for rigid solids. We believe however that such resemblances have no physical significance. The whole adsorption process for the swelling system may be unlike that of the rigid system. For example, the net heat of adsorption is often negative for the swelling system but never negative for a solid adsorbent. In this case the difference is due to the fact that in the swelling system adsorption may occur with a great increase in entropy or decrease in order whereas on a solid surface the adsorption leads to a more orderly array than in bulk liquid or a decrease in entropy. Adsorption in the swelling system is in many respects more akin to the forming of a solution than to adsorption in a rigid system.

THE PREPARATION AND UTILIZATION OF METALLIC AEROSOLS FOR FILTER PAPER TESTING¹

By J. KOHL AND R. D. ZENTNER

Tracclab, Inc., Western Division, Berkeley, California

Received July 22, 1952

The determination of filtration efficiency and particle size efficiency for filter papers used in health physics is of considerable industrial importance. To determine such efficiencies, it is necessary to employ a simulant dust of known characteristics which can be readily dispersed in aerosol form and from which the desired data may be extracted. Carbonyl iron powder has been employed as such a simulant dust. It can be obtained in known or easily measured size ranges between 0.5–50 μ , it has a spherical particle shape, can be easily dispersed in aerosol form, and lends itself readily to chemical and physical analytical techniques. Dispersion and filter testing equipment and techniques have been devised and results presented of the collection efficiency determinations for several types of filter papers by these methods. Various analytical methods are presented and the problems of filter testing with metallic aerosols are discussed.

Purpose of Project.—It has been determined that such operations as the explosion of nuclear fission weapons, the use of nuclear reactors and the treatment of irradiated materials yield solid finely-divided air-borne radioactive materials. Following A bomb tests aircraft are flown with filter paper sampling devices² for determining air-borne radioactive dust concentrations³ and filter samplers are used at ground stations for this purpose. The aerosols produced in the handling of uranium ores and metals, have been extensively studied from a pharmacologic standpoint.⁴ Moreover, it is known that cooling air passing through such air-cooled piles as the Oak Ridge and Brookhaven reactors contains dust which may become radioactive.⁵ For the purposes of air cleaning and health physics radiation monitoring, it is desirable to determine the type and concentration of particulate radioactivity by air filtration in the vicinity of these operations to determine the hazards to personnel in these areas. It is therefore necessary to know

the efficiency of the filter papers used in this monitoring, so that the absolute amount of air-borne solid radioactivity in the collected air sample may be estimated from a knowledge of the sample volume and the quantity of collected material.

Many devices exist for the laboratory determination of filter collection efficiency. Most of these are designed to test filters at breathing rates (32–85 liters/min.) with penetrating smokes whose particle size is in the region of 0.3–1.0 μ .⁶ Other methods employ tobacco smokes, lead fume, magnesium smokes and oxides of various metals, which are, in general, generated and stored in a plenum chamber until they can be delivered to an air stream passing through the filter to be tested. Plant pollen, mold spores and bacteria also have been employed. Optical, gravimetric, chemical and bacteriological methods are then used to determine the concentration of the aerosol either in the air stream on both sides of the filter or on the filter itself.⁷

For the sampling work contemplated, the most important size range for particulate radioactivity is in the region of 1–5 μ , and the rates at which such activity will be sampled in order to detect low concentrations of solids is in the vicinity of 500–1000 cubic feet per minute per square foot of filter paper. The quantity of material to be collected is approximately one microgram per square foot of filter paper. Since it is evident that papers which will sample aerosols of this size, at these comparatively high velocities cannot be so dense as to cause a large pressure drop across the paper, with a corresponding large utilization of power in the associated air-moving equipment, it was decided that a pressure drop

(1) Presented before the twenty-sixth National Colloid Symposium which was held under the auspices of the Division of Colloid Chemistry of the American Chemical Society of Los Angeles, California, June 16–18, 1952.

(2) *Chem. Eng. News*, **30**, 1999 (1952).

(3) *Nucleonics*, **10**, 10 (1952).

(4) G. Voegtlin and H. C. Hodge, "The Pharmacology and Toxicology of Uranium Compounds," N.N.E.S., VI-I, McGraw-Hill Book Co., New York, N. Y., 1949.

(5) (a) *Nucleonics*, **4**, 9 (1949); (b) *ibid.*, **4**, 28 (1949).

(6) F. T. Gueker, Jr., H. B. Pickard and C. T. O'Konski, "Handbook on Aerosols," U. S. Atomic Energy Commission, 1950, p. 123.

(7) P. Drinker and I. Hatch, "Industrial Dust," McGraw-Hill Book Co., New York, N. Y., 1936, pp. 250–260.

of 20" of water would be the greatest tolerated for candidate papers. With this requirement, it was felt that filter paper collection efficiencies of greater than 99% would be unattainable. No data, however, could be found in the literature for testing methods or for the results of tests in this high flow region. The problem of determining filter paper efficiencies in this region was considered to embrace the following requirements: (1) The design and construction of a filter tester for passing measured air flows at desired rates through a filter paper and admitting aerosols in an appropriate quantity and degree of dispersion. (2) The provision of an aerosol which simulates the properties of field aerosols and a device for delivering the aerosol to the filter tester. (3) The establishment of methods for determining collected and uncollected amounts of aerosols on the filter and in the tester.

These three problems will be discussed in this paper.

The Nature of Air-borne Metallic Dusts.—Although the literature contains many references to air-borne dusts of non-metallic nature, the problem of determining the concentration of metallic dusts was considered to be of interest since contemporary air pollutants contain components of micron size metal particulates.⁸ It is also believed that debris resulting from an atomic explosion or other nuclear operations consists of metallic oxide particles of micron dimensions.⁹ Moreover, with the increasing employment of large quantities of such toxic heavy materials as uranium and plutonium in the atomic industries, the contribution of finely-divided air-borne metallic radioactivity to the industrial hazard is important. It is known that plutonium and uranium aerosols exist as particulate metals having diameters in the 1-5 μ region.¹⁰⁻¹² Moreover, it is this size region that is the most dangerous from a personnel ingestion and absorption standpoint.¹³ In evaluations of air-borne metallic or radioactivity hazards, therefore, it is necessary to consider the filter collection efficiency properties of such aerosols.

In general, the aerosols of interest are metallic aerosols whose particle diameters lie in the range between 0.1 and 5 μ , and whose densities lie in the range of 3.5 to 19.

The Selection of a Simulant Testing Dust.—For the purposes of filter testing the use of weighable amounts of the radioactive aerosols is too hazardous to be practical. It would be difficult to obtain quantities of fissionable plutonium for filter testing and the large-scale use of either plutonium or uranium α -active aerosols in a laboratory is hazardous. Similarly, it would be both difficult and dangerous to obtain testing-scale quantities of radioactive atomic bomb debris.

For these reasons, it was desirable to employ a simulant aerosol whose characteristics would include as many properties of the aerosols of interest as possible. Moreover, data available in the literature indicates that the nature of the dust used to test filter papers has an important effect on the resulting efficiencies.¹⁴

Finally, from the point of view of economic considerations, an aerosol simulant material should be available in reasonable and inexpensive quantities.

A search of the literature of testing dusts was therefore initiated.

Simulants Reported in the Literature.—A variety of aerosols intended to reproduce the characteristics of various field aerosols are presently employed for filter testing. Cadle and Magill¹⁵ employed lamp black dispersions and

sodium chloride particles as simulants for Los Angeles smog. A number of military and civilian laboratories now use a dioctyl phthalate smoke prepared by an MIT-designed generator.¹⁶ Other aerosols employed by these laboratories included triphenyl phosphate, oleic acid, tricresyl phosphate and methylene blue. These latter smokes, however, were intended to simulate military screening agents. LaMer¹⁷ has published extensively on the generation, size-measurement and collection of mono-disperse sulfur aerosols. It is evident, however, that none of these aerosols would be very satisfactory simulants for atomic bomb debris or nuclear operations effluent.

The literature of metal powders was therefore consulted. Metal powders appeared to be satisfactory as far as the criteria noted above were concerned. Powders of over thirty metals, metal salts and alloys were uncovered which might be used; among these were alumina, cobalt, titanium, iron oxide, titanium dioxide, zinc sulfide and cadmium sulfide powders. The last two fluorescent materials were considered because some thought was given to the determination of filter loading by the measurement of fluorescence intensity. Almost all of these could be obtained in mesh sizes ranging from (-100) to (-325) from Chas. Hardy, Inc., New York 17, N. Y. The metal powder art was particularly productive in presenting potential metallic dispersants and a number of samples were ordered and examined in an effort to find a satisfactory material.

It was felt, however, that the most satisfactory method of determining the efficiency of filter materials for various sizes of aerosols was to employ a series of sharply-sized aerosols for testing each filter. In this way the simultaneous retention of the large diameter component of an aerosol and passage of the smaller diameter component might be avoided. This method imposed the limitation that the diameters of the particles in the test aerosol be accurately known. It was also desirable that all of the diameters of a given particle be similar or identical, *i.e.*, that the particle be spherical, so that any cross-sectional area presented by a particle to a filter paper will be a representative, known area. This requirement, of course, limited the potential simulants to those containing spherical particles.

Powders Containing Spherical Particles.—Microscopic examination of the powder samples procured showed that only a few proposed powders possessed the desired characteristics. Among these were carbonyl iron powder, brass powder, copper powder, bronze powder and glass powder. Of this group, carbonyl iron powder was chosen as the simulant to be employed in the filter testing experiments.

Carbonyl Iron Powder.—Finely divided carbonyl iron is procurable from the Antara Products Div., General Aniline and Film Corp. It is supplied in six powders, whose chemical compositions are all in excess of 97% Fe, but whose sizes vary from 40 to 1 μ . A summary of these properties appears below.

Grade	Iron content, %	Particle density	Reported average dia., μ
I,	99.7-99.9	7.85	20
HP	99.7-99.8	7.86	10
C	99.4-99.8	7.86	10
E	97.9-98.3	7.77	8
TH	98.1-98.5	7.79	5
SF	98.0-98.3	7.81	3

In order to obtain an accurate picture of the particle shape and size distribution of the various powder samples, microscopic methods of size distribution measurement were employed. Photomicrography, microprojection and measurement with a filar micrometer were employed to obtain size distributions of the powders. These data are presented in Fig. 1, which are based on measurements of at least 200 particles per sample.

Dispersion of the Aerosols.—A feeder of the "aspirator" type¹⁸ was employed for delivering carbonyl iron powder to the air stream. This feeder comprised an aspirator having

(8) L. C. McCabe, P. P. Mader, H. E. McMahon, W. J. Hamming and A. L. Chaney, *Ind. Eng. Chem.*, **41**, 2486 (1949).

(9) Los Alamos Scientific Laboratory, "The Effects of Atomic Weapons," McGraw-Hill Book Co., New York, N. Y. 1950, pp. 32-33.

(10) G. Voegtlin and H. C. Hodge, "Pharmacology and Toxicology of Uranium Compounds," McGraw-Hill Book Co., New York, N. Y., 1949.

(11) J. A. Leary and F. J. Fitzgibbon, "Particle Size Determination in Radioactive Aerosols by Radio-Autograph," AEC D 2791, June 7, 1949.

(12) P. R. Hammond, "Decontamination of Radioactive Waste Air I," AEC D 2711, Oct. 3, 1949.

(13) Reference 9, p. 360

(14) F. B. Rowley and R. C. Jordan, "Air Filter Performance as Affected by Low Rate of Dust Feed, Various Types of Carbon and Dust Particle Size and Density," Bulletin of Minnesota Engineering Experiment Station 16.

(15) R. D. Cadle and P. L. Magill, *Ind. Eng. Chem.*, **43**, 1331 (1951).

(16) "Handbook on Aerosols," AEC, Washington, D. C., 1950, chap. 10.

(17) V. K. LaMer, *Proc. First Natl. Air Pollut. Symp., Stanford Res. Inst.*, Nov. 1950.

(18) Bureau of Mines Information Circular 7806.

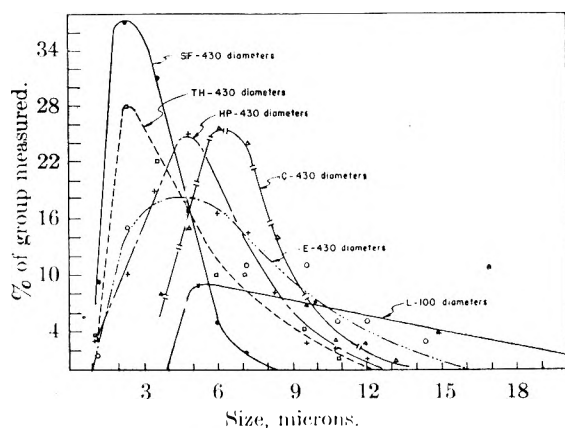


Fig. 1.—Antara carbonyl iron.

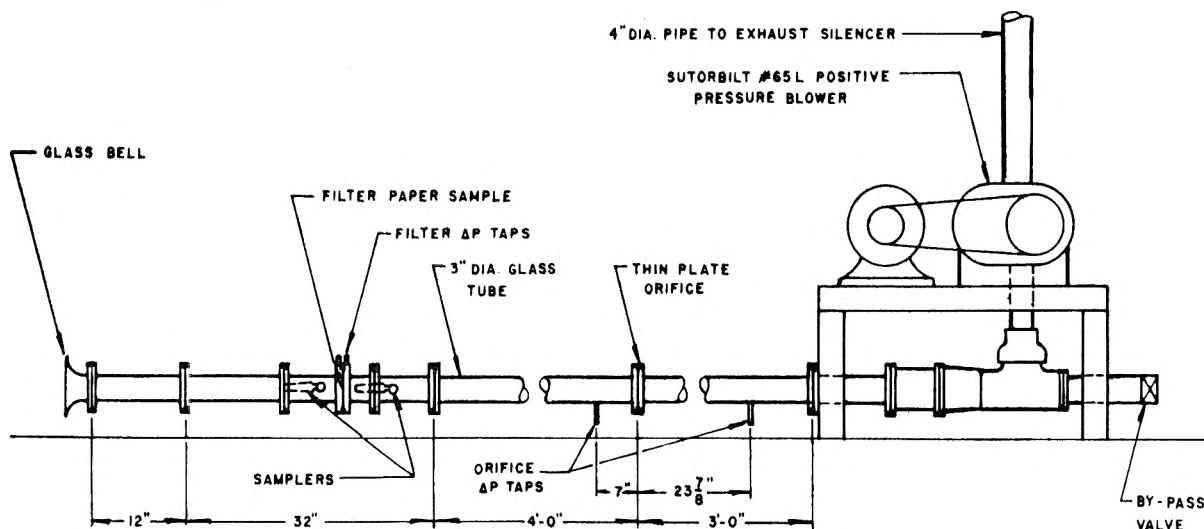


Fig. 2.—Filter testing duct.

an extension tube attached to the suction coupling. This extension led into a tube resting on a small vertical elevator. When compressed air was blown through the aspirator sufficient suction existed in the extension tube to draw carbonyl powder from the elevator tube through the extension tube to the aspirator tip. This feeder was mounted with its aspirator tip just upstream of the intake bell of the filter tester itself.

An effort was made to determine the degree of dispersion achieved, by collecting and inspecting a sample of the aerosol in front of the aspirator. This was achieved by briefly placing a greased microscope slide in the aerosol cloud a few inches in front of the aspirator tip and then examining the slide under a microscope. This experiment was repeated several times and in every case a well-dispersed sample of carbonyl iron powder was obtained on the slide. It was thus assumed that satisfactory dispersion was obtained by the aspirator.

The Determination of Iron.—Once the iron powder was collected on the filter papers, it was necessary to determine the amount thereof. This determination was accomplished by cooking the filter papers from a given run for a few minutes in hot dilute HCl to convert the iron to soluble ferric chloride, which was determined colorimetrically with the well-known ammonium mercurioacetate indicator.¹⁹ This technique permitted accurate determinations of iron on paper in the range 0.1 to 100 mg. The limiting factor for low filter loading tests was the background iron content of the filter papers tested.

Naturally, the precision and accuracy of the determination of filter paper collection efficiency are limited by the precision and accuracy of the colorimetric iron determina-

tion method employed. In the experiments of this study, an accuracy of 1% was considered adequate, since it was desired to establish the order of a series of collection efficiencies of candidate papers rather than to determine absolute efficiencies.

Testing Duct.—Figure 2 is a descriptive drawing of the filter testing duct. It includes nine feet of 3" diameter glass pipe, a filter holder, sampling ports and an orifice for metering flow. Air is drawn through the duct by a Sutorbilt No. 65L Blower at rates from 10 to 250 s.c.f.m. and at filter pressure drops ranging from 5" of H₂O to 80" H₂O.

In a test, a filter paper is placed in the wire-screen-backed holder which is mounted in the duct. Air at a known rate is drawn through the paper while dust is fed into the duct. Samples of the aerosol are withdrawn upstream and downstream of the filter for determination of the aerosol concentration at these locations.

The air samplers comprise sharp edged nozzles containing high efficiency filter paper. They are connected to a vacuum system with a flow control and metering line. Several nozzle sizes and a variable sampling air rate are used to ob-

tain a velocity into the nozzle identical with the average air velocity in the duct. Pitot tube traverses were employed to demonstrate that the filter paper acts as an effective distribution guide which provides a uniform velocity distribution downstream from the filter, even at pressure drops as low as 5" of water, except for a 1/4" thick retarded air layer adjacent to the pipe wall.

Testing Techniques. (1) **Metered Volume Technique.**—In the metered volume technique, a measured fraction of air downstream of the filter was sampled and its dust concentration determined. Knowledge of this concentration and of the dust collected by the test filter, determined by the chemical methods described, permitted calculation of the filter efficiency.

Three types of "absolute" filters were used in the sampling heads. These were ACC type 6, ACC Type 7 and an experimental high efficiency filter. The efficiency of the 6 and 7 filter materials were established at essentially 100% by testing samples of the two papers in series.

In all tests the sampler nozzle ahead of the sampling filter was cleaned of iron powder and the iron thus determined was included in the calculation. The duct was carefully cleaned after each test and the amount of iron dropping out between the test filter and sampler was considered in the calculations. A check of this technique by the mass balance method described in the following paragraph demonstrated its validity for our tests.

(2) **The Mass Balance Technique for Determination of Filter Efficiency.**—The mass balance technique was considered to be an absolute method of determining filter efficiency and was used to establish the validity of the metered volume method, which was considerably simpler to apply. The mass balance technique was carried out by using carefully weighed quantities of feed dust and by thoroughly cleaning the polished interior of the stainless steel and glass

(19) E. B. Sandell, "Colorimetric Determination of Traces of Metals," Interscience Publishers, Inc., New York, N. Y., 1950.

duct. The filter efficiency was then calculated from the ratio of the dust collected by the filter to that reaching the filter face, which was the amount of dust fed less the amount of dust falling out in the duct.

The results of a series of runs, utilizing both the mass balance and metered volume technique, indicated filter efficiencies differing by an average of only 1% for a given paper.

Two Filter Technique for Determination of Filter Efficiency.—In a third method of determining efficiency without the need for making a mass balance or taking samples, two filters were placed in series in the duct system and the aerosol was drawn through both. Assuming equal efficiency for each filter or a known efficiency for the back-up filter, it was possible to calculate the efficiency based only on a knowledge of the amount of iron collected by each filter. This technique verified the efficiencies for the papers determined by other methods and indicated, for example, an efficiency of 76% for Type SF carbonyl iron for the Type 5 paper at 20" pressure drop across the filter. This value falls in the range of values obtained by the mass balance and metered volume techniques. The two filter technique requires the assumption that negligible particle size fractionation takes place in the first filter.

Collection Efficiencies.—To determine efficiencies at flow conditions similar to those expected in air samplers, the filter papers of interest were tested at a pressure drop across the paper of 20" of water. A few efficiencies so determined with Type SF carbonyl iron powder (approx. 1.6 μ) at this pressure drop are shown in Table I.

TABLE I

Filter collection efficiency Sampler method	%	Flow rate through filter in ft./min. at 20" H ₂ O pressure drop
Whatman No. 41	67	225
Whatman No. 41H	46	338
MSA Red All-Dust Filter	91.5	519
Chemical Corps Type 5	76	775
Experimental filter impregnated with dioctyl phthalate	88	2095

In these tests up to 10 mg. of carbonyl iron dust was fed into the unit per test and dust loads of around 1–6 mg./in.² were collected on the filter being tested. Although it was found that increases in dust loading on the filter resulted in greater filter efficiencies, the studies were maintained in the low loading region to simulate field conditions.

The Effect of Particle Size on Filter Efficiency.—Studies were made to determine whether filter papers selectively removed certain sizes at either the high or the low range of the particle size distribution, or whether the filter papers collected a sample whose size distribution was representative of that of the aerosol in the test duct. In order to establish the distribution relationship between the aerosol and the collected sample, four samples for each run were analyzed: (1) the size distribution of the feed dust; (2) the size distribution of the air-borne dust upstream of the tested filter; (3) the size distribution of the dust on the tested filter; (4) the size distribution of the air-borne dust downstream from the tested filter.

The size distribution of the feed dust used in these studies, Type SF carbonyl iron powder, has been shown in Fig. 1. Size distributions of the aerosol upstream of the tested filter were collected both on greased microscope slides and on extremely efficient low-flow rate air filter papers. By examining these samples under the microscope

it was established that the aerosol upstream of the tested filter had a size distribution corresponding to that of the feed dust.

Samples were cut from the upstream filter, the tested filter and the downstream sampler filter after each of several runs with Type SF carbonyl iron powder. These samples were placed on a microscope slide, wet with xylene to secure them to the slide, and tweezed apart with dissecting needles to render the collected particles visible. The particles were then measured at approximately 1200 \times (oil immersion) with a filar micrometer. Over two hundred particles were measured in each sample.

The results of one typical run are shown in Fig. 3. It can be seen that the filter examined, Chemical Corps Type 5 paper, collected a representative sample of the feed dust; and a representative sample was similarly collected from the airstream behind the filter. In this way, it was established that this paper did collect a representative sample of the aerosol in this size range.

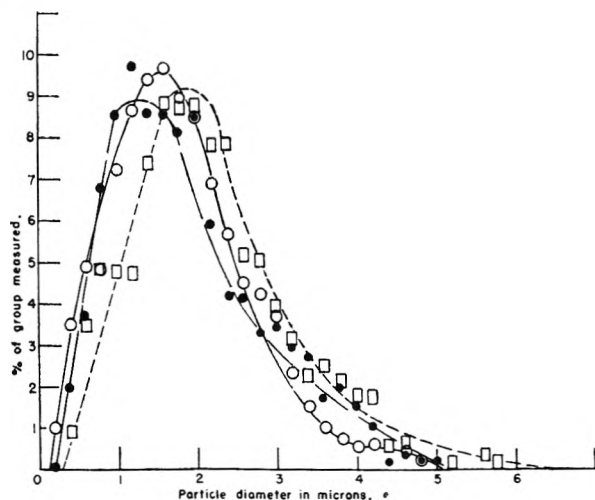


Fig. 3.—Size distribution curves, 600 particles each approximately 1213 \times : feed dust, —○—○—○—; dust on type V, —●—●—●—; dust on back sampler, —□—□—□—; —■—■—■—.

The technique described is adapted for establishing the collection of non-representative samples of aerosols by candidate filter papers. No such papers were encountered, however, in the group examined during this study.

The authors wish to thank other members of the staff of this project, and, in particular, Dr. L. R. Zumwalt, Mrs. Cornelia Mayrhofer and Mr. T. H. Mansfield, for their untiring and enthusiastic cooperation, without which this problem could not have been successfully completed.

DISCUSSION

HUMBERT MORRIS.—I should judge that your interest in this work is the protection of the human respiratory system. The upper part of the respiratory system normally traps air-borne particles larger than 5 μ , if the density is one. These particles are moved, along with mucus, to the throat and then to the stomach. Only particles smaller than 5 μ (if the density is one) have a good chance to reach the small cavities, alveoli, in the lungs, where they might be retained for a long time. Of these, only the particles which are larger than 1 μ have a good chance to settle out: the smaller ones are freely exhaled. Thus, the human lung is most

imperiled by particles in the size range of 1 to 5 μ , if the density is one. If the density is greater, as in your case where it is about 8, somewhat smaller sizes would be more appropriate. However, as you report that the filter paper collects the same particle-size distribution that impinges on it, this point may not be important.

K. J. MYSELS.—How does the effect change with the rate of air passage?

R. D. ZENTNER.—We found it was as much a function of the type of collector as anything. The collectors we used generally had their efficiency increased significantly as the air flow rate went down, largely because the aerosol was in contact with them more, and the forces tending to move the aerosols through the filter paper in stream lines were greater at higher rates of flow than at low rates of flow. In most cases as we went down in flow rate, we got efficiency of 100%, but we are not interested in low flow rates.

ANON.—Do you think the results of these tests can be applied to substances other than iron?

R. D. ZENTNER.—We felt that because we were using a particle size definitely in a region of interest and our results in many cases approximate results obtained at AEC sites, that we were not going too far wrong. Your point is a good one, because apparently the critical consideration is the centrifuging of the particles out of the air stream line on to the filter paper. This is, of course, a function of the density of the particle. Because we were working at an intermediate range, we felt we could probably extrapolate on both sides much better than if we were working at one end or the other of the density range.

ANON.—What filter areas did you employ?

R. D. ZENTNER.—In most cases we were using fractions of a square foot up to one square foot. The velocities were of the order of linear 1000 feet per minute.

SOME ELECTRICAL PROPERTIES OF COLLOIDAL SUSPENSIONS IN OILS¹

By A. BONDI AND C. J. PENTHER

Shell Development Company, Emeryville, California

Received July 22, 1952

A variety of electrical measurements have been carried out on colloidal suspensions in oils by means of a capacitor with one rotating electrode. Suspensions of soap fibers exhibited a drop of dielectric constant with increasing shear stress which has been ascribed to flow orientation of these anisometric particles. The relatively low dielectric loss of soap suspensions appears to be composed of a low frequency (ionic conduction) and a high frequency component of widely differing temperature coefficient. The dielectric loss of silica suspensions, on the other hand, gives a continuous spectrum in the frequency range studied (0.02 to 20 kc.). From the marked reduction of dielectric loss by shearing one may derive information regarding the corresponding change in geometry of the silica particle aggregates. Two novel effects have been discovered which apply to all suspensions of non-conducting particles examined; an increase in the (very small) d.c. conductivity and the appearance of a marked electrokinetic potential as they are sheared. Similarly, while the d.c. conductance of carbon black suspensions is reduced by shearing, owing to the destruction of the conducting particle chains, the d.c. conductance of deflocculated carbon black suspensions rises with shear rate as it does for other systems of non-conducting particles. This change in sign of the shear rate-coefficient of conductivity may be a sensitive criterion of deflocculation. The dielectric constant of iron particle suspensions and its shear rate coefficient are quite small and relatively insensitive to the degree of particle aggregation, hence are not a good measure of flocculation. Most striking in the experiments with non-conductive particles as well as with those on iron particles is the extremely rapid response of dielectric properties not only to acceleration but also to deceleration of shear rate. Hence the deformation of particle aggregates in the systems under discussion may be essentially elastic in nature, a fact which throws new light on their flow properties and the mechanism of motion of gels.

The degree of flocculation of colloidal suspensions in non-aqueous media has heretofore been measured by the sedimentation volume, the sedimentation rate, the flow properties and occasionally by light scattering techniques or by direct microscopic observation.²⁻⁴ The optical techniques are undoubtedly most direct and accurate and based on sound physical theory, but they are afflicted with some serious shortcomings which severely reduce their usefulness in many investigations. Among these, the small permissible concentration of solids looms largest, since that means a small interfacial area is available for adsorption. Unless the experiment be carried out in extremely pure solvents, the solid-oil interface will be swamped with adsorbable impurities from the solvent and the discrimination in deflocculating ability among the surfactants to be tested will be poor. There are also difficulties in applying the

optical methods over a wide temperature range. The suggestion by Voet,⁵ that flocculation could be observed by electrical measurements prompted exploration of the possibilities of that method in a number of fields in which we happened to be interested.

It may be recalled that Voet proposed to measure the dielectric constant of colloidal suspensions as a function of concentration and of shear by means of a cylindrical capacitor cell containing a coaxially arranged rotating electrode. This method appeared to be applicable to concentrated systems and its exploration was decided on. Since the work planned was intended to correlate with the results of viscosity measurements a broader range of shear rates and temperatures had to be covered than appeared possible with Voet's apparatus; accordingly a new apparatus was designed and built which has been described in another paper.⁶

Results

Suspensions of Non-conducting Particles.—Suspensions of soap fibers and of silica particles in oils were chosen as representative of non-conducting systems. As shown in Figs. 1 and 2 the soap par-

(1) Presented before the twenty-sixth National Colloid Symposium which was held under the auspices of the Division of Colloid Chemistry of the American Chemical Society in Los Angeles, California, June 16-18, 1952.

(2) E. K. Fischer, "Colloidal Dispersions," John Wiley and Sons, Inc., New York, N. Y., 1951.

(3) Henry Green, "Industrial Rheology," John Wiley and Sons, Inc., New York, N. Y., 1946.

(4) M. van der Waarden, *J. Colloid Sci.*, **8**, 317 (1950).

(5) A. Voet, *THIS JOURNAL*, **51**, 1037 (1947).

(6) C. J. Penther and A. Bondi, *ibid.*, **57**, in press (1953).

ticles are quite anisometric and crystalline, whereas the silica particles are amorphous essentially isometric sponges. Both solids are able to gel oils at relatively low concentrations. The dielectric constant of both solids is of about the same magnitude (around 5). The very low electrical conductivity and dielectric loss of the bulk solids is hardly related to the corresponding property of small particles with surfaces in excess of 100 m.²/g., since the surface conductance probably becomes the governing factor in their electrical behavior.

The purpose of the electrical measurements on these systems was to obtain quantitative information regarding their state of flocculation and, if possible, to learn something about the kinetics of particle motion in the gels. Flow measurements can be interpreted in a simple manner only for dilute suspensions where there is no particle interaction. The systems under study, however, are of greatest practical interest at concentrations where particle interaction dominates their mechanical properties. Viscosity measurements had given no clue regarding the mechanism of particle motion in gels. Electrical measurements which are sensitive to changes in particle aggregation and configuration appeared potentially able to give some information regarding the details of particle motion in gels. We shall see that this expectation has been fulfilled.

In the course of this work an effect has been discovered which has not previously been reported in the literature, namely, an increase in the conductivity of "non-conducting" suspensions under the influence of shear. This phenomenon has tentatively been ascribed to the transport of charges across the electrode gap by means of particle collisions. The simultaneous generation of charges on the electrodes as shear induces relative motion of gel particles and surrounding fluid interferes with the very feeble charge transfer by the collision process, and the data given should be considered preliminary pending quantitative evaluation of the two superposed phenomena.

Soap in Oil. Dielectric Constant.—Several lubricating greases composed of about 6% technical lithium soap and a highly refined mineral oil (see Table I for physical property data) were examined. The dielectric constant of these greases proved exceedingly sensitive to shear, decreasing rapidly with increasing shear rate over the entire frequency range (50 to 20,000 c./s.) and temperature range (30 to 90°) studied. In view of the anisometric shape of the soap particles this effect was to be expected and can be considered as a corollary to the flow birefringence observed on very similar systems.^{7,8} Its quantitative aspects are still puzzling, however. The extent of dielectric constant change is rather greater than one would estimate for electrically isotropic particles of similar length/diameter ratio on the basis of interfacial polarization theory.⁹ The large effect could be accounted for if one assumes that the particles are electrically anisotropic. This is a plausible assumption in view

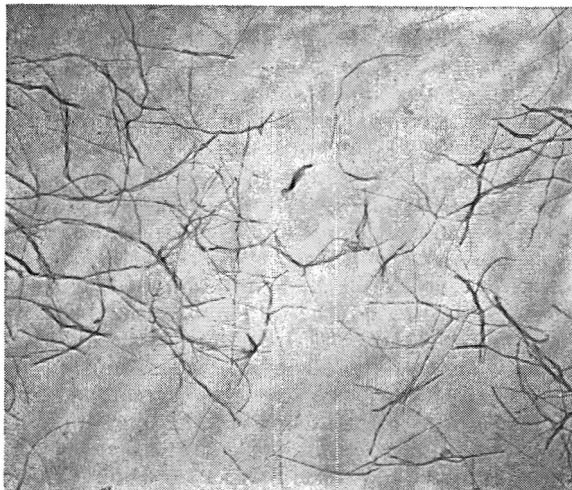


Fig. 1.—Electron micrograph of lithium soap fibers.

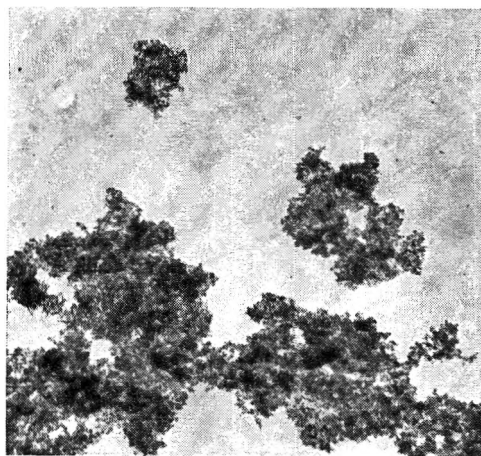


Fig. 2.—Electron micrograph of aerosil silica.

of the crystalline character of the soap fibers. In the absence of electrical measurements on soap single crystals there is no independent evidence for this guess, nor can one determine the extent of flow orientation of the soap fibers.

Their relatively large size, the high viscosity of the oil and their strong particle interaction preclude Brownian motion of the soap fibers; they therefore begin to orient instantly as shear commences. It is rather unexpected, however, that the particle orientation—as measured by dielectric constant—also follows speed reductions (down to complete stop) just as rapidly,¹⁰ since even for the free particles one would estimate a reorientation time, after removal of the shear forces, of the order of 100 sec.^{11,12} In the absence of Brownian motion one would have expected prolonged persistence of orientation after removal of the shear stress. A possible explanation is that the grease does not flow as a continuum but in discrete lumps, each one of which is deformed elastically. The deformation of the lump would likewise lead to orientation of the

(10) Namely, instantly, as observed on the oscilloscope, which was used as balance detector.

(11) A. Peterlin, *Kolloid Z.*, **86**, 230 (1939).

(12) W. Philippoff, "Viskosität der Kolloide," Steinkoff, Dresden, 1942.

(7) J. A. Brown, *et al.*, paper presented at the Annual Meeting of the National Lubricating Grease Institute, Oct., 1951.

(8) B. W. Hotten and D. S. Birdsall, *J. Colloid Sci.*, **7**, 284 (1952).

(9) R. W. Sillars, *Inst. Elect. Eng.*, **80** 375 (1937).

fibers (as in stress birefringence), the strain energy being stored in the bent fibers held together at their contact points. A macroscopic simile would be a multi-tail whip which is bent by pulling the tails. Being lubricated against each other, the lumps can relax instantly as the shear stress on them is reduced.

Increasing the temperature decreases the flow orientation effect, as shown in Fig. 3, because of the reduced viscosity and thus the reduced shear stress. In the absence of particle interaction the shear stress transmitted by the oil should have been responsible for the observed flow orientation. Plotting $\epsilon - \epsilon_0$ against the shear stress transmitted by the oil ($\dot{\epsilon}\eta_0$), however, strongly overcompensates the temperature effect instead of aligning all points on a single curve. Closer coincidence of the points obtained at several temperatures on a single curve is obtained, however, if one employs as independent variable the shear stress data derived from the flow measurements on the grease sample. This result strongly suggests that the soap crystallites are oriented by forces transmitted through the gel lattice.

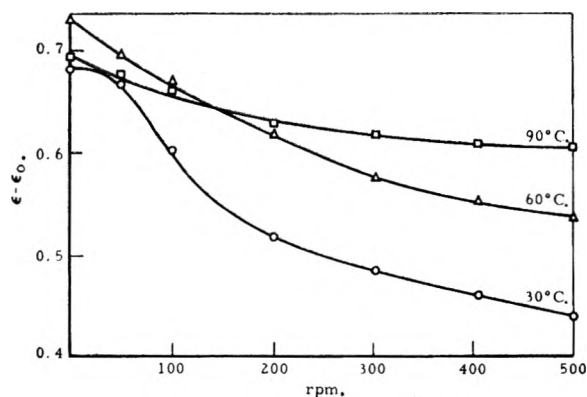


Fig. 3.—Shear induced change in dielectric constant of a lithium soap suspension at various temperatures: ϵ_0 , dielectric constant of solvent; ϵ , dielectric constant of suspension.

The dielectric loss of the greases tested is small, indicative of the fact that the bulk¹³ and the surface conductivity of the soap particles is very low. Most commercial greases exhibit higher losses¹⁴ owing to the presence of conducting oxidation products which probably accumulate in the soap/oil interface. The plot of $\tan \delta$ (the diel. loss angle) against frequency at various temperatures, shown in Fig. 4, suggests that several dissipative processes operate in this system. The low frequency losses represent undoubtedly an ionic conduction, the loss being of similar order of magnitude as the observed direct current conductivity of the system. The positive temperature coefficient of conduction is in keeping with such a mechanism. The temperature coefficients of $\tan \delta$ and of κ (d.c. conduct.) are smaller by a factor of 2.7 to 2 than that of the viscosity of the oil, indicating that the migration of ions may be along the soap/oil interface rather than through liquid.

The higher frequency loss, which in terms of

(13) T. M. Doscher and S. Davis, *THIS JOURNAL*, **55**, 53 (1951).

(14) J. N. Wilson, private communication.

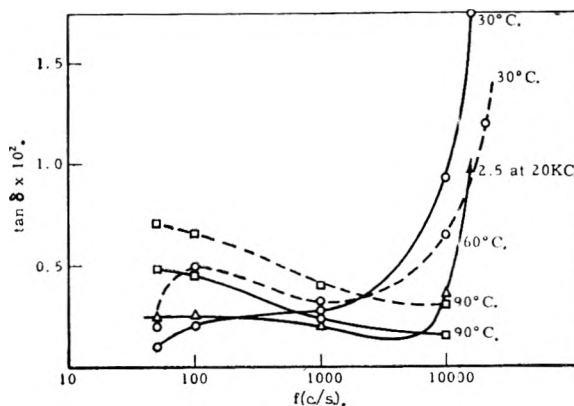


Fig. 4.—Frequency dependence of the dielectric loss of a lithium stearate grease at various temperatures, under static conditions (drawn out lines), and at a shear rate of 1000 sec.^{-1} (broken lines).

conductivity is a large multiple of the d.c. conductance, exhibits at 10 kc. a negative temperature coefficient. In the absence of data closer to the maximum, *i.e.*, to the relaxation frequency, it appears unsafe to make any guesses regarding the nature of the oscillators responsible for this loss component.

The large effect of shear on the dielectric loss, especially at low frequencies, without significantly changing the position of the maximum suggests that it is due to the collisional conduction mechanism, mentioned above and discussed in the following section, and not to changes in the state of aggregation which, as interfacial polarization losses, would be accompanied by displacement of the low frequency maximum, depending upon the growth or decrease in length/diameter ratio of the aggregates (*v.i.*).

The electrokinetic effect is rather pronounced in soap base greases, as is shown by the curves in Fig. 5, and it increases in extent with increasing temperature. This means that the relative motion of gel structure and oil increases as the temperature increases. The far more rapid decrease of oil viscosity than of gel rigidity as the temperature is raised is in agreement with this conclusion. In view of the concurrent increase in conductivity with shear rate and with temperature the observed potentials do not represent the true potentials and have yet to be corrected. The

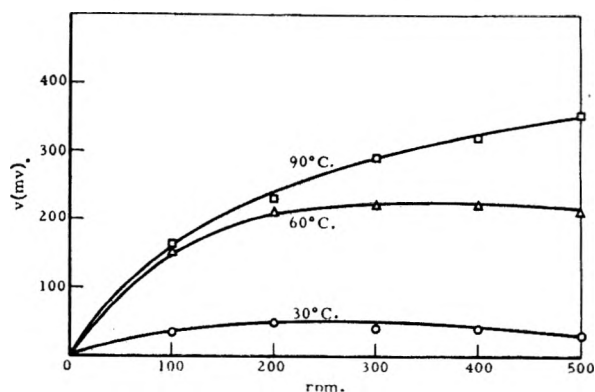


Fig. 5.—Shear induced (electrokinetic) potential using a lithium stearate grease.

grease of Fig. 5 gave the same results irrespective of the direction of the experiment. Some greases, however, do not follow the same curve as one decreases the velocity which they followed during the acceleration cycle. The nature of the resulting hysteresis loop has not yet been examined.

Silica in Oil.—Nearly isometric non-conducting particles are obtained by the combustion of silicon tetrachloride in the oxygen-hydrogen flame. The silica employed in this work¹⁵ (see Fig. 2) was presumably made by such a process. In contrast to the soap fibers one would not expect easily observable flow orientation phenomena in such systems and indeed there is only a mild effect of shearing on the dielectric constant. A far greater shear effect is experienced by the dielectric loss, which will therefore be discussed first.

The dielectric loss of silica suspensions in oils is rather high, as shown by the data in Table II, especially at low frequencies. In view of the very low loss and conductivity of bulk silica—quartz glass—the losses must be due to the relatively high surface conductivity of the silica particles. The strongly adsorbed water layer may constitute the conducting path, no special effort having been made to dry the silica powder.

TABLE I

PROPERTIES OF SUSPENSIONS USED AND OF THEIR COMPONENTS

	Silica suspension ^b	Soap suspension ^b
ASTM cone penetration ^a at 25°, dmm.	345	292
Approximate yield value, dynes/cm. ²	1500	2500
Properties of oil		
Viscosity at 30°, cs.	115	143
Viscosity at 90°, cs.	11.2	10.7
Refractive index n^{20D}	1.4800	1.4898
Dielectric constant at 30°	2.175	2.236
Temp. coefficient of dielectric constant, °C. ⁻¹	1.1×10^{-3}	1.07×10^{-3}

^a Worked 60 strokes. ^b At 6% w. solids concentration.

TABLE II

DIELECTRIC LOSS OF SILICA (AEROSIL) SUSPENSIONS IN WHITE OIL UNDER STATIC CONDITIONS

Frequency	$\tan \delta \times 10^2$			
	100 c./sec. 30°	30°	10,000 c./sec. 30°	90°
1.15% v. silica	1.75	3.1	0.36	0.46
2.35% v. silica	2.03	6.0	.36	0.66
4.9% v. silica	4.1	16.3	.62	1.81
0% silica (oil)	0.09	0.2	.13	0.1

It is well known that the presence in a non-conducting fluid of a second phase of higher conductivity gives rise to dielectric losses, which—for spherical particles—can be calculated by the Maxwell-Wagner theory. Non-spherical particles cause a far greater loss, as has been shown by Sillars.^{9,16} A typical series of loss *vs.* frequency curves for particles of different length diameter

(15) Aerosil "K" made by Degussa, Germany, received through the U. S. Navy, and Linde Silica, an equivalent American product.

(16) The authors are indebted to Prof. C. P. Smyth for directing their attention to this theory.

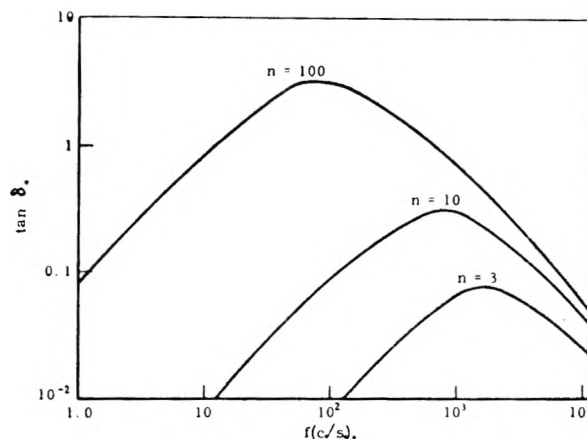


Fig. 6.—Relation between dielectric loss of a suspension and particle geometry and frequency, according to Sillars' theory: for the case: $\epsilon_0' = 2.2$; $\epsilon_2' = 5.2$; $\sigma_2 = 10^{-3}$ mho/cm., n is a function of length/diameter ratio of particles, $n = 3$ for spheres.

ratio as calculated from Sillars' theory is shown in Fig. 6.

A similar set of curves is obtained if one plots loss *vs.* frequency data of the silica suspension for various shear rates, Fig. 7a. The tentative conclusion is drawn from these results that at the highest shear rates the independent particle aggregates have a more spherical shape, and as the

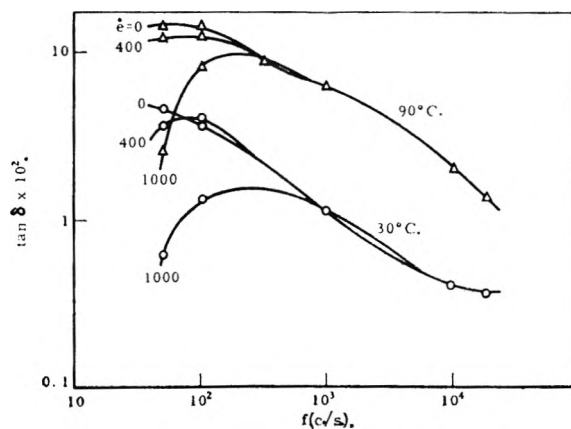


Fig. 7a.—Dielectric loss curves for a 6% w. silica suspension in white oil at shear rates varying between 0 and 1000 sec.⁻¹ and at 30° and 90°.

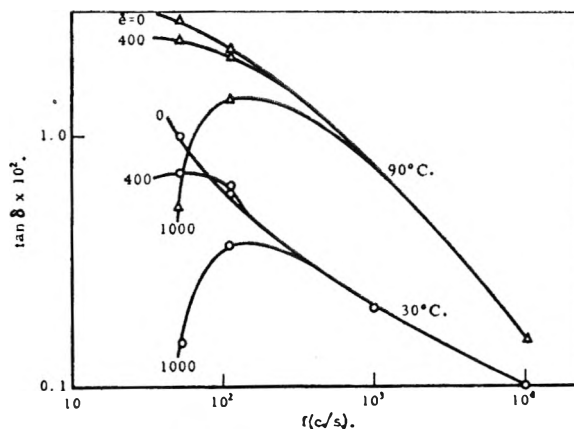


Fig. 7b.—Dielectric loss curves for a 6% w. silica suspension in white oil, deflocculated with a monolayer of dimethyl-stearylamine.

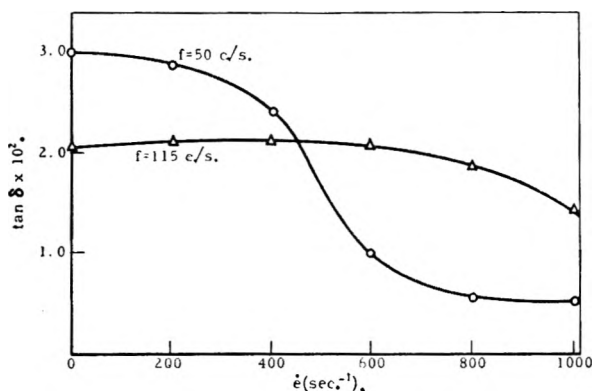


Fig. 8.—Dielectric loss of a 6%w. silica suspension in white oil as function of shear rate (at 90°).

shear rate is reduced the particles agglomerate in chain-like aggregates of increasing length/diameter ratio. At speeds below a certain value the aggregates begin to grow also in dimensions normal to the direction of flow and the loss does not show any further change, while the dielectric constant actually decreases with decreasing shear rate beyond that point (*v.i.*). The differences in slope between the curves of Figs. 6 and 7a may be due to the probably wide distribution of chain lengths in the silica suspension.

As for most semi-conductors, the temperature function of the dielectric loss, *i.e.*, the local conductivity, is exponential in character, owing to the existence of an activation energy for the motion of the conducting ions. For the case of conduction by proton transfer along a hydrogen bond bridge this activation energy is determined by the local barrier to the rotation of the hydroxyl group. A detailed discussion of this subject will be presented elsewhere.

The presence of a deflocculating agent does not change the general shape of the curves shown above, but—depending upon the nature of the interaction with the surface—changes the absolute level of the loss (see Fig. 8) and its temperature coefficient. It is one of the advantages of this method of measurement that one can obtain information regarding the behavior of surface layers in gels under specifiable conditions of mechanical history.

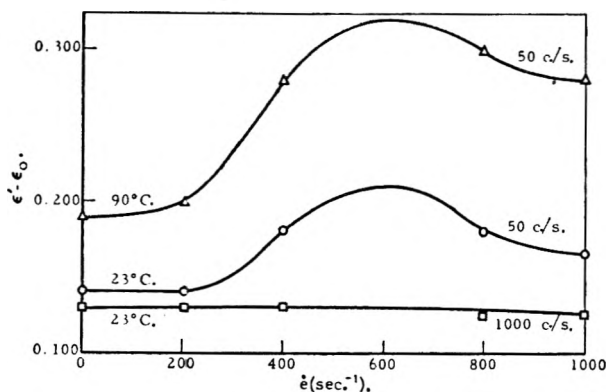


Fig. 9.—Shear effect on the real component of the dielectric constant ϵ' of a silica suspension in white oil at various frequencies and temperatures. At 90° and 1000 c./s. $\epsilon' - \epsilon_0 = 0.086$, independent of shear rate.

The dielectric constant of silica suspensions is strongly frequency-dependent, especially in the range of low frequencies, the range of anomalous dispersion, as shown in Fig. 9. The contribution of the silica to the dielectric constant of the suspension is expressed as $(\epsilon - \epsilon_0)/\varphi$ where ϵ and ϵ_0 are the dielectric constants of suspension and oil, respectively, and φ is the volume fraction of silica. According to interfacial polarization theory this specific dielectric constant increment should be independent of concentration. The data shown in Table III are not in complete agreement with this requirement of theory. The origin of this discrepancy will be explored further.

TABLE III

SPECIFIC DIELECTRIC CONSTANT INCREMENT OF SILICA IN ITS WHITE OIL SUSPENSION (AT ZERO SPEED) AT 10 KC.

Vol. concn. of silica (at 20°)	at 30° ($\epsilon - \epsilon_0)/\varphi$	at 90°
1.15%	4.2 (3.74) ^a	3.0
2.35%	4.05 (3.8)	3.4 (3.05)
4.9%	3.1 (2.96)	3.5 (2.96)

^a Values in parentheses are derived from the real component of the dielectric constant of the suspension.

The dielectric constant *vs.* shear rate curve goes through a maximum. The high speed branch of this curve may be understood in terms of the chain-aggregation mechanism which was suggested by the loss *vs.* speed curve. The low velocity branch of the curve may reflect the increasing spherical symmetry of the aggregates as the three dimensional particle network is formed.

The direct current conductivity of the silica suspension under static conditions is but a small fraction of the equivalent conductance corresponding to the a.c. losses. While the latter (in the low frequency region) decrease sharply as the suspension is being sheared, the d.c. conductance increases steadily with increasing applied shear rate.

This peculiar phenomenon may be understood as due to charge transfer from one electrode to the other through successive collisions of particles which carry the adsorbed charge in the interface (as Millikan's oil droplets did). Knowing the number of particles per unit volume, their size and the prevailing shear rate as well as the voltage gradient, one can estimate the amount of current that could be so carried, making but two plausible assumptions: the charge per particle equals one elementary charge (4.8×10^{-10} e.s.u.) and the attractive forces between the particles are sufficiently short range so that one can set the radius of the attractive force field of the particle as equal to the particle radius. From Smoluchowski's theory of orthokinetic flocculation one then obtains for the number of collisions per particle per unit time

$$\dot{n} = \frac{4}{3} \nu R^2 \dot{e} \quad (1)$$

where ν = number of particles per unit volume, R = radius of attraction sphere of a particle, \dot{e} = shear rate in sec^{-1} . The conductivity calculated from the particle collision rate—on the basis of the electron microscope radii of the smallest par-

ticles—exceeds the actually observed conductivity usually by a factor of the order 10^2 to 10^4 . This factor contains the charge transfer efficiency per collision and the number of small particles per moving aggregate, or only the latter if one assumes charge transfer to be complete on every collision. Quantitative evaluation of the d.c. conductivity data requires correction for the electrokinetic potential (and *vice versa*) which is very noticeable with silica suspensions (see Fig. 10). The conductivity increment per unit concentration for a given shear rate should reflect changes in degree of aggregation as a function of temperature and composition. The data in Table IV indicate that temperature has a relatively small effect, but that deflocculants sharply increase the number of particles, as one should expect.

TABLE IV

D.C. CONDUCTIVITY INCREASE^a OF SILICA SUSPENSIONS IN WHITE OIL DUE TO SHEARING AT A SHEAR RATE OF 400 SEC.⁻¹

Volume concentration of silica ^b	Conductivity increase per unit concentration per unit shear rate (mho cm. ⁻¹ sec. × 10 ⁻¹³)		
	60°	100°	120°
1.5%	1.4	1.45	1.57
2.35%	0.9	1.5	1.2
4.9%	1.9	2.3	2.5
4.9% + monolayer of deflocculant	25	240	270

^a Uncorrected for electrokinetic potential. ^b Aerosil K.

The electrokinetic potential of silica suspensions is of the same order as for soap suspensions. It likewise increases with increasing temperature because of the increased relative motion between oil and gel structure. For this reason it is also more pronounced the stiffer the gel, *i.e.*, the higher the solids concentration, as shown in Fig. 10. No general rule has as yet been found regarding the effect of various deflocculants on the electrokinetic potential.

Suspensions of Conducting Particles.—Suspensions of numerous species of conducting particles have been described by Voet.⁵ As all conductors have the same dielectric constant, namely, infinity, the dielectric constant of all their suspensions can be described by a single expression, which at low volume concentrations ϕ is well approximated by

$$\epsilon = \epsilon_0(1 + 3F\phi) \quad (2)$$

where ϵ , ϵ_0 are the dielectric constant of suspension and oil, respectively, and F is a shape factor, which is unity in the case of spheres and can acquire relatively large values for anisometric structures; it does not depend upon the size of the particles.

Iron Powder in Oil.—One of the main difficulties in carrying out measurements on metal powder suspensions in oils is the large density difference which leads to rapid settling of the suspensoid. The settling rate can be reduced by the use of viscous oils and very small particles. As a typical application of this equipment it appeared of interest to study the deflocculating ability of surfactants on iron powder. The latter is available in very finely divided forms derived from the decomposition of iron pentacarbonyl. The grade used (Grade SF of General Aniline and Dyestuff

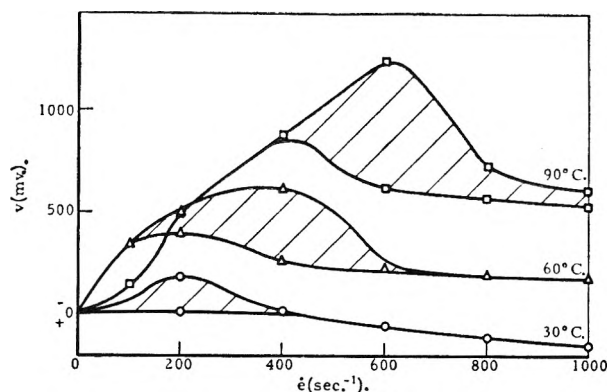


Fig. 10.—Electrokinetic potential (uncorrected) obtained when a 4.9%v. silica suspension in white oil is sheared at various speeds: the upper curves represent the (initial) maxima; the lower curves the steady state values of the potential.

Corp.) had, according to the manufacturer, a narrow size distribution with a steep maximum around 2.5μ . Sedimentation analysis of this powder in white oil (of somewhat lower viscosity than the white oil used in the electrical measurements) gave a size distribution curve with a flat maximum around 13μ . The degree of flocculation in white oil is therefore of the order $(13/2.5)^3 = 140$. Microscopic observation confirmed the average aggregate size determined by sedimentation analysis.

Settling in the cell does not affect the measurements appreciably as long as no concentrated sediment is formed. Nevertheless it appeared desirable to carry out the measurements quite rapidly after filling with the freshly stirred up suspension. Typical data are shown in Fig. 11. The shape factors are of similar magnitude as those found by Voet for other metal powder suspensions, as is their dependence upon the applied shear.

The agglomeration factor $F_{rest}/F_{infinite\ shear}$ just as the shape factor F does not reflect the size of the flocculated aggregate but only its—presumably accidental—anisometry. It should be added that, except for the rest state, the dielectric constant corresponding to any given shear rate is reproduced to within one point in the third decimal place regardless whether arrived at from higher or from lower speeds, and is attained nearly as

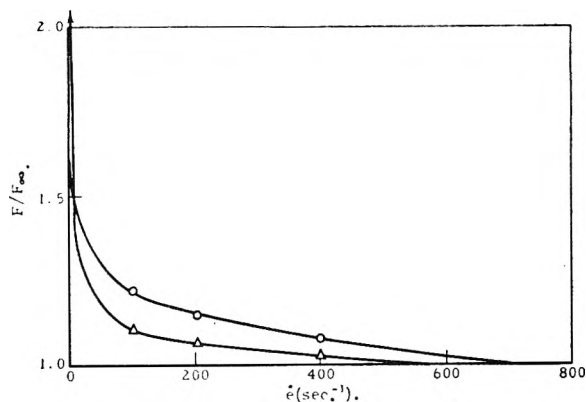


Fig. 11.—Change of agglomeration factor (determined from dielectric constant) of iron powder SF (2.7%v.) in white oil with increasing shear rate at 30°: O, iron powder in oil; Δ, iron powder plus 0.1% stearic acid in oil.

rapidly as the response of the speed changing device. Further oscillographic studies are intended for the actual measurement of the response rate of the system.

The capacity of the rest state is attained more slowly. The rate at which this takes place appears to depend very strongly upon the surface condition of the particles, being very rapid with freshly prepared straight iron/white oil blends, and quite slow in the presence of small amounts of surfactant, *e.g.*, stearic acid. This differentiation has not been observed in the rate of adjustment of the capacity to steady state values at finite rotational speeds.

As one should expect, the presence of surfactants (deflocculants) reduces the values of $dF/d\dot{\epsilon}$ (or probably more correctly $dF/d\dot{\tau}$) as shown by the curves of Fig. 11.

The dielectric loss of iron suspensions is not easily interpreted because of the contribution which eddy current losses might make, which—in contrast to the interfacial polarization losses—are strongly dependent upon particle size. Experimental data indicate that the sign as well as the magnitude of the speed coefficient of dielectric loss of these suspensions is affected by solids concentration and particle size. More data will be required, however, before a clear picture can be discerned.

The d.c. conductivity of the dilute iron suspensions is very low and does not increase with shear rate, apparently because of the small number of particles present compared to the silica and soap systems.

Carbon Black in Oil.—Few systems have been studied as frequently for their state of aggregation as the suspensions of carbon blacks in oils. Viscosity, sedimentation volume, sedimentation rate, as well as electrical methods have been employed.^{2,4,17-19} Voet likewise examined the dielectric constant *vs.* concentration and shear rate relation of carbon black suspensions.⁵ In the course of the examination of the electrical properties of acetylene black suspensions in oils it became apparent that the conductivities of such suspen-

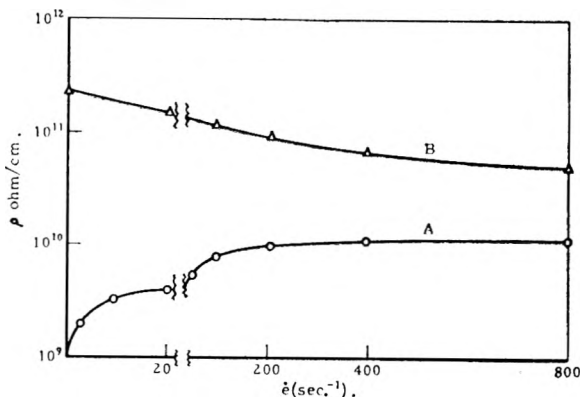


Fig. 12.—Effect of shear rate on the resistance of a carbon black suspension (10%w. of channel black) in white oil at 30°: curve A, as is; curve B, deflocculated with a monolayer of surfactant.

(17) M. J. Forster and D. J. Mead, *J. Applied Phys.*, **22**, 705 (1951).

(18) A. de Waele, *et al.*, *Nature*, **166**, 401 (1950); **167**, 244 (1951).

(19) R. G. Kinsman and R. F. Bowles, *J. Oil and Colour Chemists' Assoc.*, **34**, 592 (1950).

sions are far too high to permit reasonable values of the dielectric constant to be obtained. The same applied to several channel blacks.

The high conductivity of such blends has been generally ascribed to the formation of continuous particle chains (catenation) between the electrodes. Straining these chains leads to their breakage and thus to reduction in the conductivity of the system. Were the concentration of chains so small that they would not collide in positions leading to temporary bridging between the electrodes, a single revolution would reduce the conductivity to a very small value. The work reported here was carried out at a sufficiently high concentration to lead to gel formation. Shearing therefore never reduced the conductivity by more than an order of magnitude.

Deflocculation in such systems by means of surfactants should thus have two effects. By separating the carbon particles and preventing the formation of chains they should reduce the conduction through the suspension materially. Hence, by changing the system to one composed of non-conducting, *i.e.*, mutually insulated, particles, the application of shear should increase the conductivity by means of the collision mechanism postulated for the silica suspensions. Both of these characteristics are actually observed. Addition of a typical engine oil deflocculant may reduce the conductivity of acetylene black suspensions by a factor of nearly 10^4 and, on the other hand, the conductivity of many deflocculated carbon black suspensions is indeed found to increase with increasing shear rate, Fig. 12. Consequently the concentration of surfactant, at which the conductivity/shear rate relation changes sign may be a fairly exact measure of its deflocculating ability. That even high shear stresses may deflocculate a system, at least temporarily, to the extent of changing the sign of the conductivity/shear rate relation is apparent from the occurrence of maxima in the conductivity *vs.* shear rate curve of some carbon black-oil mixtures.

At any given speed, the magnitude of the conductance of a carbon black suspension is a relative measure of the degree of deflocculation. In solvents of low cohesive energy density, such as aliphatic hydrocarbons, alkyl siloxanes and probably also in the fluorocarbon liquids the conductivity of carbon black suspensions is high as is the degree of flocculation. In aromatic hydrocarbons, especially of the condensed type and in many polar solvents, carbon particle cohesion (flocculation) is weaker and conductivity lower than in the non-polar solvents mentioned before. The presence of even relatively small amounts of strongly adsorbable amphipathic substances which effectively coat the carbon black surface with a hydrocarbon layer reduces particle cohesion and thus conductivity to very low values. This sequence of flocculating characteristics is manifest in the data of Forster and Mead.¹⁷ If one takes the conductivity of carbon in the silicone fluid as reference and defines a degree of flocculation $D = R(\text{sample})/R(\text{silicone})$, then the numerical value of D (shown in Table V) probably represents the inverse ratio of the proba-

TABLE V

RELATIVE DEGREE OF DEFLOCCULATION OF CARBON BLACKS
IN DIFFERENT FLUIDS (DERIVED FROM CONDUCTIVITY
UNDER STATIC CONDITIONS)

Fluid	R-40 ^a	Shawinigan acetylene black ^b
In transformer oil	25	—
In linseed oil	400	90

^a Relative to the flocculation in silicone oil; calculated from data of ref. 4. ^b Relative to the flocculation in medicinal white oil; calculated from data of ref. 4 and our own value for this black in medicinal white oil.

bilities of a particle collision leading to particle adhesion or conversely the ratio of the lifetimes of adsorbed solvent or solute molecules in the interface. The latter mechanism of collision efficiency explains the strongly positive temperature coefficient of the conductivity of carbon black suspensions.

Conclusions.—The measurement of the changes of electrical properties of relatively concentrated colloidal suspensions in oils as a function of shear deformation of such systems has provided some novel insight into the kinetics of particle movement and the extent and mode of particle cohesion under dynamic conditions. The unexpectedly rapid response of the various electrical properties to positive and negative changes in strain rate suggests that particle motion in these relatively concentrated gels involves primarily elastically restorable short range displacements within "gel-lumps" which move relative to each other. Much further work is required to reconcile the results of electrical and of flow measurements on these systems.

The original aim of this work, to obtain a quantitative measure of particle aggregation, has been achieved only in part. The dielectric constant and dielectric loss data can give information regarding the shape (permanent or transient) of particle aggregates but are silent regarding the size of such aggregates. Once the theory is further developed, the dynamic contribution to the electrical conductivity of semiconducting suspensions may serve as a means to measure aggregate size. Evaluation of the local velocity differences between fluid and gel structure from the observed electrokinetic potentials also requires further development of the theory before it can be realized. The d.c. conductivity of suspensions of catenating conducting particles can be converted into a quantitative—although still relative—measure of particle cohesion in different liquid environments.

On further reflection it appears that perhaps the original question was wrong. In suspensions which are sufficiently concentrated so that particle interaction leads to a finite yield value it makes little sense to ask for the size of individual particle aggregates since, under static conditions, the whole gel is one aggregate. In sols one has either completely deflocculated individual particles (which can be measured by optical, viscometric, or sedimentation

techniques) or growing aggregates, which under static conditions would grow indefinitely until all particles present have been collected into a single aggregate. The size of aggregates in flocculating systems can therefore be defined only for dynamic conditions, namely, as the size and shape at which the cohesion of the weakest cross-section is in equilibrium with the shearing stress acting on its surfaces. While, with the present status of theory, flow measurements on concentrated suspensions can give only information regarding the resistance to deformation of the macroscopic system, it appears that electrical measurements may give insight into the transient size, shape, and internal motions of the particle aggregates which actually move past each other in the act of flow.

Acknowledgment.—The authors are greatly indebted to Dr. C. H. Klute for valuable advice on electrical measurements, and to Drs. J. N. Wilson and A. M. Cravath for stimulating discussions. Several of the measurements were carried out by Messrs. W. W. Kerlin and R. F. Fraatz.

DISCUSSION

K. J. MYSELS.—Can you elaborate on the electrokinetic effect between the two cylinders? I cannot visualize where the potential comes from.

A. BONDI.—The way I feel is that the gel skeleton is not an integral part of the gel. The skeleton which Mr. Peterson showed yesterday is just a series of solid particles that swim in the gel. As the shear is applied to this gel, parts of the gel will move at a different speed than the oil. This is all that is needed for the electrokinetic effect, *i.e.*, the solid moves at a speed relative to the liquid in which it is embedded.

K. J. MYSELS.—In order to show a measurable potential you need more than that, you need the accumulation of charges at one end of your system. Your apparatus, however, involves a rotation which prevents any such accumulation and furthermore the potential is between the two cylinders, *i.e.*, perpendicularly to the direction of flow.

A. BONDI.—I would like to point out that Garner and collaborators, as well as Weissenberg, have proposed for viscoelastic system a transport of solute to regions of reduced stress, and that the stresses between the concentric cylinders vary radially, so that the radial transport may cause the potential. [It may be best to say simply that for the present the origin of the observed potential is obscure.]

K. J. MYSELS.—I doubt that this radial motion could be important enough to cause such large electrical effects, since the shearing gradient is relatively uniform between closely spaced concentric cylinders such as yours. If this explanation were correct the net radial movement of particles should soon stop when the system reaches a steady state and hence the potential should soon reach zero.

R. D. VOLD.—According to this suggestion you have these aggregates, and if you put them in a flow field they merely deform and regain their original shape. Mr. Reich in our laboratory has been carrying out some studies on dispersing colloidal carbon in water at different levels of mechanical agitation, and gets what appears to be quasi-equilibrium between some kind of aggregate size and the level of mechanical agitation. Thus the effective size of the aggregates may well depend on the velocity gradient induced in the system.

ADSORPTION ON MONOLAYERS. VI. ADSORPTION OF THE ISOMERIC HEXANES ON CONDENSED STEARIC ACID MONOLAYERS AND ON CLEAN WATER SURFACES^{1,2}

BY KENNETH E. HAYES² AND ROBERT B. DEAN³

Contribution from the Department of Chemistry, University of Oregon, Eugene, Oregon

Received July 22, 1952

The adsorption of the isomeric hexanes on condensed stearic acid monolayers (at 8.0 Gibbs) and on clean water surfaces has been investigated using the vertical type surface balance described in paper III of this series. On water the adsorption follows type III isotherms, the amount adsorbed at any one partial pressure being greatest for *n*-hexane and decreasing in the order of the boiling points. On the condensed monolayers the adsorption follows type V isotherms. At low pressures the adsorption is independent of the nature of the hexane, while at high pressures, where the isotherms level off, the amount adsorbed appears to depend on the ability of the molecules to pack into a well ordered monolayer. The heats of adsorption on clean water are not significantly different from the heats of vaporization of the respective hexanes. On the monolayers the heats of adsorption increase with increasing adsorption, approaching the heat of vaporization asymptotically. The results are found to be incompatible with the BET theory.

It was found by Dean and McBain⁷ that many organic vapors would cause an increase in the area of sodium stearate monolayers which were held at constant surface pressure. Vapors of liquids, which have a spreading pressure greater than the surface pressure of the monolayer, would be expected to displace the monolayer and thus increase the total film area. It was observed however that vapors of some liquids having a lower spreading pressure would also cause expansion. This indicates that the vapors are adsorbed by, and form mixed films with, the stearic acid monolayer. A semi-quantitative investigation of this phenomenon was made by Dean and Li⁸ who, using a simplified form of the Gibbs' adsorption equation, calculated the amount of certain selected organic vapors on stearic acid monolayers, at various concentrations of the stearic acid.

More recently, Dean and Hayes⁴⁻⁶ have investigated the system stearic acid-*n*-hexane at 20 and 30° using more accurate experimental techniques,⁴ and have calculated the adsorption isotherms for *n*-hexane, using the complete form of the Gibbs equation.

In this way it may be shown⁵ that the amount of vapor adsorbed, Γ_1 , is given by

$$\Gamma_1 = \left[\left(\frac{\partial \pi}{\partial P} \right) - \Gamma_2 \left(\frac{\partial \mu_2}{\partial P} \right) \right] \quad (1)$$

where the subscript 1 refers to hexane and 2 to stearic acid. π is the surface pressure and P the relative partial pressure of the hexane. Koenig⁹

(1) Presented before the twenty-sixth National Colloid Symposium which was held under the auspices of the Division of Colloid Chemistry of the American Chemical Society in Los Angeles, California, June 16-18, 1952.

(2) This work was supported in part by a grant from the Frederick Gardner Cottrell Fund of the Research Corporation, and in part by a grant from the U. S. Institute of Public Health. This work, together with the contents of papers III, IV and V⁴⁻⁶ in this series is reported more extensively in the Ph.D. thesis of K. E. Hayes, Oregon, June, 1952. Now Department of Chemistry, University of Princeton, New Jersey.

(3) Chemical Division, The Borden Co., Bainbridge, N. Y.

(4) R. B. Dean and K. E. Hayes, *J. Am. Chem. Soc.*, **73**, 5583 (1951).

(5) R. B. Dean and K. E. Hayes, *ibid.*, **73**, 5584 (1951).

(6) R. B. Dean and K. E. Hayes, *ibid.*, **74**, 5982 (1952).

(7) R. B. Dean and J. W. McBain, *J. Colloid Sci.*, **2**, 383 (1947).

(8) R. B. Dean and Fa-Si Li, *J. Am. Chem. Soc.*, **72**, 3979 (1950).

(9) F. O. Koenig, "Computation of Surface Concentrations from Surface Tension Data," Academic Press, Inc., New York, N. Y., in print.

has shown how to compute $\partial \mu_2 / \partial P$ from spreading pressures.

From the data at 20 and 30° it was possible to compute the isosteric heats of adsorption of *n*-hexane on stearic acid monolayers at 25° and to assign probable structures to the mixed films. At low stearic acid concentrations it appears that hexane dissolves in the hydrocarbon chains of the monolayer to form "Duplex" films. However, at 8.0 Gibbs, 8×10^{-10} moles/cm.²,¹⁰ where the stearic acid molecules in the monolayer are close packed, there is very little room for hexane to penetrate between the chains. *n*-Hexane is adsorbed on the top of the stearic acid monolayer, as a second monolayer with its molecules oriented almost vertically.

This investigation of the adsorption of the isomeric hexanes on closed packed stearic acid monolayers and on clean water surfaces, was undertaken with a view to substantiating the postulated structures ascribed to the mixed monolayers.

Experimental

Materials.—Benzene was Baker and Adamson "B and A" quality free from thiophene and was twice distilled, the fraction boiling between 79.5 and 80° being collected. The hexanes were all Phillips Petroleum Company 99% grade. They were all twice distilled just before use, that fraction boiling within one half of one degree of the boiling point as given in National Bureau of Standard tables being collected. The hexanes and benzene were tested and found to be free from surface active impurities.

Stearic acid was from Armour and Company and was a sample from the same lot used by Ralston¹¹ in his investigations, it was recrystallized from ethanol, m.p. 69.4°. Benzene solutions of stearic acid were prepared by weighing the stearic acid and dissolving in the redistilled benzene in a volumetric flask. The concentrations used were 0.0004 and 0.00072 *M*.

Phosphoric acid solutions (0.01 *N*) were prepared from Baker and Adamson Reagent Grade phosphoric acid and this was used as the liquid phase throughout the entire investigation.

Apparatus and Methods.—The apparatus and technique are described in detail elsewhere.⁴

Results

Figure 1 shows the results of partial pressure-surface pressure data for *n*-hexane on stearic acid monolayers at $\Gamma_2 = 8.00$ and $\Gamma_2 = 0.00$ Gibbs, that is, on close packed monolayers and on clean

(10) R. B. Dean, *THIS JOURNAL*, **55**, 611 (1951).

(11) A. W. Ralston, *J. Org. Chem.*, **7**, 546 (1942).

water. These curves are typical of the behavior of all of the hexanes, the data for the other hydrocarbons being omitted for the sake of clarity.

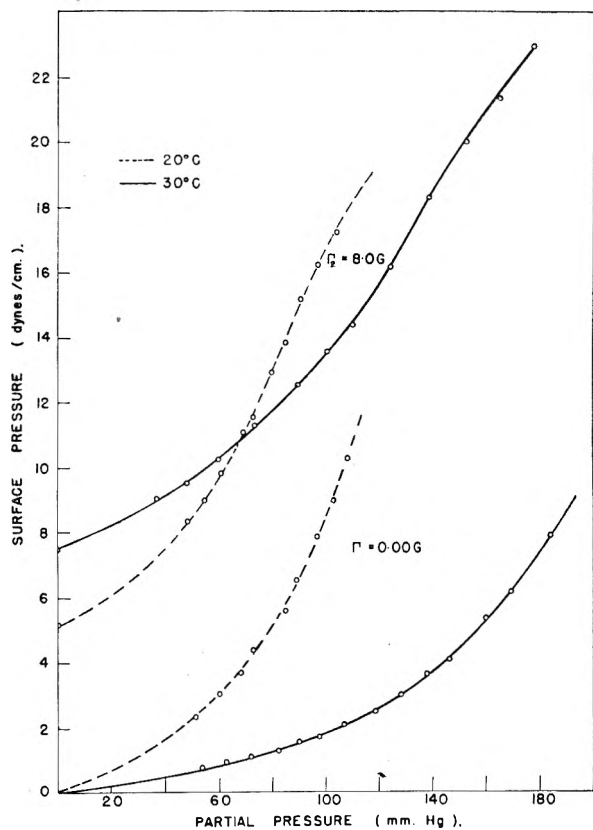


Fig. 1.—Surface pressure–relative pressure curves for *n*-hexane on clean water surfaces and on condensed stearic acid monolayers at 20 and 30°.

From these curves values of the function $\partial\pi/\partial P$ were obtained, which were then inserted into a simplified form of equation 1, namely

$$\Gamma_1 = \frac{P}{RT} \left(\frac{\partial\pi}{\partial P} \right) \quad (2)$$

and values of Γ_1 calculated.

The second term in equation 1, $\Gamma_2(\partial\mu_2/\partial P)$ is obviously equal to zero when $\Gamma_2 = 0.00$ Gibbs, *i.e.*, for the adsorption on clean water, and equation 2 is then the same as that used by Micheli¹² and Cassel and Formstecher¹³ in their investigations of the adsorption of insoluble vapors on water surfaces.

It is interesting to note that the π - P data for the adsorption of the isomeric hexanes on water, may be fitted to a degenerate cubic equation

$$\pi = aP + bP^3$$

from which values of Γ_1 may be obtained analytically. Values of Γ_1 obtained in this way are in good agreement with the values obtained by graphical differentiation of the π - P curves.

It was shown in paper IV of this series⁵ for *n*-hexane on stearic acid, that $\partial\mu_2/\partial P$ is zero or negligible for monolayers of stearic acid at 8.0 Gibbs, and we have tacitly assumed that $\partial\mu_2/\partial P$ is also negligible for stearic acid monolayers at 8.0 Gibbs

in the presence of the other hexanes. It is probable that this assumption is very near the truth. 2,2-Dimethylbutane does not appear, at first sight, to belong to the same series as the other hexanes (Fig. 3), it was thought that the anomalous behavior of this hydrocarbon might be ascribed to a different standard state.⁵ Experiments were made however, which show that the spreading pressure of stearic acid under 2,2-dimethylbutane vapors at 30° follows the same pattern as *n*-hexane.⁵

Typical adsorption isotherms for the isomeric hexanes on clean water surfaces are shown on Fig. 2 and on condensed monolayers in Fig. 3. The complete results are tabulated in Tables I and II.

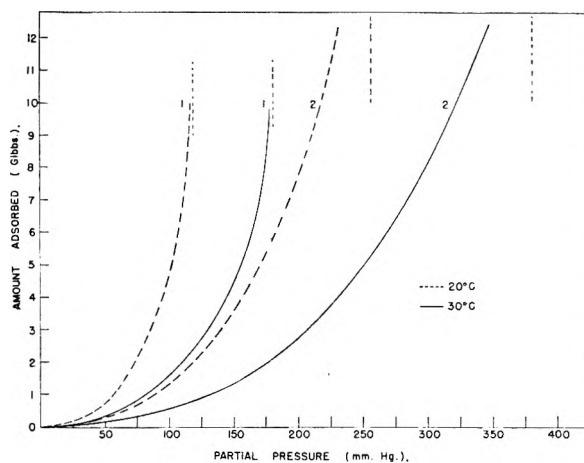


Fig. 2.—Typical adsorption isotherms for the isomeric hexanes on clean water surfaces at 20 and 30°. (The curves shown are for: 1, *n*-hexane; 2, 2,2-dimethylbutane. The other hexanes fit between these two extremes in the same order as their respective boiling points.)

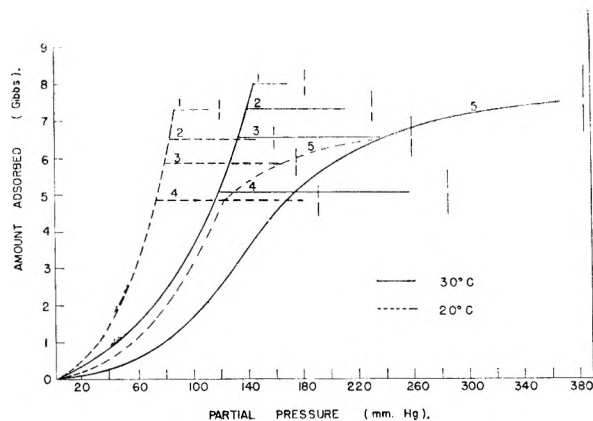


Fig. 3.—Adsorption isotherms for the isomeric hexanes on condensed stearic acid monolayers at 20 and 30°: 1, *n*-hexane; 2, 3-methylpentane; 3, 2-methylpentane; 4, 2,3-dimethylbutane; 5, 2,2-dimethylbutane.

The surface pressure data are believed to be accurate to better than ± 0.05 dyne per cm. and that relative partial pressure measurements to about ± 0.005 . By assuming maximum errors in the π - P curves it was possible to ascribe confidence limits to the adsorption isotherms. We are confident that the reported values of are accurate to better than 5%.

Heats of adsorption for the systems studied were calculated using the Clausius-Clapeyron equation.

(12) L. I. A. Micheli, *Phil. Mag.*, **3**, 895 (1927).

(13) H. M. Cassel and M. Formstecher, *Kolloid-Z.*, **61**, 18 (1932).

TABLE I

ADSORPTION OF THE ISOMERIC HEXANES ON CLEAN WATER SURFACES, AT 20 AND 30° REPORTED AS PARAMETERS IN THE GENERAL EQUATION

$$\Gamma_1 = aP + bP^3$$

Confidence limits on a are approximately ± 0.05 . Confidence limits on b are approximately ± 0.25 .

	20°		30°	
	a	b	a	b
<i>n</i> -Hexane	0.42	8.38	0.63	7.15
3-Methylpentane	.53	12.64	.29	13.46
2-Methylpentane	.36	12.42	.29	13.08
2-3-Dimethylbutane	.94	11.18	.78	13.11
2-2-Dimethylbutane	.96	15.52	.98	15.39

TABLE II

VALUES OF Γ_1 , IN GIBBS, FOR THE ADSORPTION OF THE ISOMERIC HEXANES ON CONDENSED STEARIC ACID MONOLAYERS ($\Gamma_2 = 8$ G.), INTERPOLATED TO INTEGRAL VALUES OF THE RELATIVE PARTIAL PRESSURE

I, *n*-hexane; II, 3-methylpentane; III, 2-methylpentane; IV, 2,3-dimethylbutane; V, 2,2-dimethylbutane

P	I	II	III	IV	V
A. At 30°					
0.1	0.36	0.32	0.42	0.56	0.21
.2	0.73	0.96	1.09	1.36	0.88
.3	1.32	1.92	2.19	2.75	2.22
.4	2.11	3.06	3.67	4.61	4.28
.5	3.02	5.45	6.20	5.21	5.90
.6	4.23	7.25	6.66	5.15	6.44
.7	6.12	7.44	6.72	5.21	6.92
.8	7.88	7.29	6.60	4.95	7.20
.9	8.06	7.24	6.53	4.75	7.50
B. At 20°					
0.1	0.24	0.28	0.33	0.40	0.26
.2	0.63	0.85	1.06	1.17	0.87
.3	1.16	1.82	2.41	2.72	1.83
.4	2.06	3.14	4.18	4.77	3.14
.5	3.21	5.41	5.44	5.48	4.21
.6	4.70	6.71	6.24	4.67	5.09
.7	6.69	6.46	5.00	4.67	5.63
.8	7.40	6.42	5.58	4.97	6.00
.9	7.25	5.50	5.85	5.11	6.26

As the isotherms for the isomeric hexanes on stearic acid at $\Gamma_2 = 8.0$ Gibbs are, within the limits of the experimental data, identical on the rising part of the curves (except 2,2-dimethylbutane) it follows that the heats of adsorption must also be identical. These heats are low, 4.0 kcal. at low adsorption and approach a value of 7.5 ± 0.8 kcal. asymptotically as adsorption proceeds. This value is not inconsistent with the statement that the heats of adsorption approach the heats of vaporization of the respective hexanes as the amount adsorbed increases to its maximum value. It is probable that more refined experimental techniques would enable the Γ_1 - P curves for these hexanes to be separated by an amount sufficient to prove the truth of this statement.

Heats of adsorption for the isomeric hexanes on clean water surfaces are not significantly different from the heats of vaporization of the respective hexanes.

Discussion

The surface of pure water may be considered as a "soft" surface, meaning that the actual transition

layer is diffuse to a depth of 2-3 Å. A hexane molecule, on being adsorbed at a pure water surface, becomes imbedded in a soft matrix of water molecules which surround it on all sides except the top. The attractive forces between a water molecule and a hexane molecule would be expected to be of the same order of magnitude as those between two hexane molecules. The heat of adsorption of hexane on water should therefore not differ greatly from the heat of vaporization of liquid hexane.

Further evidence that the hexane molecules are imbedded to a depth of 1-2 Å., is that 2,2-dimethylbutane fits in with this postulated behavior very well, and that the isotherms for this compound on clean water show no deviations from the typical behavior of the other hexanes. 2,2-Dimethylbutane is different from the other hexanes in that it is impossible to construct a model such that it will sit with all of its carbon atoms on a surface. If the hexane molecules on being adsorbed were to sit on the top of the water without penetration, we would expect the heat of adsorption for 2,2-dimethylbutane to start out at a value of about five-sixths of that of *n*-hexane and increase to the heat of vaporization as the amount adsorbed increases.

This is indeed the case for the adsorption isotherms of the isomeric hexanes on a stearic acid monolayer at a concentration of 8.0 Gibbs. Here we have type V isotherms which are approximately independent of composition for four of the five hexanes, at least at lower pressures. A condensed stearic acid monolayer may be considered as a "hard" surface, in that it is virtually impossible for a hexane molecule, on adsorption, to penetrate into the surface in the same way as with water. We can therefore say that the adsorbed molecules are actually sitting on the top of the hydrocarbon chains in this case. As the first molecules are adsorbed they will align themselves so as to present a system with the lowest possible energy, *i.e.*, with all six carbon atoms in contact with the surface. As the pressure is increased and the amount adsorbed increases there will come a time when it is no longer possible for all of the adsorbed molecules to lie flat, and one of two things will happen. Either multimolecular adsorption will start, or else the adsorbed molecules start to reorient themselves into a vertical position. Our data favor the latter belief, and, within the accuracy of the data, adsorption seems to cease with the completion of a somewhat tilted monolayer. The heights of the adsorbed layers have been calculated on the assumption that the density of the hexane in the film is not very different from the density of liquid hexane, and the calculated heights agree fairly well with the postulate of a tilted monolayer.

As we have already mentioned 2,2-dimethylbutane does not show the same behavior as the other hexanes. However, as this compound can only have a maximum of five carbon atoms in the surface, and as the amount adsorbed depends on the number of contacts between the adsorbent and the adsorbate it is not surprising that the initial amounts adsorbed at lower pressures should be less than for the other hexanes. The concentration at which the isotherm for 2,2-dimethylbutane levels

off does not correspond to a tilted monolayer but rather to a layer almost two molecules thick. 2,2-Dimethylbutane is a pear-shaped molecule, and the upper half of a monolayer of this hydrocarbon is full of holes, which may be filled by a second layer of molecules inverted over the first.

We have been unable to fit our data to the BET equations for type III or type V isotherms. The occurrence of type V isotherms on flat surfaces is inconsistent with the postulate of the BET theory. In that theory flat-topped type IV or type V isotherms are believed to occur when sorption is limited to the filling of pores. This is obviously not the case in our experiments and caution should be exercised in deducing pore size from other type V isotherms on solid adsorbents.

Summary

This investigation has shown that hexane vapors are adsorbed by stearic acid monolayers with the formation of liquid-expanded and intermediate films.

Adsorption proceeds beyond a monolayer on the liquid-expanded films, but appears to reach a limiting value, corresponding to a tilted monolayer, on condensed stearic acid monolayers.

Adsorption of the isomeric hexanes on clean water surfaces follows type III isotherms, and in all cases proceeds beyond the formation of a monolayer. The adsorption of any isomer at a given partial pressure is greater the higher the boiling point of the isomer.

The heats of adsorption approach the heats of vaporization of the respective hexanes at high values of the surface concentration of hexane.

DISCUSSION

ANON.—If you are going to try to put six of these groups from your isomeric hexanes on a flat surface, it will cost you about 2 or 3 kcal. for turning those carbon atoms in the adverse position, *i.e.*, putting them in the same plane, because of hindered rotation around those single bonds.

K. E. HAYES. (*Communicated*).—It is not necessary that the hexane molecules be pulled flat to within 0.1 Å. If the carbon atoms are planar within about 1 Å, the hexane

molecule will be sufficiently flat for all of the carbon atoms to be in the surface, because of the slight penetration into the surface by the adsorbed molecules.

CONWAY PIERCE.—I would like to ask about this negative heat of adsorption. To what extent of surface coverage does this extend?

K. E. HAYES.—The heat of adsorption reaches a value which is not significantly different from the heat of vaporization when the surface concentration of hexane corresponds to a complete monolayer of hexane, lying flat on the surface.

CONWAY PIERCE.—It seems to me that you are dealing with a system similar to a protein-water system, namely, a swelling system. You have your stearic acid monolayer, the hexane chains become intermixed with the hydrocarbon chains of the monolayer, and we certainly know that we have negative heats of adsorption in the swelling systems, because of the tremendous increase in entropy as we go from the bulk liquid to the adsorbed phase. I do not know to date of any system of physical adsorption on a rigid system (*i.e.*, non-swelling) in which we have a negative heat of adsorption. Now when we are talking about swelling systems, these Brunauer type V isotherms cease to have any meaning.

F. FOWKES.—I heard a paper at the Buffalo meeting by Dr. Bartell and one of his students; he talked on contact angles of water on silver in the presence of a little benzene vapor. At this point I began to worry about your "Wilhelmy" method with the platinum slide and all of the hexane vapor. Is there any way of checking to make sure that the high pressures you measure do not have any contribution from a lowered contact angle of the water on the platinum slide.

K. E. HAYES.—Only by visual examination. We realize that the "Wilhelmy" method has its limitations. As long as the slide is moving upwards the contact angles appear to be either zero or very small. We cannot of course study the desorption isotherms by our method because of this limitation.

MALCOLM DOLE.—Do you really mean negative heats of adsorption?

K. E. HAYES.—No. The heat of adsorption starts at about 4 kcal. and approaches the heat of vaporization asymptotically.

MALCOLM DOLE.—Do you mean heat is adsorbed or liberated?

K. E. HAYES.—Liberated when the vapor is adsorbed. The values less than the heat of vaporization correspond to adsorption of heat when hexane is transferred from bulk liquid to the surface.

A STUDY OF PHYSICAL ADSORPTION AT LOW COVERAGES¹

BY S. CHU LIANG

*Division of Applied Chemistry, National Research Council, Ottawa, Canada**Received July 22, 1952*

By measuring the adsorption isotherms of krypton and argon on 3 mm. glass spheres, it has been possible to show the existence of heterogeneity on the glass spheres in a semi-quantitative manner. The sites which are most difficult to clean by evacuation at 300° are also most active for physical adsorption. As the number of high activity sites increases, the surface, if left undisturbed at room temperature, appears to rearrange itself without change in the total number of adsorption sites but with a change in the activity distribution. This is viewed as a concrete evidence for the active center theory. Beyond the monolayer, the adsorption behavior approaches that of a uniform surface, thus partly accounting for the applicability of the BET equation even though a surface be heterogeneous.

Introduction

The now well known BET equation² was derived on the basis of a homogeneous surface, but it is widely used for surface measurements where the surface is strongly suspected to be heterogeneous, and with reasonable success. The experimental evidence regarding surface heterogeneity presented by Taylor and Liang³ was challenged by both Beeck and Rideal and their co-workers.⁴ While the argument has been further elucidated by Halsey⁵ and more recently by Sastri and Ramanathan⁶ it appears desirable if some independent evidence of the existence of heterogeneity can be obtained. Such is the purpose of the present work.⁷

In choosing the system to be studied, the inert gases on 3 mm. glass spheres⁸ was selected for several reasons. The manner in which the monatomic gas molecules can react is extremely limited. Since the commercial glass beads are not porous and appear to be rather smooth, the possibilities of capillary condensation and diffusion are minimized. The data obtained may thus be treated with confidence as due only to physical adsorption. Glass also offers the advantage of having a surface expected to be heterogeneous.

In the present study, the low coverage region has been emphasized because we believe only in such a way the specificity of adsorption sites can be exposed. At coverages above the monolayer, the surface becomes essentially homogeneous.

An examination of the literature reveals that accurate data at low coverages are rare. This may be due in part to the experimental difficulties involved. For example, in a small pressure of the adsorbate (10^{-2} – 10^{-3} mm.), we have found that a waiting period of 50–100 hours is necessary if the

first measurement is to represent true equilibrium. When the sample was precooled in a higher pressure of helium to the working temperature, the waiting period was shortened considerably; but the traces of impurities (less than 0.1%) in the helium were sufficient to cover the most active sites, rendering the data useless. Great care was exercised in obtaining the results presented in the following for a semi-quantitative interpretation.

Experimental

Apparatus.—The apparatus was modeled after that of Wooten and Brown⁹ using a 200-cc. bulb and 1.4 mm. capillary McLeod gage. The total geometrical space of the system was about 400 cc. The pressure could be measured at 10^{-3} mm. with 5% accuracy and at 10^{-4} mm. with 10%. Beyond 10^{-4} mm. the accuracy was too low for the measurements to have any significance. Since each run took 5–7 days, a methane regulator was used to keep the liquid nitrogen bath level constant within 3 mm. for the entire period. The temperature was followed with an oxygen vapor pressure thermometer. It was sufficiently constant ($\pm 0.05^\circ\text{K.}$) even though atmospheric pressure changes were large (± 20 mm.).

Adsorbent.—Commercial 3 mm. glass spheres of Kimble glass were used. One hundred beads were measured individually with calipers accurate to 0.1 mm. An average diameter of 3.2 mm. was obtained and used for the calculation of the apparent surface area. Five hundred beads were weighed in 50 portions and the average weight of 4.55 g. per 100 beads was obtained. The total sample weighed 249.8 g. representing an apparent total area of 1767 cm.². The adsorption chamber was made of 47.8 mm. i.d. Pyrex glass tubing and had a total wall area of about 170 cm.², thus giving a total adsorbing area of about 1940 cm.².

Gases.—The krypton and argon were Linde Air products, spectroscopically pure grade. They were used without further treatment.

Procedure.—The glass sphere sample was introduced into the adsorption chamber with no treatment of any kind. After sealing to the system, it was warmed to 300° and evacuated continuously at this temperature for 90 hours. It was then cooled and used for the study.

The standard procedure used in this study was that, after the sample was evacuated and allowed to attain the room temperature, a portion of gas was admitted, the cold bath put on and the system allowed to attain equilibrium. Normally, since physical adsorption is a fast process, an investigator when taking two readings some 10–20 minutes apart and finding the difference within experimental error, considers the reading a true equilibrium value. It was found during this study, however, that a reading so obtained could be quite misleading. In Fig. 1 are shown some typical rate of adsorption data where the "normalized"¹⁰ pressure is plotted against time. It can be seen that at least some 50 hours is required for the first equilibrium value. While other possibilities cannot be definitely ex-

(1) Presented before the twenty-sixth National Colloid Symposium which was held under the auspices of the Division of Colloid Chemistry of the American Chemical Society in Los Angeles, California, June 16–18, 1952.

(2) S. Brunauer, F. H. Emmett and E. Teller, *J. Am. Chem. Soc.*, **60**, 309 (1938). No attempt is made here to discuss the soundness of the BET equation as this has been done by many authors elsewhere.

(3) H. S. Taylor and S. C. Liang, *ibid.*, **69**, 1306, 2989 (1947).

(4) (a) O. Beeck, A. W. Ritchie and A. Wheeler, *J. Colloid Sci.*, **3**, 505 (1948); (b) E. K. Rideal and B. M. W. Trapnell, *Discussions Faraday Soc.*, No. 8, 114 (1950).

(5) G. D. Halsey, Jr., *THIS JOURNAL*, **55**, 21 (1951).

(6) M. V. C. Sastri and K. V. Ramanathan, *ibid.*, **56**, 220 (1952).

(7) In a very recent paper, published since this work was finished, Drain and Morrison (*Trans. Faraday Soc.*, **48**, 316 (1952)) gave further evidence of surface heterogeneity.

(8) The only other adsorption study on glass spheres known to the writer is that due to R. T. Davis and T. W. DeWitt (*J. Am. Chem. Soc.*, **70**, 1135 (1948)) where the experimental conditions are so different that a comparison with the present work is not possible.

(9) L. A. Wooten and C. Brown, *J. Am. Chem. Soc.*, **65**, 113 (1943).

(10) The data used in Fig. 1 are obtained from several runs at various pressure regions. In order to put different sets of data in the same graph, the pressure is "normalized" by plotting $\log p/p_0$ where p is the actual pressure and p_0 is the pressure at time = 0.

cluded, this seems to be due mainly to the cooling of the sample from room temperature, because when this equilibrium is established, subsequent additions of gas reach equilibrium within 15–30 minutes. If, however, the first equilibrium is not reached and a pseudo-equilibrium value is taken, and such values are also taken in the subsequent additions of gas, then an apparent linear portion of V_{adsorbed} vs. p is obtained, leading to an apparent simple Langmuir isotherm or "Henry Region" as observed and discussed by Dreving, Kiselev and Likhacheva.¹¹

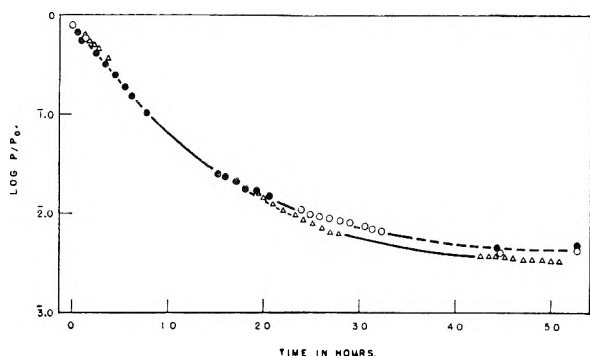


Fig. 1.—Rate of adsorption of krypton. p_0 is the initial pressure and p the pressure at time t .

Results

Because of the low pressure range in which the study was made, the thermal transpiration becomes important. All the data have been corrected for this effect.

The adsorption isotherms were measured at one temperature ($77.6 \pm 0.1^\circ\text{K}$.) only. Because the surface was ever changing, it was not possible to compare the results obtained at different temperatures and therefore the isosteric heat of adsorption could not be calculated.

With krypton two series of measurements were made. In series A, between each two runs, the sample was warmed up to 300° and evacuated at that temperature for about 24 hours. In series B, the inter-run evacuation was conducted at room temperatures (25°). With argon, the measurements were made in the series B manner only.

Krypton.—The measurements were made in the pressure range 10^{-4} –0.5 mm., corresponding to 0.2–1.25 BET monolayer.

Series A.—After each evacuation at 300° , the volume adsorbed at a fixed pressure increased. This was accompanied by a similar increase of BET V_m .¹² In seven runs, the surface area increased from $V_m = 0.044$ cc. STP to 0.075. Two runs are shown in Fig. 2 as examples. The lower pair indicates the low pressure range and the upper pair the higher pressure range. The pressure for the monolayer formation was constant at 0.11 ± 0.01 mm.

Series B.—The surface area calculated from six runs was constant at $V_m = 0.065$ –0.071 cc. STP, within the accuracy of the BET method. The pressure at which the monolayer was complete, however, increased with each run. Except in the

(11) V. P. Dreving, A. V. Kiselev and O. A. Likhacheva, *J. Phys. Chem. (U.S.S.R.)*, **25**, 710 (1951).

(12) Owing to the uncertainty of the cross-section of the krypton molecule (see R. A. Beebe, J. B. Beckwith and J. M. Honig, *J. Am. Chem. Soc.*, **67**, 1554 (1945)), throughout this paper, the surface area will be expressed at BET V_m instead of geometrical unit.

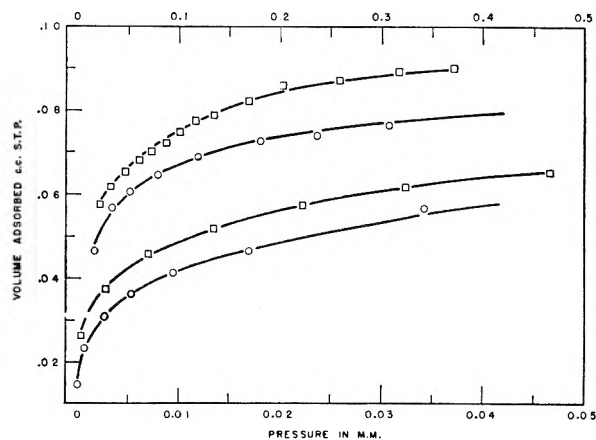


Fig. 2.—Krypton adsorption isotherms, series A: \circ , Run No. 2; \square , Run No. 6. For lower pair, use lower abscissa scale, for upper pair, use upper scale.

very low pressure region, the results of four runs shown in Fig. 3 resemble those in Fig. 2 to a certain extent. Whereas in series A the difference in adsorption at coverages above monolayer increased, in series B the difference actually decreased and finally merged into one isotherm.

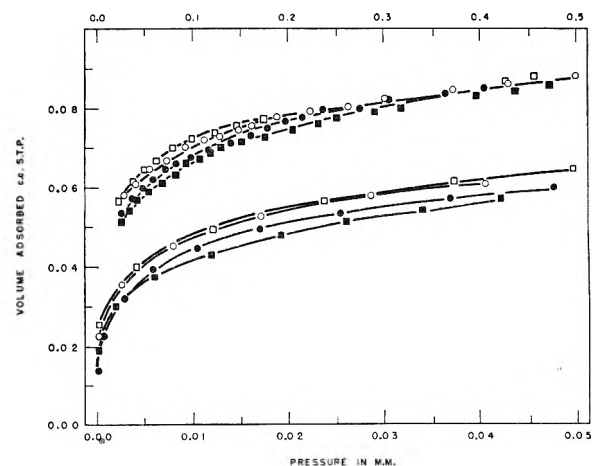


Fig. 3.—Krypton adsorption isotherms, series B. \square , Run No. 1; \circ , No. 2; \bullet , No. 3; \blacksquare , No. 4. For lower four curves use lower abscissa scale, for upper curves, use upper scale.

Argon.—The argon isotherms were measured in the range 10^{-4} –0.05 mm., or 0.05–0.20 BET V_m . The isotherms were obtained to supplement the krypton data in the coverage region $V/V_m < 0.20$. They did not obey the simple Langmuir equation.

In all cases, at coverages less than a BET monolayer, the results were found to obey the Freundlich equation. In series A, the slope decreased with each run whereas in series B as well as the case of argon, the slope increased. The changes are shown in Table I.

TABLE I
SLOPES OF FREUNDLICH ISOTHERMS

Series A		Series B		Argon	
Run No.	Slope	Run No.	Slope	Run No.	Slope
1	0.33	1	0.16	1	0.22
4	.22	2	.22	2	.24
6	.17	5	.24	3	.28

Discussion

In the method given by Hill, Emmett and Joyner¹³ for analyzing adsorption data, it was stressed by those authors that the isotherm measurements should be extended to as low coverage as possible. The present study confirms such a necessity. The straight line portion is absent at as low as 5% coverage in the present case.

The surface of the present sample can be concluded as heterogeneous from the examination of Table I. For a uniform surface, at low coverage, the slope should be unity and this is not even approximated. Secondly, if the surface were uniform and the change of the slope were due to increase (or decrease) of total surface, the slope should remain constant from one run to another instead of changing as shown in Table I. And thirdly, although the reason for an isotherm to obey a Freundlich equation is not completely known, it has been suggested by several authors as indicating an exponential distribution of sites, a type of heterogeneous surface.

It has not been possible for the writer to determine the origin of the heterogeneity of the surface studied. Recently, Boudart¹⁴ has suggested that heterogeneity in a surface may be induced by adsorption. Such is, of course, not the present case. If so, then in series B, there should be only one isotherm instead of several. Because the surface area has remained constant, the influence of adsorption on heterogeneity should be the same for every run. The present heterogeneity must therefore be in "localized" active centers. As a point of interest, in Table II are compared the BET constants evaluated from six runs, three each from series A and B, respectively. Owing to the low values of the intercept i , the constant c cannot be determined with accuracy. Nevertheless, it is possible to show that c increases gradually in series A and decreases in series B, while V_m increases in series A and remains constant in series B. These features can all be shown in accordance with the concept of active center theory.¹⁵

TABLE II

COMPARISON OF BET CONSTANTS^a

Run No.	Intercept i	Slope s	$V_m = \frac{1}{1/i + s}$	$c = \frac{1}{1 + s/i}$
Series A				
1	0.22	22.5	0.044	103
4	.075	15.8	.063	214
6	.060	13.2	.075	221
Series B				
1	0.046	14.0	0.071	306
3	.080	14.4	.069	181
5	.090	15.3	.065	171

^a For meanings of various constants, see ref. 1.

The physical mechanism may be constructed as follows. Consider a surface composed of sites of various activities. Before the sample is evacuated, the sites are covered, presumably, by chemisorbed gases. In the first evacuation at an elevated tem-

perature (300°) the low activity sites are uncovered and made available for physical adsorption. The high activity sites remained covered by chemisorption. With each subsequent evacuation at the elevated temperature sites of gradually higher activities are uncovered. Conceivably, these newly uncovered sites will also exhibit higher activity for physical adsorption. Consequently, at a fixed pressure, *e.g.*, 10^{-4} mm., the number of sites available, and therefore the quantity of gas adsorbed, increases with each evacuation. Since this addition is only at the high activity end, the increase in adsorption at all pressures below the monolayer formation will be constant. Above the monolayer formation, the specificity of the different sites vanishes so that increased adsorption in this region becomes the result of a simple expansion of surface, and proportional therefore to the surface area. Experimentally, one may expect to find a constant difference in adsorption at coverages up to the monolayer formation, and thereafter, the difference increases. It is in this above monolayer region that the surface behaves as though homogeneous and that the various theories derived on a uniform surface, including the BET equation, find best applicability. The BET constant c is a resultant value and therefore increases with the increase of high energy sites. It should perhaps be emphasized that the BET equation describes only the free energy of adsorption but not the mechanism.

If, however, the further evacuation is conducted at 25° instead of 300°, the sites still covered by chemisorption remained covered, the exposed sites continue to be available and so the surface area remains constant. But the activity distribution need not remain constant, particularly in the case of glass which has a semi-liquid structure. On standing at room temperature, the distribution attained at elevated temperature shifts gradually with a decrease in the number of the high activity sites and an increase in that of the low activity sites. As a consequence, the equilibrium pressure for a definite amount of gas adsorbed increases as the time of standing increases. After the monolayer, however, since the specificity of sites disappears and the total surface area remains constant, the equilibrium pressure should not be affected and so the several isotherms merge. The BET constant c decreases with a decrease in high activity sites.

The effects obtaining to this discussion are indeed borne out by the experimental observations in every detail. In particular, in Fig. 4 results from several runs of series A are plotted in the form of ΔV (difference in volume adsorbed) *vs.* θ (fraction of BET monolayer covered). The constancy in difference is maintained in all cases up to $\theta = 1$. If the multilayer formation is proportional to the extent of surface¹⁶ available, the difference in the range of $\theta = 1$ to 2 should follow the dotted line. In the present study the experimental accuracy beyond the monolayer formation falls off so rapidly that it is not possible to analyze the data rigorously in this higher coverage region. It is nevertheless possible to see from Fig. 3 that the convergence of the isotherms from several runs is clearly indicated.

(13) T. Hill, P. H. Emmett and L. G. Joyner, *J. Am. Chem. Soc.*, **73**, 5102 (1951).

(14) M. Boudart, *ibid.*, **74**, 1431 (1952).

(15) H. S. Taylor, *Proc. Roy. Soc. (London)*, **108A**, 106 (1926).

(16) The extent of surface is different from the total surface present.

Although the active center theory was proposed more than two decades ago, it has never been quantitatively illustrated as it is in Figs. 2 and 4. The constancy of increased adsorption over a wide pressure range cannot be otherwise explained. While this is only an isolated case, perhaps other cases will be found if the low coverage region is investigated in a similar manner.

Acknowledgment.—The writer wishes to thank Drs. J. A. Morrison and M. M. Wright for their help in preparing this paper and to Dr. I. E. Puddington for his continuing interest in this work.

DISCUSSION

ANON.—I wonder if you interpret these data to mean that the surface is constantly changing?

S. C. LIANG.—Yes!

ANON.—Wouldn't that be a criticism against what you are trying to prove. In other words, would the question of heterogeneity arise in connection with, presumably, a stable surface. Here the surface is constantly changing.

S. C. LIANG.—In the case where the evacuation was conducted at 300° the surface was always increasing, although the first increase was fairly large and the later increases were smaller. The total surface area was increas-

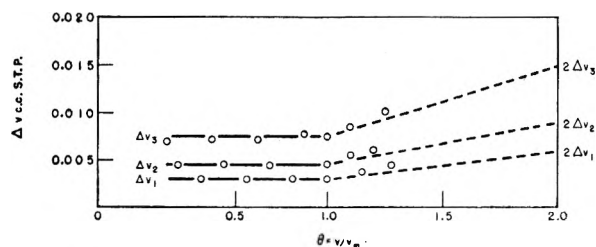


Fig. 4.—Difference in adsorption in series A as a function of coverage.

ing all the time. In the case of series B, the evaporations were conducted at room temperature and the changes were in the distribution. So that, they should give support to the active center theory. We indicated that the sites are increasing all the time at the high energy end.

R. B. DEAN.—It seems from these two papers that the BET theory works where it is not supposed to work, *i.e.*, on heterogeneous surfaces, and does not work on a homogeneous surface. I think Dr. Halsey has stated that, theoretically, it should not work on a homogeneous surface. It appears that the original postulates should be re-examined.

S. C. LIANG.—I think everybody knows that it shouldn't work in the case of either heterogeneous or homogeneous surfaces, except in so far as it describes the behavior above monolayer coverage. It does not describe the heat or entropy changes, but only the free energy changes.

ON THE STRUCTURE OF MICELLES¹

BY G. D. HALSEY, JR.

Contribution from the Department of Chemistry and Chemical Engineering, University of Washington, Seattle, Washington

Received July 22, 1952

Two factors that limit the growth of micelles and permit them to exist without phase separation have been proposed: the geometrical limit of chain length (Hartley) and the repulsive action of the charge density (Debye). It is shown that indefinitely long rod-like micelles avoid both these limitations on size, but that a third factor prevents these micelles from separating as a new phase. These rods comprise a system analogous to a one-dimensional gas, and it is well known that such a gas does not condense, but forms a polydisperse system of aggregates. Such a micelle is shown to be consistent with the observed properties of soap solutions.

Factors Governing Micelle Growth.—From studies of the intensity of scattered light it² has been established that the hypothesis of micelle formation in concentrated solutions of long-chain salts is correct. It is a remarkable fact that these aggregates of ~50 molecules form, without coagulating further to produce a separate phase of indefinite extent.

It is agreed that the attractive force causing the formation of micelles is the van der Waals attraction between the hydrocarbon portions of the molecules, and that the energy involved approximates the heat of vaporization of the corresponding hydrocarbon.

One can assert further that the charged, or in general, the hydrophilic portion of the molecule, is on the surface of the micelle. For, if once the charged ends of the molecule were built into the inside structure of the micelle, there would be no reason for the micelle not to grow indefinitely, and thus to become a separate phase. It appears then that the

finite length of the hydrocarbon chain requires that at least one dimension of the micelle be determined by it and thus remain small.

Hartley³ has proposed the so-called spherical model, in which, essentially, all three dimensions of the micelle are determined by the length of the hydrocarbon chain.

The idea that the micelle is spherical is clearly not essential to his model and indeed when one recalls that the molecules in a liquid hydrocarbon are aligned roughly parallel, it is difficult to see how the Hartley model could help but be anisotropic. At any rate, any Hartley micelle cannot exceed in size the sphere with radius equal to the length of the hydrocarbon chain. It has a definite size and shape, dictated by its structure.

Debye's observation² that the apparent molecular weight of micelles varies continuously with the concentration of salt lends support to his explanation of the finite size of micelles.

If we consider, as he did, the flat plate model for micelles, all the charge on the micelle is collected in two circular plates. The electrostatic energy of

(1) Presented before the twenty-sixth National Colloid Symposium which was held under the auspices of the Division of Colloid Chemistry of the American Chemical Society in Los Angeles, California, June 16-18, 1952.

(2) P. Debye, *Ann. N. Y. Acad. Sci.*, **51**, 575 (1950).

(3) G. S. Hartley, "Aqueous Solutions of Paraffin-Chain Salts," *Hermann et Cie., Paris*, 1936.

repulsion increases with $n^{3/2}$ where n is the number of molecules in the micelle. The van der Waals energy of attraction increases with n , and so growth ceases at a finite-sized micelle. An increase in salt concentration causes the micelle to grow by lowering the concentration of charge in the circular plates, thereby explaining the light-scattering results.

One Dimensional Growth and Micelle Formation.—Consider however a plate-like micelle of very large size with fixed surface area (charge density) and volume (number of hydrocarbon tails interacting). Then, it is clear that a more stable shape would be a rod of equal area and volume, rather than a plate. To show this, we will now modify the argument of Debye. Consider the potential at a small distance r_0 from the end of a rod of length $Z = nr_0$. r_0 is thus a characteristic spacing of charge. For large n the potential will be

$$W_e \int_0^{nr_0} \frac{dr}{r} = W_e \ln n \quad (1)$$

where W_e is the "fundamental electrical energy" of Debye. The total electrical work of forming a micelle of size N is given by the integral

$$W_e \int_1^N \ln n \, dn = N \ln N - N + 1 \quad (2)$$

This function increases more slowly than Debye's $N^{3/2}$, and thus shows the rod-like micelle to be more stable at large N .

The total energy is the sum of the electrical energy and the van der Waals energy $-W_m N$. If we maximize this sum we find for the optimum size of the rod-like micelle

$$N_0 = eW_m/W_e \quad (3)$$

rather than the expression of Debye

$$N_0^{1/2} = \frac{3}{2} \frac{W_m}{W_e} \quad (4)$$

The expression (2) which increases very slowly with N is derived only in the complete absence of counter-ions. In the presence of counter-ions only the near part of the cylinder would contribute to (1) the distant charge being cancelled out by the cloud of counter-ions in the solution. The effect is to replace the upper limit of (1) by a constant, a function not of n , but of counter-ion concentration alone. The expression (2) then becomes proportional to N and N_0 approaches infinity. Essentially, long chain ions approaching the end of a long rod feel only the near end, the distant end being obscured by a cloud of counter-ions. Therefore there is no effect of rod length on potential, the Debye model breaks down, and we are left with two finite dimensions, one at least limited by geometry, and one indefinite dimension.

It would appear then, that there would be no reason why the micelle should not continue to grow indefinitely in the long dimension. It is here however that we observe a third mechanism that can operate to maintain the micelles at finite size. An array of molecules definite and finite in size in two dimensions and indefinite in size in the third corresponds to a one-dimensional gas, that is to say, molecules fixed on a string like beads. It is known⁴

that no matter what the form of interaction, such gases cannot condense to form two phases, like two and three dimensional gases. The micelles would thus be polydisperse to an extent governed by the form of the interaction. Most simply, the distribution of sizes would have the same form as the distribution for a linear polymer in equilibrium with the monomer. It appears, however, that for a micelle all n 'mers below a certain size N are missing, where N is the smallest micelle. The size of this micelle is governed by very specific factors, both geometrical and electrical. If, then, the micelle grows by adding subsequent single ions one by one, eventually the distribution of the linear polymer would be approached. However, if the single ions add in groups of number g the dependence of size on concentration becomes more pronounced. If the single ions add in groups of $g = N$, the distribution becomes that for the linear polymer if concentration to the N 'th power is substituted for concentration to the first power. It is clear that a variety of size distributions could be explained by appropriate choice of N and g . It is not possible to write down the expression for the distribution function in terms of g , N and concentration in simple form.

It remains to consider what determines the smaller dimensions of a micelle indefinitely large in one dimension. First, one dimension must be limited by the length of the hydrocarbon chain. The second can either be limited by electrical forces, after Debye, or by the length of the hydrocarbon chain, after Hartley. In one case,⁵ it can be shown that the micelle is not limited by electrostatic factors. Scott, Tartar and Lingafelter have prepared micelles with no more than one unit charge, using octyltrimethylammonium octane sulfonate, which contains equal numbers of positive and negative paraffin-chain ions.

It is clear, then, that electrical forces need not operate to make the growth of finite-sized micelles possible. It is nevertheless possible, however, for added salt which changes the charge density of the micelle to change the net energy of association, and thus the size of the micelle. However, in the case of a rod micelle the electrical energy is not of the right form to limit indefinite growth.

Experimental Evidence.—A number of experimental observations support the idea of rod-like micelles whose length is limited by random fracture, rather than by specific forces.

Debye and Anacker⁶ were led to postulate rod-like micelles of extremely large size in a soap solution containing a large amount of salt.

Scheraga⁷ has postulated rod-like micelles in similar solutions, on the basis of flow-birefringence measurements.

Lingafelter and Minor⁸ observed that the fibrous "curd" form of soap was made up of molecules oriented perpendicular to the fiber axis, and amorphous with respect to the angle around the axis, with a slightly preferred orientation indicated.

(5) A. B. Scott, H. V. Tartar and E. C. Lingafelter, *J. Am. Chem. Soc.*, **65**, 698 (1943).

(6) P. Debye and E. W. Anacker, *This Journal*, **55**, 644 (1951).

(7) H. A. Scheraga, *J. Am. Chem. Soc.*, **73**, 5108 (1951).

(8) J. E. Minor, Thesis, University of Washington, 1950.

(4) R. H. Fowler, "Statistical Mechanics," University Press, Cambridge, 1936, § 21.231.

These fibers are presumed to be aggregates of extremely long rod-shaped micelles.

In the range of small micelles the frequently encountered minima⁹ in the specific conductivity-concentration curve may be taken to indicate that the charge on the micelle increases with concentration. Since the charge density can hardly increase with concentration, a continuous increase in micelle size is indicated.

It must be emphasized that no attempt has been made to show that the micelle when first formed is rod-shaped, but rather that its tendency to grow is in one dimension alone, and that this fact is responsible for the unusual stability of the micelle toward bulk crystallization.

I wish to thank Professor H. V. Tartar and Professor E. C. Lingafelter for many discussions.

DISCUSSION

K. J. PALMER.—It is not clear to me why spherical micelles cannot continue to grow by just forming extra double layers on the outside.

G. D. HALSEY.—You see that would put heads on the inside. Once it is possible to put heads on the inside, there would be no reason to stop doing it. That is why we just ruled out the spherical model.

K. J. PALMER.—Well, I think there is some evidence that this does occur in some systems. In the case of lipids that we have studied the dry material gives a sharp X-ray diffraction pattern which presumably represents the distance corresponding to the double length of the molecule. When this material is emulsified with small amounts of water the X-ray spacing increases and continues to do so with addition of water until the spacing triples in size. In other words the water appears to penetrate between the polar groups of the micelle which we believe consists of a whole lot of double layers because the X-ray diffraction pattern remained very sharp. In any case you can increase the water layers, so that the total spacing is three times the original spacing. The growth of these particular micelles is limited by the amount of solvent available. All of the solvent present appears to go between the double layers.

G. D. HALSEY.—In the non-aqueous?

K. J. PALMER.—No, these are aqueous. You start with the dry material and add small amounts of water.

(9) E. Gonick, *J. Am. Chem. Soc.*, **67**, 1191 (1945).

G. D. HALSEY.—But this is very, very concentrated.

K. J. PALMER.—That is right!

G. D. HALSEY.—In very concentrated solutions or slurries the micelles have most of their gegenions and mat together loosely to form a fibrous curd. The fibrous nature suggests that the micelles are long pipes roughly lined up side by side. If you add water, the gegenions are dissociated off, and the spacing between rods increases, and finally they push off into the solution.

K. J. PALMER.—In the case of lipides you don't have to break them up. The swelling can be controlled by adding a limited amount of water. The polar layers can be condensed by the addition of salt. This forces out the water. The micelles certainly consist of more than one double layer, however, because they are visible under the microscope.

IRVING REICH.—I would like to preface my question with the comment that it is unfortunate, I think, that relatively little work is done with non-ionic surface active agents, such as the polyoxyethylene fatty acid esters, and so on, because it would seem that they would permit us to clear up some of the uncertainties as to the relative influence of long range electrostatic forces and short range van der Waals forces. My question is, why are the non-ionic micelles limited in size? When you were speaking of the uncharged micelles, which I gather are made up of combinations of positively and negatively charged structures, you suggested an explanation which might apply for non-ionics, namely, that the micelles are rods which will break under thermal agitation. The trouble is, it seems to me, that this is just the sort of circumstance under which you might expect the Debye type of micelle to be formed. I believe that you pointed out that the energy of the rod micelle was less than that of the Debye micelle because of the smaller long range electrical repulsion energy. This would not be true for the non-ionic micelle, which may very well be expected to form the Debye type of micelles and grow to unlimited size.

G. D. HALSEY.—Suppose we did form Debye micelles; if they grew indefinitely they would never be micelles, but would crystallize out. Therefore in uncharged systems, the micelles must be limited in two dimensions of growth, at least, by the Hartley argument. In other words, when we do find micelles in non-aqueous systems, they can have only one axis of indefinite growth, the other dimensions must be fixed by specific structural factors.

IRVING REICH.—But assuming that you did form a rod micelle, why then should not that same molecule form under the same conditions, a plate micelle. The reason you give for the charged micelle being a rod rather than a Debye disk does not appear to apply here.

SCATTERING OF LIGHT BY LARGE SPHERICAL PARTICLES^{1,2}BY R. O. GUMPRECHT³ AND C. M. SLIEPCEVICH*Department of Chemical and Metallurgical Engineering, University of Michigan, Ann Arbor, Michigan**Received July 22, 1952*

The fundamental theory of the scattering of light by large spherical particles is discussed. A quantitative relationship between the Mie theory total scattering coefficient, K_t and the apparent or actual scattering coefficient, K_a is presented. K_a is shown to be a function of the total Mie scattering coefficient, the parameter α appearing in the Mie equations, and the half-angle, θ , of the cone which the transmitted-light-measuring instrument subtends with the illuminated spherical particle. These relationships between K_a and K_t were computed from the Mie equations and are particularly useful in the consideration of light scattered by large particles (*i.e.*, values of α up to 400). The validity of the computed values for K_a was confirmed experimentally by measurements on prepared dispersions of glass beads in water. The validity of the transmission equation is discussed from the standpoint of the geometry of the optical system used for obtaining transmission measurements.

During the past ten years considerable interest has developed in the application of the Mie⁴ theory of light scattering by spherical particles to the determination of particle size and concentration in aerosols.^{5,6} The primary advantage in using a light-scattering technique to measure particle sizes in aerosols is that it is not necessary to obtain a representative mechanical sample of the aerosol. Mechanical samples, as a rule, inherently introduce certain errors.⁷⁻⁹

In 1948 the Department of Chemical and Metallurgical Engineering of the University of Michigan initiated a graduate-student research program to develop a method for determining droplet sizes and distributions in atomized sprays based on the Mie theory of light scattering by spherical particles. Because of the large particle sizes encountered in this work, it became necessary to extend the range of the tabulated values of light-scattering functions which were in existence at that time¹⁰ to include values for particles whose radii are many times larger than the wave length of the incident light (roughly, up to 30 microns in radius). The initial computations were made by means of an IBM, Model 602-A, Calculating Punch at the University of Michigan. The computations were completed on a high-speed electronic computer, the ENIAC, which is located at Aberdeen Proving Ground, Maryland. The results of these computations were compiled in tabular form and published.^{11,12}

(1) Presented before the twenty-sixth National Colloid Symposium which was held under the auspices of the Division of Colloid Chemistry of the American Chemical Society in Los Angeles, California, June 16-18, 1952.

(2) This work was performed in partial fulfillment of the requirements for the Degree of Doctor of Philosophy in Chemical Engineering at the University of Michigan.

(3) Graduate Fellow, Department of Chemical and Metallurgical Engineering.

(4) Gustav Mie, *Ann Physik*, **25**, 377 (1908).

(5) Victor K. LaMer and David Sinclair, OSRD report No. 1857 (Sept. 29, 1943).

(6) David Sinclair and Victor K. LaMer, *Chem. Revs.*, **44**, 245 (1949). See also "Handbook on Aerosols," U. S. Atomic Energy Commission, Washington, D. C., 1950.

(7) K. R. May, "Symposium on Particle Size Analysis," p. 125-126, Supplement to *Trans. Inst. Chem. Eng.*, **25**, (1947).

(8) K. R. May, *J. Sci. Instruments*, **22**, 187 (1945).

(9) J. M. Geist, J. L. York and G. G. Brown, *Ind. Eng. Chem.*, **43**, 1371 (1951).

(10) "Tables of Scattering Functions for Spherical Particles," National Bureau of Standards Applied Mathematics Series-4, U. S. Government Printing Office, Washington, D. C., 1948.

(11) R. O. Gumprecht and C. M. Sliepevich, "Tables of Light-Scattering Functions for Spherical Particles," University of Michigan, Engineering Research Institute, Special Publication: Tables; Ann Arbor, Michigan, 1951.

General Theory

The mathematical background for the Mie theory is discussed in detail by Stratton.¹³ The basic equations may be summarized as

$$i_1 = \left| \sum_{n=1}^{\infty} \{A_n \pi_n + P_n [X \pi_n - (1 - X^2) \pi_n']\} \right|^2 = \left| i_1^* \right|^2 \quad (1)$$

$$i_2 = \left| \sum_{n=1}^{\infty} \{A_n [X \pi_n - (1 - X^2) \pi_n'] + P_n \pi_n\} \right|^2 = \left| i_2^* \right|^2 \quad (2)$$

$$K = \frac{1}{\alpha^2} \int_0^\pi (i_1 + i_2) \sin \gamma \, d\gamma = \frac{2}{\alpha^2} \sum_{n=1}^{\infty} \frac{R^2(A_n) + I^2(A_n) + R^2(P_n) + I^2(P_n)}{(2n+1)/n^2(n+1)^2} \quad (3)$$

Definitions

$$A_n = \left[\frac{(-1)^{n+1/2}(2n+1)}{n(n+1)} \right] \left[\frac{S_n'(\beta)S_n(\alpha) - mS_n(\alpha)S_n(\beta)}{S_n'(\beta)\phi_n(\alpha) - m\phi_n'(\alpha)S_n(\beta)} \right]$$

$$P_n = \left[\frac{(-1)^{n+1/2}(2n+1)}{n(n+1)} \right] \left[\frac{mS_n(\alpha)S_n'(\beta) - S_n(\beta)S_n'(\alpha)}{m\phi_n(\alpha)S_n'(\beta) - S_n(\beta)\phi_n'(\alpha)} \right]$$

where

$$S_n(\alpha) = (\pi\alpha/2)^{1/2} J_{n+1/2}(\alpha); \quad S_n(\alpha) = \partial S_n(\alpha)/\partial\alpha$$

$$\phi_n(\alpha) = S_n(\alpha) + iC_n(\alpha); \quad \phi_n'(\alpha) = \partial\phi_n(\alpha)/\partial\alpha$$

$$C_n(\alpha) = (-1)^n (\pi\alpha/2)^{1/2} J_{-n-1/2}(\alpha)$$

$$\alpha = \pi D/\lambda; \quad \beta = m\alpha$$

D = diameter of illuminated spherical droplet

λ = wave length of the incident light in the surrounding medium

m = index of refraction of droplet relative to that of the surrounding medium

$J_{n+1/2}(\alpha)$ and $J_{-n-1/2}(\alpha)$ are Bessel functions of half-integral order

$$\pi_n = \partial P_n(x)/\partial x; \quad \pi_n' = \partial^2 P_n(x)/\partial x^2$$

where

$P_n(x)$ is the Legendre polynomial of degree n (not to be confused with P_n defined above)

$X \cos \gamma$ (where γ is the angle between the direction of propagation of the scattered light and the reversed direction of propagation of the incident beam)

$R(A_n)$, $I(A_n)$, $R(P_n)$ and $I(P_n)$ refer to the real and imaginary values of the complex functions A_n and P_n , respectively.

$R(i_1^*)$, $I(i_1^*)$, $R(i_2^*)$ and $I(i_2^*)$ refer to the real and imaginary values of the complex functions i_1^* and i_2^* , respectively.

(12) R. O. Gumprecht and C. M. Sliepevich, "Tables of Functions of First and Second Partial Derivatives of Legendre Polynomials," University of Michigan, Engineering Research Institute, Special Publication: Tables; Ann Arbor, Michigan, 1951.

(13) J. A. Stratton, "Electromagnetic Theory," McGraw-Hill Book Co., Inc., New York, N. Y., 1941.

The intensity functions, i_1 and i_2 , defined above, are proportional to the intensities of the two incoherent plane-polarized components of light scattered by a single illuminated particle.

When the particle is illuminated by unpolarized light of unit intensity per unit beam cross sectional area, $\lambda^2/8\pi^2 i_1$ is the intensity (per unit solid angle) of the scattered component whose electric vector is perpendicular to the plane of observation (the plane containing the direction of observation and the direction of propagation of the incident beam), and $\lambda^2/8\pi^2 i_2$ is the intensity of the scattered component whose electric vector is parallel to the plane of observation.

When the particle is illuminated by plane-polarized light of unit intensity per unit beam cross sectional area, $\lambda^2/4\pi^2 i_1$ is the intensity of the scattered component whose electric vector is perpendicular to the electric vector of the incident beam, and $\lambda^2/4\pi^2 i_2$ is the intensity of the scattered component whose electric vector lies in the plane formed by the electric vector of the incident beam and its direction of propagation.

The scattering coefficient, K , is defined as the ratio between the scattering cross section and the geometric cross section of the spherical particle. The intensity of a parallel beam of light is reduced in traversing a dispersion of uniform spherical particles, all of diameter D , according to the transmission equation as

$$I/I_0 = e^{-\frac{K\pi D^2 n l}{4}} \quad (4)$$

where: I_0 is the intensity of the incident parallel beam and I is the intensity of the beam after traversing a distance, l , through the dispersion containing n particles per unit volume of dispersion. It should be noted that K , defined above, is based on the total amount of light scattered by a particle in all directions. For this reason, it will be referred to as K_t in the subsequent discussion.

Published values of K_t are presently available for about half a dozen values of m and for numerous values of α ranging from less than 1 up to 400.^{10,11} Considerable interest has been focussed on the values of K_t for large values of α because of the fact that K_t approaches the value 2 instead of 1. On first consideration it might appear impossible for a large spherical particle to have a scattering cross section twice the geometrical cross section. Various authors have explained this seeming anomaly, however, on the basis of Babinet's principle of diffraction by opaque circular discs.¹⁴⁻¹⁶

Babinet's principle shows that a circular opaque disc diffracts an amount of light around the edges of the disc equal to the amount of light which actually strikes the disc. Therefore, the scattering cross section is actually twice the geometric cross section. Furthermore, the major portion of the light which is scattered as a result of diffraction is scattered within a relatively small cone in the forward direction. No known type of light measuring-device can measure the intensity of only the undis-

turbed portion of the parallel beam, with the complete exclusion of light scattered in a forward direction. Previous investigators have shown that when experimentally measured light intensities are substituted in the transmission equation (4), the apparent scattering coefficient may range from a value of 1 to a value approaching 2, depending on the value of the half-angle θ of the cone which the light-measuring device subtends with the scattering particles.¹⁴ In the subsequent discussion, the apparent or actual scattering coefficient will be referred to as K_a to distinguish it from the total scattering coefficient K_t .

Since there was some question as to the validity of the diffraction theory for opaque circular discs when applied to the case of transparent spheres,¹⁶⁻¹⁷ it was necessary to obtain exact solutions of the Mie equations for the purpose of obtaining values of K_a as a function of θ for values of α ranging up to 400. Exact solutions were employed because the accuracy of approximate solutions for i_1 and i_2 as functions of γ for large particles was considered questionable.¹⁸ In addition, the ratio of K_a to K_t , subsequently referred to as R , was computed from diffraction theory and compared with the values of R computed by the Mie theory.

Theoretical Calculations

Since K_t is based on the total amount of light scattered by a particle in all directions and K_a is based on the amount of light scattered by a particle in all directions, except within a cone of half-angle θ in the forward direction, K_a may be defined in terms of the Mie theory as

$$K_a = K_t - \frac{1}{\alpha^2} \int_{\pi-\theta}^{\pi} (i_1 + i_2) \sin \gamma d\gamma \quad (5)$$

from which R may be defined as

$$R = \frac{K_a}{K_t} = 1 - \frac{1}{K_t \alpha^2} \int_{\pi-\theta}^{\pi} (i_1 + i_2) \sin \gamma d\gamma \quad (6)$$

Rayleigh¹⁹ has shown by diffraction theory that the fraction of the diffracted light falling outside of a cone of half-angle θ in the forward direction is given by

$$f = [J_0(\alpha\theta)]^2 + [J_1(\alpha\theta)]^2 \quad (7)$$

where J_0 and J_1 indicate Bessel functions of order zero and one, respectively; $\alpha = \pi D/\lambda$ (same as Mie theory); and θ is expressed in radians and is assumed to be small enough so that $\theta \simeq \sin \theta$.

Assigning a value of $K_t = 2$ to the opaque circular disc, the value of R may be defined as

$$R = \frac{1 + [J_0(\alpha\theta)]^2 + [J_1(\alpha\theta)]^2}{2} \quad (8)$$

Of interest also is a comparison between the values of the scattered light intensities at various angles in the forward direction as predicted by both the Mie theory and the diffraction theory. According to diffraction theory, the intensity of diffracted light at an angle θ with the forward direction is given by^{15,20}

(14) David Sinclair, *J. Optical Soc. Am.*, **37**, 475 (1947).

(15) W. H. Walton, "Symposium on Particle Size Analysis," p. 141-142, Suppl. to *Trans. Inst. Chem. Eng.*, **25** (1947).

(16) G. F. Lothian and F. P. Chappel, *J. Applied Chem.*, **1**, 475 (1951).

(17) L. Brillouin, *ibid.*, **20**, 1113 (1949).

(18) H. Blumer, *Z. Physik*, **38**, 935 (1926).

(19) Lord Rayleigh, *Phil. Mag.*, Sec. 5, vol. II (1881).

(20) Max Born, "Optik," Julius Springer, Berlin, 1933. Reprinted by Edwards Bros., Ann Arbor, Mich., 1943, p. 160.

$$i_s = \left[\frac{\pi D^2}{4\lambda} \right]^2 \left[\frac{2J_1(\alpha\theta)}{\alpha\theta} \right]^2 \tag{9}$$

where I_s refers to the intensity per unit solid angle for incident light of unit intensity per unit beam cross-sectional area. By the Mie theory, for unpolarized incident light

$$I_s = \frac{\lambda^2}{8\pi^2} (i_1 + i_2) \tag{10}$$

Therefore, for the purpose of comparison, the quantity $\alpha^4/2 [2J_1(\alpha\theta)/\alpha\theta]^2$ should equal the sum ($i_1 + i_2$) computed from the Mie equations. Values of ($i_1 + i_2$) computed by both the Mie theory and the diffraction theory, as well as values of R computed by equation (6) and by equation (8), are presented in Table I.

Discussion of Calculated Results

It can be seen from an inspection of Table I that the values of ($i_1 + i_2$) computed by the two methods

show only approximate agreement, but that the values of R computed by the two methods show remarkably good agreement. The latter agreement appears to be best for small values of θ , where it is seen that a maximum discrepancy of less than 2% exists for values of θ less than 1.4°. At $\alpha = 80$ the values of R computed for the various values of θ are practically identical for each of the three different indices of refraction. At $\alpha = 20$ the discrepancy between the values of R computed by the Mie theory for the three indices of refraction, and the values of R computed by the diffraction theory, increases rapidly as the value of θ is increased.

In general, it may be concluded that a very close approximation of the value of R (which may be termed a "correction factor" for the transmission equation and which is essentially independent of the index of refraction of the particles) may be obtained from the relatively simple expression given

TABLE I

α	θ°	$R(i_1^*)$	$I(i_1^*)$	$R(i_2^*)$	$I(i_2^*)$	$(i_1 + i_2)$		R	
						Mie	Dif- fraction	Mie	Dif- fraction
A.									
400	0	-2598	-81210	+2598	+81210	1.320×10^{10}	1.280×10^{10}	1.000	1.000
$m = 1.33$.2	-1817	-62640	+1818	+62670	0.7857	0.7695	0.796	0.808
$K_t = 2.031$.4	-453.5	-23200	+23270	+463.4	.1080	.1114	.599	.602
	.3	-87.94	+5786	+115.0	-5762	.006671	.005309	.574	.581
	.3	-800.6	+9678	+830.0	-9738	.01898	.01848	.553	.557
	1.0	-1299	-21.33	+1301.0	-38.50	.0003382	.00001136	.538	.545
	1.2	-898.7	-5008	+870.9	+5036	.005201	.005313	.533	.539
	1.4	-348.3	-986.4	+324.3	+1062	.0002328	.0005263	.533	.531
200	0	-1024	-20550	+1024	+20550	8.470×10^8	8×10^8	1.000	1.000
$m = 1.33$.2	-950.6	-19290	+947.2	+19300	7.461	7.075	0.941	0.943
$K_t = 2.056$.4	-755.1	-15790	+743.1	+15820	5.009	4.810	.804	.808
	.3	-505.9	-10910	+484.6	+10970	2.397	2.362	.672	.676
	.3	-285.7	-5725	+259.1	+5804	0.6661	0.6963	.599	.602
	1.0	-162.0	-1319	+137.0	+1396	.03735	.05235	.582	.582
	1.2	-161.3	+1588	+144.4	-1534	.04922	.03318	.581	.581
	1.4	-262.0	+2765	+256.3	-2745	.1531	.1311	.570	.572
150	0	-486.7	-11395	+486.7	+11395	2.602×10^8	2.532×10^8	1.0	1.0
$m = 1.44$.2	-471.5	-11000	+465.8	+11000	2.425	2.363	0.966	0.967
$K_t = 2.026$.4	-429.1	-9882	+407.6	+9871	1.954	1.913	.879	.880
	.6	-368.3	-8184	+324.9	+8162	1.338	1.318	.770	.772
	.8	-301.3	-6128	+235.0	+6094	0.7484	0.7474	.675	.676
	1.0	-241.2	-3978	+156.6	+3934	.3138	.3206	.614	.614
	1.2	-198.6	-1981	+105.2	+1932	.07710	.08305	.588	.587
	1.4	-179.2	-345.9	+89.32	+296.2	.002475	.003527	.582	.581
100	0	-127.1	-5253	+127.1	+5253	5.52×10^7	5×10^7	1.0	1.0
$m = 1.33$.2	-115.5	-5169	+118.1	+5170	5.347	4.852	0.984	0.985
$K_t = 2.101$.4	-81.89	-4922	+91.76	+4927	4.853	4.422	.940	.943
	.3	-29.69	-4530	+50.64	+4541	4.115	3.777	.875	.880
	.3	+36.07	-4015	-1.834	+4034	3.240	3.006	.801	.808
	1.0	+108.8	-3411	-60.93	+3437	2.347	2.210	.728	.737
	1.2	+181.6	-2754	-121.7	+2786	1.540	1.476	.667	.676
	1.4	+247.6	-2082	-179.0	+2119	0.8916	0.8740	.622	.631
B.									
80	0	-320.5	-3273	+320.5	+3273	2.163×10^7	2.048×10^7	1.0	1.0
$m = 1.20$	1/4							0.985 ^a	0.985
$K_t = 2.046$	1/2							.944 ^a	.943
	3/4							.885 ^a	.880
	1.0	-245.9	-2441	+272.6	+2466	1.217	1.231	.815	.808
	1.4							.709 ^a	.699
	2	-117.6	-712.6	+174.8	+766.8	0.1140	0.1783	.616	.602
	3	-76.79	+485.2	+105.1	-455.4	0.04598	0.008495	.600	.581
80	0	-84.79	-3276	+84.79	+3276	2.147×10^7	2.048×10^7	1.0	1.0
$m = 1.33$	1/4							0.985 ^a	0.985
$K_t = 2.047$	1/2							.944 ^a	.943
	3/4							.884 ^a	.880
	1.0	+21.05	-2490	-6.732	+2491	1.240	1.231	.812	.808
	1.4							.701 ^a	.699
	2	+198.9	-841.0	-168.1	+844.6	0.1489	0.1783	.606	.602
	3	+233.5	+326.7	-218.0	-319.3	0.03107	0.008495	.588	.581

TABLE I (Continued)

α	θ°	$R(i_1^*)$	$I(i_1^*)$	$R(i_2^*)$	$I(i_2^*)$	$(i_1 + i_2)$		R	
						Mie	Dif-fraction	Mie	Dif-fraction
80	0	- 111.5	- 3342	+ 111.5	+ 3342	2.236×10^7	2.018×10^7	1.0	1.0
$m = 1.44$	$1/4$							0.985 ^a	0.985
$K_t = 2.089$	$1/2$.943 ^a	.943
	$3/4$.883 ^a	.880
	1.0	- 76.24	- 2482	+ 76.97	+ 2533	1.259	1.231	.812	.808
	1.4							.705 ^a	.699
	2	- 10.58	- 713.9	+ 12.89	+ 831.6	0.1201	0.1783	.612	.602
	3	+ 17.92	+ 468.5	- 15.86	- 390.8	0.03728	0.008495	.600	.581
60	0	- 99.43	- 1798	+ 99.43	+ 1798	6.486×10^6	6.480×10^6	1.0	1.0
$m = 1.33$	$1/2$							0.967 ^a	0.967
$K_t = 1.998$	1	- 58.43	- 1536	+ 62.30	+ 1534	4.720	4.895	.881	.880
	1.4							.799 ^a	.794
	2	+ 33.53	- 891.5	- 22.01	+ 885.1	1.580	1.913	.696	.676
	3	+ 110.3	- 194.1	- 95.36	+ 187.2	0.09398	0.2125	.630	.587
	4	+ 127.0	+ 248.6	- 117.0	- 250.6	0.1544	0.02688	.619	.581
C.									
40	0	- 94.87	- 795.0	+ 94.87	+ 795.0	1.282×10^6	1.280×10^6	1.0	1.0
$m = 1.33$	$1/2$							0.985 ^a	0.985
$K_t = 1.988$	1	- 84.32	- 739.2	+ 84.90	+ 737.5	1.105	1.132	.942 ^a	.943
	1.4							.896 ^a	.894
	2	- 56.28	- 585.9	+ 58.29	+ 580.1	0.6864	0.7695	.815	.808
	3	- 20.10	- 372.9	+ 23.65	+ 362.9	.2718	.3779	.707	.676
	4	+ 12.98	- 150.1	- 8.639	+ 138.6	.04198	.1114	.663	.602
	5	+ 34.28	+ 35.10	- 30.46	- 44.24	.005292	.008376	.658	.582
	6	+ 40.96	+ 151.0	- 38.96	- 154.6	.04987	.005309	.644	.581
	7	+ 36.61	+ 188.6	- 37.15	- 185.9	.07285	.02098	.603	.572
30	0	- 73.40	- 449.6	+ 73.40	+ 449.6	4.152×10^5	4.050×10^5	1.0	1.0
$m = 1.33$	1	- 69.59	- 430.7	+ 70.47	+ 430.7	3.808	3.779	0.966	0.967
$K_t = 1.998$	2	- 58.86	- 376.8	+ 62.16	+ 376.6	2.912	3.059	.881	.880
	3	- 43.20	- 295.7	+ 49.77	+ 295.4	1.790	2.109	.782	.772
	4	- 25.36	- 199.0	+ 35.16	+ 198.6	0.8090	1.196	.708	.676
	5	- 8.308	- 99.65	+ 20.32	+ 99.42	.2030	0.5127	.672	.614
	6	+ 5.506	- 10.24	+ 6.971	+ 10.41	.002920	.1328	.666	.587
	7	+ 14.64	+ 59.45	- 3.798	- 58.70	.07209	.005642	.663	.581
20	0	- 47.00	- 214.0	+ 47.00	+ 214.0	9.602×10^4	8×10^4	1.0	1.0
$m = 1.33$	1	- 46.05	- 209.8	+ 46.53	+ 209.2	9.205	7.763	0.983	0.985
$K_t = 2.140$	2	- 43.27	- 197.4	+ 45.13	+ 195.0	8.091	7.075	.936	.943
	3	- 38.90	- 177.6	+ 42.84	+ 172.7	6.474	6.043	.872	.880
	4	- 33.28	- 151.8	+ 39.70	+ 143.9	4.646	4.810	.804	.808
	5	- 26.84	- 121.6	+ 35.80	+ 110.8	2.908	3.535	.744	.737
	6	- 20.06	- 88.92	+ 31.21	+ 75.81	1.503	2.362	.702	.676
	7	- 13.39	- 55.71	+ 26.07	+ 41.29	0.5667	1.398	.679	.631
20	0	+ 2.197	- 173.3	- 2.197	+ 173.3	6.005×10^4	8×10^4	1.0	1.0
$m = 1.20$	1	+ 3.187	- 169.5	- 2.952	+ 169.4	5.745	7.763	0.987	0.985
$K_t = 1.733$	2	+ 6.083	- 158.4	- 5.178	+ 158.3	5.021	7.075	.952	.943
	3	+ 10.67	- 140.9	- 8.748	+ 140.8	3.987	6.043	.903	.880
20	0	- 34.28	- 262.1	+ 34.28	+ 262.1	13.98	8×10^4	1.0	1.0
$m = 1.44$	1	- 33.39	- 257.9	+ 34.01	+ 258.1	13.54	7.763	0.980	0.985
$K_t = 2.622$	2	- 30.84	- 245.6	+ 33.23	+ 246.2	12.30	7.075	.923	.943
	3	- 26.92	- 226.0	+ 31.99	+ 227.2	10.44	6.043	.841	.880

^a Obtained by interpolation.

by equation (8), provided θ is kept small (preferably less than 1.5°).

On the basis of these results, it is evident that the transmission equation (4) as written above must be corrected to account for both the light transmitted, and the light scattered, in a forward direction. Thus, by inserting the correction factor, R , into the differential form of equation (4), and integrating over the distance traversed by the beam through the dispersion, the following results

$$I/I_0 = e^{-RK_t \frac{\pi D^2}{4} nl} \tag{11}$$

Geometrical Considerations

Of the various optical systems which have been used in light-transmission experiments, the lens-pinhole optical system shown in Fig. 1 is preferred for three reasons.

(1) The exact value for the half-angle θ can be calculated readily from a direct measurement of the diameter of the pinhole and the focal length of the lens. Referring to Fig. 1, light from source S is focused into a parallel beam by the lens L_1 . Lens L_2 focuses the parallel beam at the pinhole, which is located at the focal point of this lens. The pinhole must be large enough to permit all the light in the focused beam to pass through and fall on the cathode of the phototube P . It can be readily shown that the value of θ is equal to the arc tangent, r/f ,

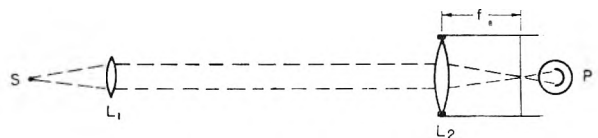


Fig. 1.—Diagrammatic illustration of a lens-pinhole type transmitted light detector.

where r is the radius of the pinhole and f is the focal length of the lens L_2 .¹⁵

(2) The value of θ is a constant and independent of the location of the illuminated particle in the path of the beam or in the fringes of the beam, so long as the diameter of the lens L_2 satisfies equation (12)

$$D_{L_2} \geq \frac{2rl}{f} + D_b \quad (12)$$

where

D_{L_2} is the diameter of lens L_2

l is the distance between lens L_2 and the most remote particle in the beam

D_b is the diameter of the parallel light beam

(3) The lens-pinhole optical system practically excludes all stray light from the phototube.

When transmission measurements are being made on a liquid dispersion of immiscible particles contained in a cell which is placed in the beam, account must be taken of the light scattered from the particles which is deflected from its original path upon crossing the boundaries of the cell, as shown in Fig. 2. It is seen that the value of θ to be

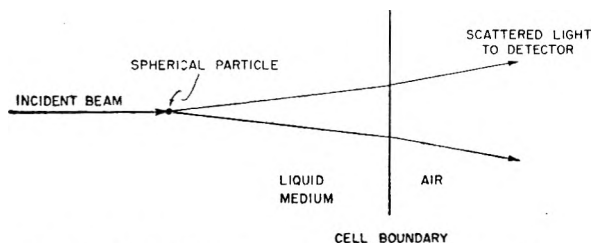


Fig. 2.—Deflection of scattered light at cell boundary.

applied to particles suspended in a liquid medium is smaller than the value of θ given by the fraction r/f . Since r/f is usually quite small, the value of θ (in radians) for particles suspended in air is given by

$$\theta = r/f$$

For particles suspended in a liquid medium in a cell, the value of θ is given by

$$\theta = r/fn_m$$

where n_m is the refractive index of the medium.

In contrast to the lens-pinhole detector, the optical system shown in Fig. 3 presents obvious difficulties, since the angle θ is not a constant but is dependent on the location of the illuminated particle in the path of the beam. Thus, in the derivation of the transmission equation from the differential equation, $-dI/I = RK_t \pi D^2/4 n dx$, when the right side is integrated from $x = 0$ to $x = l$, R cannot be taken out of the integral as a constant but must be retained under the integral sign, since it is a function of x . The result is quite cumbersome. An additional complication is that the value of R for particles near the outer edges of the beam is different from the value of R for particles in the center

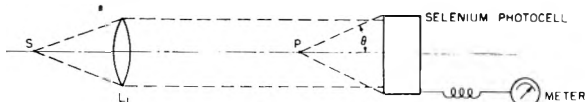


Fig. 3.—Diagrammatic illustration of the use of a photo-cell as a transmitted light detector without the lens-pinhole system.

of the beam at any given distance from the photo-cell. This variation is due to the fact that the axis of the cone subtended by the photocell with a particle at the edge of the beam is not coincident with the direction of propagation of the incident light.

From the foregoing discussion it is apparent that the transmission equation as ordinarily expressed by equation (4) cannot be used except in the case of extremely small particles, for which it is only a good approximation. The effect of not only the particle diameter but also the geometry of the optical system on the apparent scattering cross section must be considered in all cases.

Experimental Work

In the present work an optical system similar to Fig. 1 was used. It consists of a pinhole $1/8$ inch in diameter, and a lens whose focal length is $37/8$ inches, giving a value of $\theta = 0.92^\circ$ for particles suspended in air and 0.69° for particles suspended in water.

In order to test the validity of the computed values of R shown in Table I, measurements were made on the transmission of light through dispersions of glass spheres suspended in water. The glass spheres were prepared from Pyrex glass by the procedure outlined by Bloomquist and Clark.²¹ After the spheres were washed and separated into several narrow size-groups by elutriation, the sizes of the particles in the respective groups were determined by both microscopic examination and by measurement of sedimentation rates in water. From these size measurements, the geometrical cross-sectional area per gram of glass was calculated for each group. In experimentally determining the value of R for each size-group of glass beads, the quantity $(\pi D^2/4 n)$ in the modified transmission equation (11), was replaced by the product of the geometrical cross-sectional area per gram of glass beads times the concentration of glass beads in the test cell in grams per cubic centimeter, to give

$$\ln \frac{I_0}{I} = RK_t CAI \quad (13)$$

where

C = concentration of glass beads (in grams per cubic centimeter)

A = geometric cross sectional area per gram of glass beads (in square centimeters per gram)

l = length of light path through the test cell (in centimeters).

Since computed values of K_t as a function of α for a relative index of refraction equivalent to that of Pyrex glass in water were not available, it was necessary to employ the Lorenz-Lorentz relationship^{6,22} to obtain these values from the published values of K_t as a function of α for $m = 1.20$.¹¹

Once the values of all factors in the transmission equation except R were known, it was possible to calculate the value of R quite easily from simple transmission measurements.

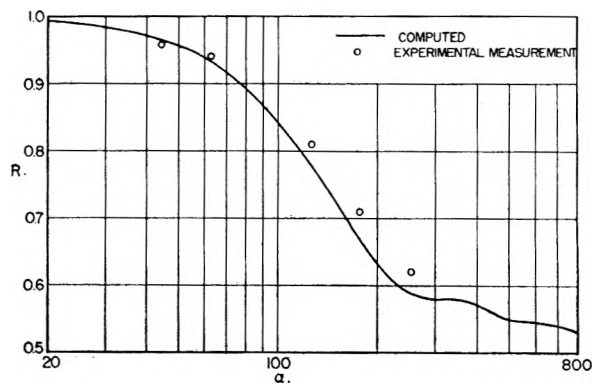


Fig. 4.— R vs. α for $\theta = 0.69^\circ$.

(21) C. R. Bloomquist and A. C. Clark, *Ind. Eng. Chem., Anal. Ed.*, **12**, 61 (1940).

(22) E. D. Bailey, *ibid.*, **18**, 365 (1946).

A comparison between the values of R determined by theory and those by experiment is shown in Fig. 4. The solid curve represents the values of R computed from diffraction theory and the circles represent the values of R determined by the glass-bead transmission measurements. The fact that the experimental points are about 5% higher than the theoretical values for the larger values of α is probably due

to the slight divergence of the supposedly parallel beam, as explained by Lothian and Chappel.¹⁶

Acknowledgment.—The Calco Chemical Division of the American Cyanamid Company provided Fellowship Grants for this work during the period 1949–51.

MEASUREMENT OF PARTICLE SIZES IN POLYDISPERSED SYSTEMS BY MEANS OF LIGHT TRANSMISSION MEASUREMENTS COMBINED WITH DIFFERENTIAL SETTLING^{1,2}

BY R. O. GUMPRECHT³ AND C. M. SLIEPCEVICH

Department of Chemical and Metallurgical Engineering, University of Michigan, Ann Arbor, Michigan

Received July 22, 1952

A mathematical derivation of a method for the measurement of particle sizes and their distribution in polydispersed systems by means of light transmission measurements combined with differential settling is presented. The method consists essentially of the combined application of Stokes' law of settling and a corrected form of the light transmission equation. The experimental equipment consists of a settling chamber, chopped-light source, light filter, a lens-pinhole optical systems a phototube pick-up and preamplifying system, a narrow-band amplifier and a strip-chart recorder. Differentiation of the "decay" curve plotted by the strip-chart recorder yields the so-called size-frequency distribution curve of the aerosol in the settling chamber. An example of an analysis of an aerosol produced by spraying kerosene from a conventional swirl-chamber nozzle is given.

Introduction

In the previous paper the relationship between the apparent scattering coefficient and the total scattering coefficient as computed from the Mie theory was shown to be dependent on both the size of the particle and the geometry of the optical system employed to measure the intensities of the transmitted light. This relationship is conveniently expressed as the ratio of the apparent scattering coefficient to the total scattering coefficient and is designated by R . The correct transmission equation for a dispersion of spherical particles, all of diameter D , is therefore

$$I/I_0 = e^{-RKt} \frac{\pi D^2}{4} nl$$

or its equivalent form

$$-\ln \frac{I}{I_0} = RKt \frac{\pi D^2}{4} nl \quad (1)$$

where

I_0 is the intensity of the incident parallel beam

I is the intensity of the beam after traversing a distance, l , through a dispersion containing n spherical particles per unit volume of the dispersion

K_t is the Mie-theory total-scattering coefficient, or the ratio between the total scattering cross section and the geometric cross section of the spherical particles^{4,5}

(1) Presented before the twenty-sixth National Colloid Symposium which was held under the auspices of the Division of Colloid Chemistry of the American Chemical Society in Los Angeles, California, June 16–18, 1952.

(2) This work was performed in partial fulfillment of the requirements for the Degree of Doctor of Philosophy in Chemical Engineering at the University of Michigan.

(3) Graduate Fellow, Department of Chemical and Metallurgical Engineering.

(4) "Tables of Scattering Functions for Spherical Particles," National Bureau of Standards Applied Mathematics Series—4 U.S. Government Printing Office, Washington, D. C. (1948).

(5) R. O. Gumprecht and C. M. Sliepceovich, "Tables of Light-Scattering Functions for Spherical Particles," University of Michigan, Engineering Research Institute, Special Publications: Tables; Ann Arbor, Michigan, 1951.

Derivation of Equations

A polydispersed system may be considered as being composed of a multitude of monodispersed systems; therefore, the transmission equation becomes

$$-\ln \frac{I}{I_0} = \frac{\pi l}{4} \sum_i R_i K_i D_i^2 n_i \quad (2)$$

In equation (2), I , I_0 and l can be measured readily, and R_i and K_i are related to D_i . Therefore, since D_i and n_i are independent unknowns in this equation, another relationship is required.

If light-transmission measurements are made on a dispersion containing particles above the colloidal size range, the intensity of the transmitted light will gradually increase as the particles settle out under the influence of gravity. If tranquil settling takes place, the size range of particles settling out during any interval of time can be computed from Stokes' law

$$D = k/\sqrt{t} \quad (3)$$

where

D = diameter of the largest particle present in the light beam after an elapsed time, t , from the start of settling; and

$$k = \sqrt{\frac{18h\mu}{g_1(\rho_1 - \rho_2)}}$$

where

h = settling height

μ = viscosity of the settling medium

g_1 = local acceleration of gravity

$(\rho_1 - \rho_2)$ = difference in density of the dispersed particles and the surrounding medium

Equation (3) can be used to replace the variable, D , in equation (2) by a quantity which is readily measured, namely, t , as shown below.

In equation (2), n_i refers to the number of particles (per unit volume of dispersion) of diameter D_i contained in any one of the arbitrary monodis-

persed systems of which the polydispersed system is assumed to be composed. Obviously, it would be impractical to attempt to define a polydispersed system composed of a random distribution of particle sizes in terms of a summation of truly monodispersed systems. Therefore, the polydispersed system is assumed to be composed of an arbitrary number of systems, each of which is composed of a relatively narrow size range of particles. If a term N is defined as the number of particles of average diameter D per unit volume of the dispersion per unit range of particle diameter,⁶ then in the limit, as the size range of particle diameters in each arbitrary system, approaches zero

$$\Sigma n_i = \int_0^{\infty} N dD \quad (4)$$

where NdD is equal to the number of particles having diameters between D and $D + dD$ per unit volume of the dispersion.

Equation (2) can now be rewritten as

$$\ln I = \ln I_0 - \frac{\pi l}{4} \int_0^{\infty} RK_t D^2 N dD \quad (5)$$

Differentiating equation (5) with respect to t yields

$$\frac{d \ln I}{dt} = - \frac{\pi l}{4} RK_t D^2 N \frac{dD}{dt} \quad (6)$$

By means of equation (3), D can be eliminated from equation (6). Thus

$$d \ln I / dt = \frac{\pi l}{8} k^2 t^{-1/2} RK_t N \quad (7)$$

Solving for $RK_t N$

$$RK_t N = \frac{8}{\pi k^2} \frac{1}{t} \frac{dI}{dt} t^{3/2} \quad (8)$$

From light-transmission measurements on a dispersion undergoing tranquil settling with time, the relationship between I and t can be measured directly. Thus, from a curve of I vs. t , the quantity $RK_t N$ can be calculated from the value of I and the slope of the curve at a given time t . Likewise, the value of D can also be calculated from Stokes' law at the same given time t . Therefore, $RK_t N$ can be obtained as a function of D . Finally, since R and K_t are known functions of D (as discussed in the previous paper), N can be calculated as a function of D to obtain the so-called size-frequency distribution curve. Since the total number of particles of all sizes per unit volume of the dispersion is given by

$$\Sigma n_i = \int_0^{\infty} N dD \quad (4)$$

the total surface area of the particles per unit volume of dispersion is

$$S = \pi \int_0^{\infty} N D^2 dD \quad (9)$$

The total volume of the particle per unit volume of the dispersion is

$$V = \frac{\pi}{6} \int_0^{\infty} N D^3 dD \quad (10)$$

Discussion

In deriving the above expressions it was assumed that the sizes of the particles and the properties of the settling medium were such that Stokes' law of settling was valid; that is, for a value of the Reynolds number for the particle between about 0.0001 and 2.0.⁷ For Reynolds numbers outside of this range, modified expressions for the settling velocity must be employed. It was also assumed that settling occurs in a perfectly tranquil medium. When thermal convection currents are likely to be troublesome, it seems more practical to insulate the settling chamber or surround it with a constant-temperature bath than to contend with the complex problem of stirred settling.⁸ In addition, the actual width or thickness of the light beam was assumed to be negligibly small compared to the settling height of the chamber. For example, when the width of the beam is 1% of the settling height, the error in the calculated value of the particle diameter is about 0.5% and the error in the calculated value of N is about 1.5% in the opposite direction. Thus, the errors in the calculated values of the surface and volume of the particles per unit volume of the suspension due to the assumption of negligible beam width are less than 1%.

Experimental Work

The experimental equipment used in the present work for the analysis of drop sizes produced by spray atomizers consists of a settling chamber 10 feet in height with a cross section measuring 3 feet by 3 feet. A filtered chopped-light source, a lens-pinhole optical system, a phototube and a preamplifier are mounted on the settling chamber. The preamplified signal is introduced into a high-gain narrow-band amplifier which feeds into a strip-chart recorder.

The light source consists of a 6-volt fixed-focus auto-spotlight bulb located at the focus of a camera viewer lens, $5/8$ -inch in diameter with a 3-inch focal length. The light beam is chopped at 300 cycles per second by means of a spinning aluminum disc having ten $5/8$ -inch holes equally spaced on a diameter of 4 inches. The disc is driven by an 1800-r.p.m. synchronous motor. A constant level of light intensity is obtained by the use of a regulated 6-volt power supply for the light bulb. Essentially monochromatic light is obtained by the use of a Baird interference-type filter which has a peak transmission at $4700 \pm 50 \text{ \AA}$. and a band width of 100–150 \AA . at one-half of maximum transmission.

The transmitted light receiver consists of a 3-inch diameter by $3/8$ -inch focal length condensing lens with a $1/8$ -inch pinhole behind the lens at the focus. The light which passes through the pinhole falls on the cathode of a 929 vacuum phototube which is mounted in a light-tight housing. The a.-c. voltage developed at the plate of the phototube is fed to the grid of a cathode-follower type of impedance transformer mounted in the same housing with the phototube. The preamplified signal passes through a shielded cable to the main amplifier, where it is amplified, rectified and finally introduced into a strip-chart recorder. The amplifier is equipped with a gain control and a 300-cycle parallel T filter which eliminates the effects of stray 60-cycle pickup. Stable amplifier operation is obtained by the use of an electronically regulated "B" voltage power supply.

The strip-chart recorder plots a continuous record of the intensity of the modulated light which falls on the cathode of the phototube. The curve obtained during the period when the dispersion is settling in the settling chamber has sometimes been referred to as a "decay" curve because of its similarity to curves illustrating radioactive decay. A

(7) J. H. Perry, "Chemical Engineers' Handbook," 3rd Ed., McGraw-Hill Book Co., Inc., New York, N. Y., 1950, p. 1019.

(8) "Handbook on Aerosols," U.S. Atomic Energy Commission, Washington, D. C., 1950, Chapters 7 and 8.

(6) J. M. Dalla Valle, "Micromeritics," 2nd Ed., Pittman Publishing Corporation, New York, N. Y., 1948, p. 51.

typical decay curve is illustrated in Fig. 1. This curve was obtained during the settling of an aerosol produced by the pressure atomization of 50 ml. of kerosene at 700 pounds per sq. in. from a conventional swirl-chamber type nozzle.

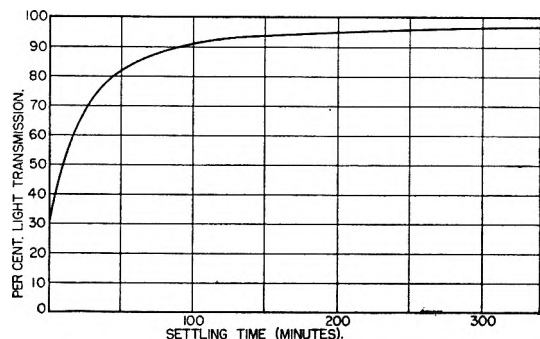


Fig. 1.—Per cent. light transmission elapsed vs. settling time for kerosene fog.

Figure 2 illustrates the size-frequency distribution curve which was calculated from the decay curve shown in Fig. 1 by the methods outlined above. The area under the curve is equal to the total number of kerosene droplets per cubic centimeter of aerosol in the chamber. Such factors as coagulation and evaporation of droplets and thermal convection during the settling period were assumed to be negligible. Further elaboration on these points is considered beyond the scope of the present paper.

Acknowledgment.—The Calco Chemical Division of the American Cyanamid Company provided Fellowship Grants during the period 1949–51.

DISCUSSION

ANON.—The light diffracted from the first particle could strike another particle, and also be diffracted, and in that way, you might get more transmitted light than the calculated value.

R. O. GUMPRECHT.—Yes, that is true. However, the lens-pinhole optical system limits to a great extent the amount of secondary scattered light which actually reaches the phototube. The amount of secondary, tertiary, etc., scattered light which will be recorded as “transmitted” light is a function of the optical density of the dispersion. The higher orders of scattered light are likely to be troublesome only in extremely dense dispersions. In the more useful ranges of optical densities employed in the present work, we have been unable to detect the effects of secondary and higher orders of scattered light.

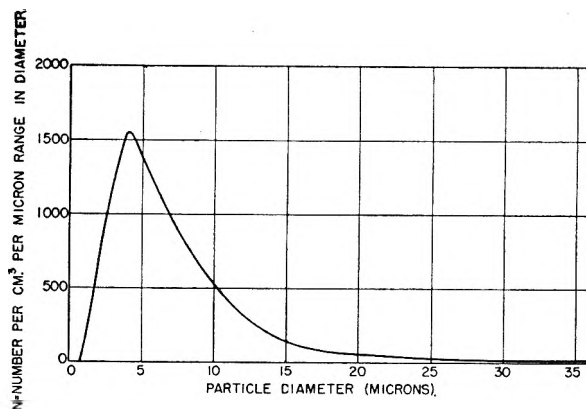


Fig. 2.—Size-frequency distribution curve for kerosene sprayed at 700 p.s.i.

D. P. GRAHAM.—How many values of partial wave values are required?

2nd Question (in answer to D. P. Graham). Values of α of 400 required about 420 terms in the Mie theory series summations.

D. P. GRAHAM.—Did you do anything at all with absorbing substances?

R. Q. GUMPRECHT.—Not at this time.

R. B. DEAN.—In your diffraction theory did you allow for the transmitted light which came through the center of your transparent droplets and was refracted by a small enough angle to be caught in your recording system?

R. O. GUMPRECHT.—Both the Mie theory and the diffraction theory predict that the ray of light scattered by a large particle at 180° (that is, in exactly the forward direction) has an intensity higher than that of any other scattered ray. The ray scattered at *exactly* 180° , however, carries zero energy and does not contribute to the calculated values of either K , or R since its dimensions are: intensity *per unit solid angle* for a beam of unit intensity per unit beam cross sectional area. In order to calculate the amount of light scattered in the forward direction, for the purpose of comparing it with the amount scattered in all other directions, it is necessary to integrate the scattered intensities over some finite solid angle. For example, both the Mie theory and the diffraction theory show that 40% of the beam attenuation produced by a particle whose α value equals 400 is due to light scattered in the forward direction within a cone whose half angle is four tenths of a degree.

ROLE OF SURFACE ACTIVE AGENTS IN WETTING¹

BY FREDERICK M. FOWKES

*Shell Development Company, Emeryville, California**Received July 22, 1952*

A mechanism for the wetting of cotton by aqueous solutions of wetting agents is proposed which allows prediction of sinking times of cotton yarn for a variety of wetting agents. The equations require data on the relation between concentration and surface tension of solutions of the wetting agent. Penetration of solutions of wetting agents into porous hydrophobic solids proceeds at a rate determined by the cosine of the contact angle ($\cos \theta$) of the advancing front on the cotton fibers. As the value of $\cos \theta$ is found to be a linear function of surface tension (γ') for a large variety of surface active agents, values of γ' may be identified with values of $\cos \theta$. An equation derived on this basis ($\log t_s = A + B\gamma'$) can be used to predict sinking times in various wetting tests. Data obtained with Aerosol OT, Aerosol MA and Tergitol 4 illustrate this point. The value of γ' depends on the concentration of agent in the surface region of the solution. This concentration (c') becomes less than the bulk concentration (c) during penetration if the agent is heavily adsorbed on cotton. With solutions of Nonic 218 and Triton X-100, for example, $c - c'$ is often much larger than c ; thus diffusion becomes the main rate-determining factors in wetting with these materials. Values of the diffusion constant, D , appear to decrease from 4×10^{-6} cm.²/sec. in dilute solutions to 1.5×10^{-6} cm.²/sec. in concentrated solutions composed mainly of micelles. The relations of sinking time to diffusion and to surface tension may be used additively to predict rates of wetting for a wide variety of surface active agents.

The wetting of hydrophobic cotton yarn by aqueous solutions of surface active agents is used as an example of the general problem of penetration of liquids into porous phobic solids with the aim of demonstrating the rate-determining factors in such phenomena.

First, the relation of surface activity of wetting agents to rates of wetting was investigated. It is shown that the contact angle (θ) on cotton of aqueous solutions of wetting agents is the factor which determines rates of wetting, and that the rate of wetting is an exponential function of $\cos \theta$. For a given test, $\cos \theta$ alone determines the sinking time. Second, the effect of adsorption of wetting agents during penetration was studied. It is shown that if wetting agents are heavily depleted by adsorption onto the cotton during penetration, the replenishment of the advancing front by diffusion from the bulk of solution becomes the factor which determines rates of wetting. Because of this adsorption phenomenon, which was demonstrated by heavily adsorbed substances such as Triton X-100² and Nonic 218,² the relation of rates of wetting to contact angle was demonstrated with solutions of Aerosol OT,² Aerosol MA² and Tergitol 4,² in which adsorption and diffusion have negligible effect on rates of wetting.

Effects of Surface Activity on Rates of Wetting.

—The traditional approach to penetration of porous solids is to approximate the path of flow by a parallel bundle of smooth-walled capillaries. In such a system the rate of penetration is proportional to the adhesion tension, $\gamma \cos \theta$, where γ is the boundary tension of the advancing liquid and θ its contact angle on the capillary walls. However, in the case of cotton threads, the rate of penetration is not proportional to $\gamma \cos \theta$, nor is its direction parallel to the fibers.

(1) Presented before the twenty-sixth National Colloid Symposium which was held under the auspices of the Division of Colloid Chemistry of the American Chemical Society in Los Angeles, California, June 16-18, 1952.

(2) Aerosol OT, from American Cyanamid Company, is the sodium salt of di-2-ethylhexyl sulfosuccinate. Aerosol MA is the dihexyl derivative. Tergitol 4, from Carbide and Carbon Corp., is the sodium salt of a highly branched alkanol sulfate. Triton X-100, from Rohm and Haas, is a condensate of ethylene oxide with an octyl phenol; the polyether chain has about 9 units. Nonic 218, from Sharples Chemicals, is a condensate of ethylene oxide with a dodecyl mercaptan; this polyether chain also has about 9 units.

It is well-known that the logarithm of sinking time is a linear function of the logarithm of the concentration of wetting agent.³ It is now shown that the logarithm of sinking time is also a linear function of the cosine of the contact angle or of surface tension, and that this function is identical for many wetting agents. A theoretical basis for this relation is proposed in this section.

In this study rates of wetting were determined for gray unboiled cotton yarn as supplied for the Draves-Clarkson sinking test.³ These skeins were 54 inch loops of yarn weighing five grams apiece and containing 120 threads. In a cross section of each thread there were 100-200 cotton fibers. The yarn has a surface of natural waxes and oils which makes it hydrophobic. In this study the oils were rinsed out with benzene (at 25°). The hydrophobic nature of the waxy surface was demonstrated by the "capillary depression" of water; the top 14-20 cm. of skeins submerged vertically in water were not penetrated by distilled water. Calculations based on a model system of capillaries having the same wall perimeter per unit area of water-air interface (600-800 cm./cm.²—determined by measurement of photomicrographs of cross-sections of cotton thread) show that this "capillary depression" may be accounted for with a contact angle (θ) of water on this cotton of 107°. Because of this similarity of the surface of waxy cotton to other waxes it is proposed to use the contact angles (θ) of aqueous solutions on paraffin wax to represent the values of θ for solutions of wetting agents on cotton.

Rates of penetration of wetting solutions into cotton yarn can be measured with a variety of tests. Two of these were used in this study; the Draves-Clarkson sinking test with three-gram hook³ and the yarn bundle method.⁴ When this yarn was floated on top of water, as in the yarn-bundle test, the penetration was observed to occur from the sides of threads and yarn in a direction perpendicular to the length of the fibers (see Fig. 1). After entry the solution appeared to travel a short

(3) C. Z. Draves and R. G. Clarkson, *Am. Dyestuff Repr.*, **20**, 201 (1931). See also *Year Book of Am. Assoc. Textile Chemists and Colorists*.

(4) S. M. Edelstein and C. Z. Draves, *Am. Dyestuff Repr.*, **38**, 343 (1949).

distance through the threads parallel to the fibers. In slow wetting, penetration occurred at few points and solutions traveled parallel to the fibers for several millimeters. In rapid wetting, however, penetration occurred at many more points and parallel travel was negligible.

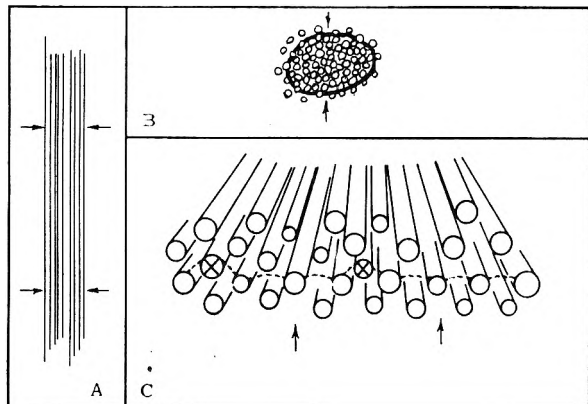


Fig. 1.—A, skeins are penetrated by water entering from all sides and in a direction perpendicular to the length of the skein; B, cross section of skein of yarn shows water entering from periphery and moving toward the center; C, within a thread evenly spaced hydrophobic fibers prevent movement of the water meniscus (dashed line), except where fibers marked x intersect the meniscus and permit it to advance.

The rate of wetting of waxy cotton cloth or yarn (as measured by the various wetting tests) depends on the rate of wetting of the individual threads. The following mechanism for the wetting of threads is visualized. In threads, the close and even spacing of hydrophobic fibers, on contact with the wetting solution, forms a series of highly curved menisci which prevents passage of water or wetting solutions.⁵ Indeed, wetting solutions can penetrate the fibers only at points where imperfections in spacing and alignment occur. In Fig. 1C penetration is shown to occur where fibers labeled X lie partly between adjacent fibers of a lower layer. Where these intersect the meniscus between fibers of the lower row, the meniscus moves forward along the length of the newly wet fiber, like a zipper, for some distance. At some other place where the solution is in contact with the thread another such intersection may occur and the meniscus again moves forward. Thus, in steps, the solution moves through the thread perpendicularly to the fibers, with a rate proportional to the frequency of such intersections.

The degree of imperfection may be expressed as shown in Fig. 2. Here fiber 3 lies above the water meniscus between fibers 1 and 2, and its distance from the meniscus is shown to be $d - r \cos \theta$, where d is the distance of fiber 3 from the plane of fibers 1 and 2, r is the radius of a fiber and θ the contact angle. When $d - r \cos \theta$ has a small enough value, such as d'' , penetration occurs.⁶ Only a small proportion of the values of $d - r \cos \theta$ are as small

(5) A. B. D. Cassie, *Disc. Faraday Soc.*, No. 3, 242 (1948); D. J. Crisp and W. H. Thorpe, *ibid.*, No. 3, 210 (1948).

(6) The value of d'' increases with curvature of the meniscus which is proportional to the hydrostatic pressure drop across the meniscus. As sinking times measure the slowest penetration in a test piece of cotton, the portion that is rate-determining will have little hydrostatic head and d'' will therefore be small.

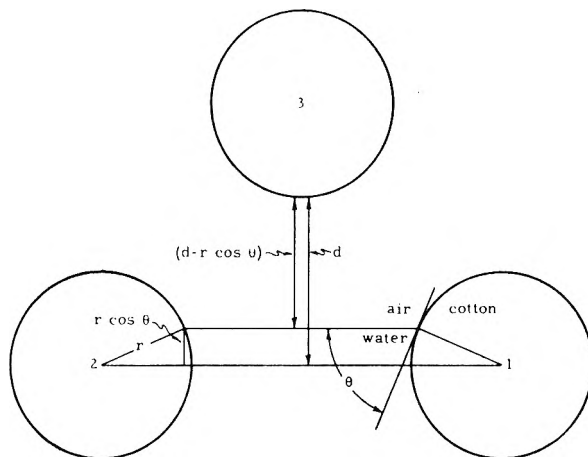


Fig. 2.—Cross section of three fibers in a thread showing how decrease of contact angle (θ) brings the water-air interface closer to fiber 3. The curvature of the meniscus is not shown because the radius of curvature of the meniscus (near the top of a skein) is large (on the order of 400μ) compared with the diameter of fibers ($10-20\mu$).

as d'' , so this proportion (y) may be represented by a distribution function such as

$$y = ae^{-(d' - r \cos \theta)/d''} \quad (1)$$

in which d' represents the average value of d . This shows that the proportion of cases where $d' - r \cos \theta$ equals or exceeds d'' increases as an exponential function of $\cos \theta$.

If the rate of wetting of threads is proportional⁷ to y , then the rate of wetting of cotton test pieces ($1/t_s$) is also proportional to y . Thus

$$1/t_s = a'e^{-(d' - r \cos \theta)/d''} \quad (2)$$

or

$$\log t_s = -\log a' + 2.303 d'/d'' - 2.303 (r/d'') \cos \theta \quad (3)$$

Here the sinking time (t_s) in a given test is determined by only the contact angle (θ). The test constant a' relates the sinking time to the number of threads which must be wetted consecutively before sinking of the skein occurs; when a' is large, sinking is rapid.

Equation (3) now relates wetting times to values of contact angle. It appears that contact angles of aqueous solutions on wax may be related to the surface tension. Figure 3 shows that the following relation holds reasonably well for five commercial wetting agents⁸

$$\cos \theta = 1.68 - 0.035\gamma \quad (4)$$

Thus equation (3) may be changed to relate sinking times to surface tension

$$\log t_s = A + B\gamma \quad (5)$$

in which the test constants are combined in A , and B is a constant, depending on relatively invariable quantities.

It should be emphasized that the values of sur-

(7) The proportionality constant a' depends on the number of threads to be wet consecutively before sinking occurs. It also depends on the driving force for penetration, which, though it includes a surface tension term, is relatively constant in the range under consideration.

(8) The constants in equation (4) are for wetting agents which adsorb to give a methyl or alkyl surface; other constants may be required for aromatic or fluorocarbon surfaces.

TABLE I

SINKING TIMES AND SURFACE PROPERTIES OF SOLUTIONS OF STANDARD WETTING AGENTS

Measurements at $25 \pm 1^\circ$; Draves-Clarkson tests with 3-g. hook; contact angles (θ) are one-minute values on paraffin wax; surface tensions, γ , are one-minute values by Wilhelmy method

Wetting agent	c , %	γ , dynes/cm.	θ , degrees	t_s (Draves), sec.	t_s (yarn bundle), sec.
Aerosol OT	0.01	45.3	81.5	29.0; 29.0; 27.0
	.02	41.2	75	10.2; 10.4; 10.2	52.2; 56.2; 55.0
	.03	38.7	71	5.9; 5.9; 5.9	24.7; 24.0; 24.6; 23.5
	.04	36.8	68	13.2; 15.0; 14.0; 15.0
	.06	34.5	61.5	6.5; 6.5; 6.5; 7.0
	.10	31.1	54	0	2.4; 2.8; 2.7; 2.4
Aerosol MA	.12	33.4; 33.0; 33.8
	.15	42.0	76.5	20.5; 20.4; 20.5
	.20	40.4	71.5	24.8; 30.1; 38.0; 38.2; 29.2
	.25	38.4	...	6.0; 5.9; 6.0	13.2; 15.5; 13.0; 19.2
	.3	36.9	67.5	3.8; 3.8; 3.8	8.3; 9.8; 6.2; 12.2; 8.4
	.5	32.8	56	2.2; 2.7; 2.5; 2.5
Tergitol 4	.05	41.6	78	17.0; 16.2; 15.0; 17.5; 18.2; 17.0; 18.3; 20.5; 17.0; 16.2; 15.2
	.075	38.9	74	8.6; 8.8; 8.1; 7.1; 7.1; 7.1; 8.2	20.6; 26.2; 22.0; 22.0; 25.0
	.1	37.3	71	3.3; 3.6	11.8; 12.0; 12.3; 9.8
	.12	36.1	68	6.5; 6.7; 7.2; 7.2; 5.7; 6.2; 6.5

face tension and contact angle used in this derivation represent the values at the front of the penetrating liquid and must therefore be determined so as to represent all of the surface active material in solution. With relatively homogeneous wetting

agents, surface tensions may be determined in the usual manner. For some mixtures, dynamic surface tensions may be required.

Surface tensions (γ) of solutions of wetting agents are known to be a linear function of the logarithm of the concentration (c), such as the following integrated form of the Gibbs adsorption equation

$$\gamma = C - \frac{2.303 RTZ \log c}{N\sigma}$$

where C is the intercept of γ at $\log c = 0$. Z is the number of particles per molecule in solution and σ is the surface area per adsorbed molecule. By using this expression for γ in equation (5), we obtain

$$\log t_s = A + BC - BD \log c \quad (6)$$

where BD , the slope of the straight line of the $\log t_s$ vs. $\log c$ relation, equals $2.303B RTZ/N\sigma$, and thus is a constant for any given wetting agent varying with σ/Z for different wetting agents. Equation (6) has been known as a useful empirical relation for years.³

Experimental evidence is offered in Table I and Fig. 4 to support the $\log t_s$ vs. γ relation of equation (5). These data are sinking times by the two sinking tests mentioned previously, and values of surface tension and contact angle for solutions of three well-known and homogeneous wetting agents, Aerosol OT, Aerosol MA and Tergitol 4.

Effects of Adsorption and Diffusion on Rates of Wetting.—The extent of adsorption of surface active agents on paraffin wax (used to simulate waxy cotton) was determined with Gibbs' adsorp-

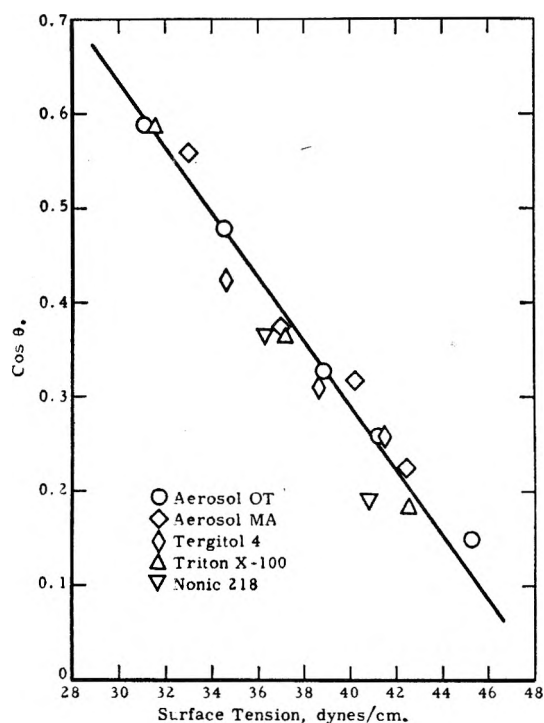


Fig. 3.—Contact angles of aqueous wetting solutions may be accurately estimated from surface tension data.

tion equation to give the area of cotton interface per adsorbed molecule (σ_1^9)

$$\sigma_1 = 2.303 (RTZ/N) \times d \log c/d (\gamma \cos \theta) \quad (7)$$

The values of σ_1 may be compared with values of areas per molecule in the surface of the solution, σ_s , computed from the more usual form of the Gibbs equation

$$\sigma_s = -2.303 (RTZ/N) \times d \log c/d \gamma \quad (8)$$

Values of σ_1 and σ_s are summarized in Table II, together with values of S_i , the interfacial area per adsorbed gram of agent.

TABLE II

AREA OF ADSORBED SURFACE ACTIVE AGENTS

Calculations by Equations (7) and (8). Basic data listed in Tables I and IV

Agent	M	Z	Area per molecule at surface, σ_s , \AA^2	Area per molecule at interface, σ_1 , \AA^2	Area per gram at interface, S_i , m^2
Nonic 218	562	1	61.5	53.2	570
Triton X-100	577	1	52.4	51.9	542
Aerosol OT	444	2	137	154	2090
Aerosol MA	388	2	103	118	1830
Tergitol 4	292	2	132	135	2790

The weight of surface active agent adsorbed on 5-g. skeins of cotton was then determined with rise of surface tension as a measure of depletion of wetting agent from solutions (see Table III). The surface area per gram of cotton, S_i , was computed from these measurements to be 3986 cm^2 . This is in agreement with the $3,100 \text{ cm}^2$ per gram estimated from microscopic examination of cotton fibers.

TABLE III

ADSORPTION OF SURFACE ACTIVE AGENTS ON COTTON AT 25° Gray, unboiled cotton 5-g. skeins, rinsed in benzene and dried. Surface tensions by Wilhelmy method.

Agent	Weight of soln., g.	Surface tension		Concentration, %		Gram adsorbed	Area of cotton, S_c , cm^2/g .
		Initial	Final	Initial	Final		
Nonic 218	100	31.5	32.5	0.02	0.017	0.0030	3420
	83	32.5	35.0	.017	.012	.0041	4730
	67	35.0	38.6	.012	.007	.0033	3820
Triton X-100	50	31.7	38.5	.012	.005	.0035	3980
	50	31.7	38.8	.012	.0049	.0035	3980
Average							3986

Triton X-100 and Nonic 218 are extracted from solution by adsorption on hydrophobic cotton to a much greater extent than the ionic wetting agents, as shown by the values of S_i in Table II; for this reason these may be expected to show a reduced rate of wetting. Table IV shows that indeed this is so. For example, in Fig. 4 it is seen that a Draves-Clarkson sinking time of 10 seconds requires a surface tension of 40–41 dynes/cm., yet with both Nonic 218 and Triton X-100, the concentration necessary to give the above rate of wetting is much more than that required to give a surface tension of 40–41 dynes/cm. The surface tension required by Fig. 4 for a given sinking time (t_s) may be represented by γ' , which is attained by concentration c' of a surface active agent. In Table IV values of c' and $c - c'$ are shown. Here

(9) F. M. Fowkes and W. D. Harkins, *J. Am. Chem. Soc.*, **62**, 3377 (1940).

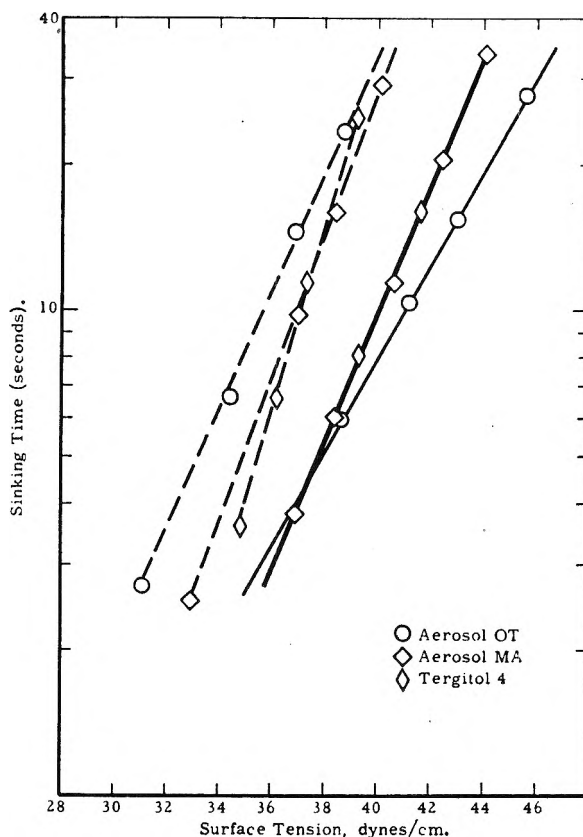


Fig. 4.—Rates of wetting as a function of surface tension: solid lines, Draves test (3-g. hook); dashed lines, yarn bundle test.

$c - c'$ shows the concentration required to provide fast enough diffusion to maintain γ' at the advancing front of the penetrating solution. It can be shown that surface transport is so fast that it is not a rate-determining factor in the Draves-Clarkson test.

If the advancing front of penetrating liquid is to maintain surface tension γ' , then the surface must be supplied with surface active molecules at a rate dm/dt (g./sec. cm^2) equal to the rate of depletion which is the product of dm/ds (grams of agent adsorbed on a cm^3 of test cotton) and ds/dt (the rate of penetration in $\text{cm}./\text{sec}.$)

$$dm/dt = dm/ds \times ds/dt \quad (9)$$

Now by Fick's first law of diffusion¹⁰

$$dm/dt = D \times dc/dx \quad (10)$$

where D is the diffusion constant and x the distance from the surface. dc/dx can be evaluated by Fick's second law and has been shown to be¹⁰

$$dc/dx = \frac{(c - c')e^{-x^2/4Dt}}{\sqrt{\pi Dt}} \quad (11)$$

At the surface $x = 0$, so this reduces to

$$dc/dx = (c - c')/\sqrt{\pi Dt} \quad (12)$$

Now dm/ds of equation (9) can be shown to be the surface area per gram of cotton, S_c , divided by the product of S_i (the area per gram of adsorbed

(10) A. L. Geddes, "Physical Methods of Organic Chemistry," Part I, A. Weissburger, Ed., 2nd ed., Interscience Publishers, Inc., New York, N. Y., 1949, pp. 554–561.

TABLE IV
WETTING RATES AND SURFACE PROPERTIES OF SOLUTIONS OF NONIC 218 AND TRITON X-100
All measurements at $25 \pm 1^\circ$. Values of γ' corresponding to values of t_s (below) were obtained from Fig. 4

Agent	c , %	γ , dynes/cm.	θ degrees	t_s (Draves), sec.	γ'	c'	$(c - c')$
Nonic 218	0.301	52.3	...				
	.303	44.5	...				
	.305	40.8	79				
	.306	39.7	...				
	.31	36.3	68.5				
					Av.		
	.32	31.0	...	25.8; 25.0; 26.8 (25.9)	43.1	0.0037	0.0163
	.33	28.7	40.5	16.0; 14.0; 14.9 (14.9)	41.2	.0048	.0232
	.34	27.8	...	10.4; 10.2; 9.6 (10.1)	40.1	.0057	.0343
	.35	27.9	40.0	7.5; 7.5; 7.5 (7.5)	39.3	.0064	.0436
.37	28.0	...	4.6; 4.6; 5.5 (4.9)	38.1	.0076	.0624	
.1	28.1	40.0	3.2; 3.2; 3.0 (3.2)	36.1	.01004	.090	
Triton X-100	.003	42.5	79.5				
	.006	37.1	69.0				
	.012	31.7	54.0				
	.03			19.0; 18.7; 19.3 (19.0)	42.7	0.0032	0.0268
	.04			13.2; 13.6; 13.8 (13.5)	41.1	.0037	.0363
	.07			7.2; 7.2; 7.3 (7.2)	39.0	.0047	.0653

agent at the water-wax interface) and v , the volume of interfiber space per gram of cotton

$$dm/ds = S_c/vS_i \quad (13)$$

Equations (12) and (13) may now be combined with (9) and integrated to give

$$c - c' = \frac{1}{2} \times \frac{S_c}{S_i} \times \left(\frac{\pi}{t_s}\right)^{1/2} \times \frac{1}{\sqrt{D} v/s} \quad (14)$$

where v/s is a test constant which is equal to the area of the water-air interface per gram of cotton.

With equation (14) and the data of Tables II-IV, values of $\sqrt{D}v/s$ may be calculated. These have been calculated for sinking times obtained by the Draves-Clarkson test with solutions of Nonic 218 and Triton X-100. Table V shows that $\sqrt{D}v/s$ is nearly constant for all tests, varying from 0.6 for dilute solutions to 0.4 for concentrated solutions. This variation is probably caused by the change of D when the critical concentration for micelle formation (CMC) is exceeded. Values of D may be estimated by use of the Stokes-Einstein equation

$$D = kT/6\pi r\eta \quad (15)$$

An average value of the molecular radius r for these molecules may be estimated to be 6.5 Å., and for "Hartley" micelles to be 25-30 Å., which gives $D = 4 \times 10^{-6}$ cm.²/sec. for the molecules and $D = 1 \times 10^{-6}$ cm.²/sec. for the micelles. The CMC as estimated from surface tension data, is 0.035% for Nonic 218 and 0.015% for Triton X-100. The 0.04% solution of Nonic 218 is nearly free of micelles so the molecular value of D (4×10^{-6} cm.²/sec.) may be used to calculate v/s from the known value of $\sqrt{D}v/s$. For this solution v/s , the average area of water surface per gram of cotton, is then 285 cm.²/g. This is a reasonable value, since the simplest geometrical surface of the outside of a gram of cotton skein is about 80 cm.². Table V shows values of D calculated for $v/s = 285$ cm.²/g., which decrease from 4×10^{-6} cm.²/sec. for solutions at the CMC to 1.5×10^{-6} cm.²/

sec. for solutions composed almost entirely of micelles.

TABLE V

DIFFUSION CONSTANTS CALCULATED WITH EQUATION (14)
 $S_c = 3986$ cm.²/g.; D calculated for $v/s = 285$ cm.²/g.

Agent	c , %	$c - c'$, %	S_i , m. ² / g.	t_s (Draves- Clarkson, sec.)	\sqrt{D} \times v/s	D , cm. ² / sec. \times 10^{-6}
Nonic 218	0.040	0.0343	570	10	0.57	4.0
	.070	.0610	570	4.9	.46	2.6
	.100	.090	570	3	.40	2.0
Triton X-100	.03	.0268	542	19.0	.53	3.4
	.04	.0363	542	13.5	.47	2.7
	.07	.0653	542	7.2	.35	1.5

These calculations show that diffusion is a rate-determining step in wetting when adsorption is heavy, and that diffusion can account quantitatively for the concentration of wetting agent needed to give a desired sinking time. Further, equation (14) may be used to calculate $(c - c')_t$ for other wetting agents, using $\sqrt{D} \times v/s = 0.6$ for concentrations below the CMC , 0.5 at concentrations twice the CMC , etc.

The yarn bundle sinking test also demonstrates diffusion as a rate-determining factor. In Fig. 5 sinking times are shown for solutions of Nonic 218 in beakers of three different diameters. In this test the sinking cotton scavenges the surface film from the whole beaker; dust particles on the surface of the solution can be seen to travel rapidly toward the sinking cotton while it is sinking. This film is replenished by diffusion of agent into the entire surface of the solution. Consequently, surface films are supplied to the sinking cotton at a more rapid rate in beakers of larger diameter, and sinking times are shorter, as shown in Fig. 5. The values of v/s are much larger than in the Draves-Clarkson sinking test, but only with the smallest beakers (4 cm. in diameter) were values of D comparable with those of Table V. Values of D for the largest beakers were

about 4×10^{-7} cm.²/sec. The discrepancy is caused by surface transport becoming a rate-determining step in this type of test. As shown by Crisp,¹¹ surface films are transported at about 30 cm./sec. under unit surface tension gradient. Though this rate exceeds by far the rate of transport required in the Draves-Clarkson sinking test, it becomes an important rate-determining step in surface sinking tests with heavily adsorbed agents, especially when the surface area of the solution is large and the sinking rapid. This is probably the reason for the slower than normal sinking observed with Aerosol OT in the yarn bundle test (Fig. 4).

It should be noted that in the systems where diffusion is the main rate-determining step in wetting, increase of temperature should result in more rapid sinking, for diffusion rates generally increase with temperature.

Conclusions.—It has been shown that the rate of wetting of cotton in the Draves-Clarkson sinking test or similar immersion tests is a function of only the contact angle of the solution on wax, and of the extent of adsorption. Equations (5) and (14) relate these factors so that with only a knowledge of the relation of surface tension to concentration for a given wetting agent one can calculate the sinking times as a function of concentration. Furthermore, since the relation of surface tension to concentration of wetting agents is known to be predictable from molecular structure (by consideration of critical concentrations for micelle formation and areas per adsorbed molecule), these equations can be used to correlate wetting properties of surface active agents with their molecular structure.

Experimental Details

The surface active agents were used as supplied by the manufacturers. Distilled water was used for all solutions. All measurements were made at $25 \pm 1^\circ$. The cotton skeins, supplied by Hooker and Sanders, Inc., New York, were rinsed three times in fresh C.P. benzene and then air-dried before use. Only skeins weighing 4.9–5.1 g. were used.

Yarn bundle sinking tests were made with one inch clips of yarn weighing approximately 0.093 g. and containing 120 threads. These were placed on the surface of solution in a beaker with a diameter of 6.5 cm. (unless noted otherwise), and time to submerge measured.

Surface tensions were measured by the Wilhelmy method with a platinum plate 0.005 inch thick. Contact angles were measured on drops by means of a microscope with special goniometer eyepiece.

Molecular weights were supplied by manufacturers for the ionic wetting agents. Molecular weights of Nonic 218 and Triton X-100 were measured ebullioscopically in a tetrahydrofuran-water azeotrope.

Acknowledgments.—The measurements of sinking times, adsorption, surface tension and contact angles were made by Miss Helen Robbins. The molecular weight measurements were done by

(11) D. J. Crisp, *Trans. Faraday Soc.*, **42**, 619 (1946).

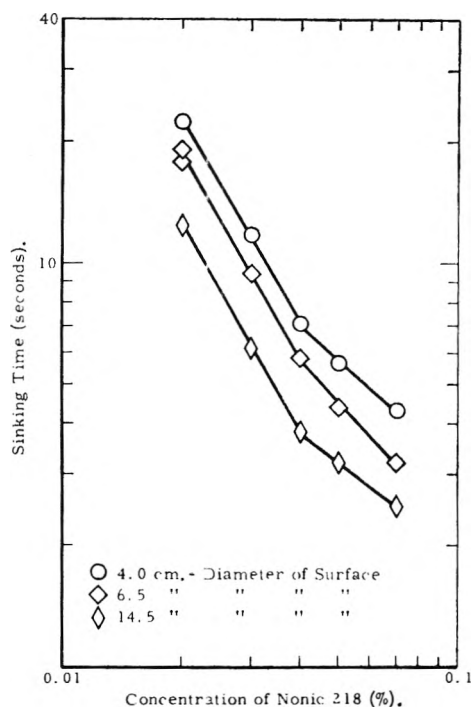


Fig. 5.—In the yarn bundle sinking test Nonic 218 wets more rapidly in beakers of larger surface area.

Shell Development Analytical Department, using a method devised by R. U. Bonnar.

DISCUSSION

ANON.—I have the problem of wetting powders with alcohol. What agents would increase the rate of penetration of alcohol into these powders?

F. M. FOWKES.—I don't know. It seems to me that alcohol by itself would wet and penetrate rapidly into a variety of powdered materials, such as the oily (or hydrophobic) and the hydrophilic materials. Extremely phobic powders (such as Teflon) may require special wetting agents, however.

IRVING REICH.—It seems to me, that in the course of the development here you assumed that the total surface area of the cotton was wet by the aqueous solutions. Actually sinking occurs before all the surface is wet.

F. M. FOWKES.—The Cotton hydrometer method of observing sinking, such as described by Grunfest *et al.*, (*Am. Dyestuff Repr.*, **36**, 225 (1947)), can be used to show that about 90% of the sample is wetted when sinking occurs in the Draves-Clarkson test with 3-g. hook. The dry part of the skein, at sinking, is presumed to be a central tapered core. When the solution has penetrated to this core, sinking occurs. If 6-g. weight were used the dry core would be longer and sinking would occur with less penetration. In the derivation one treats penetration at a level in the yarn where the penetration is representative of the whole skein.

IRVING REICH.—The actual per cent. of surface wetted at sinking time would depend on the weight of the hook used.

F. M. FOWKES.—The weight of the hook was 3 g.

A NEW METHOD OF MEASURING DIFFUSION COEFFICIENTS^{1,2}

BY KAROL J. MYSELS AND D. STIGTER

*Contribution from the Department of Chemistry, University of Southern California, Los Angeles 7, California**Received July 22, 1952*

The new method uses fritted glass to immobilize the liquid in which diffusion occurs, but differs from the conventional fritted glass diaphragm method in that the whole liquid is immobilized. The need for stirring any part of the liquid is thus obviated. The method is particularly adapted for tracer work and is being used to determine the self-diffusion coefficient of micelles of association colloids tagged by solubilized dyes.

While many excellent methods of measuring diffusion coefficients are available, there does not seem to be any adapted for precise measurements in macromolecular tracer systems. The need for such a method became apparent in the determination of self-diffusion coefficients of micelles using solubilized water-insoluble dyes for tagging the micelle, as has been suggested earlier.³

The presence of tracers produces no density gradients, hence common methods using wide channels cannot be used because unavoidable convection currents would cause excessive errors. Immobilization of the liquid in small capillaries seems necessary despite the accompanying danger of surface diffusion. The conventional porous diaphragm method depends critically on maintaining uniformity of concentration in the two compartments (which has been shown recently to require vigorous stirring^{4,5}) and on the complete immobilization of the solution in the diaphragm. A sharp and permanent boundary must exist between these regions. If stirring leads to any mechanical "pumping" of the solution through the diaphragm, it may cause large methodical errors when applied to slowly diffusing macromolecular systems even though it is harmless for rapidly diffusing simple ions.

The new method immobilizes the *whole* solution in two relatively thick (1-2 cm.) fritted glass discs. Thus any need for stirring is obviated. At the beginning, one disc (*i.e.*, its pores) is filled with solution containing tracer and the other with tracerless solution. The discs are clamped together and submerged in mercury to prevent evaporation while diffusion proceeds. They are then separated and the amount of tracer in each disc determined.

The diffusion coefficient is computed from the measured transport by comparison with the behavior of a substance of known diffusion coefficient, D . In our case sodium chloride diffusing between 0.2 and 0.7 N concentrations was chosen, as it has

an unusually small variation⁶ of diffusion coefficient with concentration.

Calculations

The ratio R of transport across the plane of separation of the discs at a time t to the transport at equilibrium is a dimensionless quantity which can be readily shown² to depend only on t and the diffusion coefficient D for any given system, provided D is independent of concentration and the concentrations are originally uniform on each side of the plane. In particular, R is independent of the original concentrations and of the direction of diffusion. These relations are true for discs of any arbitrary shape.

If the same R is obtained at times t_1 and t_2 for two substances, then

$$t_1 D_1 = t_2 D_2$$

This relation is used to calculate the unknown diffusion coefficient. Since D_1 for the calibrating substance and t_2 for the unknown are both known, it requires only the knowledge of the time t_1 required by sodium chloride to reach the same R . This is interpolated from several calibrating experiments on a plot of R vs. $\sqrt{t_1}$. This plot is linear up to about $R = 0.6$ and then gently curves to reach $R = 1$ at infinity.

One can determine experimentally the volumes V_u and V_l of the two discs, the concentration C_0 of the solution placed in the lower disc (assume that in the upper = 0) and the amounts A_u and A_l found in the two discs by analysis at the end of the experiment. One may then calculate the transport at infinity, as $T_\infty = C_0 V_l V_u / (V_l + V_u)$ and an average transport $T = (A_u/2) + (C_0 V_l - A_l)/2$. Of course R is T/T_∞ .

If R is thus computed it is very insensitive to small errors in the position of the original boundary. Thus if the boundary is formed at a small volume Δ below the surface of the lower disc (at which separation occurs), the concentration in this volume Δ will be substantially equal to $C_0/2$ within a very short time. It is then easy to show² that T and R are completely independent of Δ .

Experimental

The discs are cut from fritted glass cylinders of medium porosity (average pore diameter 14μ) $1'' \times 2''$ or $4''$ whose sides are glazed by fusion immediately after sintering.⁷ Alternate methods of closing the pores are fusion of the fritted cylinder into a glass tube, which is quite difficult and reduces the porosity near the walls, or imbedding the cylinder in lucite, which gives a less inert coating. Two discs are always cut immediately adjacent to each other and their

(1) Presented before the twenty-sixth National Colloid Symposium which was held under the auspices of the Division of Colloid Chemistry of the American Chemical Society in Los Angeles, California, June 16-18, 1952.

(2) This work has been conducted as part of Office of Naval Research Project No. NR 054-254. A much more detailed account is presented under the same title in mimeographed First Technical Report, ONR Project No. NR 054-254, available from the senior author, The Library of the University of Southern California, or the Library of Congress.

(3) R. B. Dean and J. B. Vinograd, *THIS JOURNAL*, **46**, 1091 (1942); H. W. Hoyer and K. J. Mysels, *ibid.*, **54**, 966 (1950).

(4) R. H. Stokes, *J. Am. Chem. Soc.*, **72**, 763 (1950).

(5) J. M. Nielsen, A. W. Adamson and J. W. Cobble, *ibid.*, **74**, 446 (1952).

(6) R. H. Stokes, *ibid.*, **72**, 2243 (1950).

(7) Supplied by the Corning Glass Works, Corning, New York.

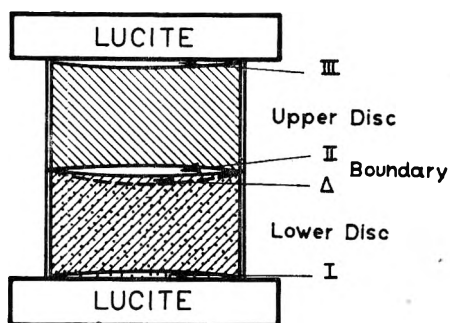


Fig. 1.—Schematic representation of the diffusion cell showing in an exaggerated manner the spaces I, II and III occupied by the free liquid and the formation of the boundary below the surface of the disc.

original relative position preserved so as to maintain closely matching surfaces. A height of about 13 mm. seems to be optimum. A greater height prolongs the measurement unduly; a lesser one reduces the amount available for analysis.

The cell is shown schematically in Fig. 1 and its assembly in a clamp in Fig. 2. The porous discs are mounted with Araldite 101 cement⁸ in lucite rings for ease of handling and aligning. The two porous discs are held between two lucite discs in the stainless steel clamp which ensures rigidity and reproducibility of alignment and allows immersion in mercury to prevent evaporation and leakage.

Filling of the porous discs with a solution (and its removal) is done by gradual displacement of a miscible liquid. When the porosity of the disc is uniform up to the impervious wall, slow flow under gravitational forces of 1.5 pore volumes is sufficient to replace over 99.9% of the original liquid. When the porosity is not uniform, as many as ten volumes may be necessary. We always use a 50–70% excess above the minimum required. This displacement is rather slow and careful protection from evaporation is necessary. Burets may be used to dispense NaCl solutions but syringes are used with detergent to avoid loss of dye to stopcock grease or elastomers.

Analysis.—Sodium chloride concentrations were determined by direct conductimetry after dilution to a known volume, using a Jones-Dike bridge,⁹ properly designed cells and Shedlovsky's¹⁰ equivalent conductivity values. The conductivity of the water used was always determined and subtracted. Dye contents were determined with 10-mm. cells in a Beckman UV spectrometer using a wide slit at the absorption maximum and correcting for any turbidity measured in the region of negligible absorption.

Volume Determination.—Because of unavoidable unevenness of the disc surface, there are spaces between the discs, as shown in Fig. 1. Each of them amounts to about 0.02 cc. The liquid in the middle space is always considered a part of the upper disc. The liquid in these free spaces is collected (with a pipet for NaCl solutions and small squares of cleansing tissues for detergent solutions) and added to that contained in the pores of the corresponding disc. The volumes of each disc are determined by filling both discs with the same solution, assembling, disassembling and determining the solute content of each. Using NaCl solutions the mean deviation is about 0.002 cc. for a volume of approximately 2 cc. Using solubilized dye the mean deviation is about 0.01 cc. due to the lower precision of colorimetric analysis and there is no significant difference between the volumes determined by the two methods.

Calibration.—Sodium chloride solutions 0.7 *N* in the lower and 0.2 *N* in the upper disc are used for calibration. This avoids the presence of very dilute solutions in which surface diffusion is significant,^{4,5} gives sufficient amounts of solute for precise analysis and utilizes the unusually broad minimum⁶ of the *D vs. concn.* curve for this salt. The value for 0.5 *N*, $D = 1.474 \times 10^{-5}$ cm.²/sec., is used in further computations. The values of time for various values of *R* are read from a graph of deviation from linearity with respect to \sqrt{t} .

(8) Supplied by CIBA, New York.

(9) P. H. Dike, *Rev. Sci. Instruments*, **2**, 379 (1931).

(10) T. Shedlovsky, *J. Am. Chem. Soc.*, **54**, 1405 (1932).

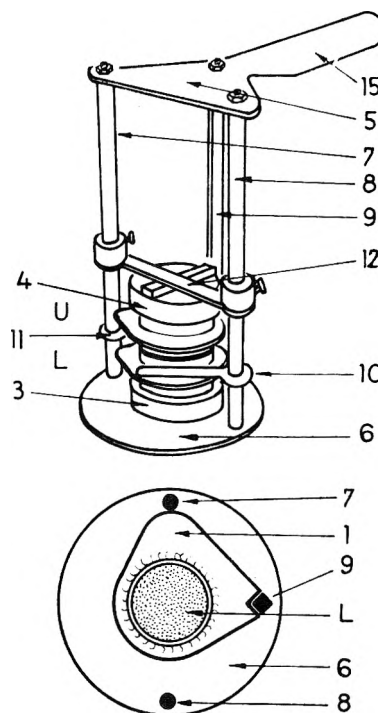


Fig. 2.—The diffusion cell is formed by porous discs U and L (each in a lucite ring) and is closed by lucite discs 3 and 4. It is held by springs 10, 11 and 12 in a clamp formed by plates 5 and 6 connected by rods 7, 8 and 9. Handle 15 serves to hold the cell under mercury.

The boundary between two different solutions is formed by filling the discs with the two solutions, clamping the lower one in position, drying the outside, submerging its lower edge in mercury and drying its upper surface. The upper porous disc, covered with the upper lucite disc and with a drop of the solution hanging from its lower surface, is lowered into position, the excess liquid squeezed out, and after closing the upper spring and drying the outside, the whole cell is submerged in mercury.

In this process there is a small amount of unavoidable mixing of the two solutions, and some of the liquid from the lower disc is pressed out, so that the boundary is effectively formed at a small volume Δ (Fig. 1) below the surface of the lower disc. The material balance shows that this volume amounts to about 0.01 cc. with an average deviation of about 0.005 cc.

As has been shown above, under Calculations, the value of Δ does not affect the average transport ratio *R*. That the initial mixing is of no significance may be seen from Table I, which compares results of short time diffusion experiments with values predicted on the basis of long time results. Significant mixing would lead to consistently higher experimental values and require a zero time correction, but this is not the case.

TABLE I

SHORT TIME DIFFUSION EXPERIMENTS				
0.7 <i>m</i> NaCl in lower disc; 0.2 <i>m</i> NaCl in upper disc				
Time, min.	Δ , cc.	Calcd.	Transport ratio, % Found	Difference
2.5	+0.004	2.1	1.9	-0.2
3	+ .012	2.3	2.6	+ .3
9	+ .040	6.0	5.8	-.2
5.0% Aerosol MA + Orange OT in lower disc; 5.0% Aerosol MA in upper disc				
128	+0.004	6.2	6.4	-0.2
164	.000	7.0	7.1	-.1

Density gradients which act to stabilize the boundary are present in calibration runs using NaCl. In tracer experiments there are in principle no density gradients and in

practice there may be even minute destabilizing ones. The method seems, however, to be completely insensitive to such inversions of density because in two runs in which sodium chloride solutions were used in inverted position (*i.e.*, 0.7 *N* in the upper and 0.2 *N* in the lower disc), the values of *R* deviated by -0.6% and +1.1% from the calibration line for 11 hr. and 17 hr. experiments, respectively. (Dr. R. J. Williams has found that discs of coarse porosity are no longer insensitive to such extreme inversions of density gradient but are still satisfactory for tracer work).

Temperature control is provided by an air-bath whose temperature varies by $\pm 0.05^\circ$ with a period of approximately 1 minute at $25 \pm 0.1^\circ$. The mercury cups are supported on rubber in an almost vibrationless way although strong vibrations seem to have no effect.

Accuracy and Precision.—The above results show that the method seems to eliminate most sources of methodical errors except that of adsorption and surface diffusion in the particular system studied. The presence of these effects is indicated by a discrepancy between volumes determined using tracer and using NaCl and may be ascertained by using discs of different porosities.

The precision depends on the value of *R*, showing a flat minimum near *R* = 0.65. The reproducibility of measurements with sodium chloride corresponds to about $\pm 0.5\%$ in the value of *D* and with dye solution it corresponds to the analytical error. Thus in 5% Aerosol MA, Orange OT in three different discs gave four results averaging 1.089×10^{-6} cm.²/sec. with a mean deviation of 1.2%, while oil blue (which is appreciably water-soluble) gave three results averaging 1.156×10^{-6} cm.²/sec. with a mean deviation of 1.1%.

DISCUSSION

S. C. LIANG.—Would the dye affect the diffusion of the micelles because of the amount of dye present in the micelle?

K. J. MYSELS.—That is a very good question. However, the amount of dye employed was on the average less than one dye molecule per micelle. Therefore such an effect would be very small. Furthermore the dye was so com-

pletely water-insoluble and very soluble in oil so that it should be located well inside the micelle. Also in electrophoretic measurements we used several different dyes to see if they gave the same results and found that they did. I do not think we are changing things very much but we plan to check this point by comparing different dyes in diffusion.

IRVING REICH.—I would like to just go a stage further on the question just asked. Obviously the molecule or two of dye locked within the micelle will not affect the speed of diffusion very much. But there is so much to be understood about the geometry and the energetics of the micelle. It may be a highly sensitive structure. Might it not be possible for the micelle to let's say, double in size because of the presence of even one molecule of the dye?

K. J. MYSELS.—If there was a large effect by one kind of dye, presumably different kinds of dyes would give very different results and we propose to consider this effect at a later time.

MALCOLM DOLE.—Could not dye molecules diffuse from one micelle to another micelle by some kind of chain effect? The solubility of the dye in the solvent, even if the dye is very insoluble, may make this kind of an effect possible.

K. J. MYSELS.—If the dye is completely insoluble in water, then in order for them to jump from one micelle to another, the micelles must be very close together, in fact the micelles must touch, which is very unlikely.

MALCOLM DOLE.—It is also unlikely that the dye is completely insoluble.

K. J. MYSELS.—The solubility of the dye in water is estimated at perhaps 1/10,000 of the solubility in the soap solution. Hence for 10,000 dye molecules which are entrapped inside the micelles there is only one which is in the water. Even if this one were diffusing ten times faster than the micelles it would introduce only an error of $1/10$ of 1%.

PREDICTION OF GAS-ADSORBENT EQUILIBRIA¹

BY F. D. MASLAN,² M. ALTMAN AND E. R. ABERTH

Department of Chemical Engineering, New York University, New York, N. Y.

Received July 22, 1952

It has been found that a modified Polanyi-Dubinin theory can be used to correlate the adsorption of various gases on activated carbon, silica gel and activated alumina with good accuracy both above and below the critical point. In this modification the adsorbate is considered as a highly compressed gas, and its volume and fugacity are calculated at the adsorption temperature. The method has been tested on nine systems and good checks with experimental results are obtained. Binary gas adsorption can be predicted from single gas adsorption data when $N_{12}V_{12} = N_1V_1 + N_2V_2$. This method has been tested on the system oxygen-nitrogen-activated carbon with success.

It is desirable to be able to predict gas adsorption equilibria from a minimum of experimental data. The Polanyi-Dubinin theory offers a route to this goal.

Single-Gas Adsorption.—The modification of the Polanyi-Dubinin adsorption theory proposed by Lewis and his co-workers³ is given by

$$\left[\frac{RT}{V'} \ln \frac{f_s}{f} \right]_I = \left[\frac{RT}{V'} \ln \frac{f_s}{f} \right]_{II} \quad (1)$$

when

$$N_I V'_I = N_{II} V'_{II} \quad (2)$$

where *f* = fugacity of the gas at adsorption pressure and temperature, *f_s* = fugacity of saturated liquid at adsorption temperature, *N* = moles adsorbed per unit weight adsorbent, *R* = gas law constant, *T* = adsorption temperature, degrees absolute, and *V'* = molal volume of saturated liquid at a vapor pressure equal to adsorption pressure. The subscripts I and II refer to different sets of adsorption conditions. In the above relationships the adsorbate is assumed to be a saturated liquid. Lewis, *et al.*, found that good correlation could be obtained using the above equations and definitions below the critical point. Data for many hydrocarbons correlated well. Branching of the generalized correlation curves, NV' vs. $(RT/V') \ln f_s/f$, were obtained for saturated and unsaturated hydrocarbons.

Whereas the substitution of fugacities for pres-

(1) Presented before the twenty-sixth National Colloid Symposium which was held under the auspices of the Division of Colloid Chemistry of the American Chemical Society in Los Angeles, California, June 16-18, 1952.

(2) National Research Corp., Cambridge, Mass.

(3) W. K. Lewis, E. R. Gilliland, B. Chertow and W. P. Cadogan, *Ind. Eng. Chem.*, **42**, 1326 (1950)

tures in the original Polanyi theory is theoretically sound to account for the non-ideality of the gases, no justification can be found on theoretical grounds for assuming that the molal volume of the adsorbate is equal to the saturated liquid volume at a temperature where the vapor pressure equals the adsorption pressure. While this correlation is useful below the critical points of the gases and has been successful in this region, extrapolation above the critical point has been found to be impractical and the method breaks down.³ The difficulty in determining a liquid volume above the critical point is obvious.

However, many adsorption temperatures are above the critical temperature of the adsorbed gas. In order that a generalized correlation may hold over the entire temperature range for a particular gas, a consistent set of assumptions is needed to provide a unique relationship between the pressure and volume of the adsorbed gas at any one temperature. If one considers the adsorbate as a highly compressed gas and that the gas has the same escaping tendency from the surface of the adsorbent as from a saturated liquid-vapor interface, then it is possible to respecify the volume (V) and fugacity (f_s) for equation 1. In order to calculate this fugacity, the pressure of the adsorbed gas must be obtained. This is done by plotting the vapor pressure curve for the liquefied adsorbate and extrapolating it to the desired adsorption temperature. If the temperature is below the critical temperature of the gas, then the adsorbate pressure is identical with the vapor pressure, and the fugacity is the same as defined by Lewis, *et al.* If the temperature is above the critical temperature of the gas, the extrapolation appears justified on the basis of experimental data discussed by Brunauer.⁴ He reports results that show that no discontinuity occurs in the adsorbed phase on passing the critical temperature.

Once the pressure of the adsorbate is known, the molal volume of the compressed gas (V) may be calculated from an equation of state or from a compressibility chart. The fugacity (f_s) may be obtained by familiar thermodynamic equations or from a fugacity coefficient chart.

Using the method outlined above, adsorption data for the two systems oxygen-activated carbon and nitrogen-activated carbon,⁵ are plotted in Fig. 1. It was found that the experimental data could be correlated over the full temperature range of 0 to -150° with an average deviation of 3%. This temperature range covers the region from below the critical points of the gases to a region considerably above them and hence can be regarded as a rather critical test of the assumptions. The points for both of the gases show a smooth transition as the curve crosses the respective critical temperatures. This helps justify the assumption made in the extrapolation of the vapor pressure curve above the critical point.

The fact that the two gases can be correlated by a single curve indicates that their adsorption

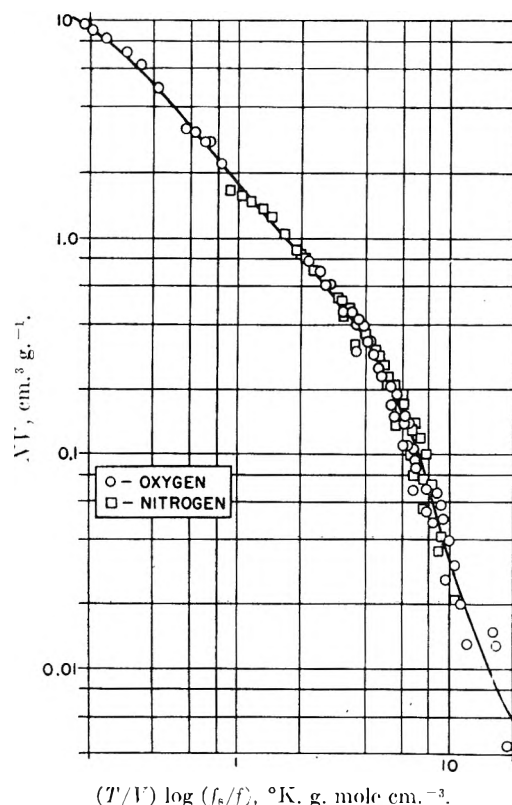


Fig. 1.—Adsorption potential diagram for oxygen-activated carbon and nitrogen-activated carbon over the temperature range 0 to -150° .

characteristics on activated carbon are very similar.

The method was tested again successfully by plotting adsorption data for oxygen and nitrogen on activated alumina and silica gel as shown in Figs. 2 and 3, respectively.⁵ The data for activated alumina (Fig. 2) cover a temperature region of -150 to -175° . It can be seen that the data for both of the gases give smooth curves and small deviations. In this case the oxygen and nitrogen curves do not coincide. This might be accounted for by a difference in adsorption characteristics on activated alumina.

The data for silica gel in Fig. 3 cover the temperature range -130 to -150° . This is part of the same region covered in Fig. 1. However, it will be noted that the silica gel figure has a separate curve for oxygen and for nitrogen, while one curve correlates the data on activated carbon. No explanation for this behavior can be offered at present other than to assume that the difference is caused by different adsorption characteristics on the silica gel than on the activated carbon.

As a further test of this method, data for adsorption of hydrogen on activated carbon⁶ are successfully correlated with a deviation of less than 2% in Fig. 4. These data cover the temperature region 55 to 69°K . The thermodynamic data, the vapor pressure and the PVT data for hydrogen were obtained from a recent National Bureau of Standards publication.⁷ The curve for the hydrogen-acti-

(4) S. Brunauer, "Adsorption of Gases and Vapors," Vol. 1, Princeton University Press, Princeton, N. J., 1945.

(5) M. Altman, D.Sc. Thesis, New York University, University Heights, New York, 1952.

(6) W. V. Dingenin and A. V. Itterbeck, *Physica*, **6**, 49 (1939).

(7) H. W. Woolley, "Natl. Bur. Stds., Research Paper RP 1932," Vol. 41, 1948.

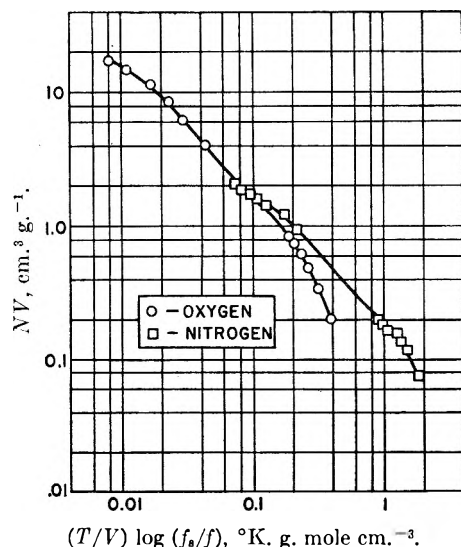


Fig. 2.—Adsorption potential diagram for oxygen-activated alumina and nitrogen-activated alumina over the temperature range -150 to -175° .

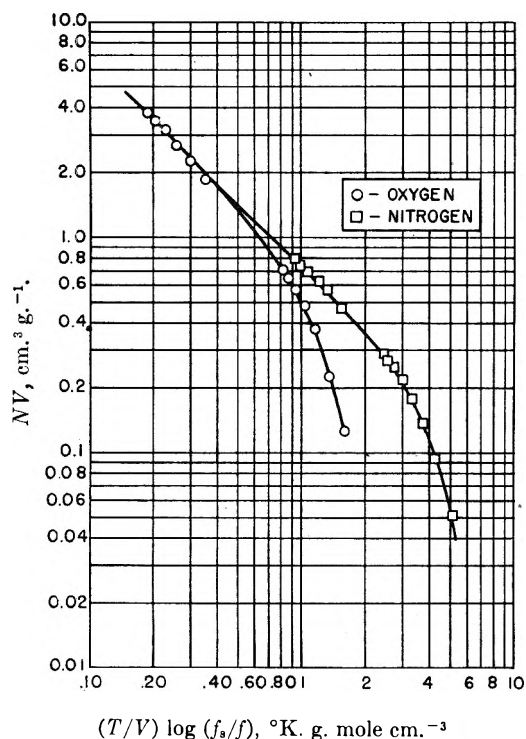


Fig. 3.—Adsorption potential diagram for oxygen-silica gel and nitrogen-silica gel over the temperature range -130 to -150° .

vated carbon system cannot be directly compared with that of Fig. 1 because the carbon was different.

The excellent results obtained with these seven systems, especially above the critical points, appear to justify this correlation method. It is hoped that in the future data on other gases will be available for further testing.

Data on the adsorption of propane and propylene on activated carbon⁸ at temperatures of 0 to -30° did not correlate well by use of this method. Since

(8) E. R. Aberth, M.Ch.E. Thesis, New York University, University Heights, New York, 1952.

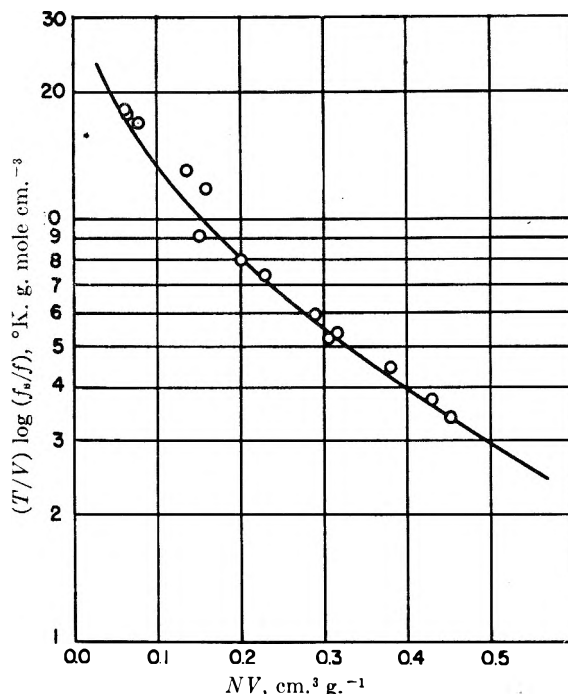


Fig. 4.—Adsorption potential diagram for hydrogen-activated carbon over the temperature range 55 to 69° K.

these data were at temperatures about 120° below the respective critical points and near the normal boiling points, it is believed that the assumption of a compressed gas is no longer justified as most of the adsorbate is undoubtedly present as liquid. This probably can account for the breakdown of the correlation method in these cases.

Binary Gas Adsorption.—The method used above for single gas adsorption can be extended to multi-component adsorption. In the following discussion the case of binary gas adsorption will be considered.

The adsorption potential theory states that the work required to bring a gas from the gas phase into the adsorbed phase is equal to its free energy change. Extending this to binaries, if two gases are adsorbed at the same time, the total work is equal to the sum of the work done on each gas, provided there is no energy change on mixing. Hence

$$[NRT \ln f_s/f]_{12} = [NRT \ln f_s/f]_1 + [NRT \ln f_s/f]_2 \quad (3)$$

where the subscript 12 represents the binary gas mixture and subscripts 1 and 2 represent the pure components. The other quantities in equation 3 are as defined previously.

Applying the law of additive volumes to the adsorbate, the assumption is made that the total volume of the adsorbed gas is equal to the sum of the volumes of the individual components of the gas mixture

$$N_{12}V_{12} = N_1V_1 + N_2V_2 \quad (4)$$

In order for the final relationship to be specific and give only a single result, the adsorption potential corresponding to the left side of equation 3 must be constant for a certain value of $N_{12}V_{12}$, no matter what are the values of N_1V_1 and N_2V_2 .

Dividing equation 3 by $N_{12}V_{12}$ and cancelling R gives

$$T/V_{12} \ln (f_{s12}/f_{12}) = T/V_{12} [\ln (f_{s1}/f_1)^{n_1} + \ln (f_{s2}/f_2)^{n_2}] \quad (5)$$

where

$$n_1 = N_1/N_{12} \text{ and } n_2 = N_2/N_{12}$$

Since

$$N_{12} = N_1 + N_2 \quad (6)$$

$$n_2 = 1 - n_1 \quad (7)$$

Rearranging equation 5 and taking the antilogarithm gives

$$f_1^{n_1} f_2^{1-n_1} = f_{s1}^{n_1} f_{s2}^{1-n_1} / f_{s12} / f_{12} \quad (8)$$

Equation 8 is a general relationship between the pure gas and binary gas fugacities. For a given amount of adsorbate of a certain composition, the denominator of the right side of the equation may be found from a generalized adsorption potential curve at ordinate $N_{12}V_{12}$. The two fugacities in the numerator are calculated as described previously for pure gases. This leaves the gas composition in equilibrium with the adsorbate, as represented by the left side of the equation, unknown. The solution for the two gas fugacities f_1 and f_2 can be handled by trial and error or at low pressures by the following method.

At low pressures the fugacity can be taken as being equal to the partial pressure of the gas with only a slight error. If the total pressure is one atmosphere, then

$$f_1 + f_2 = 1 \quad (9)$$

and

$$f_2 = 1 - f_1$$

Therefore equation 8 may be written for one atmosphere as

$$f_1^{n_1} (1 - f_1)^{1-n_1} = f_{s1}^{n_1} f_{s2}^{1-n_1} / f_{s12} / f_{12} \quad (10)$$

In this equation all values are known for a specified adsorbate amount and composition except f_1 . Once the correct value of f_1 is obtained, the gas phase composition can be readily calculated.

The gas-adsorbent equilibrium is then completely established.

Equation 10 was tested on the system oxygen-nitrogen-activated carbon for which experimentally determined values of relative volatilities are available.⁶ The results are given in Table I. The calculated results compare quite closely with the experimental ones. Even though the temperatures range from below to above the critical points, the average deviation is only 10% and the maximum is 19%. This system is a good one for such a test as the relative volatilities are small and the adsorption characteristics of oxygen and nitrogen are similar. Since the prediction method gives good results on this system, a similar or better accuracy might be expected with other systems having larger relative volatilities.

Lewis and co-workers⁹ used an equation derived by Broughton for the prediction of binary equilibria from single component data with only fair results. This equation was tested also on the oxygen-nitrogen-activated carbon system and results are given in Table I. They are about the same as those from equation 10 except for the -150° case. This is considerably in error.

TABLE I

COMPARISON OF EXPERIMENTAL AND CALCULATED RELATIVE VOLATILITIES FOR OXYGEN-NITROGEN-ACTIVATED CARBON SYSTEM

Temp., °C.	Relative volatilities		
	Exptl.	Eq. 10	Lewis, <i>et al.</i> , ec.
-150	1.7	2.1	2.9
-130	1.5	1.3	1.3
-110	1.3	1.2	1.3

The explanation for this large deviation is that integration of the Broughton equation requires extrapolation of the pure isotherm data to very low pressures which can introduce errors. These errors become larger as more gas is adsorbed, and in these results the largest deviation occurred at -150° where the largest amount of gas is adsorbed.

(9) W. K. Lewis, E. R. Gilliland, B. Chertow and W. P. Cadogan, *Ind. Eng. Chem.*, **42**, 1319 (1950).

MACROMOLECULAR PROPERTIES OF POLYVINYLPIRROLIDONE: MOLECULAR WEIGHT DISTRIBUTION

BY L. E. MILLER¹ AND F. A. HAMM²

General Aniline & Film Corporation, Central Research Laboratory, Easton, Pennsylvania

Received July 15, 1952

This paper discusses the application of the well known Svedberg equation to polyvinylpyrrolidone, a synthetic high polymer. The dependence of sedimentation constant on concentration and molecular weight is described. The configuration of the molecule in solution in terms of axial ratios and root mean square distance between the ends of the randomly kinked chain is discussed; viscosity and translational diffusion data were used. From the empirical relation between sedimentation constant and molecular weight, several equations are derived for defining different type average molecular weights. Special emphasis was placed on the quantitative analyses for polydispersity. Four methods are compared. It is demonstrated that the best method for describing the molecular heterogeneity is based on a recent procedure in which the number distribution of sedimentation constants, $g(s)$ versus s , is determined from ultracentrifugal velocity diagrams. The limitations on the attempt to plot "true" molecular weight distributions ($g(s)$ vs. M) are discussed; an approach to such a distribution is outlined.

Introduction

The synthetic high polymer, polyvinylpyrrolidone, has recently acquired a national interest as a blood plasma extender. Its preparation, properties and applications in the blood field and in other branches of medicine have been summarized in book form.³ This polymer in 3.5% aqueous solution containing physiological inorganic salts has been known in Germany as "Periston." The medical profession in Germany, both military and civilian, has used this material as a blood plasma extender since about 1940. It was the primary purpose of this investigation to determine the molecular weights of a representative number of samples, with special emphasis on their molecular weight distributions. This latter aspect is important because of the extended clinical evaluations being conducted here as well as abroad. Throughout the remaining text this polymer will be referred to as PVP.⁴

The macromolecular properties of PVP have been studied by means of sedimentation velocity, diffusion and viscosity techniques and compared with the results of earlier workers. Although an extended viscosity program⁵ has been carried out in this Laboratory, only a brief consideration, sufficient to corroborate the other discussions, is given herein.

A critical evaluation of the existing methods for polydispersity analysis by means of the sedimentation velocity and diffusion diagrams and the results obtained by applying each of these techniques to the same experimental data is presented and compared.

Experimental

Samples.—The polymer PVP is a hygroscopic white solid. The amount of water retained by the "dry" material is a function of the relative humidity; it may be as high as 15%. Although the experimentation was not limited to the samples

listed in Table I, only those which are pertinent to the discussions have been included. The samples represent both large and small scale experimental preparations.

TABLE I

Samples	Description	Fikentscher K
I	Unfract. material	33
II	First fraction of I	38
III	Second fraction of I	37
IV	Fifth fraction of I	29
V	Unfract. material	29
VI	First fraction of V	21
VII	Unfract. material	29
VIII	Unfract. high mol. wt.	71
IX	Unfract. very high mol. wt.	109

Samples II, III and IV are the precipitates which result from an incremental addition of diethyl ether to a 20% (initial concentration) solution of sample I in methanol. Subsequent work in this Laboratory,⁶ as well as theoretical considerations by Flory⁶ and Scott,⁷ have established that less polydispersed fractions can be obtained by precipitation from more dilute solutions. (The solute concentration at first signs of precipitation is about one third of the initial value.) Sample VI represents a different type of fractionation procedure. An acetone slurry was made of sample V; it was stirred for four hours, and then the mixture was allowed to layer overnight. The clear supernatant acetone layer contained the soluble lower molecular weight portions. The acetone was removed using a steam-bath and vacuum. The residue after dissolution in water was spray dried. This sample of PVP is represented by number VI. The Fikentscher⁸ K-values given in Table I were determined from the relative viscosity of 1% aqueous solutions. These values are often used as a qualitative indication of the weight average molecular weight.

Diffusiometry.—The translational diffusion coefficients (D) reported in this work were determined in a Klett⁹ electrophoresis apparatus using a Tiselius type 11 cc. analytical cell. The boundaries were recorded by means of the Longworth scanning technique. A plot of $1/H^2_{max}$ vs. time for each experiment yielded a straight line which intercepted the time axis between minus 3000–5000 seconds. According to Longworth,¹⁰ the straight line relationship is a criterion that the diffusion across the boundary interface was not significantly disturbed. The boundaries were made by positioning the cell components in the conventional way. It was not necessary to sharpen the boundaries by capillary withdrawal of the solvent even for the more dilute solutions. The zero times recorded were of the same order of magnitude as others quoted in the literature.¹¹ Although the apparent

(1) Bell Telephone Laboratories, Inc., Allentown Laboratory, 555 Union Boulevard, Allentown, Penn.

(2) Burroughs Adding Machine Company, Research Activity, 511 No. Broad St., Philadelphia, Penna.

(3) "PVP Polyvinylpyrrolidone," Compiled and Published by General Aniline & Film Corporation, Development Department, 230 Park Avenue, New York, N. Y., March, 1951.

(4) Sterile solutions of polyvinylpyrrolidone for physiological use are marketed by the General Aniline & Film Corporation under the trade name "Plasdone."

(5) S. Siggia and G. G. Stoner, this Laboratory; unpublished works.

(6) P. J. Flory, *J. Chem. Phys.*, **12**, 425 (1944).

(7) R. L. Scott, *ibid.*, **12**, 178 (1945).

(8) H. Fikentscher, *Cellulosechemie*, **13**, 60 (1932).

(9) Klett-Tiselius Electrophoresis Apparatus, Klett Mfg. Co., 179 East 87th St., New York 28, N. Y.

(10) L. G. Longworth, *Ann. N. Y. Acad. Sci.*, **41**, 269 (1941).

(11) K. G. Stern, S. J. Singer and S. Davis, *J. Biol. Chem.*, **167**, 321 (1947).

time at which diffusion began was determined in the manner just described, an alternate scheme, first described by Lamm,¹² was used in the computation of the diffusion coefficients. The percentage mean deviation for the calculated diffusion coefficients within each experiment was usually not more than 5%.

As a check on the over-all validity of the experimental technique, the diffusion coefficient was determined for a pure substance for which the value is known to a high degree of precision. Eimer and Amend C.P. saccharose was chosen as the standard. A value of $D_{20} = 4.589 \times 10^{-6}$ cm.²/sec. was obtained for the diffusion coefficient of a 1.0011% aqueous solution. Gosting and Morris¹³ have reported a value of $D_{21.90} = 5.148 \times 10^{-6}$ cm.²/sec. determined by the Gouy interference technique. When corrected to 20° this value becomes 4.507×10^{-6} cm.²/sec. The reproduction of the diffusion coefficient of saccharose to within 1.8% of the value reported by Gosting and Morris suggests that the diffusion coefficients for PVP tabulated in Table III can be considered reliable.

It is significant to note that during the early stages of this work the authors found that the well known temperature correction

$$D_{20} = D_t \times \frac{T_{20}}{T} \times \frac{\eta_t}{\eta_{20}} \quad (1)$$

gave spurious results when applied to PVP. The diffusion coefficient for sample I determined at 5.0° was $D_{5.0} = 5.41 \times 10^{-7}$ cm.²/sec. which, when corrected to 20.0° by means of equation 1, becomes $D_{20} = 8.62 \times 10^{-7}$. The diffusion coefficient of sample I was also determined at 21.4°. The value of $D_{21.40} = 4.16 \times 10^{-7}$ cm.²/sec. was obtained. This becomes 3.90×10^{-7} cm.²/sec. when corrected to 20.0° by means of equation 1. These results imply that changes in the shape of the molecule with temperature require that another term be introduced in the formula for temperature correction. Although the exact form of the term to be added is not known at this time because only two experimental points have been determined, the assumption of a straight line relationship makes it possible to determine an approximate value of $D_{20.00}$ by interpolation. The interpolation is justified in this case because of the relatively short temperature range over which the interpolation takes place (21.4–20.0°). The approximate value of $D_{20.0}$ determined by this interpolation was 4.81×10^{-7} cm.²/sec. This value was used as the diffusion coefficient for sample I in all subsequent calculations. Care was taken during the remainder of this work to carry out all the experiments as closely as possible at the same temperature (20°).

The comparatively high diffusion coefficient determined at 5° is an indication that the polymer molecule is more tightly coiled at the lower temperature, thus more closely approaching the simple spherical behavior. Any tendency for a dependence of diffusion coefficient on concentration would be enhanced at higher temperatures. On the basis of this observation the deviation from Newtonian flow reported in the viscosity section of this paper might be predicted. In this regard it is advisable when large differences in diffusion coefficient or sedimentation constant are obtained to examine carefully the experimental conditions from which they were derived. Any suggestion of a dependence of frictional coefficient on temperature or polydispersity will automatically invalidate the use of equation 1 for temperature correction.

According to Singer,¹⁴ $f_s \cong f_D$ when the polymer molecule is not oriented by the centrifugal field. In a later section of this paper it will be shown that the sedimentation constant at 60,000 r.p.m. is equal within experimental error to the sedimentation constant at 45,000 r.p.m. Thus $f_s \cong f_D$, and the diffusion coefficients may be expected to be concentration dependent only when a concentration dependence of sedimentation constant is found. Because the reproducibility of sedimentation experiments is considerably better (3–5%) than the diffusion experiments it was not considered necessary to determine the concentration dependence of diffusion wherever there was no concentration dependence of sedimentation constant. As a further check on this

hypothesis, the diffusion coefficient for sample V was determined at concentrations of 0.25 and 1.00%. The values are $D_{20} = 5.98 \times 10^{-7}$ and $D_{20} = 6.33 \times 10^{-7}$, respectively. While it is true that a difference of about 6% exists between these two values, it is doubtful as to whether any significance can be attached to the difference. Because the expected reproducibility of diffusion coefficients from experiment to experiment is usually of the order of 5–10%, these data indicate qualitatively that no significant dependence of diffusion coefficient on concentration exists for sample V. In this regard it is important to note that no skewness was observed in the diffusion diagrams for all of the samples listed in Table III. A significant concentration dependence of diffusion would be expected to result in a skewness in the diffusion diagram which would increase with increasing time. It is reasonable, however, to expect a concentration dependence with increasing molecular weight because concentration dependence was found for the sedimentation constants for the samples in this range. The diffusion coefficients listed in Table III are based on data determined only for 1% solutions. A few typical diffusion diagrams are illustrated in Fig. 1.

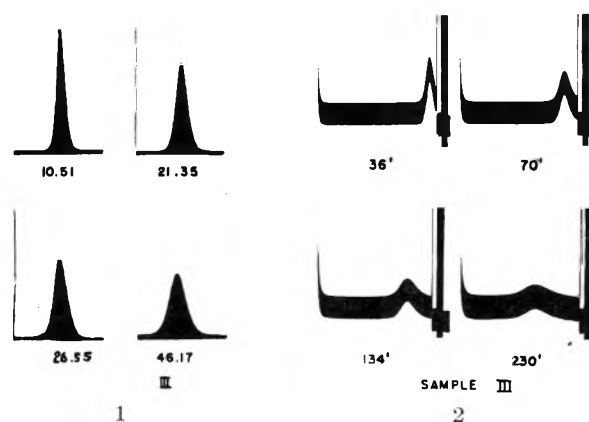


Fig. 1.—Diffusion diagrams: 1% solution, magnification 1, time in hours after boundary was made.

Fig. 2.—Sedimentation diagrams: 1% solution, magnification 1.5, time after full rotor speed.

Sedimentation.—The sedimentation constants for PVP reported in Table III were determined in a Spinco ultracentrifuge.¹⁵ From 8–10 photographs were taken of the sedimenting boundary with the time interval usually being 32 minutes. The calculations were made in the conventional manner as described by Svedberg and Pedersen¹⁶; 6–8 separate computations for sedimentation constant were made for each ultracentrifugal run. The percentage mean deviation of the calculated s within each experiment was seldom more than 5%, and the reproducibility from experiment to experiment was found to vary between 3 and 5%. A few typical sedimentation diagrams are shown in Fig. 2.

Figure 3 illustrates the relationship between the sedimentation constant and the concentration of the polymer in solution. For sample I no concentration dependence of sedimentation constant was observed between the range of concentrations from 1.0–0.25%; a slight decrease in sedimentation constant was observed at the 2% concentration. The molecular weights listed in Table VI were calculated using sedimentation constants determined at 1% concentration; these values for a (samples I through VII in Table III) are equivalent to those at infinite dilution. This assumption could only be made in the case of low molecular weight material ($K \cong 20$ –30) because as is seen on Fig. 3, increasing molecular weight PVP (samples VIII and IX) showed a definite concentration dependence of sedimentation constant. The decrease in sedimentation constant of sample I at the high (2%) concentration is very probably due to the effect of the broad distribution of sedimentation constants (see Fig. 9). At the highest concentration the relative amounts of the high molecular weight material is

(12) O. Lamm, *Nova. Acta. Reg. Soc. Upsaliensis*, **10**, 1 (1937).

(13) L. J. Gosting and M. S. Morris, *J. Am. Chem. Soc.*, **71**, 1998 (1949).

(14) S. J. Singer, *J. Polymer Sci.*, **2**, 290 (1947).

(15) Spinco Model E Ultracentrifuge (Analytical Refrigerated), Specialized Instruments Corporation, Belmont, California.

(16) T. Svedberg and K. O. Pedersen, "The Ultracentrifuge," University Press, Oxford, 1940.

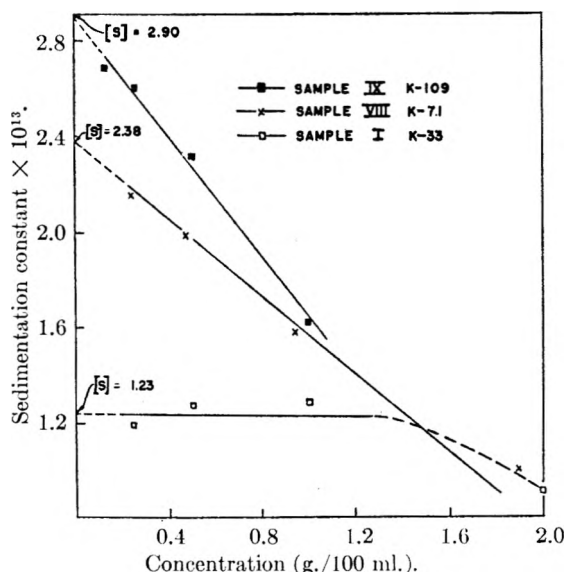


Fig. 3.—Dependence of sedimentation constant on molecular weight and concentration.

very probably adequate to cause an appreciable molecular interaction, resulting in the observed decrease in sedimentation constant.

The sedimentation constant for sample V at 45,000 r.p.m. was determined to be $s_{20} = 1.17 \times 10^{-13}$ sec.⁻¹ which was not considered significantly different from the value at 60,000 (Table III). The reproduction of the same sedimentation constant at two different rotor speeds suggests the absence of an alignment of the polymer in the ultracentrifugal field.

One possible source of error in these determinations of sedimentation constant was the temperature at which the ultracentrifugal run was made. The average temperature during the sedimentation run was usually 23–24°. It has already been shown that the frictional coefficient of the PVP molecule is temperature dependent and that the temperature correction for diffusion does not apply. It follows therefore that the usual temperature correction for sedimentation does not completely describe the change in sedimentation constant with temperature. However, because the difference in temperature was not large (3–4°), the error introduced by the configurational change with temperature is not expected to be greater than the over-all probable error in the determination of diffusion coefficients. The values for molecular weight determined by the Svedberg equation are therefore not adversely affected.

Viscosity.—The relative viscosity measurements primarily used to determine the intrinsic viscosities of the PVP samples were determined at 24.85° in Ostwald-Fenske type viscometers with the flow times for water of the order of 300 seconds.¹⁷ The values used were average measurements of two analysts, with the maximum deviation from the mean being of the order of ±0.1 second. This variation results in a maximum possible error of 1.5% at the lowest concentration (0.125%) and decreases to 0.5% probable error at the highest concentration (1.500%).

The intrinsic viscosities were determined by plotting $\ln \eta_{rel}/c$ vs. c for five concentrations between the range 0.1250 to 1.500%.

The temperature dependence of the molecular frictional coefficient discussed earlier suggested the possibility that PVP solutions exhibit structural viscosity. The relative viscosity of a number of 0.5% solutions of PVP was determined at two different temperatures (24.85 and 35.00°) and in two viscosimeters of distinctly different bore sizes. Flow times for water at 25.85° were 356.86 and 76.66 seconds. All of the samples exhibited a departure from Newtonian flow but to a varying degree, depending upon the average molecular weight. The differences observed were all too great to be accounted for on the basis of the relatively

high experimental error (< 1.5%) introduced by the large capillary bore size.

If the viscosity temperature coefficient is defined as $d\eta_{rel}/dT \cdot T_1^2$ and the "flow time" coefficient as $d\eta_{rel}/dt \cdot t_1^2$, where T_1 is the temperature and t_1 is the flow time for water, the data can be presented in a convenient manner as shown in Table II.

TABLE II

PVP Sample	Temp. coefficient	Flow time coefficient
I	0.591×10^{-3}	0.357×10^{-4}
IX	9.56×10^{-3}	3.28×10^{-4}

An increase by an order of magnitude of 10 is observed between samples I and IX. (For Newtonian flow, both these coefficients would equal zero.) These data serve to emphasize the inaccuracies inherent in the characterization of the average molecular weights by means of a single relative viscosity determination such as afforded by the use of the Fikentscher K-value. A single relative viscosity measurement is a function of the molecular weight distribution. It is conceivable that a very small fraction of high molecular weight material could contribute disproportionately to the measured relative viscosity.

Although the electrophoretic mobility of PVP is reported¹⁸ to be pH sensitive, the viscosity of PVP as a function of pH and ionic strength has not been studied. On the basis of the chemical structure of the polymer no significant electroviscous effect is anticipated. The polymer is essentially non-ionic and should be only very weakly amphoteric.

TABLE III

PVP Sample	$D_{20} \times 10^7$	% MD^a	$s_{20} \times 10^{13}$	% MD^a	$[\eta]$
I	4.81	5.05	1.28	3.91	0.24
II	4.14	1.62	1.42	3.52	0.33
III	4.27	4.34	1.27	7.87	...
IV	5.87	8.32	1.13	4.42	...
V	6.33	3.86	1.10	1.82	0.19
VI	7.55	6.10	0.82	3.66	.13
VII	5.94	3.96	1.03	3.88	.20
VIII	[2.38] ^b	5.73	1.14
IX	[2.90] ^b	1.24	1.99

^a The percentage mean deviations represent an average of all the individually determined values. Lower % MD 's could have been reported by a propitious choice of values to be averaged. ^b These are the intrinsic values determined by extrapolation to infinite dilution. The % MD 's are for the 1% solutions.

Partial Specific Volume.—The partial specific volume can be determined in a number of ways.¹⁹ One of two methods used in this Laboratory will be described. The following general equation serves as a basis for discussion

$$\bar{V} = V + Z_1(\partial V/\partial Z_2)_{T,P} \quad (2)$$

where

\bar{V} = partial specific volume of solute
 V = specific volume of solution
 Z_1 = weight fraction of solvent
 Z_2 = weight fraction of solute

At infinite dilution this equation reduces to

$$\bar{V} = V_\infty + (\partial V/\partial Z_2)_{T,P} \quad (3)$$

In practice the specific volume of the solution is plotted (ordinate) against the weight fraction of solute (PVP) on large graph paper. The partial specific volume for PVP is therefore simply the

(18) R. A. Sullivan, F. M. Palermi and R. Annino, Paper 59, Meeting-in-miniature, New York Section of ACS, Feb. 8, 1952, Hunter College, New York, N. Y.

(19) See for instance S. Glasstone, "Textbook of Physical Chemistry," D. Van Nostrand Co., Inc., New York, N. Y., 1946.

(17) The authors are indebted to L. J. Lohr of the analytical section of this Laboratory for viscosity and density measurements and for the Dumas nitrogen assay.

algebraic sum of the ordinate intercept (infinite dilution) plus the slope of the straight line.

Aqueous solutions of three distinctly different samples were made so as to be about 5% on a weight-volume basis. The exact PVP concentration for these solutions were determined by Dumas nitrogen assay.¹⁷ Four more solutions for each PVP sample were made by quantitative dilution so that a concentration range from about 0.1 to 5% was covered. Calibration of the Dumas nitrogen assay demonstrated that these analyses were accurate to $\pm 1\%$. The density of each solution was determined¹⁷ at 24.85°. The mean deviations were $\pm 0.0002-3$. The accuracy of the nitrogen assay limits the accuracy of the value for \bar{V} . The plot of Z_2 against V resulted in straight lines to which all the points fell closely.

Samples I, IX and an unlisted (Table I) sample gave values of 0.8057, 0.7995 and 0.8805 for \bar{V} , respectively. Wide variations in polydispersity and molecular weight were included in these samples. The mean value is 0.802 with a mean deviation of ± 0.004 . However, because of the limitations imposed on Z_2 by the concentration assay, the value of $\bar{V} = 0.802 \pm 0.008$ cc./g. for $0 \leq C \leq 5\%$ is reported.

Refinements in the determination of the partial specific volume were not necessary because an error of 1% results in an error of roughly 4% in the quantity $(1 - \bar{V}\rho)$. This quantity affects the value of molecular weight inverse linearly just as the translational diffusion coefficient does. Because the probable error in the determination of this latter parameter is usually greater than 4%, the accuracy in the reported value for \bar{V} is adequate. The Kjeldahl procedure for nitrogen assay was found to give abnormally low results.¹⁷

Although the partial specific volume is based on density measurements made at 24.85°, the molecular weights calculated for 20° are not affected by this temperature difference. The value of \bar{V} should not be strongly temperature dependent.

Theoretically for ideal solutions and for ideal determinations of s and D , the partial specific volume should be determined with an accuracy of $\pm 0.2\%$. In practice²⁰ accuracies in the determination of \bar{V} for proteins are often of the order of $\pm 0.6\%$. Nevertheless, the reproducibility in the evaluation of the diffusion coefficient usually is the most serious factor limiting the accuracy in the determination of molecular weight when using equation 4; this was the case in these experiments.

Water of Hydration.—Adair and Adair²¹ have developed a method for the determination of water of hydration by a comparison of the partial specific volume of the protein crystal with the partial specific volume in the anhydrous state. There are limitations to this method which were emphasized by Adair and Adair and also by Oncley.²² Most methods for the determination of the amount of water associated with macromolecules in solution leave much to be desired. In this work a rough

approximation of the water associated with the PVP molecule in solution was obtained from the difference in partial specific volume of the "anhydrous" material was taken as the reciprocal of the density measured in a suspending medium in which the spray dried PVP was immiscible. The density of PVP in petroleum ether was determined pycnometrically¹⁷ to be 1.13 g./cc. This value in conjunction with the previous determination of the partial specific volume of the PVP in aqueous solution yielded a value of 0.084 g. water per gram of PVP, or roughly 0.5 mole of water per monomer unit. This is of the same order of magnitude as the hydration reported in the literature for various proteins.^{22,23} The significance of this calculated water of hydration for PVP is admittedly doubtful, primarily because the spray-dried material is not anhydrous as described in an earlier section, however an order of magnitude is suggested.

Diffusion Coefficients from the Sedimentation Diagrams.—Sedimentation diagrams have long been used as a convenient source for an estimation of the diffusion coefficients. Until recently this method has presumably only been reliable for application to highly homogeneous samples, any significant polydispersity contributing materially to the spreading of the boundary and thus directly to the error in the determination of D . During an earlier phase of this work the diffusion coefficients of PVP were determined from the sedimentation diagrams using the height-area method for computation. Because of an awareness of the effect of polydispersity on the determination of D in this manner, only the earlier photographs in each sedimentation run were used. Notwithstanding this precaution, the values of D determined in this manner were in very poor agreement with the values determined in the conventional separate experiments.

Alberty²⁴ and more recently Brown and Cann²⁵ have derived a technique for determining the diffusion coefficient from electrophoresis diagrams even when there is a significant spreading of the boundary due to electrophoretic heterogeneity. The corresponding method for sedimentation has been described by Baldwin and Williams.²⁶ According to this method the diffusion coefficient may, to an approximation, be written as a power series the first two terms of which approximate a straight line. The apparent diffusion coefficient, calculated, for instance, by applying the method of second moments to the sedimentation diagrams, can be plotted against time. The extrapolation to zero time would then yield the true diffusion coefficient with the effects of the polydispersity of the sample presumably being eliminated. This was done and Fig. 4 represents such curves for samples II and V, and Table IV is a tabulation of the results of a number of such determinations for D compared

(23) E. J. Cohn and J. T. Edsall, "Proteins, Amino Acids and Polypeptides," Reinhold Publ. Corp., New York, N. Y., 1943.

(24) R. A. Alberty, *J. Am. Chem. Soc.*, **70**, 1675 (1948).

(25) R. A. Brown and J. R. Cann, *THIS JOURNAL*, **54**, 364 (1950).

(26) R. L. Baldwin and J. W. Williams, *J. Am. Chem. Soc.*, **72**, 4325 (1950). This method is described in greater detail by R. L. Baldwin, *et al.*, in Paper XXI, Symposium on Complex Ions and Polyelectrolytes, Ithaca, N. Y., June 18-21, 1951.

(20) (a) G. Kegeles, *J. Am. Chem. Soc.*, **68**, 1670 (1946); (b) T. L. McMeekin, *et al.*, *ibid.*, **71**, 3298 (1949).

(21) G. S. Adair and M. E. Adair, *Proc. Roy. Soc. (London)*, **B120**, 422 (1936).

(22) J. L. Oncley, *Ann. N. Y. Acad. Sci.*, **41**, 121 (1941).

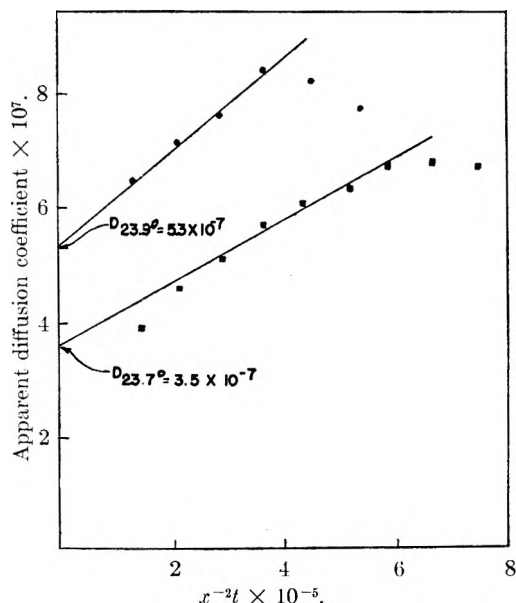


Fig. 4.—Determination of diffusion coefficient from sedimentation diagrams: —●— Sample II; —■—, Sample V.

with values determined from previously described conventional experiments.

TABLE IV
DIFFUSION COEFFICIENTS (D_{20})

PVP Sample	From conventional experiments, cm. ² /sec. × 10 ⁷	From sedimentation diagrams, cm. ² /sec. × 10 ⁷	Difference, %
I	4.81	3.9	- 21
II	4.14	4.8	+ 15
IV	5.87	3.1	- 47
V	6.33	3.1	> -100

It is apparent from Table IV and Fig. 4 that the method outlined above is totally unreliable for use as an accurate determination of the diffusion coefficient for PVP. An examination of Fig. 4 reveals that the apparent diffusion coefficient (D^*) does not always closely approximate a straight line function of time. For this reason care must be exercised in the application of this technique to the evaluation of diffusion coefficients. The degree of unreliability of this method appears to be related to the average value of D .

There appears to be no good substitute for determining diffusion coefficients from conventional experiments.

Molecular Weights.—The molecular weights of samples I through VII were computed by means of the well known Svedberg¹⁶ equation

$$M = RT_s / ((1 - \bar{v}_p)D) \quad (4)$$

These values are presented in graphical form as a function of the sedimentation constants in Fig. 5. These results are in general agreement with those reported by Scholtan²⁷ who found that the molecular weight was a parabolic function of the sedimentation constant. In the low molecular weight range ($M = 20,000$ to $40,000$) the relationship of molecular weight to sedimentation constant can be

(27) W. Scholtan, *Die Makromolekulare Chemie*, **7**, 209 (1952). This publication appeared while our manuscript was in preparation.

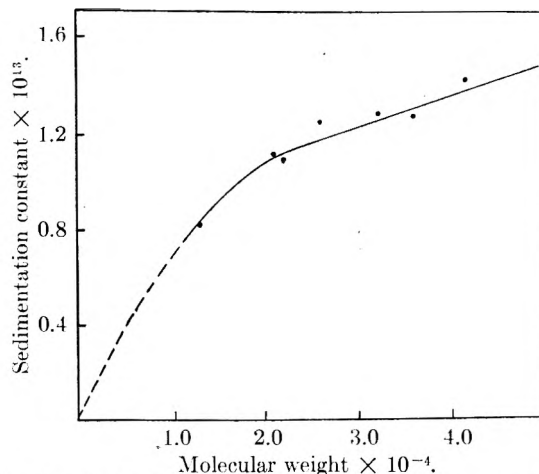


Fig. 5.—Molecular weight versus sedimentation constant.

expressed with sufficient accuracy by the straight line function

$$s = 0.73 \times 10^{-13} + 0.17 \times 10^{-17} M \quad (5)$$

Average molecular weights may be determined from Fig. 5 by a single measurement of sedimentation constant. For the straight line portion of this curve the value of M should be precise within limits of 5–10%. To obtain a more absolute value a more careful consideration of the effect of polydispersity on the molecular weight must be made. More will be said about this in a later section.

To develop a direct answer as to what type average molecular weight is obtained from sedimentation velocity–diffusion measurements one must have a knowledge of the type average sedimentation constant and diffusion coefficient derived from these experiments. Gralén²⁸ has shown that if the second moment method of computation is applied to the diffusion diagrams, then a weight average diffusion coefficient is determined. We have used this second moment of analysis so that a D_w is assumed for the subsequent discussion.

No one has yet identified the type average sedimentation constant determined directly from sedimentation velocity diagrams, the type average probably being different, depending on the molecular configuration and distribution of molecular sizes. For practical purposes this means a consideration of all types of average s taken in conjunction with the weight average D_w must be made to determine the type average molecular weight. Singer²⁹ has illustrated the general formulas for the three molecular weight averages derivable from a combination of weight average D and number, weight and weight-maximum sedimentation constant. It has just been demonstrated that the molecular weight can be represented over a considerable range by a straight line function of the sedimentation constant (equation 5). The frictional coefficient during ultracentrifugation may then be written as

$$f_i = M_i(1 - \bar{v}_p)/(a + bM_i) \quad (6)$$

where a and b are the coefficients appearing in the straight line function (equation 5).

(28) N. Gralén, *Kolloid. Z.*, **95**, 188 (1941).

(29) S. J. Singer, *Polymer Bull.*, **1**, 79 (1945).

Assuming weight averages for both parameters (D_w, s_w) involving frictional coefficients, the general equation for average molecular weight becomes

$$M_{ww} = \frac{\sum n_i M_i^2 / f_i}{\sum n_i M_i / f_i} = \frac{\sum n_i M_i^2 ((a + b M_i) / M_i (1 - \bar{v} \rho))}{\sum n_i M_i ((a + b M_i) / M_i (1 - \bar{v} \rho))} \quad (7)$$

where the subscript i refers to the i th molecular species.

This equation reduces to

$$M_{ww} = \frac{1 + (b/a)M_w}{(1/M_n) + (b/a)} = \frac{M_n(1 - (b/a)M_w)}{1 + (b/a)M_n} \quad (8)$$

The fact that the ratio b/a is not vanishingly small attaches some importance to equation 8. If this ratio were small, then equation 8 would reduce to M_n as stated by Singer.²⁹ From similar reasoning the type of molecular weight resulting from a number average, s_n , and weight average, D_w , can be described as

$$M_{nw} = \frac{M_n \sum n_i M_i \left[\sum \frac{1}{n_i M_i} + \frac{b}{a} \sum 1 \right]}{1 + (b/a)M_n} \quad (9)$$

This relation is more complex than that illustrated in equation 8 for M_{ww} ; the quantities n_i and $n_i M_i$ cannot be reduced to the more simple terms M_n , M_w or M_z .

Similar equations can be derived for other combinations of average sedimentation constant with average diffusion coefficients. However, the nature of equations 8 and 9 serves to illustrate how complex the average molecular weight would be if the *exact* type of average sedimentation constant were known. The true value for s is undoubtedly a mixed average. If a more rigorous description of the relationship between s and M such as a parabolic function for the full length of the curve in Fig. 5 were substituted in equation 6, the problem of describing the molecular weight average would increase the desirability of considering the molecular weight *distribution* in preference to a detailed study of so-called average molecular weights. Furthermore, a knowledge of the molecular weight distribution is more important from practical considerations. This aspect will be considered in some detail in the latter parts of this paper.

The molecular weight as determined by the sedimentation velocity-diffusion method described earlier can also be presented as a function of intrinsic viscosity as done by Dialer and Vogler³¹ and Scholtan.²⁹ The equation for the Staudinger relationship between intrinsic viscosity and molecular weight is given in Table V. The values determined by the earlier workers were also determined by sedimentation velocity-diffusion methods; they are included for comparison.

TABLE V

$[\eta]$	$= 4.1 \times 10^{-5} M^{0.65}$	this work
$[\eta]$	$= 6.4 \times 10^{-5} M^{0.58}$	ref. 30
$[\eta]$	$= 1.4 \times 10^{-5} M^{0.70}$	ref. 27

As can be seen from Table V, there is only qualitative agreement between the three equations. This discrepancy can be partly explained on the

(30) K. Dialer and K. Vogler, *Die makromolekulare Chem.*, **6**, 191 (1951).

basis of differences in experimental conditions. Of greater importance is the observation reported by Frank and Breitenbach³¹ who have noted that the coefficient in the Staudinger equation varies considerably with the degree of molecular heterogeneity of the polymer sample. It will be shown that the samples used in this work were of varying degrees of homogeneity. It is reasonable to expect that the homogeneity of samples from different laboratories would vary through at least as great a range as the samples within one laboratory. If this is the case, the discrepancies noted are not surprising. The magnitude of the exponents of M should be expected to decrease with increasing molecular weight as predicted from theory.³² This effect was also noted for PVP by Scholtan.²⁷ Reliance on the equations given in Table V for a weight average molecular weight is often a matter of convenience. In view of what is now known about PVP, the accuracy of the molecular weight would be largely dependent upon the molecular weight distribution as well as the experimental conditions used to evaluate viscosity.

Molecular Configuration.—A knowledge of the diffusion coefficients and molecular weights previously discussed permits an evaluation of their frictional ratios according to the method outlined in a number of texts.³³ The method described by Oncley²² was used to determine the contribution to the molecular frictional ratio due to asymmetry and hydration. Use of the value of hydration determined earlier suggests that any appreciable departure from the theoretical behavior for a spherical shape is due only to a minor degree to the hydration of PVP in aqueous solution. The average ratios (a/b) of the PVP molecule in solution can be easily determined from the frictional ratios by use of tables of correspondence given by Svedberg and Pedersen.¹⁶ These results are tabulated in Table VI.

TABLE VI

PVP	Mol. wt.	Diffusion, f/f_0	Viscosity increment, ν	Axial ratios (a/b)		$R_s \times 10^{-8}$, cm.
				Diffusion	Viscosity	
I	32,000	1.96	30.0	19.1	16.9	149
I	41,500	2.11	41.3	23.0	20.8	169
III	36,000	2.14	...	24.0	...	158
IV	23,000	1.80	...	15.1	...	125
V	21,000	1.73	23.8	13.8	11.6	120
VI	13,000	1.70	16.3	13.1	11.3	95
VII	21,000	1.84	25.0	16.3	15.0	120
VIII	142	...	43.8	...
IX	248	...	60.8	...

The axial ratios of polymer molecules in solution have also been derived from viscosity measurements. This type of computation has also been described in some detail by Oncley²² and so only the results are included in Table VI. In each case the axial ratios have been derived assuming a 1 elon-

(31) H. P. Frank and J. W. Breitenbach, *J. Polymer Sci.*, **VI**, 609 (1951).

(32) J. G. Kirkwood and J. Riseman, *J. Chem. Phys.*, **16**, 565 (1948).

(33) See for example: A. Weissberger, "Physical Methods in Organic Chemistry," Interscience Publ., Inc., New York, N. Y., 1944. Part I. H. Neurath, *Chem. Revs.*, **30**, 357 (1942); A. E. Alexander and P. Johnson, "Colloid Science," University Press, Oxford, 1949.

gated ellipsoid shape model. The axial ratios derived from viscosity represent measurements made at 24.85°; the comparable ratios from diffusion are based on data corrected to 20.0°.

Recent theoretical considerations^{32,34} have indicated that the shape model assumed is not a sufficient characterization of a high polymer in solution, the randomly coiled polymer chain being a more accurate description of the configuration. A more accurate description of the state of the molecule may be obtained by calculating the root mean square distance between the ends of the chain. According to Kirkwood and Riseman³²

$$R_0 = Z^{1/2}b \quad (10)$$

where R_0 is the root mean square distance, Z is the degree of polymerization and b is the statistical length of the monomer unit. The determination of b as described by Kirkwood and Riseman made it possible to compute the R_0 's given in Table VI. As a further experimental test of the Kirkwood-Riseman theory, the values of the diffusion coefficients were computed by means of the K-R equations. The diffusion coefficients computed from the K-R theory making use of intrinsic viscosity data are compared in Table VII with the values obtained earlier in the conventional manner. Because the intrinsic viscosity was determined from data taken at 24.85°, the values of diffusion coefficients calculated from the K-R theory were corrected to 20.0° by means of equation 1.

TABLE VII

Sample	$D_{20} \times 10^7$ cm. ² /sec.	
	Exptl.	K-R Theory
I	4.81	6.52
II	4.14	5.55
III	4.24	6.08
IV	5.87	7.89
V	6.33	8.39
VI	7.55	11.35
VII	5.94	8.39

The values calculated from theory are in most cases in good agreement with the experimental values when cognizance is taken of certain approximations made in the original theory, and the fact that the temperature correction by equation 1 does not compensate for changes in molecular frictional coefficients with temperature.

Analysis for Polydispersity.—The term polydispersed as used in this work should be defined for the sake of clarity. The PVP samples described herein exhibit only one peak in the sedimentation diagram as illustrated by Fig. 2. There exists, however, a distribution of molecular weights about this single mean. The attention of this research has been directed toward a more complete description of this distribution (polydispersity). There are a number of methods which have been used as a characterization of polydispersity based on an analysis of the diffusion diagrams.³³ Gralen³³ was perhaps the first to show that the ratio of the diffusion coefficient computed by the statistical (second moment) method ($D\sigma$) to the coefficient determined by height-area method (D_{HA}) may be used to characterize the polydispersity of the sample. This follows from the fact that the height-area method is valid only for essentially monodispersed systems. This technique was applied to a number of PVP samples with the results shown in Table VIII.

TABLE VIII

Sample	$D\sigma \times 10^7$, cm. ² /sec.	$D_{HA} \times 10^7$, cm. ² /sec.	$D\sigma/D_{HA}$
III	4.27	3.89	1.10
IV	5.87	6.19	0.95
VII	5.94	5.97	0.99

The deviation of the ratio, $D\sigma/D_{HA}$, from unity is proportional to the degree of molecular polydispersity. Although qualitatively these results agree with those described later, no significance can be attached to the ratios given in Table VIII because the differences in D computed by each method are close to or within the deviations from the mean exhibited by each series of calculations. For this reason, this method of ratios should be applied only when there is a much broader distribution of diffusion coefficients than exhibited by these PVP samples. Neurath³³ has described a method for analyzing a compound diffusion curve for its component parts by calculating the first, second and third moments of the diffusion diagram. This method was also applied in a limited way in this Laboratory with negative results. This method is very probably limited in application to those polymers which have discrete components which can be separated by ultracentrifugal analysis. Because the ultracentrifuge diagrams of PVP exhibit only one maximum in the dn/dx curve, the polymer has a Gaussian distribution. This type of polydispersity does not lend itself readily to an analysis such as just described.

The final method for the analysis of the diffusion diagrams for polydispersity used in this work has also been fully described in the literature.³³ In this technique the experimental diffusion curve is transformed to normal coordinates and compared with the normal distribution curve. Since the areas under the normal probability curve and the normalized experimental curve are equal, the magnitude of the peak displacements is a measure of the polydispersity of the sample. Of the several methods for analyzing the diffusion diagrams for polydispersity, this latter method has met with the most success. This method of diffusion analysis was applied to five PVP samples and the diffusion diagram for saccharose. In the case of saccharose, only a very slight deviation from the normal was observed. On Fig. 6 are plotted the normalized diffusion diagrams for PVP samples V, VII for comparison with the normal probability curve. There is a significant departure from the normal for both of these samples as well as a qualitative indication of differences in the degree of polydispersity. In this investigation at least two diagrams of each experimental diffusion run were normalized; the normalized curves were identical in each case. If an arbitrary assignment of a number from one to ten is made, depending upon the degree of deviation in heights of the peaks from the peak of the normal curve, a qualitative tabulation of degree of polydispersity can be made as in Table IX where the highest number denotes the largest amount of polydispersity.

The sedimentation-velocity diagrams can also be normalized as described by Svedberg and Pedersen.¹⁶ In this case the theoretical sedimentation curve was calculated making use of the diffusion coefficients determined from the previously described conventional experiments. The calculated curve is then the sedimentation diagram which would have resulted if there were no spreading of the boundary due to molecular heterogeneity. This method is essentially a normalization to the same height; the area between the experimental curve and the curve predicted by theory for a presumed monodispersed system is then the spreading of the boundary which is due to heterogeneity alone.

Figure 7 represents such a series of curves for PVP sample II. Only one example of each of these normalization procedures is given in this paper; the choice was arbitrary. The times noted for each curve are the times after the rotor had reached full speed. It is interesting to note that only a relatively small portion of the total boundary spreading is due to polydispersity, and that this polydispersity is manifest only after relatively long times. This property has important applications which will be elaborated on in the last method for determining polydispersity. The fact that only a minor portion of the spreading of the sedimenting boundary is due to molecular heterogeneity renders this method rather insensitive for polydispersity analysis. Because the differences between the experimental and theoretical curves are small, a relatively minor error in the determination of

(34) W. Kuhn and H. Kuhn, *Helv. Chim. Acta*, **28**, 1533 (1945).

(35) N. Gralen, Dissertation, Uppsala (1944).

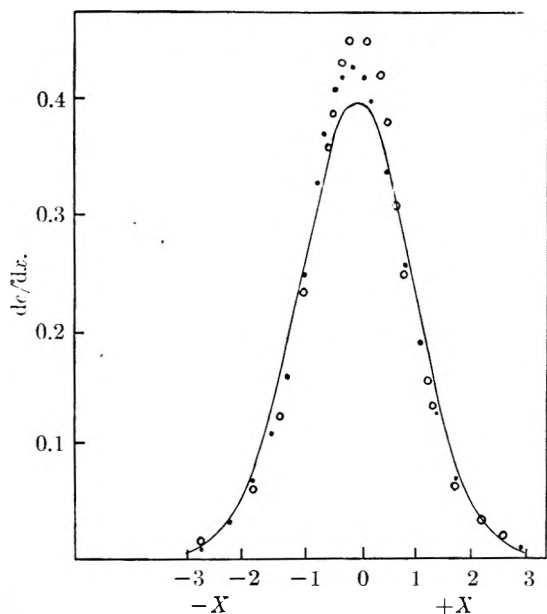


Fig. 6.—Normalized diffusion diagrams: —, normal distribution; ●, sample V; ○, sample VII.

felt that these differences can be accounted for by the comparative insensitivity of both methods.

Ultracentrifugal analysis has proved to be a more valuable tool in the study of polymolecularity. Lansing and Kraemer³⁶ have determined the molecular weight distribution of gelatin with the use of the equilibrium ultracentrifuge by assuming a logarithmic distribution function and determining the non-uniformity coefficient of the distribution. Jullander³⁷ has extended the applicability of this technique to the velocity ultracentrifuge and introduced a third parameter to describe the skewness of the distribution function. This three parameter distribution function was applied by Jullander to the analysis of the polymolecularity of nitrocellulose. In his case the average molecular weights were on the order of 100,000 to 300,000. It was possible in this range to show that the diffusion was negligible, and hence the total spreading of the boundary was due to a distribution of molecular weights. The technique described by Jullander is, however, somewhat limited to those polymers which have diffusion coefficients sufficiently small so that the spreading of the boundary during the ultracentrifugal run is due almost completely to a distribution of molecular sizes.

Polydispersity determined from sedimentation equilibrium experiments has been described by Wales,³⁸ *et al.*, for polystyrene polymers and fractions thereof. Molecular weight distribution curves, analogous to the $g(s)$ vs. M distribution described later in this paper, are shown. Significant polydispersity in the polystyrene fractions and the advantage of this equilibrium ultracentrifugal analysis are illustrated. The time required to reach equilibrium (up

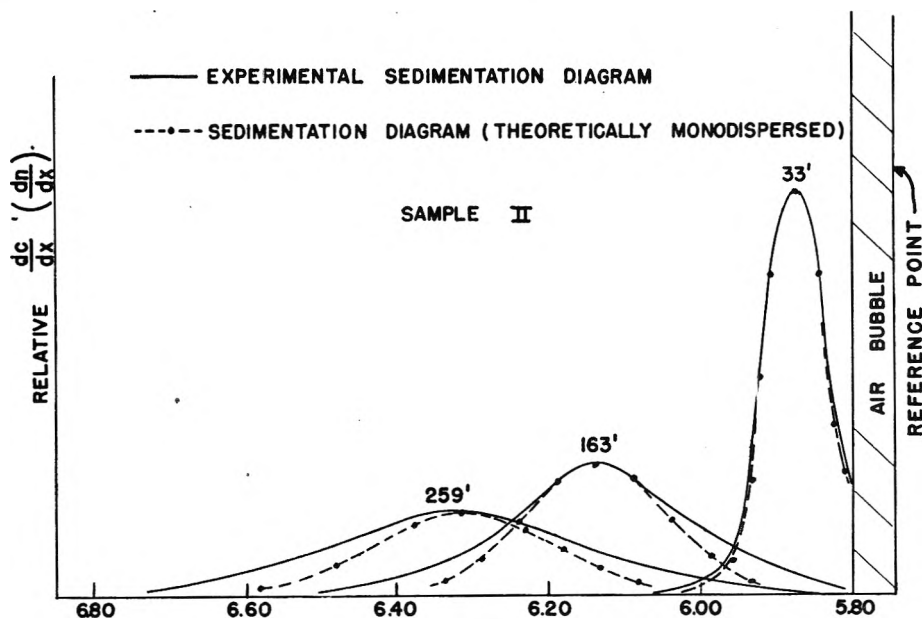


Fig. 7.—Polydispersity from normalization of sedimentation diagrams.

diffusion coefficient may result in inaccuracies in the determination of relatively polymolecularity. A tabulation of relative polydispersity from this type of sedimentation analysis is included in Table IX. There is only qualitative agreement between the tabulation for polydispersity by the normalization of the sedimentation and diffusion diagrams. It is

TABLE IX

Polydispersity decreases from 10 as an arbitrary maximum; numbers are relative. The blank spaces indicate no normalization

PVP Sample	Polydispersity from Normalization	
	From diffusion	From sedimentation
I	7	..
II	..	6
III	3	..
IV	2	2
V	6	8
VII	10	5

to two weeks) is an undesirable aspect, nevertheless this work represents an important contribution toward a much needed technique for determination of molecular weight distribution without relying on fractionation procedures.

The procedure outlined by Baldwin and Williams²⁶ and described in more detail by Williams, *et al.*,³⁹ is especially valuable for application to materials which are significantly polydispersed but which also have a relatively high average diffusion coefficient. Figure 7 shows that the PVP samples discussed in this work have these properties. The diffusion of the polymer contributes in a major way to the spreading of the boundary, and hence cannot be disregarded in an evaluation of polydispersity.

The theory for the analysis of the sedimentation-velocity diagrams for the distribution of sedimentation constants

(36) W. D. Lansing and E. O. Kraemer, *J. Am. Chem. Soc.*, **57** 1369 (1935).

(37) J. Jullander, *Arkiv Kem., Mineral. Geol.*, **21A**, 8 (1945).

(38) M. Wales, *et al.*, *THIS JOURNAL*, **52**, 983 (1948).

(39) J. W. Williams, *et al.*, *J. Am. Chem. Soc.*, **74**, 1542 (1952).

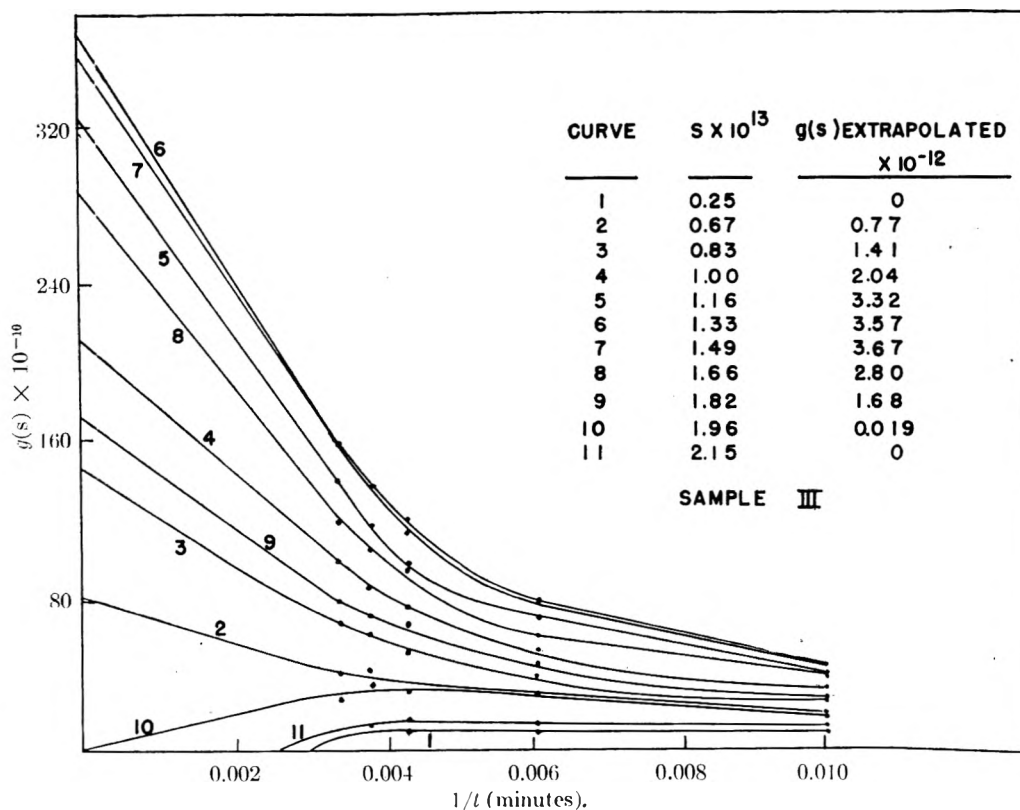


Fig. 8.—Extrapolation for distribution function.

has been described by Gosting⁴⁰ and thus will not be given in detail. An apparent distribution function, $g^*(s)$, can be calculated from each photograph of the sedimenting boundary by means of the equation

$$g^*(s) = \frac{dn \omega^2 \times t}{dx \Sigma dn/dx} \quad (11)$$

where $\Sigma dn/dx$ represents the area under the sedimenting boundary, x is the abscissa position along the dn/dx curve for a particular sedimentation constant s after time t , and ω is the angular velocity of the ultracentrifuge rotor in radians/second.

The apparent distribution function computed by means of equation 11 has not yet had the boundary spreading due to diffusion eliminated, however because

$$g^*(s) \longrightarrow g(s) \quad (12)$$

$$t \longrightarrow \infty$$

the true distribution function, can be obtained by extrapolating to infinite time.

The procedure consists of first making a determination of zero time. The zero times in this work were found to be of the order of a few minutes as reported by the original authors.²⁶ From a knowledge of zero time it is possible by means of equation 11 to compute an apparent distribution function by assuming that the total spreading of the boundary was due completely to a distribution of molecular species. According to equation 12, if the apparent distribution function is plotted *versus* $1/t$, and extrapolated to infinite time, the true distribution function is obtained. On Fig. 8 is shown a representative plot of typical apparent distribution functions *versus* $1/t$. Each curve on Fig. 8 represents the magnitude of $g^*(s)$ *versus* $1/t$ for each sedimentation constant which was chosen arbitrarily on the first photograph. The curves which turn downward and go to zero indicate that at that value for s on the first photograph the dn/dx was high not because of a large amount of material with that particular s , but because molecules with

different values of s were "presumably" present due to diffusion. Conversely, the curves which turn upwards with increasing time imply that a considerable amount of material with that particular s -value was present at that point on the first photograph. The extrapolated value of $g^*(s)$ for infinite time could then be plotted *versus* the corresponding sedimentation constants. In practice, the extrapolation of the $g^*(s)$ curves was done on large graph paper so that the ordinate scale could be enlarged. This resulted in a more accurate determination of $g^*(s)$ than is implied by Fig. 8.

For most of these calculations, from 10–12 points on the first sedimentation diagram were selected. The change in the distribution function for each of these points was then followed over the complete sedimentation run which usually consisted of 10 photographs spaced 32 minutes apart. Because neither the slope nor the curvature of the $g^*(s)$ *vs.* $1/t$ curves were found to change appreciably during the earlier portions of the sedimentation experiment, it was possible to eliminate computations for some of the diagrams so that usually five or six sedimentation diagrams were used. As the time of sedimentation increases, the increment of change along the abscissa becomes smaller so that increasing the time of sedimentation will not appreciably decrease the distance to be extrapolated. This aspect serves to note limitations in this technique which are now considered. The slope and the rate of change of the slope of the $g^*(s)$ *vs.* $1/t$ curve is different for each series of points. Extrapolation beyond the last experimentally determined point (longest time) must depend on the judgment of the analyst. This could result in variations unless a convention for extrapolation were adopted. In this work a straight line was used for extrapolation beyond the last experimental point with the slope of this straight line being decided by the slope and curvature indicated by the last three or four points. Although the curves certainly do not approach infinity as a straight line, it was decided that this convention was more reliable than trusting to an estimate of the curvature. Furthermore, if the extrapolation technique is self-consistent, the distribution curves obtained are relatively correct. The height of the peak in the final $g(s)$ *vs.* s curve (Figs. 9, 10 and 11) therefore depends somewhat on the method of extrapolation. Thus, in terms of ultimate accuracy some

(40) L. J. Gosting, *J. Am. Chem. Soc.*, **74**, 6, 1548 (1952). This paper, involving the solution of the sedimentation velocity equation to yield the distribution of sedimentation constants, appeared after the preparation of this manuscript.

room is provided for equivocation. However, the real value of this approach, the polydispersity distribution, is not impaired if the extrapolation analysis is consistent.

If the extrapolated distribution functions are plotted against the corresponding sedimentation constants, valuable distribution curves are formed. Figures 9 and 10

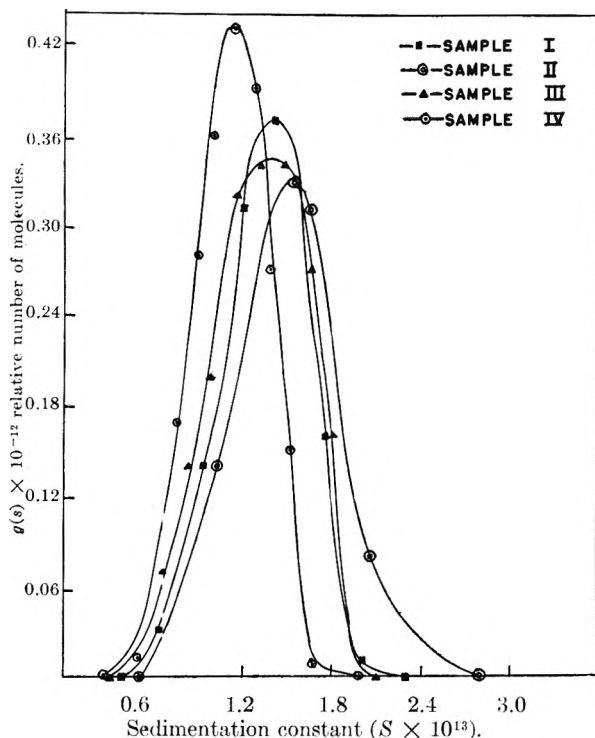


Fig. 9.—Distribution of sedimentation constants (normalized).

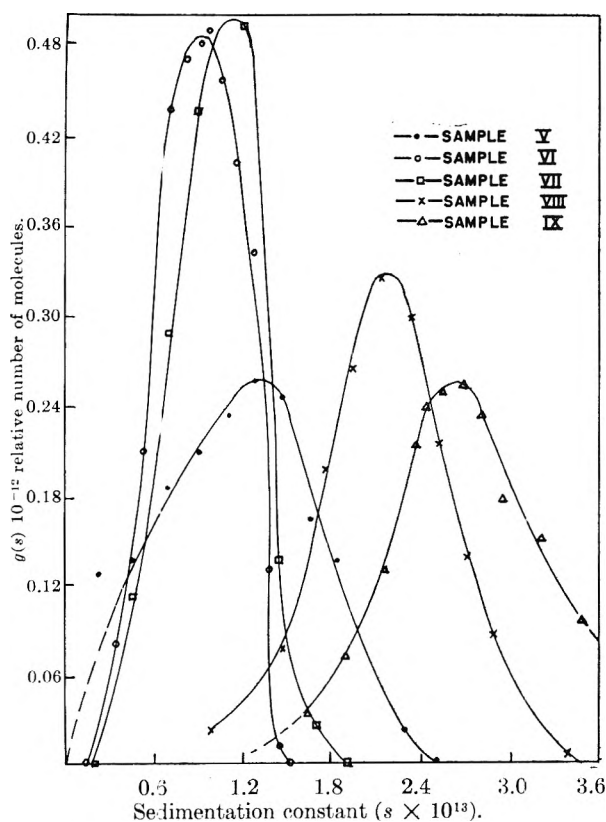


Fig. 10.—Distribution of sedimentation constants (normalized).

illustrate the results *after* normalization. This normalization is desirable because all the curves now encompass unit areas so that the differences in polydispersity between the various samples are better illustrated. These curves can be considered as a good representation of the relative number of molecules *versus* sedimentation constant.

The accuracy of these curves can be considered as good as the reproducibility of the extrapolated values of the distribution function. To check on this accuracy, sedimentation diagrams of sample V were determined at rotor speeds of 45,000 and 60,000 r.p.m. The distribution functions of sample V determined from these two experiments are nearly superimposable. Figure 11 is a plot of these data; the curves were not normalized so that a good idea of the reproducibility of the original results could be gained. The deviations are greatest at the high and low s -values. This is due to the greater probable error in measuring the magnitude of the index of refraction gradient on both sides of the peak where the values of dn/dx are small (see Fig. 2). This error is not serious because the number of molecules at these regions of the spectrum is small.

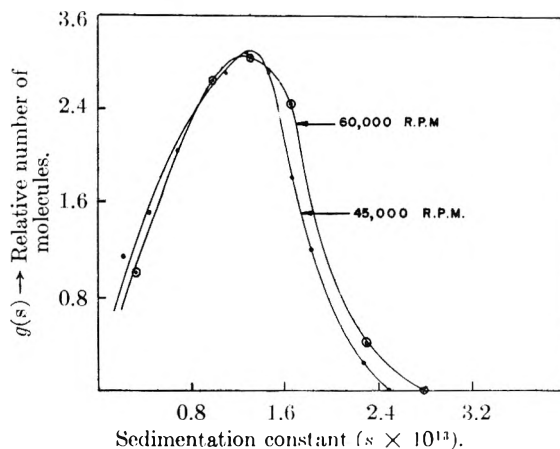


Fig. 11.—Reproducibility of distribution analysis, sample V.

A convenient measure of the polydispersity of the PVP samples represented on Figs. 9 and 10 is the width of the curve at half the maximum height, or the ordinate value of the peak. An examination of Fig. 9 reveals that the fractionation carried out on sample I did little more than to change the magnitude of the average sedimentation constant within the fractions. The widths of the distribution curves at one-half the maximum of samples II and III are nearly the same as or only slightly less than sample I. Sample IV is the only fraction which shows any appreciable decrease in polydispersity. This is very probably due to the more efficient separation possible after the decrease in concentration caused by the removal of samples II and III. As has been indicated earlier, it has been known for some time in this Laboratory⁶ that more efficient fractionation is obtained if the precipitation is carried out from more dilute solutions of the polymer. These data, however, have not yet been treated quantitatively and hence will not be presented in any detail at this time. Current fractionations are being carried out using 5% solutions of PVP instead of 20% solutions as described earlier. The fractions which result are considerably narrower in distribution. These observations are qualitative confirmations of the theories of Flory⁶ and Scott⁷ which were developed from thermodynamic treatments of heterogeneous polymers in solution. According to Flory, practically no fractionation will result from a precipitation technique unless the concentration of the polymer is less than the critical concentration which is given by

$$V_{2(\text{critical})} = 1/(1 + \sqrt{x}) \quad (13)$$

where x is the degree of polymerization of the polymer molecule, and V_2 is the volume fraction of the polymeric solute in the solution. Thus for PVP of an average molecular weight of 22,000, x equals 200, and $V_{2(\text{critical})}$ equals 0.067. Using the value of 1.13 g./cc. for the density of PVP, this becomes 7.5% (*i.e.*, no appreciable fractionation should occur unless the concentration of PVP is less than 7.5% on a weight basis).

The theoretical interpretation of this lack of efficient fractionation is given by both Flory and Scott. Because the polymer-polymer interaction is stronger than the polymer-solvent interaction, there is incomplete separation between the solution and the swollen polymer phases. The concentration of the low molecular weight material in the precipitated phase is always higher than the concentration of the same low molecular weight material in the solution phase due to the strong polymer-polymer interaction. The efficient separation of the low molecular weight material from the swollen precipitate phase is possible only in the presence of a large supernatant phase so that the difference in concentration (with respect to the low molecular weight material) is as large as possible. Another significant prediction of these theories is that the higher the average molecular weight of the material to be fractionated, the more dilute it is necessary to make the solution from which the precipitation takes place.

The distribution of sample VI (Fig. 10) is significantly narrower than sample V. The fractionation of sample VI was achieved by an acetone extraction technique which was described earlier. A comparison of the distribution obtained by precipitation methods and the distribution resulting from an extraction procedure suggests that the extraction method is superior if a narrow distribution of molecular weights is desired. This, however, is a conclusion which becomes meaningful only after a more careful evaluation of the experimental conditions under which these experiments were performed. For example, in the case of the precipitation fractionation (Fig. 9) the precipitate was removed immediately after precipitation. During the extraction technique, the PVP-acetone mixture was allowed to layer overnight. It is reasonable to expect that ample time for equilibration must be allowed for efficient fractionation. Scott has predicted that the distribution obtained by a precipitation fraction should be essentially similar to the distribution obtained by extraction techniques except for a low molecular weight "tail" which should be present in the case of the precipitation methods. It is evident, in any case, that this method of analyzing for the distribution function from the sedimentation diagrams would be extremely useful in the evaluation of the various factors affecting the fractionation of heterogeneous polymers. Similarly, modifications in the original synthesis of the polymer might alter the reaction kinetics which in turn might give rise to other molecular weight distributions which could be determined using this polydispersity analysis.

The information yielded by the distribution curves resulting from the method of analysis just described can be compared with other known methods for determining molecular weight distributions. In fact, this ultracentrifugal sedimentation analysis should be considered for use as a calibration standard for other more indirect methods. The

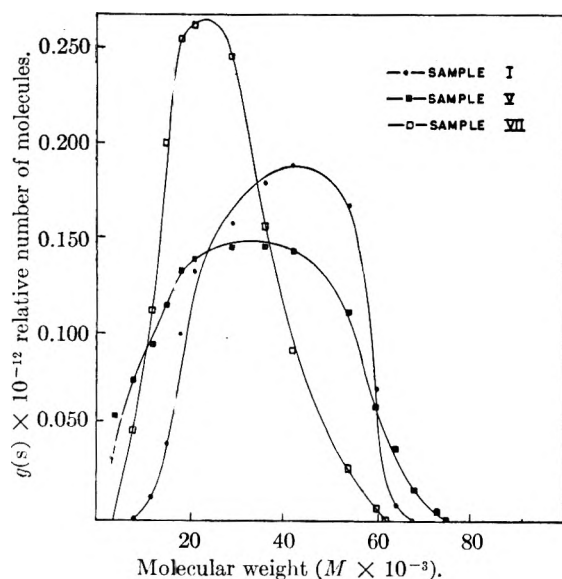


Fig. 12.—Molecular weight distribution (normalized).

results of an extensive refractionation program⁴¹ on PVP carried out in this Laboratory are in qualitative agreement with the distributions described in this paper. This unpublished distribution analysis is based on a graphical plot of the Fikentscher K -values representing the relative viscosities of 1% solutions of the fractions. It has been verified that the distributions are at least as broad as those reported herein, while there is some disagreement about the percentage of the total in each size class.

Because the correspondence between the sedimentation constants and K -values of PVP has been indicated in Tables I and III, it is possible to compare directly the distributions determined by the two methods. The amount found in each size class (characterized by a certain K -value) by fractionation is determined by weighing the dried precipitates. A comparison of the distributions found by the analyses of sedimentation diagrams and by fractionation techniques is presented in Table X.

TABLE X

K	Size class $s \times 10^{12}$	Composition sample I, % Fractionation	Sedi- mentation
0-26	0 -0.90	13.1	18.2
26-30	0.90-1.10	13.2	21.1
30-34	1.10-1.25	17.9	19.9
34-38	1.25-1.39	44.1	17.0
38-∞	1.39-∞	11.7	23.1

The disagreement between the two methods which can be seen in Table X can be resolved by the fact that the distribution curves determined in this work (Figs. 9 and 10) are a true number distribution *versus* sedimentation constant, whereas the distributions determined by fractionation-refractionation techniques are the results of viscosity measurements which are weight average values. The discussions earlier in this paper which outlined the complexities involved in the analysis of average values of molecular size by viscosity determinations are sufficient justification for considering the distribution curves obtained by the analysis of the sedimentation diagrams more reliable.

The correspondence between molecular weights and sedimentation constants (Fig. 5) taken in conjunction with the normalized distributions of sedimentation constant (Figs. 9 and 10) makes it possible to plot the distribution of average molecular weights for the PVP samples as is shown in Fig. 12. The curves in Fig. 12 illustrate the comparative breadths of the molecular weight distributions.

Although the distribution curves shown in Fig. 12 are sufficiently accurate for practical purposes, they cannot be considered "true" number molecular weight distributions in a strict sense. This stems from the fact that the sedimentation constants determined experimentally were average values, and the molecular weights were computed from average values of s and D ; the molecular weight *versus* sedimentation constant relationship (Fig. 5) must be considered an "apparent" s vs. M curve. It is therefore necessary to consider the effect of polydispersity on the experimentally derived relationship illustrated in Fig. 5. A procedure for this analysis may be outlined as follows.⁴²

The experimental relationship between s and M may be written as

$$M^* = \phi(s^*) \quad (14)$$

where M^* and s^* are the values of each parameter determined by experimentation. As was noted earlier these values represent average values which depend on the shape, size and polydispersity of the sample in question as well as the type of mathematical analysis used for the computations. For purposes of analyses it has been assumed that M^* is a weight-weight average molecular weight (calculated from s_w and D_w) and that s^* is a weight

(41) S. Siggia and N. Floramo, this Laboratory, unpublished works.

(42) The authors are indebted to Professor J. G. Kirkwood, Chairman of the Department of Chemistry, Yale University, for outlining these methods of treatment.

average sedimentation constant. (The same procedure may be applied for other combinations of average molecular weight and average sedimentation constant.) The weight average sedimentation constant can be written as

$$s_w = s^* = \left(\frac{\sum_i c_i s_i}{\sum_i c_i} \right) \quad (15)$$

where the subscript i represents the i th species of the corresponding parameter. The concentration is

$$c_i = n_i M_i / Nv \quad (16)$$

where N represents Avogadro's number and v the volume of the solution. In terms of molecular weight s^* becomes

$$s^* = \left(\frac{\sum_i n_i M_i s_i}{\sum_i n_i M_i} \right) \quad (17)$$

The molecular weight resulting from a weight average diffusion coefficient and a weight average sedimentation constant has been given by equation 7 where f_i represents the frictional coefficient corresponding to the i th molecular species. Equation 14 becomes

$$\frac{\sum_i n_i M_i^2 / f_i}{\sum_i n_i M_i / f_i} = \phi \frac{\sum_i n_i M_i s_i}{\sum_i n_i M_i} \quad (18)$$

It is certainly true that the molecular weight distribution is continuous rather than composed of a number of discrete species as implied by equation 18. The summation over the molecular spectrum is then

$$\int_{-\infty}^{\infty} MG(M) dM \quad (19)$$

$G(M)$, the molecular weight distribution, may be written in terms of the known sedimentation constant distribution as

$$G(M) = g(s) ds / dM \quad (20)$$

Equation 19 hence becomes

$$\int_{-\infty}^{\infty} M(s) g(s) ds \quad (21)$$

Henceforth the quantity $M(s)$ will simply be represented by M . Substitution of this integral for the summation of the discrete molecular weight distributions in equation 18 yields

$$\frac{\int_{-\infty}^{\infty} M^2 g(s) ds / f}{\int_{-\infty}^{\infty} M g(s) ds / f} = \phi \left\{ \frac{\int_{-\infty}^{\infty} s M g(s) ds}{\int_{-\infty}^{\infty} M g(s) ds} \right\} \quad (22)$$

The relationship between the molecular frictional coefficient and the molecular weight has been given by Svedberg.¹⁶ Substitution of this relation in equation 22 results in

$$\int_{-\infty}^{\infty} s M g(s) ds / \int_{-\infty}^{\infty} s g(s) ds = \phi \left\{ \frac{\int_{-\infty}^{\infty} s M g(s) ds}{\int_{-\infty}^{\infty} M g(s) ds} \right\} \quad (23)$$

Equation 23 can be considered a representation of the "true" molecular weight dependence on sedimentation constant for perfectly monodispersed systems expressed in terms of the weight average

values of s and M and the number distribution of sedimentation constants [$g(s)$].

Similar relations may be derived by assuming that the experimental sedimentation constant is a number average. Although this was shown not to be the case by equation 8, a true number average $s(s_n)$ can be obtained by determining the first moment of the $g(s)$ vs. s curves (Fig. 9 and 10) which, by the nature of the original theory, are implicitly number distributions. This case is being considered further but will not be included herein.

Equation 23 may be applied to the experimentally determined relations in the following manner. Assume that the true molecular weight can be expressed in terms of the sedimentation constant by means of the infinite series

$$M = a_1 s + a_2 s^2 + a_3 s^3 + \dots \quad (24)$$

Equation 23 becomes

$$\frac{\int_{-\infty}^{\infty} s(a_1 s + a_2 s^2 + a_3 s^3 + \dots) g(s) ds}{\int_{-\infty}^{\infty} s g(s) ds} = \phi \frac{\int_{-\infty}^{\infty} s(a_1 s + a_2 s^2 + a_3 s^3 + \dots) g(s) ds}{\int_{-\infty}^{\infty} (a_1 s + a_2 s^2 + a_3 s^3 + \dots) g(s) ds} \quad (25)$$

Now let

$$p_n = \int_{-\infty}^{\infty} s^n g(s) ds \quad (26)$$

Equation 25 now reduces to

$$\frac{(a_1 p_2 + a_2 p_3 + a_3 p_4 + \dots)}{p_1} = \phi \left\{ \frac{(a_1 p_2 + a_2 p_3 + a_3 p_4 + \dots)}{(a_1 p_1 + a_2 p_2 + a_3 p_3 + \dots)} \right\} \quad (27)$$

Because the $g(s)$ vs. s curves had been determined for a number of samples, it was possible to evaluate p_n (equation 26) for each sample. This was accomplished by normalizing the $g(s)$ vs. s curves (Figs. 9 and 10) and integrating numerically. To simplify the computations, it was assumed that all but the first three terms in equation 24 could be dropped. In this case three second-order algebraic equations in three unknowns (a_1 , a_2 and a_3) were obtained. Each equation represented a specific PVP sample for which s , M and $g(s)$ vs. s were known.

The solution of simultaneous equations of this type can usually be obtained by a process of iteration if approximate values of the common roots are available. In this work, the three PVP samples were chosen so that extremes in heterogeneity and average molecular weight were represented. The experimentally determined values of M and s (Table III) were substituted in equation 24 for these three PVP samples yielding three approximate equations in three unknowns. The approximate values of a_1 , a_2 and a_3 were obtained by simultaneous solution of these three first-order equations. These values of a_1 , a_2 and a_3 were used as a starting point for the exact solution of equation 27 by iteration. It was found, however, that with the use of the approximate values determined from the experimental curve it was not

possible to extract a common root from the three equations. The process of solution of simultaneous equations by iteration is only effective if the approximate values fall within the interval of convergence to a common root. Therefore, one must draw the conclusion that the "true" relationship between s and M for monodispersed systems is not the same as the experimental relationship established by measurements on polydispersed samples.

It has not been possible at the time of this writing, because of the complexity of the equations to be solved, to derive an exact solution to this problem. It is indicated, however, that unless the measurements are carried out on highly homogeneous samples, *molecular weight* distributions determined from sedimentation constant distributions cannot be considered as true number distributions.

While Fig. 12 does not represent the "true" molecular weight distribution in the strict sense of the word, for all practical purposes it is the most accurate distribution which can be drawn until an exact solution of equation 27 is obtained or until

the molecular weight-sedimentation constant relationship is investigated for truly monodisperse material.

Acknowledgments.—The authors wish to thank Lt. Colonel Collins, Quartermaster Research and Development Laboratories, Harold W. Coles, Chemistry Laboratories, and especially W. H. Stahl, Biochemistry Laboratory Section, Philadelphia Quartermaster Depot, Department of the Army, Philadelphia, Pennsylvania, for their cooperation in permitting our using the Spinco ultracentrifuge and Klett electrophoresis apparatus.

G. L. Miller, Institute for Cancer Research and the Lankenau Hospital Research Institute, Philadelphia, Pennsylvania, kindly demonstrated important experimental techniques in regard to diffusion.

The authors also take pleasure in acknowledging D. L. Fuller, O. F. Hecht, P. C. Miller, S. Siggia, G. G. Stoner and J. M. Wilkinson for many interesting discussions and Professor J. G. Kirkwood of Yale University for guidance regarding the theory.

THE ADDITION OF IODINE TO TETRAMETHYLAMMONIUM IODIDE

BY H. W. FOOTE AND MICHAEL FLEISCHER^{1,2}

Department of Chemistry, Yale University, New Haven, Connecticut

Received May 3, 1952

The system tetramethylammonium iodide-iodine-toluene has been studied by the solubility method at 6 and at 25°. The compounds $(\text{CH}_3)_4\text{NI}_3$, $(\text{CH}_3)_4\text{NI}_5$ and $(\text{CH}_3)_4\text{NI}_{11}$ were found to be stable phases at both temperatures. In addition, the compound $(\text{CH}_3)_4\text{NI}_{10}$ was found at 6° and the compound $(\text{CH}_3)_4\text{NI}_9$ at 25°. The dissociation pressures of the compounds at these temperatures were calculated from the solubility data.

Introduction

One of the simplest and most convenient methods available for studying binary addition compounds is to add as a third component a liquid which dissolves only one of the two original components, and then determine the phase relations by solubility experiments in the ternary system. This method has been found especially useful in studying the addition of iodine to iodides, and by its use, the stability relations of the polyiodides of cesium,³ rubidium,⁴ potassium⁵ and ammonium⁶ have been worked out in this Laboratory. This work had shown that the stability of the alkali triiodides increased with increasing size of the cation. It seemed of interest to study the addition of iodine to tetramethylammonium iodide to determine whether the stabilities of the polyiodides formed were in accord with the previous work. In addition, the fact that tetramethylammonium iodide was reported in the literature to form a pentaiodide and enneaiodide increased the interest in this system,

since the only binary polyiodides formed by the alkalis are RbI_3 , CsI_3 and CsI_4 . The results were also expected to furnish an interesting comparison with the behavior of ammonium iodide, which forms only one stable polyiodide, NH_4I_3 .

The results obtained were so unusual that they were set aside for many years in the hope that further study could be made. In view of recent work⁷ on the structure of tetramethylammonium pentaiodide, it seems worthwhile to put our results on record in the hope that others may take up the problem.

Previous Work.—Addition compounds of iodine and tetramethylammonium iodide were first prepared by Weltzien,⁸ who obtained the triiodide and the pentaiodide by crystallization from alcohol solutions. Geuther,⁹ by the same method, prepared the pentaiodide and also the enneaiodide, $(\text{CH}_3)_4\text{NI}_9$. Much later, all three compounds were again prepared by the same method by Chattaway and Hoyle,¹⁰ who were unable, however, to prepare a heptaoidide. The only attempt to study their stability relations was that made by Strömholm,¹¹ who used the theoretically sound method of shaking

(1) From a thesis submitted by Michael Fleischer to the faculty of the Graduate School of Yale University in partial fulfillment of the requirements for the degree of Doctor of Philosophy, 1933.

(2) Present address—U. S. Geological Survey, Washington 25, D. C. Prof. Foote died on January 14, 1942.

(3) H. W. Foote, W. M. Bradley and Michael Fleischer, *THIS JOURNAL*, **37**, 21 (1933).

(4) H. W. Foote and Michael Fleischer, *ibid.*, **44**, 633 (1940).

(5) H. W. Foote and W. M. Bradley, *ibid.*, **36**, 673 (1932).

(6) H. W. Foote and W. M. Bradley, *ibid.*, **37**, 29 (1933).

(7) R. J. Hack and R. E. Rundle, *J. Am. Chem. Soc.*, **73**, 4321 (1951).

(8) C. Weltzien, *Ann.*, **99**, 1 (1856).

(9) A. Geuther, *ibid.*, **240**, 66 (1887).

(10) F. D. Chattaway and George Hoyle, *J. Chem. Soc.*, **123**, 654 (1923).

(11) D. Strömholm, *J. prakt. Chem.*, [2] **67**, 348 (1903).

the iodide with ether saturated with iodine, and then analyzing the resulting solution to determine the amount of iodine taken up by the salt. His results, which were not of great accuracy, indicated the existence of the tri-, penta- and enneaiodides.

Experimental Results.—The experimental procedure used and the purification of iodine and toluene have been described.⁶ Tetramethylammonium iodide was obtained from the Eastman Kodak Co. It was ground and kept in a desiccator. Six closely agreeing analyses on two different lots showed an iodine content of 63.16% (theoretical 63.13), which was unchanged after a recrystallization. The salt was therefore used without further purification.

The results obtained in the system $(\text{CH}_3)_4\text{NI}-\text{I}_2$ -toluene at 6 and at 25° are given in Table I. They were so unusual that many more experiments were made than had been contemplated. Every one made has been included in Table I. As tests showed that the solid phases were not solvated and that no $(\text{CH}_3)_4\text{NI}$ was dissolved by the toluene, the composition of the solid phase was calculated in each experiment from the known original charge and the determined iodine concentration of the solution. This calculation always affords results closer to the true composition of the solid phase than does direct analysis of the wet residue, which always contains excess iodine deposited by evaporating solvent. All compositions in Table I are given in weight per cent.

These results bring up a number of interesting points. It will be noted that at the low iodine end of the system there is but little difference in the iodine content of the solutions whether the solid is a mixture of $(\text{CH}_3)_4\text{NI}$ and $(\text{CH}_3)_4\text{NI}_3$ or a mixture of $(\text{CH}_3)_4\text{NI}_3$ and $(\text{CH}_3)_4\text{NI}_5$. The difference shows at both temperatures, but is so slight that it might be ascribed to experimental error were there no other evidence that the triiodide exists. The very low solubilities at these two isothermal invariant points show that both compounds are quite stable, having low dissociation pressures.

As the stability range of the triiodide is so small, it is nearly impossible to prepare it pure from toluene solutions. However, alcohol dissolves the compound as a whole where toluene dissolves iodine only, and the solubility relations in the former solvent are such that the triiodide can be recrystallized. This was done, using the conditions recommended by Chattaway and Hoyle,¹⁰ and excellent crystals were obtained. These contained no solvent, as shown by a closed tube test. Analysis showed 55.52% available iodine (theoretical 55.80%). These crystals were used as starting material in some of the determinations. The solubilities found agreed well with those found when the iodide was used.

The solubility relations in this portion of the system bring out both the weakness and strength of the method employed in this work to study polyiodides and their dissociation pressures by the use of solvents in which the iodides themselves are not soluble. If two compounds—in the present case the triiodide and penta-iodide—both happen to have very low dissociation pressures, the iodine concentration in solution is necessarily low at both iso-

TABLE I

 $t = 6^\circ, M = (\text{CH}_3)_4\text{N}$

No.	I_2 in soln., wt. %	I_2 in solid, wt. %	Solid phases present
1	0.036	6.51	MI and MI ₃
2	.033	50.00	MI and MI ₁
3	.034	54.95	MI and MI ₃
4	.045	58.41	MI ₃ and MI ₅
5	.045	59.34	MI ₃ and MI ₅
6	.047	59.81	MI ₃ and MI ₅
7	.053	69.85	MI ₃ and MI ₅
8	.039	70.05	MI ₃ and MI ₅
9	.49	71.68	MI ₅
10	.97	71.72	MI ₅
11	1.51	71.74	MI ₅
12	1.61	72.53	MI ₅ and MI ₁₀
13	1.58	78.08	MI ₅ and MI ₁₀
14	1.59	81.87	MI ₅ and MI ₁₀
15	1.60	83.70	MI ₅ and MI ₁₀
16	1.58	83.98	MI ₅ and MI ₁₀
17	1.70	85.39	MI ₁₀
18	1.71	85.01	MI ₁₀
19	1.77	84.95	MI ₁₀
20	1.85	84.78	MI ₁₀
21	1.88	85.04	MI ₁₀
22	1.94	85.07	MI ₁₀
23	1.99	84.99	MI ₁₀
24	2.00	84.98	MI ₁₀
25	2.19	85.02	MI ₁₀
26	2.27	85.33	MI ₁₀ and MI ₁₁
27	2.28	85.47	MI ₁₀ and MI ₁₁
28	2.28	85.68	MI ₁₀ and MI ₁₁
29	2.31	85.92	MI ₁₀ and MI ₁₁
30	2.57	86.33	MI ₁₁
31	5.71	86.41	MI ₁₁
32	9.41	86.67	MI ₁₁
33	10.11	88.21	MI ₁₁ and I ₂
34	10.31	93.79	MI ₁₁ and I ₂
$t = 25^\circ$			
35	0.067	11.32	MI and MI ₁
36	0.066	50.00	MI and MI ₃
37	0.088	59.52	MI ₃ and MI ₅
38	0.083	70.00	MI ₃ and MI ₅
39	0.56	71.48	MI ₅
40	1.95	71.77	MI ₅
41	2.56	75.91	MI ₅ and MI ₉
42	2.54	82.12	MI ₅ and MI ₉
43	2.79	83.47	MI ₉
44	2.81	83.50	MI ₉
45	2.83	83.55	MI ₉
46	2.86	83.53	MI ₉
47	3.26	83.55	MI ₉
48	3.53	83.66	MI ₉ and MI ₁₁
49	3.54	84.10	MI ₉ and MI ₁₁
50	3.55	84.74	MI ₉ and MI ₁₁
51	3.55	85.18	MI ₉ and MI ₁₁
52	3.64	86.33	MI ₁₁
53	4.02	86.32	MI ₁₁
54	5.20	86.38	MI ₁₁
55	13.55	86.29	MI ₁₁
56	14.74	86.53	MI ₁₁
57	15.61	86.90	MI ₁₁ and I ₂
58	15.52	92.14	MI ₁₁ and I ₂

thermal invariant points, and the difference in concentration at the two points may be within the experimental error of determination. In such a case, the solubility determinations would not be sufficient to prove the existence of the lower of the two compounds. On the other hand, knowing that both can exist, it is possible to calculate the dissociation pressures of the compounds from the solubility determinations.

Using a solvent, for instance alcohol, which dissolves both components, the range of concentrations in which a compound is stable may be greatly enlarged or reduced. In the present case, the solubilities in alcohol are sufficiently different to permit crystallization of both the triiodide and the penta-iodide. The dissociation pressures could not, however, be calculated from the solubilities at the isothermal invariant points, since the solution contains both components.

The existence of the penta-iodide at both temperatures is very satisfactorily demonstrated by the results. The average of the five results on this compound is 71.68% available iodine; the formula $(\text{CH}_3)_4\text{NI}_6$ requires 71.63%.

The results also show very clearly the existence over a wide range of concentrations at both temperatures of a compound not previously prepared, $(\text{CH}_3)_4\text{NI}_{11}$. The average of the eight closely agreeing results on this compound is 86.41% available iodine; the formula above requires 86.33%. This is the first compound reported which has ten atoms of iodine added to an iodide. At first glance, it seems rather surprising that a compound stable over such a large concentration range should have been missed by previous workers. However, they all crystallized their preparations from alcohol solutions. A few experiments in the iodine-rich portion of the system $(\text{CH}_3)_4\text{NI}-\text{I}_2-95\%$ alcohol showed that the compound $(\text{CH}_3)_4\text{NI}_{11}$ is stable only over an extremely small concentration range in this solvent.

Besides the three polyiodides already discussed, there is unquestionably a fourth compound present at each temperature. Much to our surprise, the results showed clearly that two different compounds were present at the two temperatures. At 6°, the average of the nine results on the compound was 85.03% available iodine, and seven of the nine differed from the average by less than 0.1%; the formula $(\text{CH}_3)_4\text{NI}_{10}$ requires 85.03%. However, the five results at 25° show just as convincingly that the compound present at that temperature was $(\text{CH}_3)_4\text{NI}_9$. The average of the five results is 83.52% available iodine; the formula $(\text{CH}_3)_4\text{NI}_9$ requires 83.47%, and in each of the five results, the composition found differs from the theoretical by less than 0.1%. Furthermore, it should be noted that, at 6°, not only experiments 17 to 25, but also experiments 15 and 16 definitely exclude $(\text{CH}_3)_4\text{NI}_9$ as the solid phase. Likewise, at 25°, not only experiments 43 to 47, but also experiments 48, 49, and 50 exclude $(\text{CH}_3)_4\text{NI}_{10}$ as the solid phase.

It was thought possible that the results might be due to metastable solid phases at one or both temperatures. To test this possibility, a mixture was rotated at 6° in the usual way. The solution was analyzed, and the results given under No. 21 in

Table I were obtained. Leaving the solid phase undisturbed, a calculated amount of iodine was added, and the bottle was resealed and rotated a week at 25°. The solution was again analyzed with the results given under No. 46 in Table I. Another bottle was rotated first at 25°, the results obtained being given under No. 44 in Table I. Leaving the solid phase undisturbed, toluene was added, and the bottle was resealed and rotated a week at 6°, and the solution analyzed with the results given under No. 22 in Table I. It is evident that the $(\text{CH}_3)_4\text{NI}_{10}$ formed at 6° changed to $(\text{CH}_3)_4\text{NI}_9$ at 25° and *vice versa*. The results cannot be due to the presence of metastable phases. There must, therefore, be a transition temperature at some temperature between 6 and 25°.

The existence of three such compounds as $(\text{CH}_3)_4\text{NI}_9$, $(\text{CH}_3)_4\text{NI}_{10}$ and $(\text{CH}_3)_4\text{NI}_{11}$ is certainly surprising, perhaps even improbable. It is rather unsafe, however, to speculate on what might be expected in addition compounds. Those reported here are certainly no more unexpected than CsI_3 and CsI_4 , or $\text{CdSO}_4 \cdot 8/3\text{H}_2\text{O}$, or the numerous hydrates of FeCl_3 , to cite some well-authenticated compounds.

The dissociation pressures of the binary polyiodides have been calculated by the method previously used.⁴ Table II gives the results obtained,

TABLE II

Solids present	I ₂ in soln., wt. %	I ₂ in soln., mol. %	<i>c/c₀</i>	Dissociation pressure, mm.
<i>t</i> = 6°, M = $(\text{CH}_3)_4\text{N}$				
MI ₁₁ and I ₂	10.21	3.96 (<i>c₀</i>)
MI ₁₁ and MI ₁₀	2.285	0.84	0.212	0.0116
MI ₁₀ and MI ₆	1.59	.58	.147	.0080
MI ₆ and MI ₃	0.046	.017	.0042	.00023
MI ₃ and MI	0.034	.012	.0031	.00017
<i>t</i> = 25°				
I ₂ and MI ₁₁	15.57	6.27 (<i>c₀</i>)
MI ₁₁ and MI ₉	3.54	1.31	0.209	0.0656
MI ₉ and MI ₆	2.55	0.94	.150	.0469
MI ₆ and MI ₃	0.086	.031	.0050	.00156
MI ₃ and MI	0.067	.024	.0039	.00121

assuming the vapor pressure of iodine to be 0.0546 and 0.313 mm. at 6 and 25°, respectively. These values, obtained by interpolation of the data given in the "International Critical Tables," differ slightly from the values given by Gillespie and Fraser,¹² 0.0556 and 0.309 mm. at 6 and 25°, respectively. The older values were used so that the dissociation pressures calculated would be consistent with those given in our earlier papers. For the three polyiodides present at both temperatures, the heats of dissociation have been calculated by the van't Hoff equation. ΔH is calculated to be -15,000 calories for $(\text{CH}_3)_4\text{NI}_{11}$, -16,600 calories for $(\text{CH}_3)_4\text{NI}_6$ and -17,000 calories for $(\text{CH}_3)_4\text{NI}_3$.

It may be noted that preliminary experiments on the system $(\text{CH}_3)_4\text{NI}-\text{I}_2$ -benzene indicated that the binary polyiodides richer in iodine than the penta-iodide do not appear as solid phases, being replaced by two or more ternary polyiodides containing benzene of crystallization. In this respect, the behav-

(12) L. J. Gillespie and L. H. D. Fraser, *J. Am. Chem. Soc.*, **58**, 2260 (1936).

ior of $(\text{CH}_3)_4\text{NI}$ differs from that of NH_4I , which forms no ternary polyiodides from benzene solution,

and resembles that of CsI , which forms one, and of RbI , which forms two such compounds.

ESTIMATION OF HETEROGENEITY FROM DIFFUSION MEASUREMENTS

By P. A. CHARLWOOD¹

Courtauld Institute of Biochemistry, Middlesex Hospital Medical School, London, W.1, England

Received May 7, 1952

An expression has been derived for the standard deviation of the distribution of diffusion constants of a mixture. It requires the calculation of the fourth moments of refractive index gradient curves, or equivalent calculations from interference patterns. A procedure has been worked out for using interference patterns. An empirical curve-fitting method is of great use in some cases in obtaining corrected values of $D_{2,0}$ and $D_{4,2}/D_{2,0}$. Both experimental and theoretical patterns confirm that the use of moments higher than the second is impracticable in cases where the degree of heterogeneity is low. Efforts should, therefore, be made to attain a high degree of accuracy in the measurement of D_A and $D_{2,0}$ for proteins.

Introduction

Recently considerable attention has been given to the problem of relating the heterogeneity of proteins to their electrophoretic behavior. The general method followed has been to observe the manner in which certain mathematical characteristics of the electrophoretic patterns change with time.²⁻⁸ Similarly, the related problems of determining the distributions of sedimentation constants and molecular weights from ultracentrifuge data have been studied.⁹⁻¹³ Little comparable information is available on the subject of diffusion.^{10,11,14}

Until a few years ago, all accurate diffusion experiments relied upon the Lamm¹⁵ scale method, or various schlieren optical methods, from which the refractive index gradient curves of diffusing boundaries are obtained. Different ways of defining diffusion constant, in terms of the methods which may be used to analyze these curves, have been discussed by Gralén.^{10,16} In the case of ideal diffusion of a single, homogeneous substance all treatments lead to the same result (within, of course, the appropriate limits of error). Otherwise, averages of various types ensue. Thus, the average D_A , obtained by the height and area method, is defined by

$$D_A^{-1/2} = \sum \alpha_i D_i^{-1/2} \quad (1)$$

where the molecular species of diffusion constant D_i forms a fraction α_i of the mixture, α_i being expressed in terms of the total refractive increment. This result, given by Quensel,¹⁴ assumes independent and ideal diffusion of all constituents. Gralén¹⁶

has shown that the mean value, $D_{2,0}$, derived by the statistical method is

$$D_{2,0} = \sum \alpha_i D_i / \sum \alpha_i = \sum \alpha_i D_i \quad (2)$$

If the specific refractive increments of all components may be regarded as identical, the proportions, α , then refer to weight concentrations, and $D_{2,0}$ becomes a weight average value.

In an attempt to use the ratio $D_{2,0}/D_A$ as a measure of polydispersity, Gralén¹⁰ encountered difficulties such as skew boundaries, values of $D_{2,0}/D_A$ distinctly lower than unity (contrary to theory), and other anomalies due to the non-ideal behavior of his cellulose solutions. The method pointed out by Herdan,¹⁷ for deriving the standard deviations of molecular weight distributions from different types of average, is capable of extension to diffusion constants. The object of the present work was to explore the possibility of applying the method, not only to refractive index gradient curves, but also to the interference patterns now used for the accurate measurement of diffusion.¹⁸⁻²⁶

Theory

From the formulas given by Gralén¹⁶

$$D_{2,0} = m_2/2m_0t \quad (3)$$

and

$$D_{4,2} = m_4/6m_2t \quad (4)$$

where m_0 , m_2 and m_4 refer, respectively, to the area of the refractive index gradient curve, and its second and fourth moments about the maximum ordinate. The appropriate apparatus constants are assumed to be taken into account. For a single substance, i , behaving ideally, equations 3 and 4 give, by multiplication

$$m_4 = 12m_0t^2D_i^2 \quad (5)$$

For a mixture of such components, diffusing ideally and independently about a common origin, the refractive index gradient curve which results is ob-

(1) I.C.I. Research Fellow in the University of London.

(2) R. A. Alberty, *J. Am. Chem. Soc.*, **70**, 1675 (1948).

(3) R. A. Alberty, *THIS JOURNAL*, **53**, 114 (1949).

(4) R. A. Alberty, E. A. Anderson and J. W. Williams, *ibid.*, **52**, 217 (1948).

(5) E. A. Anderson and R. A. Alberty, *ibid.*, **52**, 1345 (1948).

(6) R. L. Baldwin, P. M. Laughton and R. A. Alberty, *ibid.*, **55**, 111 (1951).

(7) R. A. Brown and J. R. Cann, *ibid.*, **54**, 364 (1950).

(8) D. G. Sharp, M. H. Hebb, A. R. Taylor and J. W. Beard, *J. Biol. Chem.*, **142**, 217 (1942).

(9) R. L. Baldwin and J. W. Williams, *J. Am. Chem. Soc.*, **72**, 4325 (1950).

(10) N. Gralén, Inaugural Dissertation Uppsala, 1944.

(11) I. Jullander *Arkiv. Kemi Mineral Geol.*, **21**, No. 8, 1 (1945).

(12) W. D. Lansing and E. O. Kraemer, *J. Am. Chem. Soc.*, **57**, 1369 (1935).

(13) M. Wales, F. T. Adler and K. E. Van Holde, *THIS JOURNAL*, **55**, 145 (1951).

(14) O. Quensel, Dissertation, Uppsala, 1942.

(15) O. Lamm, *Nova Acta Regiae Soc. Sci. Upsalienis*, **10**, 1 (1937).

(16) N. Gralén, *Kolloid Z.*, **95**, 188 (1941).

(17) G. Herdan, *Nature*, **163**, 139 (1949).

(18) C. A. Coulson, J. T. Cox, A. G. Ogston and J. S. I. Philpot, *Proc. Roy. Soc. (London)*, **A192**, 382 (1948).

(19) L. J. Gosting and M. S. Morris, *J. Am. Chem. Soc.*, **71**, 1998 (1949).

(20) G. Kegeles and L. J. Gosting, *ibid.*, **69**, 2516 (1947).

(21) L. G. Longworth, *ibid.*, **69**, 2510 (1947).

(22) L. G. Longworth, *Rev. Sci. Instruments*, **21**, 524 (1950).

(23) A. G. Ogston, *Proc. Roy. Soc. (London)*, **A196**, 272 (1949).

(24) A. G. Ogston, *Biochem. J.*, **45**, 189 (1949).

(25) H. Svensson, *Acta Chem. Scand.*, **5**, 72 (1951).

(26) H. Svensson, *ibid.*, **5**, 1410 (1951).

TABLE I
EXAMPLE OF CURVE FITTING PROCEDURE, AS APPLIED TO BOVINE PLASMA ALBUMIN RESULTS
Temperature 25.0°, $v = 30.74$, phosphate buffer $\mu = 0.1$, pH 7.4; all X_r values are expressed in cm.

A. Time of diffusion ~ 200 sec.					
r	23.75	24.75	25.75	26.75	30.74
X_r (measured)	0.1955	0.1619	0.1300	0.1005	0.0000
X_r (from curve)	0.19547	0.16189	0.13019	0.10036	0.00000
Difference (microns)	-0.3	-0.1	+1.9	-1.4	0.0
B. Time of diffusion ~ 380 sec.					
r	22.75	23.75	24.75	25.75	30.74
X_r (measured)	0.1773	0.1507	0.1247	0.0991	0.0000
X_r (from curve)	0.17771	0.15021	0.12422	0.09972	-0.00005
Difference (microns)	+4.1	-4.9	-4.8	+6.2	-0.5

tainable by addition of the ordinates of the individual curves. Consequently, moments of the composite curve can be derived by addition of the corresponding moments of the contributing curves. Thus, if component i forms a proportion α_i (defined above) of the total, and m_0 represents the area under the main curve, the contribution to the fourth moment made by this component is $12 m_0 \alpha_i D_i^2$. By addition, for the composite curve

$$m_4 = 12 m_0 \sum \alpha_i D_i^2$$

or

$$m_4/12 m_0^2 = \sum \alpha_i D_i^2 = D_{4,2} D_{2,0} \quad (6)$$

The following relation holds, analogous to the equations of Herdan,¹⁷ for the standard deviation, σ , of $D_{2,0}$

$$\sigma = \sqrt{\{(\sum \alpha_i D_i^2 / \sum \alpha_i) - (\sum \alpha_i D_i / \sum \alpha_i)^2\}} = \sqrt{\{D_{4,2} D_{2,0} - D_{2,0}^2\}} \quad (7)$$

$$\sigma / D_{2,0} = \sqrt{\{(D_{4,2} / D_{2,0}) - 1\}} = \sqrt{\{(m_4 m_0 / 3 m_2^2) - 1\}} \quad (8)$$

The requisite moments can be computed directly from refractive index gradient curves; but, in order to apply this formula to interference patterns of the Gouy type, it is necessary to find methods of deriving both second and fourth moments of the equivalent curves. The equation given by Ogston²⁴ is, in his notation

$$m_2/2m_0 = D_{2,0} = \int_0^\infty \left(\frac{\lambda}{2} \frac{\partial r}{\partial \theta_r}\right)^2 \theta_r dx / 2 \int_0^\infty \theta_r dx = \frac{\lambda^2}{24v} \int_0^\infty \theta_r d \left[\frac{\partial r}{\partial \theta_r} \right]^2 = \frac{F^2 \lambda^2}{24v} \int_0^\infty X_r d \left[\frac{\partial r}{\partial X_r} \right]^2 \quad (9)$$

We denote the integral by the symbol I_3 , so that

$$D_{2,0} = F^2 \lambda^2 I_3 / 24v$$

In a similar manner

$$m_4/12m_0 = D_{4,2} D_{2,0} = \int_0^\infty \left(\frac{\lambda}{2} \frac{\partial r}{\partial \theta_r}\right)^4 \theta_r dx / 12 \int_0^\infty \theta_r dx = \frac{\lambda^4}{960v} \int_0^\infty \theta_r d \left[\frac{\partial r}{\partial \theta_r} \right]^4 = \frac{F^4 \lambda^4}{960v} \int_0^\infty X_r d \left[\frac{\partial r}{\partial X_r} \right]^4 \quad (10)$$

This integral is denoted by I_5 , so that

$$D_{4,2} D_{2,0} = F^4 \lambda^4 I_5 / 960v$$

From equations 9 and 10, at any given time

$$D_{4,2} / D_{2,0} = 3c I_5 / 3 I_3^2 \quad (11)$$

Ogston²⁴ has shown that I_3 is given fairly accurately by computing the sum $\sum X_r \delta(\delta r / \delta X_r)^3$ over the whole range of interference bands from $r = 0$ to $r = v$. It is feasible to compute I_5 in an analogous manner, when equation 11 can be employed. Of course, the absolute value of $D_{2,0}$ can be obtained only from values of I_3 at two or more times. Equations 8 and 11 were tested by calculations based on normal Gaussian curves (see Discussion).

Experimentally it was not always possible to locate all the inner interference minima, and sometimes the last few occupied anomalous positions, for reasons mentioned later (see also reference 20). The terms representing these inner bands make substantial contributions to I_3 and I_5 . In order, therefore, to improve the accuracy an empirical curve-fitting procedure was evolved. The values of X corresponding to the last four measured minima (and also $X = 0$, which refers to $r = v$) were expressed in terms of r . Of the functions proposed, a simple parabolic one proved to have the dual advantages of representing X with sufficient accuracy (Table IA,B), and of providing simple integrations. Thus if

$$X_r = a + br + cr^2 \quad (12)$$

the constants a , b and c can be determined by the standard procedure of minimizing the squares of the deviations of X . Then, as

$$(d\theta_r / dX_r) = 1/(b + 2cr), \quad d(d\theta_r / dX_r)^2 = \{-6c/(b + 2cr)^3\} dr$$

and

$$d(d\theta_r / dX_r)^4 = \{-10c/(b + 2cr)^5\} dr$$

Substituting y for $(b + 2cr)$

$$\int X_r d \left[\frac{\partial r}{\partial X_r} \right]^2 = -6 \int \{c(a + br + cr^2)/(b + 2cr)^3\} dr = -3 \int \{1/4cy^2 - (b^2 - 4ac)/y^3\} dy = \left[3/4cy - (b^2 - 4ac)/y^2 \right]_{y_1}^{y_2} \quad (13)$$

and similarly

$$\int X_r d \left[\frac{\partial r}{\partial X_r} \right]^4 = \left[5/12cy^3 - (b^2 - 4ac)/y^4 \right]_{y_1}^{y_2} \quad (14)$$

The limits of integration are determined as follows. That part of I_3 or I_5 obtained by summation is worked out for values of r from 0 to, say, 23.75. Since the products $X_r \delta(\delta r / \delta X_r)^3$ and $X_r \delta(\delta r / \delta X_r)^5$ for $r = 23.75$ cover part of the interval between $r = 23.75$ and $r = 24.75$, one limit for the integrations is taken to correspond, in this case, to $r = 24.25$. The other, of course, corresponds to $r = v$. Illustrations of the results of applying these parabolic end-corrections are given in Table II.

Experimental Conditions and Limitations

Materials Used.—Diffusion experiments were carried out using glycine, sucrose, bovine plasma albumin, or mixtures of these. Sucrose and glycine of "Analar" quality were weighed out and solutions made up volumetrically. No special precautions (*e.g.*, drying of the solids) were observed. The glycine-sucrose mixture was made by mixing

TABLE II
SUMMARY OF RESULTS OF DIFFUSION MEASUREMENTS

		$D_{4,2}/D_{2,0}$									
		D_A		$D_{2,0}$			Obsd.				
		Obsd.	Expected	Uncor.	Cor.	Expected	First time mark		A later time mark		
Temp.,	Sucrose	52.2	52.0	51.7	52.0	52.0	0.983	0.977	0.976	0.961	1.000
24.9°	Sucrose + glycine	72.0	72.3	77.0	78.0	79.5	1.143	1.033	1.009	1.046	1.119
Temp.,	Bovine plasma albumin	6.81	6.87	6.86	7.10		0.970	0.997	0.952	0.987	
25.0°	Bovine plasma albumin + sucrose	20.8	20.0	74.7	35.1	35.8	1.545	1.209	1.990	1.362	1.348

25 ml. of each individual solution. The bovine plasma albumin was a crystalline "Armour" product, as used by Creeth.²⁷ A solution of about 1% concentration was dialyzed against phosphate buffer (ionic strength 0.1, pH 7.4). The albumin-sucrose mixture was prepared by mixing 10 ml. of the dialyzed protein solution with 20 ml. of the phosphate buffer in which had been dissolved a weighed amount of sucrose.

Diffusion Experiments.—These were made in the Gouy diffusometer^{18,23} according to the technique described by Creeth.²⁷ There were few departures from this procedure. With solutions containing sucrose or glycine, time-marks were recorded at intervals of 15 seconds, and the boundary was sharpened several times during the period of temperature equilibration. The only other modification was the use of a thermostated boundary former, to be described elsewhere. The temperature during these experiments was 25°. All results have been expressed in units of 10^{-7} cm.² sec.⁻¹, corrected, where necessary, for buffer viscosity.

The general conditions used should have been such that the record possessed the following characteristics. At the first time-mark used for measurements the boundary should have attained a symmetrical configuration, producing interference bands in the correct relative positions, but the layers of solution which significantly affect the positions of the innermost bands should not have spread beyond the confines of the boundary stop. As the light intensity is relatively greater among the inner bands, the rate of scanning had to be high enough to allow the accurate location of these bands in the record, but not so high that the outer minima and reference trace were severely underexposed. However, the accuracy of location of the outermost minimum is not so critical in the estimation of $D_{2,0}$ or σ as in the determination of D_A . The positions of the minima, more particularly the inner ones, are affected by the presence of Fraunhofer bands.²³ The difficulties associated with the inner bands may be compared with those which arise in locating the base-line near the ends of Lamm¹⁸ scale or schlieren curves.¹⁰ This problem is even more acute when moments higher than the second are under consideration.^{6,28} The errors just mentioned would be greatly diminished by the wedge filter and the shape of the stop used in the American version of the apparatus.²⁹

In all experiments the total solute concentration was about 1% by weight, giving about 30 interference minima. If lower concentrations had been used, a cell with a longer optical path (*e.g.*, references 22 and 30) would have been required in order to obtain a reasonable number of bands for the computations.

Results and Discussion

The computation of the moments of a continuous function from measurements made at discrete intervals involves errors which can in some cases be allowed for. To test the magnitude of such errors for a normal Gaussian curve, the expression $m_4 m_0 / 3m_2^2$ was computed for $y = e^{-x^2}$ between the limits $x = \pm 4$, ordinates being taken at intervals of 0.1 unit. The value obtained was 1.0013, an error of rather more than 0.1% being involved. A similar computation, based on a theoretical interference

(27) J. M. Creeth, *Biochem. J.*, **51**, 10 (1952).

(28) E. M. Bevilacqua, E. B. Bevilacqua, M. M. Bender and J. W. Williams, *Ann. N. Y. Acad. Sci.*, **46**, 309 (1945).

(29) L. J. Gosting, E. M. Hanson, G. Kegeles and M. S. Morris, *Rev. Sci. Instruments*, **20**, 209 (1949).

(30) H. Svensson, *Acta Chem. Scand.*, **3**, 1170 (1949).

trace and using equation 11, gave a somewhat larger error (see below).

The experimental results are shown in Table II. Corrected values refer to the use of the parabolic curve-fitting method for the innermost bands. The expected values are based upon the following information in the literature: for sucrose the work of Gosting and Morris,¹⁹ for glycine the value given by Ogston¹⁸ at 20°, and for the bovine albumin the data of Creeth.²⁷

C_t values²¹ have been calculated at two different times for the interference patterns of sucrose and of bovine plasma albumin, as shown in Table IIIA, B. Departure from a constant value may be attributable to various causes, such as errors in the measurement of v or X_r . Calculation disposes of this suggestion, which would only be permissible on the basis of errors far exceeding the known errors of measurement. That the drift is not due mainly to a defect of the cylindrical lens^{22,25} is clear from its disposition in the optical system, and the fact that in Table IIIA the C_t values tend to increase, while in IIIB they are more inclined to decrease. The main cause of the deviations must, therefore, be the non-Gaussian form of the boundary, ascribable to either (a) the lapse of too short a time since the formation of the original sharp, but arbitrarily shaped boundary, (b) concentration dependence of the diffusion constant, or (c) presence of more than one molecular species. For sucrose (c) can be ignored, and (b) is disproved by the results of Gosting and Morris.¹⁹ Hence, it follows that the main reason is (a), arising from the restrictions imposed on the times of observations (see Experimental). The greater regularity of C_t at the later time (Table IIIA) confirms this. The variation in C_t values is still some 2-3 times larger than that shown by Gosting and Morris,¹⁹ taking into account the absolute magnitudes.

The values of D_A and $D_{2,0}$ for both sucrose and bovine plasma albumin show good agreement with the results of previous workers. The effect of the end-corrections on the $D_{2,0}$ values is fairly small. Although $D_{2,0}$ for bovine albumin is some 4% greater than D_A the difference is not highly significant. Thus, Ogston,²⁴ working with lactoglobulin, found $D_A = 7.15$ and $D_{2,0} = 6.94-7.02$. That his ratio $D_{2,0}/D_A$ is less than unity is reasonably attributable to experimental error, as is the case with many of the results of Gralén¹⁰ and Pedersen.³¹ In some cases Gralén¹⁰ did obtain ratios much too low to be explained by the ordinary errors of measurement. Table II shows values of $D_{4,2}/D_{2,0}$ less than unity for both sucrose and the albumin. This

(31) K. O. Pedersen, "Ultracentrifugal Studies on Serum and Serum Fractions," Almqvist and Wiksells, A.B., Uppsala, Sweden, 1945.

TABLE III

C_t VALUES FOR SUCROSE AND FOR BOVINE PLASMA ALBUMIN

A, sucrose, temp. 24.9°, $v = j_m = 28.97$	B, bovine plasma albumin, temp. 24.9°, $v = j_m = 30.74$, phosphate buffer pH 7.4, $\mu = 0.1$			
	Approximate times of diffusion (sec.)			
	45	105	200	515
	C _t (cm.)	C _t (cm.)	C _t (cm.)	C _t (cm.)
0	1.4802	0.9628	1.7142	1.1304
1	1.4854	.9628	1.7149	1.1310
2	1.4882	.9642	1.7207	1.1304
3	1.4905	.9647	1.7238	1.1304
4	1.4912	.9644	1.7299	1.1310
5	1.4952	.9646	1.7319	1.1318
6	1.4976	.9646	1.7334	1.1309
7	1.4961	.9640	1.7343	1.1309
8	1.4986	.9651	1.7345	1.1299
9	1.5051	.9657	1.7348	1.1285
10	1.5040	.9648	1.7347	1.1279
11	1.5067	.9642	1.7345	1.1274
12	1.5076	.9671	1.7338	1.1263
13	1.5075	.9645	1.7383	1.1284
14	1.5077	.9657	1.7384	1.1274
15	1.5151	.9656	1.7343	1.1300
16	1.5121	.9708	1.7355	1.1284
17	1.5166	.9697	1.7333	1.1257
18	1.5174	.9700	1.7272	1.1250
19	1.5162	.9662	1.7217	1.1233
20	1.5175	.9647	1.7193	1.1159
21	1.5220	.9670	1.7242	1.1170
22	1.5066	.9767	1.7089	1.1180
23	1.5178	.9626	1.7003	1.0996
24	1.5368		1.6927	
25	1.5264			

must be ascribed partly to the non-ideal shape of the boundary, but also to the errors consequent upon the use of a discontinuous computation to approximate to an integral. As a check on the latter an ideal set of X_r values was calculated, giving a constant C_t for the r values of the sucrose boundary, *i.e.*, $r = 0$ to $r = 28.97$. Computation of these values over the whole range gave $D_{4,2}/D_{2,0} = 1.0055$. In order to make an even closer comparison with the results derived from the experimental X_r values, the ideal values were used to compute the appropriate products from $r = 0$ to $r = 24.25$, and the curve-fitting procedure was adopted for the interval $r = 24.25$ to $r = 28.97$. The ratio thus obtained was 0.980, considerably closer to the experimental figures.

The sucrose-glycine mixture gave values of D_A and $D_{2,0}$ in satisfactory agreement with expectation, and $D_{4,2}/D_{2,0}$ ratios all greater than unity. From the corrected ratios, $\sigma/D_{2,0}$ becomes 18 and 22% at two different times, compared with the known value of 34.5%. The sucrose-bovine plasma albumin mixture, consisting of components possessing widely different diffusion constants, presented difficulties which were scarcely noticeable with the previous mixture. A compromise was essential in selecting the scanning speed and the time-marks at which measurements were made. The value of D_A agreed fairly well with that anticipated, but the uncorrected value of $D_{2,0}$ was more than double theoretical. This was due to the anomalous positions of the innermost bands, as indicated in

TABLE IV

THE POSITIONS OF THE INTERFERENCE MINIMA OBTAINED WITH A MIXTURE OF SUCROSE AND BOVINE PLASMA ALBUMIN
Temp. 25.0°, $v = 29.29$, phosphate buffer $\mu = 0.1$, pH 7.4, time of diffusion ~ 160 sec.

r	X_r (cm.)	$-\delta X_r$ (cm.)	r	X_r (cm.)	$-\delta X_r$ (cm.)
8.75	0.5398	0.0488	17.75	0.2158	0.0261
9.75	.4910	.0432	18.75	.1897	.0250
10.75	.4478	.0419	19.75	.1647	.0237
11.75	.4059	.0369	20.75	.1410	.0214
12.75	.3690	.0350	21.75	.1196	.0178
13.75	.3340	.0321	22.75	.1018	.0233
14.75	.3019	.0298	23.75	.0785	.0355
15.75	.2721	.0289	24.75	.0430	
16.75	.2432	.0274			

Table IV. Successive values of $-\delta X_r$ should form a decreasing sequence. This did not hold for the last two measurements, due, no doubt, to the inevitable compromise mentioned above. In applying the parabolic correction method the anomalous bands were omitted. Then $D_{2,0} = 35.1$, in excellent agreement with the calculated figure. For the reason just discussed, the uncorrected $D_{4,2}/D_{2,0}$ ratios were also much too high, but the corrected values gave $\sigma/D_{2,0}$ as 46 and 60%, respectively, at two times, the expected percentage being 59.

In addition to the experimental results described here, those of Gralén¹⁶ and of Svensson²⁶ are in a form suitable for the calculation of $D_{4,2}/D_{2,0}$ ratios. As a measure of the consistency of Gralén's values for gluten, we obtain $\sigma/D_{2,0} = 24, 35$ and 34% at the three different times recorded in Table I of reference 16; but there is no absolute value to serve as a standard. The integral type of interference method used by Svensson^{25,26} lends itself very simply to the computation of various moments. The quantity $D_{4,2}/D_{2,0}$, derived from the figures of Svensson²⁶ for sucrose, was 0.935. As this seemed very low, the calculation was repeated on the set of figures which would apply to a normal Gaussian boundary.²⁵ This produced a result, 0.929, even lower still, from which it must be concluded that the errors due to computing at finite intervals are much greater than in the Gouy interference method.

The ratio $D_{4,2}/D_{2,0}$ is preferable to $D_{2,0}/D_A$, because it gives the standard deviation of the distribution of diffusion constants (whatever this distribution may be), which is the measure of dispersion most commonly used. However, in view of the difficulties of carrying out sufficiently precise measurements, and the unavoidable errors of computation, it seems unlikely that it will be possible to make use of the ratio $D_{4,2}/D_{2,0}$ in cases where it would be most useful and interesting, *i.e.*, when $\sigma/D_{2,0}$ is small. The best practical approach to the use of diffusion measurements for characterizing protein heterogeneity seems to lie in placing emphasis on precise determinations of $D_{2,0}$ and D_A , their ratio being used as a semi-quantitative estimate.¹⁰ The American form of the Gouy interference method²⁹ is probably sufficiently advanced to deal with low molecular weight materials, but further work will almost certainly be necessary to discover what refinements of technique will produce results of comparable accuracy with proteins.²⁷

Symposia in Book Form

AGRICULTURAL CONTROL CHEMICALS

- Labeling Requirements for Insecticide Controls for Economic Poisons under Federal Law
- Public Health Aspects of Agricultural Chemicals
- Pharmacology and Toxicology of Some Important Economic Poisons
- Toxicity of Spray Residue of Fresh and Processed Fruits and Vegetables
- Some Poisonous Residue Factors in Use of Two New Organic Insecticides
- Use of Residual Spray Materials in a Typical Food Industry
- Plus 52 other papers

PRICE.....\$2.50 per Copy



ANALYTICAL METHODS IN THE FOOD INDUSTRY

- Measurement of Filth in Foods by Microanalytical Methods
- Determination of Water in Some Dehydrated Foods
- Determination of Amino Acids
- Some Aspects of Control Methods in the Canned Food Industry
- Measurement of Color Changes in Foods
- Quality Control Methods in Frozen Food Production and Distribution
- Measurement of Oxidative Rancidity

PRICE.....\$1.50 per Copy



ORDER FROM:

SPECIAL PUBLICATIONS DEPT. AMERICAN CHEMICAL SOCIETY 1155 16th ST., N.W., WASHINGTON 6, D. C.

Announcing - - - -

- - - Advances in
Chemistry

Series

Volume

No. 6

AZEOTROPIC DATA

Table I. Binary Systems

Formula	B-Component Name	B.P., ° C.	Azeotropic Data B.P., ° C. Wt. % A	Ref.
1 A	Argon	-186	Nonazeotrope, V-L	164
2 Na	Nitrogen, 500-1500 mm.	-195	Nonazeotrope	255
3 AgCl	Silver Chloride	1550	Nonazeotrope	263
4 Cl ₂ Pb	Lead chloride	954	Nonazeotrope	263
5 BCl ₃	Boron Chloride	11.5	Nonazeotrope	263
6 BiH ₃	Bismuth hydride	-92.5	Nonazeotrope	262
7		-100	Nonazeotrope	262
8		100	Nonazeotrope	262
9		180	Nonazeotrope	262
10		43	Nonazeotrope	262
11		77.2	Nonazeotrope	262
12		62	Nonazeotrope	262
13		60	Nonazeotrope	262
14		65	Nonazeotrope	262
15		80	Nonazeotrope	262
16		42	Nonazeotrope	262
17		52	Nonazeotrope	262
18		62	Nonazeotrope	262
19		263	Nonazeotrope	262
20		263	Nonazeotrope	262
21		262	Nonazeotrope	262
22		262	Nonazeotrope	262
23		262	Nonazeotrope	262
24		262	Nonazeotrope	262
25		262	Nonazeotrope	262
26		262	Nonazeotrope	262
27		262	Nonazeotrope	262
28		262	Nonazeotrope	262
29		262	Nonazeotrope	262
30		262	Nonazeotrope	262
31		262	Nonazeotrope	262
32		262	Nonazeotrope	262
33		262	Nonazeotrope	262
34		262	Nonazeotrope	262
35		262	Nonazeotrope	262
36		262	Nonazeotrope	262
37		262	Nonazeotrope	262
38		262	Nonazeotrope	262
39		262	Nonazeotrope	262
40		262	Nonazeotrope	262
41		262	Nonazeotrope	262
42		262	Nonazeotrope	262
43		262	Nonazeotrope	262
44		262	Nonazeotrope	262
45		262	Nonazeotrope	262
46		262	Nonazeotrope	262
47		262	Nonazeotrope	262
48		262	Nonazeotrope	262
49		262	Nonazeotrope	262
50		262	Nonazeotrope	262
51		262	Nonazeotrope	262
52		262	Nonazeotrope	262
53		262	Nonazeotrope	262
54		262	Nonazeotrope	262
55		262	Nonazeotrope	262
56		262	Nonazeotrope	262
57		262	Nonazeotrope	262
58		262	Nonazeotrope	262
59		262	Nonazeotrope	262
60		262	Nonazeotrope	262
61		262	Nonazeotrope	262
62		262	Nonazeotrope	262
63		262	Nonazeotrope	262
64		262	Nonazeotrope	262
65		262	Nonazeotrope	262
66		262	Nonazeotrope	262
67		262	Nonazeotrope	262
68		262	Nonazeotrope	262
69		262	Nonazeotrope	262
70		262	Nonazeotrope	262
71		262	Nonazeotrope	262
72		262	Nonazeotrope	262
73		262	Nonazeotrope	262
74		262	Nonazeotrope	262
75		262	Nonazeotrope	262
76		262	Nonazeotrope	262
77		262	Nonazeotrope	262
78		262	Nonazeotrope	262
79		262	Nonazeotrope	262
80		262	Nonazeotrope	262
81		262	Nonazeotrope	262
82		262	Nonazeotrope	262
83		262	Nonazeotrope	262
84		262	Nonazeotrope	262
85		262	Nonazeotrope	262
86		262	Nonazeotrope	262
87		262	Nonazeotrope	262
88		262	Nonazeotrope	262
89		262	Nonazeotrope	262
90		262	Nonazeotrope	262
91		262	Nonazeotrope	262
92		262	Nonazeotrope	262
93		262	Nonazeotrope	262
94		262	Nonazeotrope	262
95		262	Nonazeotrope	262
96		262	Nonazeotrope	262
97		262	Nonazeotrope	262
98		262	Nonazeotrope	262
99		262	Nonazeotrope	262
100		262	Nonazeotrope	262

CONTENTS

Table of Azeotropes and Nonazeotropes	1
<i>L. H. Horsley</i>	
Table I. Binary Systems	3
Table II. Ternary Systems	250
Table III. Formula Index	267
Bibliography	308
Vapor-Liquid Equilibrium Diagrams of Alcohol-Ketone Azeotropes as a Function of Pressure	315
<i>E. C. Britton, H. S. Nutting, and L. H. Horsley</i>	
Graphical Method for Predicting Effect of Pressure on Azeotropic Systems	318
<i>H. S. Nutting and L. H. Horsley</i>	
Graphical Method for Predicting Azeotropism and Effect of Pressure on Azeotropic Constants	321
<i>L. H. Horsley</i>	

329
pages,
cloth
bound, \$4

Published by
AMERICAN CHEMICAL SOCIETY
1155 Sixteenth Street, N.W.
Washington, D. C.